ISSN 0711-6659

canadian acoustics
acoustique canadienne

SEPTEMBER 1995 SEPTEMBRE 1995
Volume 23 -- Number 3 Volume 23 -- Numéro 3

PROCEEDINGS ISSUE

ACOUSTICS WEEK IN CANADA
SEMAINE CANADIENNE D'ACOUSTIQUE
1995
ACOUSTICS WEEK IN CANADA
SEMAINE CANADIENNE D'ACOUSTIQUE

CAHIER DES ACTES

canadian acoustics

acoustique canadienne

THE CANADIAN ACOUSTICAL ASSOCIATION
P.O. BOX 1351, STATION "F"
TORONTO, ONTARIO M4Y 2V9

L'ASSOCIATION CANADIENNE D'ACOUSTIQUE
C.P. 1351, SUCCURSALE "F"
TORONTO, ONTARIO M4Y 2V9

CANADIAN ACOUSTICS publishes refereed articles and news items on all aspects of acoustics and vibration. Articles reporting new research or applications, as well as review or tutorial papers and shorter technical notes are welcomed, in English or in French. Submissions should be sent directly to the Editor-in-Chief. Complete instructions to authors concerning the required camera-ready copy are presented at the end of this issue.

CANADIAN ACOUSTICS is published four times a year - in March, June, September and December. The deadline for submission of material is the first day of the month preceeding the issue month. Copyright on articles is held by the author(s), who should be contacted regarding reproduction. Annual subscription: $10 (student); $35 (individual, corporation); $150 (sustaining - see back cover). Back issues (when available) may be obtained from the CAA Secretary - price $10 including postage. Advertisement prices: $350 (centre spread); $175 (full page); $100 (half page); $70 (quarter page). Contact the Associate Editor (advertising) to place advertisements.

ACOUSTIQUE CANADIENNE publie des articles arbitrés et des informations sur tous les domaines de l'acoustique et des vibrations. On invite les auteurs à soumettre des manuscrits, rédigés en français ou en anglais, concernant des travaux inédits, des états de question ou des notes techniques. Les soumissions doivent être envoyées au rédacteur en chef. Les instructions pour la présentation des textes sont exposées à la fin de cette publication.

ACOUSTIQUE CANADIENNE est publiée quatre fois par année - en mars, juin, septembre et décembre. La date de tombée pour la soumission de matériel est fixée au premier jour du mois précédant la publication d'un numéro donné. Les droits d'auteur d'un article appartiennent à (aux) auteur(s). Toute demande de reproduction doit leur être acheminée. Abonnement annuel: $10 (étudiant); $35 (individuel, société); $150 (soutien - voir la couverture arrière). D'anciens numéros (non-épuisés) peuvent être obtenus du Secrétaire de l'ACA - prix: $10 (affranchissement inclus). Prix d'annonces publicitaires: $350 (page double); $175 (page pleine); $100 (demi page); $70 (quart de page). Contacter le rédacteur associé (publicité) afin de placer des annonces.

EDITORIAL

Bienvenue à l'édition 1995 des actes de l'*Acoustique Canadienne*. Ce numéro présente le programme complet ainsi que les résumés de deux pages du symposium technique de la Semaine canadienne d'acoustique 1995 qui se tiendra à Québec, en octobre prochain. Comme c'est devenu la tradition, les Actes comptent un nombre impressionnant de rapports de recherche. La rencontre sera tout aussi impressionnante. Au plaisir de vous y voir!

Au cas où vous ne le sauriez pas, j'aimerais attirer votre attention sur le fait que le 12 mai 1995, l'Assemblée de la santé mondiale a adopté la résolution WHA48.9 intitulée, "La prévention des déficiences auditives". Cette résolution invite chaque pays à élaborer des stratégies de contrôle des causes majeures de pertes auditives. Le but est la prévention des pertes auditives, principalement chez les enfants et les personnes âgées. Outre des causes médicales, les effets du bruit sont explicitement reconnus comme étant une cause qui peut mener à des atteintes auditives, et des démarches en vue d'élaborer des règlements et des lois sont recommandées afin de limiter les expositions nocives. Tous les pays sont vivement encouragés à véhiculer de l'information sur l'audition et à éduquer la population au sujet de la protection et de la conservation de l'audition. La résolution charge aussi l'Organisation mondiale de la Santé de faciliter les coopérations techniques dans le but d'aider à prévenir les pertes auditives, à participer à l'évaluation des pertes auditives et à faire en sorte qu'elles soient considérées comme un problème de santé publique, à supporter les efforts des pays qui, individuellement, planifient et implantent des actions à l'égard des pertes auditives, et enfin

Welcome to the 1995 Proceedings Issue of *Canadian Acoustics*. It contains details of the final programme, and two-page summaries, of the Technical Symposium of Acoustics Week in Canada 1995 to be held in Quebec City in October. As is quickly becoming the norm, this is an impressive collection of research reports. The meeting will clearly be equally as impressive. See you there!

In case you are not aware, I'd like to bring to your attention to the fact that, on 12 May 1995, the World Health Assembly adopted resolution WHA48.9: "Prevention of Hearing Impairment". This resolution urges every country in the world to begin work on plans for the control of the major causes of hearing loss. The focus is on prevention of hearing loss, especially for children, and also in the elderly. In addition to medical conditions that may lead to hearing loss, the effect of noise is explicitly recognized, and regulatory and legislative steps are recommended to limit harmful exposure. Significantly, all countries are urged to disseminate information on hearing and to educate their population about hearing protection and conservation. The resolution also instructs the World Health Organization to facilitate technical cooperation to help prevent hearing loss, to participate in the assessment of hearing loss as a public health problem, to support the efforts of individual countries to plan and implement action regarding hearing loss, and to promote research. I will publish the full resolution in the December issue.

à promouvoir la recherche. Je publierai la résolution complète dans le prochain numéro.

ACOUSTICAL INTERFACE™ SYSTEM

precision acoustical measurements with your FFT, scope or meter

PS9200 POWER SUPPLY

■ Dual Channel ■ 9V "Radio" Battery
■ Portable ■ 50 Hours Operation
■ Low Noise ■ LED Status Indicator

7000 SERIES MICROPHONES

■ Type 1 Performance ■ ¼, ½ and 1 Inch Models

4000 SERIES PREAMPLIFIERS

■ 2Hz to 200kHz ± 0.5db ■ Removable Cable ■ PS9200 and 7000 Series Compatible

NEW LOW COST PRECISION MEASUREMENTS

■ **SINGLE CHANNEL SYSTEM UNDER $1,200**
■ **DUAL CHANNEL SYSTEM UNDER $2,000**
(½ or 1 inch microphones)

ACO Pacific, Inc.
2604 Read Avenue
Belmont, CA 94002
(415) 595-8588

ACOUSTICS BEGINS WITH ACO

PROCEEDINGS OF ACOUSTICS WEEK IN CANADA 1995
ACTES DE LA SEMAINE CANADIENNE D'ACOUSTIQUE 1995

Table of Contents / Table des matières

ECKEL

Noise Control Products & Systems

for the protection of personnel... for the proper acoustic environment...

engineered to meet the requirements of Government regulations

Eckoustic® Functional Panels

Durable, attractive panels having outstanding sound absorption properties. Easy to install. Require little maintenance. EFPs reduce background noise, reverberation, and speech interference; increase efficiency, production, and comfort. Effective sound control in factories, machine shops, computer rooms, laboratories, and wherever people gather to work, play, or relax.

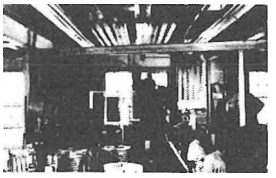

Eckoustic® Enclosures

Modular panels are used to meet numerous acoustic requirements. Typical uses include: machinery enclosures, in-plant offices, partial acoustic enclosures, sound laboratories, production testing areas, environmental test rooms. Eckoustic panels with solid facings on both sides are suitable for constructing reverberation rooms for testing of sound power levels.

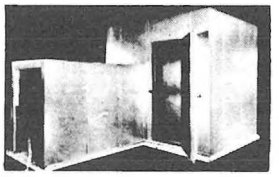

Eckoustic® Noise Barrier

● **Noise Reduction Curtain Enclosures** ● **Machinery & Equipment Noise Dampening**

The Eckoustic Noise Barrier provides a unique, efficient method for controlling occupational noise. This Eckoustic sound absorbing-sound attenuating material combination provides excellent noise reduction. The material can be readily mounted on any fixed or movable framework of metal or wood, and used as either a stationary or mobile noise control curtain.

Acoustic Materials & Products for dampening and reducing equipment noise

Multi-Purpose Rooms

Rugged, soundproof enclosures that can be conveniently moved by fork-lift to any area in an industrial or commercial facility. Factory assembled with ventilation and lighting systems. Ideal where a quiet "haven" is desired in a noisy environment: foreman and supervisory offices, Q.C. and product test area, control rooms, construction offices, guard and gate houses, etc.

Audiometric Rooms: Survey Booths & Diagnostic Rooms

Eckoustic Audiometric Survey Booths provide proper environment for on-the-spot basic hearing testing. Economical. Portable, with unitized construction.

Diagnostic Rooms offer effective noise reduction for all areas of testing. Designed to meet, within ±3 dB, the requirements of MIL Spec C-81016 (Weps). Nine standard models. Also custom designed facilities.

An-Eck-Oic® Chambers

Echo-free enclosures for acoustic testing and research. Dependable, economical, high performance operation. Both full-size rooms and portable models. Cutoff frequencies up to 300 Hz. Uses include: sound testing of mechanical and electrical machinery, communications equipment, aircraft and automotive equipment, and business machines; noise studies of small electronic equipment, etc.

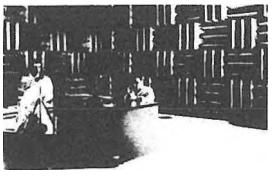

For more information, contact

ECKEL INDUSTRIES OF CANADA, LTD., Allison Ave., Morrisburg, Ontario • 613-543-2967

ECKEL INDUSTRIES, INC

Acoustics Week in Canada 1995 / Semaine Canadienne d'Acoustique 1995

Wednesday, October 25, Morning / mercredi, 25 octobre, matinée

	Salle Suzor Côté	Salle Morrice Lismer
	Psycho-physio acoustics / psycho-physio acoustique **Chair / Présidente: C. Laroche**	**Vibrations** **Chair / Président: L. Cheng**
8:40 - 9:00	*Combined use of behavioral and electrophysiological methods to explore human sound localization abilities* T. Leroux, J. B. Kelly	
9:00 - 9:20	*The influence of head protectors on warning sound localization ability in the horizontal plane* M. Fortin, R. Hétu	*Vacuum activated damping pads: a new, clean and more efficient tool to control impact noise at the source* M. Amram
9:20 - 9:40	*Pertes et gains par insertion associés au port de protecteurs de tête: conséquences pour la perception des avertisseurs sonores* R. Hétu, D. Mouneyres, H.T. Quoc, S. Denis	*Recent developments on the optimization of viscoelastic coating* L. Cheng
9:40 - 10:00	*A field investigation of conditions governing the use of auditory warning signals in industry* R. Hétu, S. Denis	*A model on self-damping of stranded cables in random transverse vibration* A. Leblond, L. Cloutier, C. Hardy, L. Cheng
10:00 - 10:20	*Détermination des caractéristiques acoustiques optimales des alarmes de recul installées sur les véhicules lourds* C. Laroche	*A simplified model for predicting vibrations of airplane fuselage* J. Missaoui, L. Cheng
10:20 - 10:40	*Développement d'un questionnaire de dépistage des incapacités auditives dans le bruit chez les travailleurs ayant été exposés au bruit* P. Fournier, C. Laroche	*A hybrid approach for vibrational analysis of coupled structures* M. Hatam, L. Cheng, D. Rancourt
10:40 - 11:00	*Active noise cancellation vs passive sound attenuation: help or hindrance?* S.M. Abel, D.L. Spencer	*Primary calibration of accelerometers by laser interferometry at the national research council* G.S.K. Wong, A.K. Agarwal, L. Wu
11:00 - 11:20	*Distorsion product otoacoustic emissions: computer modelling and experimental data* C. Giguère, H. Kunov, P. Madsen	*Methods of earthquake protection for vibration isolated equipment* P.J. Lama, S. Fey
11:20 - 11:40	*One-trial memory integration of music and film: a direct test* A.J. Cohen	
11:40 - 12:00	*Digital audiometer for precise testing of hearing in the 0 Hz -> 22,000 Hz range* M. Roland-Mieszkowski, D. Roland-Mieszkowski	
12:00	*Lunch - Déjeuner - Place Montcalm*	

Acoustics Week in Canada 1995 / Semaine Canadienne d'Acoustique 1995

Wednesday, October 25, Afternoon / mercredi, 25 octobre, après-midi

	Salle Suzor Côté	Salle Morrice Lismer
	Architectural Acoustics / Acoustique architecturale **Chair / Président: J.G. Migneron**	**Experimental methods / Méthodes expérimentales** **Chair / Président: Y. Champoux**
1:30 - 1:50	*Statistical energy analysis applied to lightweight constructions. Part 1: Sound transmission through floors* T.R.T. Nightingale, R.J.M. Craik, J.A. Steel	*A reference specimen for air flow resistance measurements* W.T. Chu
1:50 - 2:10	*Statistical energy analysis applied to lightweight constructions. Part 2: Joints between floors and party walls* T.R.T. Nightingale, J.A. Steel	*A unified approach for the two ASTM standards for impedance tube measurements* W.T. Chu
2:10 - 2:30	*Statistical energy analysis applied to lightweight constructions. Part 3: Measurements and predictions of flanking transmission* T.R.T. Nightingale, J.A. Steel, R.J.M. Craik	*Experimental characterization of the noise generation mechanism of percussion drill steel rods under laboratory controlled conditions* C. Lesage, R. Oddo, Y. Champoux
2:30 - 2:50	*Sound transmission through gypsum board walls* A.C.C. Warnock, J.D. Quirt	*Experimental investigations of riveted plates in the low, mid and high frequency range* H. Kaffel, O. Beslin, J. Nicolas
2:50 - 3:10	*Intelligibility of public address system, choice and disposition of ceiling speakers* J.G. Migneron, W. Wu	*Sound from resonances in sports equipment: can it be used to evaluate athletic performance?* D.G. Browning, R.H. Mellen, M.A. Jarrell
3:10 - 3:30	*Flanking in warehouse to residential conversions* D.B. Larson, R.A. Strachan	*Acoustic backscatter characterization of in-vitro fetal lungs; determination of alveolar sacs size* S. Hakim, K.L. Watkin
3:30 - 3:50	*Numerical modeling of fire stops at the intersection of floors and load bearing party walls* T.R.T. Nightingale	*Maximum likelihood deconvolution of ultrasonic signals for biological tissue classification* I. Diouf, K.L. Watkin
3:50 - 4:10	*Degradation of wood stud wall sound isolation by electrical boxes* T.R.T. Nightingale	*Acoustic localization using ice-mounted geophones in the Canadian high arctic* S.E. Dosso, Capt. R.W. Van Der Pryt, R.I. Verrall
4:10 - 4:30	*A summary of the CEN draft building acoustics model applied to a lightweight double leaf construction* T.R.T. Nightingale	
4:30 - 4:50	*Acoustic design of the new Ford theatre, Vancouver* J.C. Swallow	
4:50 - 5:10	*Scale-model tests of the effectiveness of novel sound-absorber configurations for industrial-noise control* M. Hodgson	
5:10 - 5:30	*Sound flanking through weak elements in composite walls constructions: a case study* B. Chapnik	

Acoustics Week in Canada 1995 / Semaine Canadienne d'Acoustique 1995

Thursday, October 26, Morning / jeudi, 26 octobre, matinée

	Salle Suzor Côté	Salle Morrice Lismer
	Noise control / Contrôle du bruit **Chair / Président: F. Laville**	**Life-span changes in speech perception / Changements à long terme dans la perception du langage** **Chair / Président: D. Jamieson**
9:00 - 9:20	*Noise and vibration sources of handheld grinders* J.L. Wojtowicki, J. Nicolas	*Self-reported and objectively-measured changes in speech perception with age* M.F. Cheesman, K.G. Greenwood
9:20 - 9:40	*Vibratory measurements to estimate mechanical properties of composite materials* B. Mercier, A. L'Espérance, J. Nicolas	*Development of perceptual distinction between phonemic contrasts in a first and second language* E.B. Slawinski
9:40 - 10:00	*Rayonnement acoustique produit lors du choc inélastique entre une sphère et une plaque mince rectangulaire* P. Troccaz, R. Woodcock, F. Laville	*Perception, production and acquisition of English /r/ and /l/ speech contrasts by Korean listeners* K. Yu, D.G. Jamieson
10:00 - 10:20	*Noise reduction in a factory workplace using ray tracing method* J.L. Wojtowicki, J. Nicolas	*Perception of a fricative-stop continuum by adults and children* KM. Krueger, M.M. Hodge, T.M. Nearey
10:20 - 10:40	*The effects of firing patterns, meteorology and terrain on community noise exposures from a military rifle range* C.W. Wakefield	*Perceptions of dialect change in the speech of adult Canadians living in Alabama* M.J. Munro, T.M Derwing
10:40 - 11:00	*Long range outdoor sound propagation model* A. Boudreau, A. L'Espérance, J. Nicolas, G. Daigle	*Perceptual change in adults: acoustic factors affecting the identification of English /r-l/ Japanese listeners* J.S. Logan, K. BharrathSingh
11:00 - 11:20	*Mufflers, nozzles and air guns: from research to applications in noisy work environments* P. Fortier	*Evaluation of VS image echodensities during contraction of the lingual musculature* J.L. Miller, K.L. Watkin
11:20 - 11:40	*Low frequency insertion loss of finite length flexible segments in piping systems* B.V. Chapnik, J.G. Curie	*Children's integration of auditory information* P. Allen, J. Nelles
12:00	*Lunch - Déjeuner - Place Montcalm*	

Acoustics Week in Canada 1995 / Semaine Canadienne d'Acoustique 1995

Thursday, October 26, Afternoon / jeudi, 26 octobre, après-midi

	Salle Suzor Côté	Salle Morrice Lismer
	Active noise and vibration control / Contrôle actif du bruit et des vibrations **Chair / Président: A. Berry**	**Numerical methods / Méthodes numériques** **Chair / Président: K. Fyfe**
1:30 - 1:50	*Active control of sound with foam-PVDF composite material* C. Guigou, C.A. Gentry, J. Pan, C.R. Fuller	*Étude vibroacoustique d'une coque cylindrique soumise à une excitation solidienne* S. Boily, F. Charron
1:50 - 2:10	*Multimodal sound pressure field in a cylindrical duct* F. Houïel, A. L'Espérance	*On the computation of acoustic modes of cavities with irregular shapes* J. Missaoui, L. Cheng
2:10 - 2:30	*A robust, low-computational, near optimal convergence speed, multi-channel filtered-X LMS algorithm* M. Bouchard, B. Paillard	*A 3D variational BEM formulation for the elastoacoustic vibration problem in viscous compressible flow* F. Erchiqui, A. Gakwaya
2:30 - 2:50	*Active noise control system to reduce the noise emitted by a large industrial stack* A. L'Espérance, M. Bouchard, F. Houïel, J.C. Dubé	*Diffraction and radiation by a panel immerged in a diffuse field* H. Nélisse, O. Beslin, J. Nicolas
2:50 - 3:10	*Active control of plate volume displacement: simulation and experimental results* F. Charette, A. Berry, C. Guigou	
3:10 - 3:30	*Active enhancement of the transmission loss of a panel via minimization of the volume velocity: theoretical and experimental results* M. Ruiz, A. Berry, F. Charette, C. Guigou	
3:30 - 3:50	*Active control of acoustic radiation using strain sensors* P. Masson, A. Berry, J. Nicolas	
4:00	*Annual General Meeting - Assemblée générale annuel*	

Combined use of behavioral and electrophysiological methods to explore human sound localization abilities

Tony Leroux[1] and Jack B. Kelly[2]

1 Programme Audiologie/Orthophonie, Université d'Ottawa
545, avenue King-Edward, Ottawa (Ontario) K1N 6N5

2 Laboratory of Sensory Neuroscience, Department of Psychology, Carleton University
1125 Colonel By Drive, Ottawa (Ontario) K1S 5B6

1. Introduction

Le matériel franco-québécois d'évaluation des capacités auditives centrales utilisé au Québec a fait récemment l'objet de critiques [1]. Ces critiques remettent en question la validité de ces épreuves en raison de problèmes de normalisation et de contrôle de certaines variables comme la compétence linguistique et les capacités cognitives des sujets. Ces faiblesses sont réelles et des travaux doivent être entrepris pour permettre l'élaboration d'épreuves pouvant corriger ces difficultés [2]. À l'intérieur de ce cadre, la localisation auditive apparaît comme un moyen privilégié d'apprécier le fonctionnement du système auditif central. D'une part, les capacités de localisation semblent relativement indépendantes des capacités linguistiques et cognitives puisque les comportements de localisation apparaissent très tôt chez l'humain durant la période qualifiée de pré-linguistique. D'autre part, plusieurs recherches ont révélé le potentiel diagnostique de certaines épreuves de localisation qui permettant d'identifier des dysfonctions du système auditif central [3-8]. En outre, les travaux réalisés par McEvoy et Picton [9-12] ouvrent la voie à l'intégration des mesures électrophysiologiques à des tâches comportementales de localisation et de latéralisation ce qui permet d'envisager la création d'épreuves objectives d'évaluation de ces capacités auditives centrales. Le présent article rapporte les résultats d'une étude exploratoire intégrant les réponses comportementales et électrophysiologiques obtenues lors d'une tâche impliquant la détection de signaux acoustiques masqués présentés binauralement.

2. Méthodologie

Sujets

Les sujets qui ont participé à cette étude sont 5 jeunes adultes âgés de moins de 35 ans présentant une acuité auditive normale. De plus, les sujets ne présentaient aucun antécédent d'atteinte à l'audition que ce soit au niveau otologique, familial ni aucune exposition significative au bruit.

Procédures expérimentales

À l'aide du système électro-acoustique numérique développé par Tucker-Davis Technology (TDT) et d'un logiciel conçu pour contrôler ce système (Balance 9)[13], un click et un bruit blanc masquant sont générés et transmis simultanément au sujet par le biais d'écouteurs. Le logiciel Balance 9 permet de contrôler très précisément: 1) la différence interaurale de temps pour le signal et le bruit masquant, 2) la différence interaurale d'intensité pour le signal et le bruit masquant et 3) le rapport signal sur bruit. Ainsi, un délai temporel interaural allant de -1000 μsec à +1000 μsec par pas de 100 μsec et une différence interaurale d'intensité allant jusqu'à 30 dB par pas de 1 dB peuvent être appliqués indépendamment au signal et au bruit masquant. De même, le rapport signal sur bruit peut être varié de -100 à +100 par unité.

Dans le cadre de cette étude exploratoire, le bruit masquant a été confiné à trois différences interaurales temporelles: 0, +600 et -600 μsec. Le signal, un click, est quant à lui déplacé temporellement d'une oreille à l'autre en utilisant des différences interaurales de temps allant de +1000 à -1000 μsec par pas de 100 μsec en présence du bruit masquant. La différence interaurale d'intensité a été fixée à 0 dB tant pour le signal que pour le bruit masquant pour obtenir essentiellement une différence interaurale temporelle. Le rapport signal sur bruit a été varié de -10 à 5 par pas de 5. La durée du bruit masquant et du signal étaient identiques, soit 100 μsec.

Pour chacune des situations temporelles du bruit masquant (n=3), les différentes situations d'écoute données par la combinaison des rapports signal sur bruit et des différences interaurales de temps du signal (n=84) ont été présentées aléatoirement à raison de 10 présentations pour chacune des combinaisons. De même, 10 présentations dont le signal est volontairement omis étaient intégrées aléatoirement pour chacun des rapports signal sur bruit utilisés pour éviter que le sujet ne se borne à détecter un signal pour toutes les présentations.

Le sujet, placé à l'intérieur d'une chambre anéchoïque, contrôle le déroulement de l'expérimentation à l'aide d'une souris modifiée qui transmet au système TDT l'ordre d'émettre une nouvelle stimulation et qui permet de recueillir, suite à la stimulation, le jugement du sujet quant à la détection ou la non-détection du signal à travers le bruit masquant. Pour chacune des 84 combinaisons étudiées, le logiciel Balance 9 donne une probabilité de détection variant de 0 à 1 tenant compte des réponses du sujet pour les stimulations où une cible était présente et celles où la cible était volontairement omise.

Afin de recueillir les réponses électrophysiologiques, 4 électrodes étaient placées sur la tête des sujets. Une électrode fixe a été placée au vertex et deux électrodes inversées ont été placées sur les lobes d'oreilles. Une dernière électrode était placée au centre du front près de la ligne d'implantation capillaire pour servir de mise à la terre. Ces électrodes ont été reliées à un pré-amplificateur lui-même relié au Nicolet Spirit™ permettant la mesure des potentiels évoqués auditifs du tronc cérébral. Le Nicolet Spirit™ était relié au système TDT qui émet un signal électrique permettant la mise en route synchronisée de la mesure électrophysiologique avec l'envoi des stimuli acoustiques au sujet. Pour chacune des combinaisons étudiées lors des manipulations comportementales, 1000 stimulations ont été recueillies et moyennées pour former la la réponse électrophysiologique composite des ondes I à V.

3. Résultats

Réponses comportementales

La figure 1 montre clairement que lorsque le signal et le bruit masquant partagent la même zone temporelle, la probabilité de détection du signal devient aléatoire. Cette observation se répète peut importe la zone temporelle dans laquelle se trouve le bruit masquant. Cet effet varie en largeur de bande temporelle et peut être retrouvé dans une gamme de rapport signal sur bruit d'environ 10 dB.

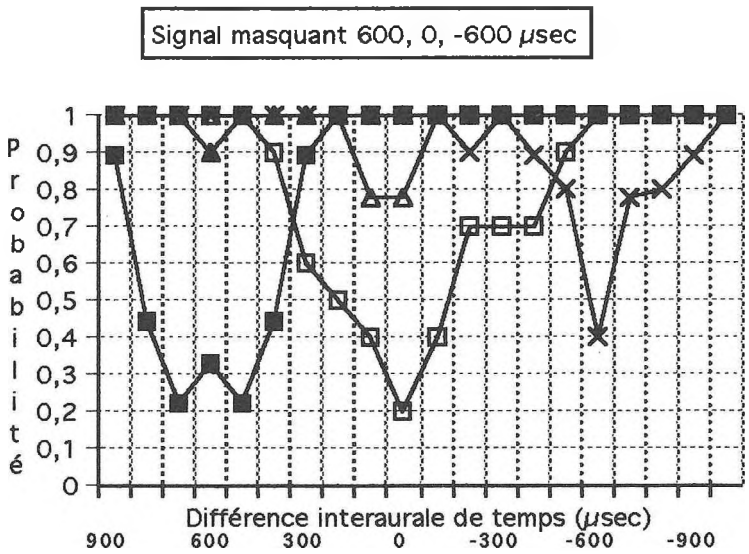

Figure 1 Probabilité de détection d'un click au travers d'un bruit masquant dont la différence interaurale de temps est varié à 600, 0 et -600 μsec. La figure présente les résultats d'un seul sujet.

Réponses électrophysiologiques

Contrairement aux réponses comportementales, les tracés électrophysiologiques obtenus jusqu'à maintenant ne diffèrent pas d'une situation d'écoute à l'autre. Les ondes I à V sont facilement identifiables et leur latence est stable, même en-deça du seuil comportemental de détection du signal. Ces résultats peuvent s'expliquer par la durée utilisée (100 μsec) à la fois pour le signal et le bruit masquant; ce qui a pour effet de générer une bouffée de bruit blanc dans ce dernier cas. Il est probable que, même en l'absence du click, la bouffée de bruit blanc soit suffisamment rapide et intense pour produire un effet "onset" propre à stimuler une réponse des sites générateurs du nerf auditif et du tronc cérébral. Des manipulations sont en cours pour tenter de contrecarrer cet effet indésirable.

4. Discussion

Les résultats comportementaux semblent mettre en évidence l'existence, au niveau du système auditif central, de bandes que l'on pourrait assimiler au fonctionnement d'une bande critique oeuvrant dans le domaine temporel. Avec la mise en place d'une procédure instrumentale appropriée, des données électrophysiologiques pourraient permettre d'identifier les sites neurologiques responsables de l'établissement de ces bandes critiques temporelles. Un examen approfondi des caractéristiques normales de ces bandes critiques temporelles est en cours au niveau comportemental. Les résultats de cette étude posent un premier jalon dans le développement d'épreuves évaluant les capacités auditives centrales de façon plus objective tout en se libérant des contraintes linguistiques

5. Références

[1] Huard, É. (1992) Quelques réflexions concernant les troubles centraux. Bulletin de la Corporation Professionnelle des Orthophonistes et Audiologistes du Québec, vol. 4(3), pp. 29-44.

[2] Bilodeau, S. (1993) L'audiologiste et le trouble auditif central chez l'enfant. Bulletin de la Corporation Professionnelle des Orthophonistes et Audiologistes du Québec, vol. 5(1), pp. 12-13.

[3] Altman, J.A., Rosenblum, A.S. Lvova, V.G. (1987) Lateralization of a moving auditory image in patients with focal damage of the brain hemispheres. Neuropsychologia, vol. 25(2), pp. 435-442.

[4] Cornelisse, L.E. and Kelly, J.B. (1987) The effect of cerebro-vascular accident on the ability to localiza sounds under conditions of the presedence effect. Neuropsychologia, vol. 25, pp. 449-452.

[5] Cranford, J.L., Boose, M. and Moore, C.A. (1990) Tests of the precedence effect in sound localization reveal abnormalities in multiple sclerosis. Ear and Hearing, vol. 11 pp. 282-288.

[6] Hochster, M. and Kelly, J.B. (1981) The precendence effect and sound localization by children with temporal lobe epilepsy. Neuropsychologia, vol. 19, pp. 49-55.

[7] Poirier, P., Lassonde, M., Villemeure, J.-G., Geoffroy, G. and Lepore, F. (1994) Sound localization in hemispherectomized patients. Neuropsychologia, vol. 32(5), pp. 541-553.

[8] Poirier, P., Miljours, S. Lassonde, M. and Lepore, F. (1993) Sound localization in acallosal human listeners. Brain, vol. 116, pp. 53-69.

[9] McEvoy, L.K., Picton, T.W. and Champagne, S.C. (1991a) Effects of Stimulus Parameters on Human Evoked Potentials to Shifts in the Lateralization of a Noise. Audiology, vol. 30, pp. 286-302.

[10] McEvoy, L.K., Picton, T.W. and Champagne, S.C. (1991b) The Timing of the Processess Underlying Lateralization: Psychophysical and Evoked Potential Measures. Ear and Hearing, vol. 12(6), pp. 389-398.

[11] McEvoy, L.K., Picton, T.W., Champagne, S.C., Kellett, A.J.C. and Kelly, J.B. (1990) Human Evoked Potentials to Shifts in the Lateralization of a Noise. Audiology, vol. 29, pp. 163-180.

[12] Picton, T.W., McEvoy, L.K. and Champagne, S.C. (1991) Human Evoked Potentials and the Lateralization of a Sound. Acta Otol. (Stockh), suppl. 491, vol. 139-144.

[13] Larivière, J. (1993) Balance9. Private softw are development. Laboratory of Sensory Neuroscience, Department of Psychology, Carleton University.

The influence of head protectors on warning sound localization ability in the horizontal plane

Martin Fortin and Raymond Hétu,
Groupe d'acoustique de l'université de Montréal,
C.P. 6128, Succ. Centre-ville, Montréal, H3C 3J7

Head protectors are extensivley used in the industrial work environment. To the best of our knowledge, their potential influence on sound localization ability has not as yet been investigated. Previous studies [1-2] have shown that hearing protectors impair sound localization in the horizontal plane to a significant degree and that this influence is likely due to disruption in spatial resolution resulting from their effect on the geometry of the pinna and/or concha [1-2]. Findings from these studies have shown increased within-quadrant and front-rear confusions for both broadband noise signals and third - octave band noises in quietnon-reverberant conditions. Data are currently being collected in our laboratory on insertion loss and directional transfer functions associated with head protectors. Preliminary analyses indicate that their effect on the geometry of the head or pinna might also disrupt the ability to localize warning signals. This may have serious implications in terms of occupational safety in industrial settings. The purpose of this study is to characterize localization errors in the horizontal plane, for a quiet non-reverberant situation, arising from wearing head protectors, with a view of adapting the acoustic characteristics of warning signals accordingly.

Methods

Participants

Twelve normal hearing listeners with mean age of 23,5 (±2) years were recruited among the students of the Université de Montréal. None had prior experience with sound localization experiments. Participants had to meet the following inclusion criteria:
-audiometric thresholds no higher than 20 dB HL (re:AINSI-S3.6 [3]) between 0.25 and 6 kHz;
-interaural difference in hearing thresholds smaller than 20 dB between 0.25 and 6 kHz;
-normal tympanogram;
-negative history of professionnal noise exposure;
-negative history of pathologies associated with hearing loss.

Procedure

The experimental paradigm was the identification of visible sources or categorization. Sixteen loudspeakers, 22.5° apart and 90 cm away from the center of the head of the listener, were operated in a hemi-anechoic chamber. The twelve subjects were tested under six listening conditions: unprotected, wearing a fire-fighter helmet, a Tyvek hood, a welder's mask, an aluminized hood and Bilsom Vicking 29 earmuffs. Two signal spectra were tested in each listening condition: a random noise with a flat spectrum between 125 and 8000 Hz (pink noise) and a six harmonics complex sound (warning sound) the fundamental of which was 500 Hz. The two signals were numerically desgined and equalized to take into account the frequency response of the loudspeakers. Two signal durations were tested in each listening condition, namely, 0.25 and 1.5 seconds.The latter allowed the contribution of free head/torso movements on the part of the subject but the former did not.

A complete run in a listening condition consisted of 2 stimuli for each loudspeaker, for a total of 32, presented in a quasi-random order. Signal level was set at 80 dBA with a ±2 dB randomized variation. The order of testing of the listening conditions, the signal spectra and duration were all randomized. Statistical analysis of the dara was performed using randomized block factorial design Anova.

Results and discussion

Table 1 presents the means and standard deviations of the localization errors in terms of total percentages; percentages are also given for within quadrant errors, front-rear and left-right confusions as a function of the three independent variables considered. A powerful effect of signal duration on global sound localization performances in the horizontal plane can be observed. Compared to long duration signals, short signals led to a significant increase in sound localization errors ($p<0.0001$ for all listening conditions). Spectral content had a significant effect for long duration signals ($p<0.0001$). Compared to the wideband noises, the warning sounds led to a significant increase in sound localisation errors for all test conditions.

Furthermore, a significant duration and spectral content interaction ($p<0.01$) was found. Generally speaking, earmuffs and the aluminized hood were the only protectors that led to a significant increase in sound localization errors when the long duration wideband noise was presented. On the whole, all protectors disrupted to some extent sound localization ability in the horizontal plane but performance differed from one protection condition to another with exception of the Tyvek hood compared to the welder's mask ($p=0.2625$). The aluminized hood was the most disruptive head protector in regard to global spatial resolution. Compared to all other head protectors, the aluminized hood led to a significant increase in errors for most of the signals except for the 0.25 s warning sound where performance was similar to the one associated with the earmuff condition ($p=0.5284$).

Within quadrant errors refer to sharp spatial resolution as compared to gross orientation. Since whereabout orientation remains relatively intact, these errors are not critical with respect to safety in the workplace. As in global sound localization performances, findings for within quadrant resolution indicate a signal duration effect, and a spectral content effect with long duration signals. However, there are no significant signal duration ($p=0.8694$) and spectral content ($p=0.5468$) effect with the aluminized hood, the most disruptive head protector with regard to this type of error. Interestingly, on the whole, within quadrant resolution was not blurred by wearing the fire-fighter helmet ($p=0.4662$).

Front-rear confusions refer to gross orientation and, consequently, are the most important type of error in danger signal localization in the workplace. Signal duration was again the most powerful factor with regard to front-rear resolution in the horizontal plane ($p<0.0001$ for all conditions). With long duration signals, there are virtually no front-back confusion whatever the protection condition, with the exception of the aluminized hood.

Table 1. Mean (+standard deviation) pourcentage localization errors as a function of signal parameters and listening condition.

Signals	Listening condition	Total pourcentage	Within quadrants	Front-rear confusions	Left-right confusions
Short (0.25 s) warning signal	Unprotected	25.8(17.0)	16.1(11.1)	10.7(8.6)	0.3(1.0)
	Fire-fighter helmet	48.2(9.0)	27.3(8.0)	23.5(7.7)	0.3(1.0)
	Tyvek hood	62.2(13.9)	26.3(8.2)	40.2(11.9)	0.9(1.6)
	Welder's mask	65.1(12.3)	35.9(10.5)	33.0(13.1)	0.3(1.0)
	Earmuffs	74.7(10.2)	33.3(8.6)	45.8(8.6)	1.5(3.2)
	Aluminized hood	80.7(10.3)	33.1(10.2)	44.9(11.4)	9.5(10.6)
Short (0.25 s) pink noise	Unprotected	18.0(10.4)	15.1(9.1)	3.0(4.0)	0.3(1.0)
	Fire-fighter helmet	44.8(15.8)	21.6(7.5)	25.9(12.0)	0.6(1.4)
	Tyvek hood	58.3(9.5)	28.1(10.7)	34.5(11.1)	0.0(0.0)
	Welder's mask	63.0(8.3)	37.5(7.9)	29.2(12.1)	0.0(0.0)
	Earmuffs	63.8(11.7)	26.3(10.4)	42.9(9.5)	0.0(0.0)
	Aluminized hood	75.0(7.9)	36.2(8.0)	43.8(9.9)	0.6(1.4)
Long (1.25 s) warning signal	Unprotected	0.5(1.2)	0.5(1.2)	0.0(0.0)	0.0(0.0)
	Fire-fighter helmet	8.1(11.4)	7.8(11.5)	0.3(1.0)	0.0(0.0)
	Tyvek hood	23.2(15.5)	20.1(13.4)	3.3(3.9)	0.3(1.1)
	Welder's mask	27.3(15.8)	24.5(14.9)	3.3(4.4)	0.0(0.0)
	Earmuffs	39.1(20.0)	35.4(20.5)	3.9(5.6)	0.3(1.0)
	Aluminized hood	65.9(20.2)	37.8(13.0)	20.2(16.1)	11.9(13.9)
Long (1.25 s) pink noise	Unprotected	1.3(2.1)	0.8(1.4)	0.3 (1.0)	0.6(1.4)
	Fire-fighter helmet	1.6(2.1)	1.0(2.0)	0.6 (1.4)	0.0(0.0)
	Tyvek hood	8.1(7.0)	3.9(5.0)	4.2 (5.2)	0.6(1.4)
	Welder's mask	6.5(3.9)	5.2(3.6)	1.5 (2.4)	0.0(0.0)
	Earmuffs	16.9(14.9)	14.6(12.4)	2.4 (3.5)	0.3(1.0)
	Aluminized hood	36.7(21.7)	31.3(17.8)	6.25(8.9)	0.0(0.0)

In order to achieve, with the aluminized hood, the same level of performance as with the other models of protector, subjects had to benefit from both the long duration and the wide spectrum of the signal. Therefore, spectral content had a significant effect only when combined with the long duration signal attended to with the aluminized hood ($p<0.0001$).

Contralateral confusions occur only with highly distorted interaural difference information. As can be seen from Table 1, the aluminized hood was the only model of protector associated with a significant degree of left-right confusions. Interestingly, spectral content was the only significant factor regarding the aluminized hood contralateral resolution ($p<0.0001$); signal duration had no effect ($p=0.9491$). Using a wide spectrum signal, almost no contralateral confusion could be osberved.

To sum up, all the protectors tested had some disruptive influence on sound localization ability in the horizontal plane, the worst being the aluminized hood. It is interesting to note that significant front-rear confusions were observed a plastic coated paper (Tyvek) hood equipped with a transparent plastic screen for vision. Such errors were generally prevented when the subjects had enough time to move their head while judging the whereabouts of sound signals. Such finding bears implications for auditory warning signal design for industrial settings.

Acknowledgement

The research presented above has been financially supported by the Institut de recherche en santé et en sécurité du travail de Québec. The protectors were kindly provided by Safety Supply inc.

References

[1] Noble,W. & al.(1990). The effect of various hearing protectors on sound localization in the horizontal and vertical planes. Am.Ind.Hyg. Assoc.J. 51(7):370-77.

[2] Abel, S.M. & Armstrong, N.M.(1993). Sound localization with hearing protectors. The Journal of Otolaryngology 22(5):357-63.

[3] ANSI-S3.6. (1969). Specifications for Audiometers, R1979, American National Standard Institute, New-York.

Pertes et gains par insertion associés au port de protecteurs de tête: conséquences pour la perception des avertisseurs sonores

Raymond Hétu, Delphine Mouneyres, Hung Tran Quoc, Stéphane Denis
Groupe d'acoustique de l'université de Montréal,
C.P. 6128, Succ. Centre-ville, Montréal, H3C 3J7

Les protecteurs de tête tels que les cagoules et masques peuvent-ils affecter la perception auditive des travailleurs qui les utilisent? En l'absence d'études pertinentes, ce projet visait à caractériser, dans un premier temps, les pertes ou les gains par insertion associés au port de ces protecteurs en prenant en compte l'angle d'incidence du signal sonore dans le plan horizontal et vertical.

Méthodologie

Dispositif et procédure de mesure

Un simulateur mécano-acoutique de tête recouvert d'une pellicule simulant la compliance de la peau a récemment été mis au point au Laboratoire de génie mécanique de l'Université de Toronto [1]. Sa mise au point bénéficie de nouvelles mesures anthropométriques. Le simulateur a été installé sur un torse de mannequin Kemar fixé sur une base rotative couvrant 360°. Celle-ci était entraînée par un moteur pas à pas dont la précision de 0.2° était assurée par contrôle numérique. La source sonore était constituée d'un haut-parleur (Belisle Acoustique DE45 Titanium) couplé à un cornet (BSE-9040) fixé à une potence permettant d'en varier l'élévation de -30 à +90° tout en maintenant une distance exacte de 1 mètre avec l'entrée du conduit auditif de la tête artificielle. La potence était recouverte de laine minérale pressée. Le dispositif était installé dans une cabine semi-anéchoïque. Les microphones installés dans les coupleurs de Zwislocki de la tête artificielle étaient branchés à un analyseur bi-voie (HP-35670A) opéré par l'intermidiaire d'un micro-ordinateur.

Un bruit de spectre large (0.2-10 kHz) présenté à un niveau global de 100 dB SPL a été utilisé comme signal. La perte par insertion (différence entre nvieau de pression acoustique relevé aux microphones du simulateur en l'absence et en présence du protecteur) a été mesurée en fonction de 36 azimuts et de 13 élévations dans la gamme de fréquences entre 0.2 et 6.3 kHz.

Modèles de protecteurs de tête évalués

Un premier échantillon de 4 modèles de protecteurs fait l'objet du présent compte rendu. Ceux-ci ont été fournis par la firme Safety Supplies. Il s'agit d'un masque de sablage en cuir (SS446M003), d'un masque de sablage avec aduction d'air (SS627K134), d'une cagoule pare-chaleur aluminisée (SS09T004) et d'un casque de soudage (767C145) monté surchapeau de sécurité. Des données ont également été recueillies sur un casque de sapeur-pompier, sur une cagoule pare-poussière, un respirateur d'urgence ainsi que des protecteurs anti-bruit. Elles ne sont pas présentées ici faute d'espace.

Résultats et discussion

La Figure 1 illustre les valeurs de perte ou de gain par insertion en fonction de la fréquence et de l'azimut à une élévation de 0° pour 4 modèles de protecteurs, tel que mesuré à l'oreille gauche du simulateur de tête. Les valeurs négatives d'azimut réfèrent à des position controlatérales par rapport à cette oreille. On observe que les trois cagoules présentent un comportement acoustique similaire. Celui-ci est caractérisé par des gains en basses fréquences et des pertes en hautes fréquences. Selon le protecteur considéré, la fréquence à laquelle le gain culmine varie: 0.2 kHz pour le casque de sablage, 0.25 kHz pour la cagoule aluminisée et 0.315 kHz pour la cagoule en cuir. Les gains sont maxima et voisins de 10 dB quand la source se situe à l'arrière de la tête. On observe en outre pour le casque de sablage un gain de 5 dB entre 0.63 et 0.8 kHz.

Au-delà de ces fréquences, les pertes par insertion sont d'autant plus importantes que la fréquence du signal est élevée. Ainsi, à 0° d'azimut, la perte atteint 19 dB à 6.3 kHz pour le casque de sablage, 29 dB à 5 kHz pour la cagoule aluminisée et 22 dB à 4 kHz pour la cagoule en cuir. Les pertes sont généralement plus importantes quand la source se situe du côté opposé à l'oreille à laquelle la mesure est effectuée, soit de l'ordre de 30 dB pour les trois protecteurs à 6.3 kHz entre +50 et +60° .

En résumé, ces trois types de masques induisent un effet d'écran pour les signaux sonores de hautes fréquences en particulier dans les zones frontales. Par contre, ils agissent comme amplificateur pour les signaux de fréquences inférieures à 1 kHz en particulier lorsque la source se situe à l'arrière de la tête.

La Figure 1 décrit également la réponse du masque de soudage. Dans ce cas, on observe des gains sur toute la gamme de fréquences quand la source se situe dans le secteur controlatéral arrière. Ainsi, on observe un gain de 18 dB à 1.6 kHz lorsque la source se situe à -110°. Le gain est de l'ordre de 7-8 dB entre 2 et 6.3 kHz en présence d'une source sonore située à 180°. Par ailleurs, on note une perte par insertion dans le secteur frontal, culminant à 14 dB à 2.5 kHz (azimut de 0°). L'effet est légèrement accusé dans le secteur avant controlatéral et atténué dans le secteur ipsilatéral.

Bien que les effets de l'élévation de la source ne soient pas représentés graphiquement, on peut les résumer en affirmant que, pour le masque de soudage, ce facteur contribue à diminuer et les gains et les pertes. Par contre, dans le cas du masque en cuir, on observe des pertes nettement plus importantes en hautes fréquences à certaines élévations (e.g. 60°). Les deux autres modèles de masques présentent des comportements intermédiaires.

Les résultats présentés plus haut ont des conséquences importantes en termes de santé et de sécurité du travail. D'un côté, les effets de gain par insertion observés peuvent se traduire par une augmentation de l'exposition sonore du fait de porter un protecteur de tête. Ainsi, le port du masque de soudage peut induire une augmentation de l'exposition à un bruit de spectre plat de 10 dBA ou plus si la source se situe à l'arrière du travailleur. En incidence aléatoire, cette augmentation est estimée à 5 dBA. Par ailleurs, le port de protecteurs de tête peut affecter la détection d'avertisseurs sonores. Par exemple, la perte par insertion appliquéeà un signal frontal combinée au gain associé à un bruit de masque situé à l'arrière peuvent élever le seuil de détection de près de 20 dB avec un masque de soudage.

References

1. Rakanski, D., Kunov, K. Desing of a human head simulator for studying the speech transmission characteristics of protective masks and transducer systems. University of Toronto, Institute of Biomedical Engineering, 1990.

[Projet subventionné par l'IRSST]

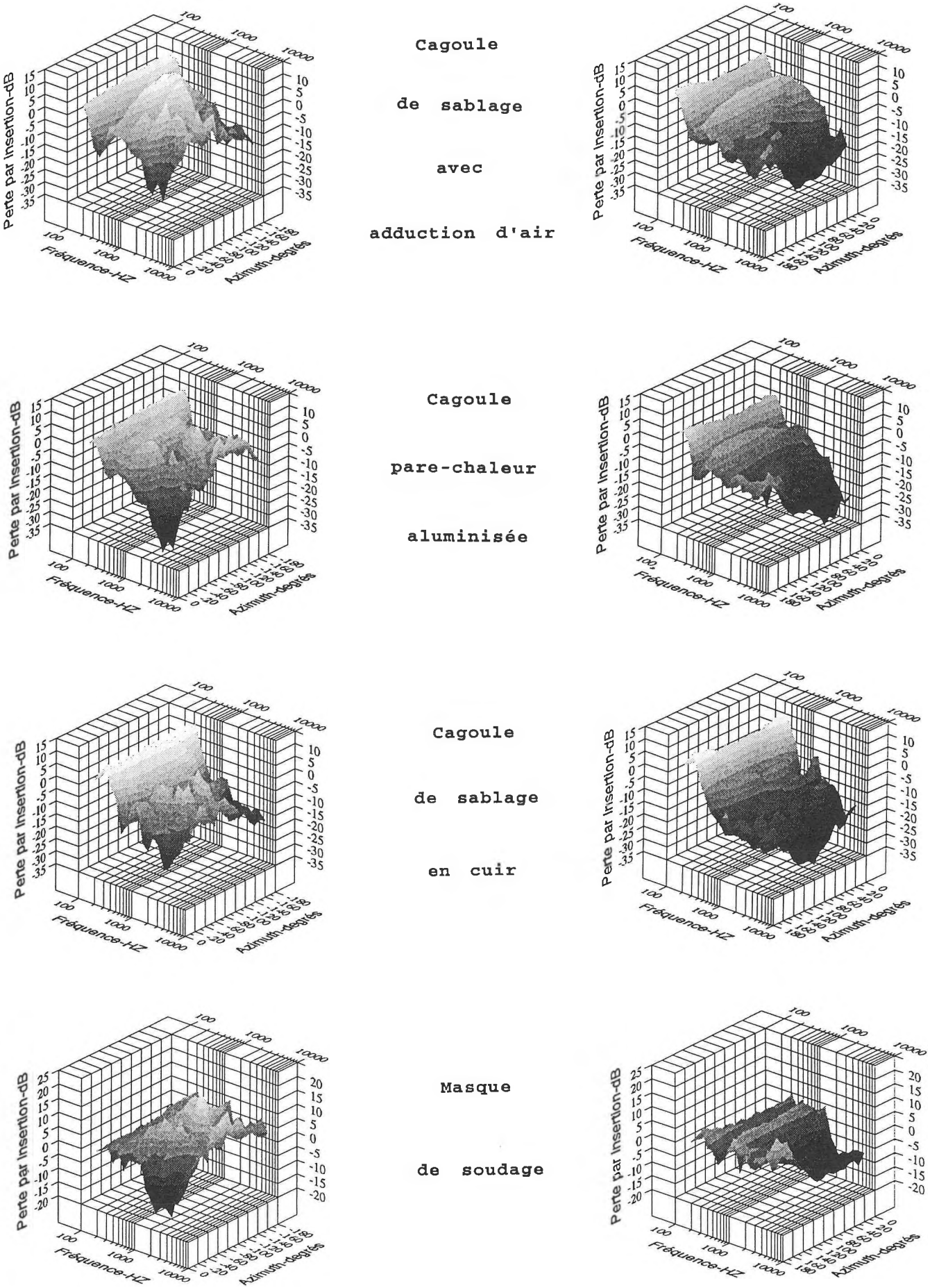

Figure 1. Perte ou gain par insertion associé à différents protecteurs de tête en fonction de la fréquence et de l'azimut

A Field Investigation of Conditions Governing the Use of Auditory Warning Signals in Industry

Raymond Hétu and Stéphane Denis
Groupe d'acoustique de l'université de Montréal,
C.P. 6128, Succ. Centre-ville, Montréal, H3C 3J7

A framework has been proposed for systematic analysis of possible mismatches between auditory demands and capacities in the workplace [1]. At present, very little information is available concerning the conditions governing perception of auditory warning signals (AWS) in industry. In a preliminary study conducted in a large steel mill [1], it was found that signals were too faint with respect to the prevailing background noise in more than one case out of three, and too loud in one case out six. This finding confirmed the need for systematic data collection on the conditions governing the use of auditory warning signals in industry. The present study was undertaken as part of a demonstration project, initiated by the Institut de recherche en santé et sécurité du travail (IRSST). The aim was to characterize the effectiveness of defective production signals and danger signals in different industrial settings.

Method

Plants visited

A total of 8 plants participated in this study. The bipartite occupational health and safety committee was first contacted for consent to participate in the study. The plants included the following industrial sectors: metal products, wires (n=2), auto parts, domestic appliances, printing and steel structures. They employed from 70 to over 400 workers.

Equipment and procedure

In each plant, a representative of the health and safety committee organized the visit. AWS were identified in each department. They were recorded under the quietest possible conditions. Then, a representative 10-s sample of the noise surrounding workers targeted by the signal was recorded. Measurement equipment included a BK-2231 sound level meter with BK4155 free-field microphone and a Sony MZ-1 magneto-optic digital recorder. The samples were later assessed using a BK-2123 analyzer. Horns operated on vehicles were recorded at a distance of 4 meters directly in front or behind.

Data treatment

The data were analyzed using DETECTSOUND™ [2-3]. Masked thresholds for AWS were determined in relation to prevailing background noise, with reference to the median normal hearing sensitivity of 55-year old males. Recognition threshold, based on findings from a field study [3], were set at +12 above estimated masked thresholds. The appropriate frequencies for signal design ranged from 0.25 to 3 kHz. A minimum of 4 recognizable spectral components was required for a signal to be judged as adequate [4]. An absolute limit of 105 dB SPL was also included in the assessment criteria, given that AWS should not induce temporary or permanent threshold shift.

Results

In all 8 plants visited, there was no one explicitly in charge of AWS. No register for such signals had been put together, nor was there any maintenance schedule.

In fact, when a signal source proved to be defective, maintenance electricians were asked to take charge of repairs and adjustments. In most places visited, AWS were identified by the safety personnel while we were conducting data collection in their plant. In other words, AWS were not considered as a safety issue even if an explicit health and safety policy was in effect in all 8 participating plants.

Fire alarmss

In most of the plant visited, it was not possible to assess one particular type of signal, namely, fire alarms, because it would have required that production be stopped for a significant period of time. It was nevertheless noteworthy that no routine testing of such signals existed in most places. In one plant, evacuation exercises were conducted yearly, but workers were directly alerted by foremen during such exercises. This procedure did not allow the plant to test the effectiveness of the alarms in all work areas. When assessing such alarms, it was found that they were too faint in over 50% of the work areas. In another plant, the fire alarm was the same signal as the one announcing coffee breaks, except that it was operated in a continous mode. That particular signal was inaudible to all workers who were engaged in the most common high-noise activities in this structural steel plant, i.e., gouging, grinding and chiselling.

Stationary signals

In all the plants visited, process AWS were being used. The more automated the process, the more frequent the use of AWS. Typically, signal sources were installed by equipment manufacturers and had not been adjusted to the sound environment in which the machinery was installed and operated. Horns activated when operating moving cranes constituted the most common type of danger signal used. Systematic analysis of stationary signals, including fire alarms, showed that they were too faint to be recognized over the background noise in half (50%) of the 124 assessed conditions under which they were used (Figure 1). No single component of these signals met the recognition threshold for normal listeners. Furthermore, less than 20% of the stationary signals actually met the ergonomic design criterion of 4 recognizable spectral components.

In most plants, signal audibility was to some extent inversely related to the level of background noise. However, it was striking to find that, in the most quiet plant visited (with maximum backround noise levels below 85 dBA in all but one work area), less than 15% of the stationary signals were adequate. This was due mainly to the fact that very high frequency components (≥3.15 kHz) were used for process signals and moving crane signals. In such cases, the signals were actually often too loud; they were said to be very annoying by workers who took part in the data collection.

In the more noisy work environments visited, AWS effectiveness was further assessed with account taken for high frequency noise-induced hearing loss combined with effective individual protection. In such cases, the signal design window was restricted to frequencies below 2 kHz. But this constraint was not routinely taken into account in the workplaces surveyed.

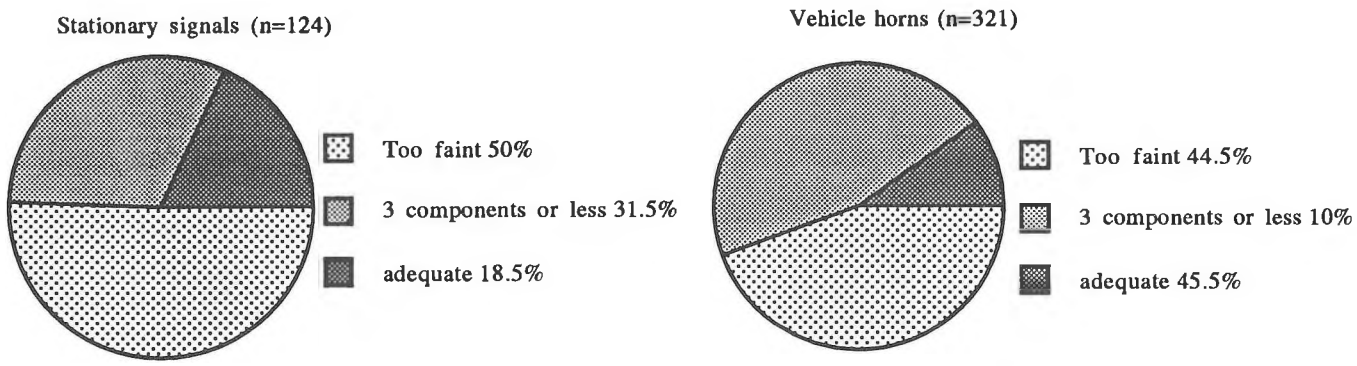

Figure 1. Assessment of sound warning signals under a specified number of conditionsgoverning their use in 8 factories. Adequate signal level was defined as 4 spectral components that reached at least 12 dB over the masked threshold for unprotected normal male listeners.

Lift truck horns

Lift trucks were quite extensively used in all plants visited. In most the lift truck, operators had de-actived or muffled the backup signal because it was felt to be too annoying. It is interesting to note that these vehicles operate in reverse gear for a significant lenght if not most of the time. The backup signal is thus on for long periods and loses its effectiveness as warning for people who work in areas of lift truck circulation. Another striking feature of the backup signals is that they consisted of one or two pure tones whose frequencies fell in a range of 1 to 3 kHz. The use of pure tones makes the signal highly sensitive to geometric interferences. The frequencies chosen happen to fall in a range in which human auditory localization is poorest for pure tones. The above observations call for a serious re-examination of the usefulness and effectiveness of backup signals.

As for the horns, a very wide variation of sound power could be observed. In some plants, there was a correlation between the mechanical power of the truck and the acoustic power of the horn, even though the various vehicles circulated in the same sound environement. In no instance was the horn specifically adjusted to the background noise in the work area. As a result, horns were found to be adequate in less than 50% of the 321 assessed conditions under which they are used, as indicated in Figure 1. Horns were definitely too faint in nearly 45% of the conditions. In one particular plant, the production process relied heavily on the use of lift trucks. Ten different models of trucks were used. Among them, the maximum third-octave band output level at 4 meters was lower than 80 dB SPL for 2 trucks; it ranged between 80 and 86 for a group of 4 trucks, and between 90 and 97 dB SPL for another group of 4. Accordingly, those with the faintest horns were found to be adequate for only the most quiet area of the plant, shipping and warehouse. They nevertheless circulated in other much noisier areas. Furthermore, in three of the most noisy production areas, the most powerful horn was too faint to be recognized over the background noise. Overall, lift truck horns had recognizable spectral components in less than 35% of the conditions under which they were uses in the plant. This example illustrates the fact that horns from lift trucks are not considered to be an important safety device. It also points to the need for adjustable horns that can meet the requirements imposed by different sound environments in a given plant.

Discussion

The above findings suggest that AWS are not being considered as a safety issue in industry. The lack of a register, of assessment and maintenance routine, and the lack of signal adjustment to listening conditions, point to a lack of awareness of the auditory demands in the industrial work environment. This situation might reflect what was pointed out in an analysis of the prevailing paradigm concerning hearing in industry [4-5], namely, that there is little if anything to be heard when the overriding concern is to protect one's hearing against high noise levels.

Observations reported above call for a systematic review of current industrial hygiene practice regarding acoustic signalling. If indeed AWS are used to transmit important information about production processes and danger situations, they need to be systematically assessed, and redesigned or replaced when minimal perceptibility criteria are not met. This implies having access to some kind of repertory of signal sources with proper specifications on frequency components and sound power levels. These observations also raise the need for adjustable sound sources, especially for vehicle horns, in order for such devices to meet the different requirements imposed by the various sound environments that typically characterize industrial settings. A simplified model of AWS propagation would also help safety personnel to specify the sound power of devices such as fire alarms that must cover large work areas under variable noise and propagation conditions.

References

1. Hétu, R. Mismatches between auditory demands and capacities in the industrial work environment. Audiol, 1994, 33: 1-14.
2. Laroche, C., Tran Quoc, H., Hétu, R., McDuff, S. Detectsound: A computerized model for predicting the detectability of warning signals in noisy workplaces. Appl Acoust, 1991, 32:193-214.
3. Tran Quoc, H., Hétu, R. , Laroche, C. Computerized assessment and prediction of the audibility of sound warning signals for normal and hearing impaired individuals. in Mattila, M. and W. Karwowski (eds.) Computer Applications in Ergonomics, Occupational Safety and Health. Amsterdam: Elsevier, 1992 : 105-112.
4. Patterson, R.D. Auditory warning sounds in the work environment. Phil. Trans. R. Soc. Lond. 1990, B327: 485-492
5. Hétu, R. The hearing conservation paradigm and the experienced effects of occupational noise exposure. Canad. Acoust., 1994, 22(1): 3-19.

Détermination des caractéristiques acoustiques optimales des alarmes de recul installées sur les véhicules lourds
(Determination of optimal acoustical characteristics for reverse alarms installed on heavy vehicles)

Chantal Laroche
Audiology/Speech-Language Pathology Program, University of Ottawa, 545 King Edward, Ottawa, Ontario, K1N 6N5

INTRODUCTION

Le Comité de réglementation sur le Code de sécurité pour les travaux de construction, composé de membres du patronat et du syndicat et de la Commission de la Santé et de la Sécurité au travail (CSST), a formulé le désir que soit réalisée une étude qui permettrait de réduire de façon significative le nombre d'accidents, souvent mortels, reliés au recul de véhicules lourds comportant ou non des alarmes de recul (Laroche et al., 1991a). Il désire particulièrement réviser l'article 3.10.12 du Code de sécurité (1994) qui prévoit la conformité des alarmes de recul avec la norme SAE-J994(1985).

Cette étude constitue la troisième phase d'un projet portant sur la propagation acoustique à l'arrière des véhicules lourds munis d'une alarme de recul. Elle fait suite à une étude sur la propagation acoustique des alarmes de recul à l'arrière de véhicules lourds (Ross et al., 1992) et au développement d'un logiciel de simulations de propagation acoustique des alarmes de recul (logiciel ALARME; Laroche et al. 1993). Ces deux études ont démontré qu'il existe des interférences acoustiques importantes qui peuvent compromettre la sécurité des travailleurs. La présente étude vise à identifier les caractéristiques acoustiques qui permettraient la conception d'une alarme de recul plus sécuritaire. La recherche de ces caractéristiques s'est faite à partir de paramètres acoustiques théoriques, de simulations d'alarmes de recul avec le logiciel ALARME, de mesures d'alarmes de recul sur le terrain, de commentaires d'appréciation d'intervenants du secteur de la construction et de simulations de la perception auditive des travailleurs à l'aide du logiciel Détectson (Laroche et al., 1991b).

PARAMÈTRES ACOUSTIQUES THÉORIQUES

Le principal critère pour évaluer le niveau d'efficacité de l'alarme est sa capacité à générer un niveau sonore uniformément décroissant c'est-à-dire sans interférences acoustiques de plus de quelques décibels (Laroche et al., 1993). De plus, les alarmes doivent posséder des caractéristiques acoustiques qui permettent leur détection, leur reconnaissance et leur localisation auditive par des travailleurs ayant ou non des atteintes auditives. Pour ce faire, il faut que le contenu fréquentiel soit distinct du bruit ambiant et ait au moins deux composantes audibles. Idéalement, la fréquence fondamentale du son complexe devrait être comprise entre 150 et 1000 Hz. Le spectre ne doit pas dépasser 3000 Hz, zone fréquentielle où la surdité est plus marquée. De plus, il faut que le niveau de pression sonore se situe entre 10 et 25 dBA au-dessus du seuil masqué et ait un niveau global entre 65 et 105 dBA. Enfin l'alarme ne doit pas générer plus de 6 signaux sonores différents et le délai entre les pulses doit véhiculer une information qui revêt un certain caractère d'urgence. (Patterson, 1982; ISO 7731, 1986; Laroche et al., 1991b)

SIMULATIONS AVEC LE LOGICIEL ALARME

Les simulations réalisées à l'aide du logiciel ALARME ont permis de démontrer que les alarmes comportant 3 ou 4 fréquences génèrent des patrons de propagation présentant de faibles variations du niveau sonore, c'est-à-dire rarement supérieures à 5 dB pour une distance de 1 mètre. Ces variations peuvent atteindre 15 à 20 dB lorsqu'une seule composante fréquentielle est utilisée (Laroche et al., 1993). Plusieurs combinaisons de fréquences se sont avérées intéressantes. De plus, les résultats démontrent que lorsque l'alarme est visible à l'arrière des véhicules, les interférences acoustiques sont moins fréquentes.

VALIDATIONS TERRAIN

Un simulateur d'alarmes répondant aux caractéristiques acoustiques identifiées à partir des simulations et des paramètres acoustiques théoriques a été développé par la firme DAP Électronique Canada Ltée. Le simulateur a été installé à deux emplacements différents sur 3 types de véhicules lourds (camion à benne, chargeur, niveleuse) et des mesures de pression acoustique ont été effectuées conformément à la norme CEI 804 (1985). Pour chaque position et chaque véhicule, des combinaisons de 3 et de 4 fréquences ont été mesurées. Des mesures de signaux comportant 6 fréquences ou un balayage en fréquences ont aussi été réalisées. L'écart entre les simulations et les mesures in-situ est généralement inférieur à 8 dBA, la plus grande disparité se produisant soit près du véhicule (moins de 1 mètre), soit sur les côtés (à 45^{o}). La figure 1 montre un exemple de résultat pour la niveleuse. La mesure a été réalisée sur une ligne centrale s'éloignant de l'arrière du véhicule, le simulateur d'alarme étant installé directement à l'arrière et générant les fréquences de 1000, 1150 et 1300 Hz.

De façon générale, les alarmes ayant 4 fréquences sont meilleures que celles ayant 3 fréquences. Les alarmes ayant 6 fréquences présentent moins d'interférences acoustiques, mais aucune amélioration significative n'a été notée si on les compare à des alarmes de 4 fréquences. Conformément aux résultats des simulations, les alarmes positionnées de façon à être visibles par une personne à l'arrière du véhicule présentent moins d'interférences acoustiques. La

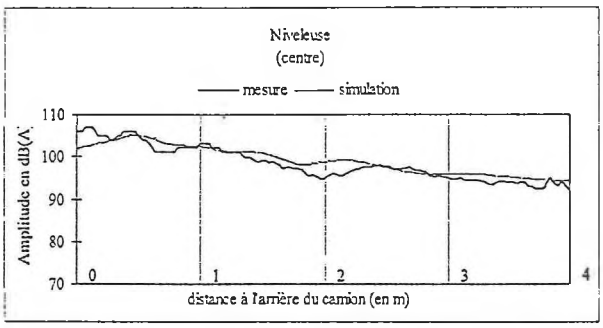

Figure 1. Variation du niveau de pression sonore en s'éloignant de l'arrière de la niveleuse. Alarme visible générant un son complexe de 1000, 1150 et 1300 Hz.

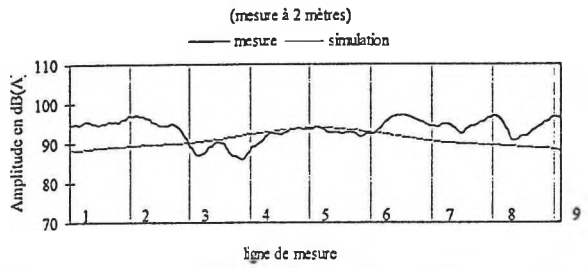

Figure 2. Variation du niveau de pression sonore à 2 mètres à l'arrière du camion à benne. Alarme non-visible générant un son complexe de 1000, 1150 et 1300 Hz.

figure 2 illustre un exemple où l'alarme de 1000, 1150 et 1300 Hz est peu visible sur le camion à benne. La mesure a été prise sur une ligne de 2 mètres qui contournent le véhicule. On note alors des variations plus marquées du niveau sonore.

Des intervenants du milieu de la construction ont été invités à évaluer et à commenter à l'aveugle 5 alarmes différentes. Deux d'entre elles avaient obtenu de bons résultats lors des essais terrain et deux autres avaient obtenu des résultats médiocres. La dernière alarme était celle déjà installée sur le véhicule du chantier de construction. Aucun consensus n'a été obtenu. Les alarmes de 4 fréquences ont été peu populaires à cause de leur tonalité trop agressante. L'alarme présentant le contenu fréquentiel 1000, 1150 et 1300 Hz a obtenu le plus grand nombre de votes et de bons résultats sur le terrain. Les intervenants ont aussi mentionné qu'ils ne croyaient pas à la nécessité d'avoir des catégories d'alarmes selon le type de véhicule lourd, car cette option ne ferait qu'accentuer la cacophonie qui règne sur les chantiers.

VALIDATIONS AVEC DÉTECTSON MD

L'alarme de recul retenue à l'étape précédente a été analysée à l'aide du logiciel Détectson MD (Laroche et al, 1991b) afin d'évaluer sa perception par les travailleurs. La simulation a tenu compte du bruit ambiant (bruit typique de chantiers de construction), du port de protecteurs auditifs (bouchons EAR et serre-tête Peltor H7A) et de la capacité auditive des travailleurs (seuils d'audition et sélectivité fréquentielle). Les résultats démontrent que l'alarme comprenant des composantes fréquentielles entre 1000 et 1300 Hz, de 95 dB SPL chacune, rencontre les critères d'audibilité et de reconnaissance pour l'ensemble des travailleurs. La figure 3 illustre un exemple d'analyse menée avec Détectson pour des individus de 55 ans atteints de surdité indemnisable et portant des bouchons EAR. Seules deux composantes fréquentielles de l'alarme peuvent être visualisées sur la figure à cause de l'analyse en tiers d'octave que réalise Détectson, mais il est clair que ces deux composantes rejoignent la zone hachurée qui correspond à la zone fréquentielle et de niveau sonore (dB SPL) requise pour assurer la reconnaissance du signal.

CONCLUSION

Il ressort donc de cette étude qu'un signal pulsé d'une durée de 400 msec, comportant 3 fréquences de 1000, 1150 et 1300 Hz de 95 dB SPL s'avère la combinaison la plus appropriée pour remplacer les alarmes de recul existantes. Par ailleurs, les alarmes de recul devraient être installées de telle sorte qu'elles soient visibles par une personne placée à l'arrière du véhicule. Quelques éléments de localisation auditive mériteraient d'être vérifiés avant d'adopter le signal sonore proposé (Laroche, 1994). Pour s'assurer de son audibilité et de sa reconnaissance,

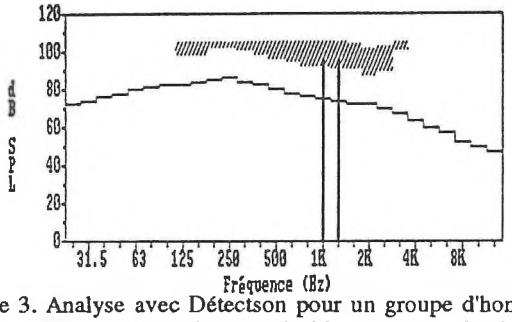

Figure 3. Analyse avec Détectson pour un groupe d'hommes de 55 ans atteints de surdité indemnisable et portant des bouchons EAR

il serait aussi intéressant de valider le signal retenu lorsqu'interfèrent différents bruits ambiants typiques des chantiers de construction. Enfin, les recommandations émises ci-haut peuvent servir de base à la révision de l'article 3.10.12 du Code de sécurité pour les travaux de construction (1994).

Remerciements:
Cette étude a été réalisée grâce à une subvention de recherche de l'IRSST octroyée à Chantal Laroche alors qu'elle était chez Sonométric Inc.

Références:

CEI 804 (1985). Sonomètres intégrateurs-moyenneurs. Bureau Central de la Commission Électrotechnique International.

Code de sécurité pour les travaux de construction (1994). S2.1, r.6, Gouvernement du Québec.

ISO 7731 (1986). Danger signals for workplace- Auditory danger signals.

LAROCHE, C., HÉTU, R & NICOLAS, J.(1990). Conception et validation d'un modèle informatisé de détection de signaux sonores de danger en milieux de travail bruyants. Rapport d'étape, Programme de recherche subventionnées, IRSST, RS-89-05, mars 1990.

LAROCHE, C., L'ÉSPÉRANCE, A. & HÉTU, R. (1991a). Des alarmes de recul qui tuent! Travail et Santé, 7,9-13.

LAROCHE, C., TRAN QUOC, H., HÉTU, R. & McDUFF, S. (1991b). "Detectsound": A computerized model for predicting the detectability of warning signal in noisy workplace. Applied Acoustics, **32**, 193-214.

LAROCHE, C., LEFEBVRE, L., ROSS, M.J. & LAROCQUE, R. (1993). Détermination des caractéristiques acoustiques optimales des alarmes de recul. Phase II: Mesures terrain et mise au point d'un modèle de propagation sonore. Rapport final, Programme de recherche subventionnée, IRSST, CR-92-05, mars 1993.

LAROCHE, C. (1994). Review of the literature on sound source localization and applications to noisy workplace. Acoustique Canadienne, **22**(4), 13-18.

PATTERSON, R.D. (1982). Guidelines for auditory warning systems on civil aircraft. CAA Paper 82017, Civil Aviation Aothority, London.

ROSS, M.J., LAROCHE, C. & LAROCQUE, R. (1992). Détermination des caractéristiques optimales des alarmes de recul. Phase I: Inventaire des véhicules lourds, des réglementations et des normes relatives aux alarmes de recul. Commandite spéciale, IRSST.

SAE J994b MAR85 (1985). Alarm-Backup-Electric-Performance, Test and Application.

Développement d'un questionnaire de dépistage des incapacités auditives dans le bruit chez les travailleurs ayant été exposés au bruit
(Development of a screening tool measuring auditory capacities in a noisy environment among workers exposed to industrial noise)

Paula Fournier et Chantal Laroche
Programme d'audiologie et d'orthophonie, Université d'Ottawa,
545, ave. King-Edward, Ottawa (Ontario) K1N 6N5

INTRODUCTION

La mesure de la **sélectivité fréquentielle** permet de prédire la capacité de détecter un son, tel que la parole ou un signal avertisseur, en présence de bruits de fond (Hétu et Tran Quoc, 1994). Il est connu que l'élargissement des filtres auditifs est associé à une baisse de sélectivité fréquentielle (Tran Quoc et al., 1991). D'ailleurs, une perte cochléaire, comme une surdité due à l'exposition au bruit, engendre l'élargissement des filtres auditifs (Florentine et al., 1980; Tyler, 1986). La mesure des paramètres des filtres auditifs peut donc servir d'indicateur des capacités auditives faisant appel à la sélectivité fréquentielle.

Afin de mieux documenter ce phénomène, le Groupe d'Acoustique de l'Université de Montréal a développé récemment une **procédure clinique quantitative** permettant de prédire la capacité auditive faisant appel à la sélectivité fréquentielle chez les sujets atteints d'une perte auditive de nature neuro-sensorielle. La sélectivité fréquentielle est déterminée en calculant la largeur de bande de fréquence d'un **filtre rectangulaire équivalent (FRE)**, qui est définie comme étant "la largeur de bande de fréquences, en Hertz, d'un filtre rectangulaire laissant passer la même puissance acoustique d'un bruit blanc qu'un filtre de résonance centré à la même fréquence" (Hétu et Tran Quoc, 1992).

La mesure des filtres auditifs présente plusieurs attraits. D'une part, elle promet d'être fort pour la réadaptation professionnelle (Hétu et Tran Quoc, 1994; ibid., 1992). D'autre part, la mesure de la sélectivité fréquentielle pourrait contribuer au diagnostic différentiel (Hétu et Tran Quoc, 1994).

Cette procédure peut toutefois s'avérer longue à compléter dans un contexte clinique où les contraintes budgétaires se font ressentir. La mesure des caractéristiques des filtres auditifs pour cinq fréquence exige, en effet, entre 40 et 50 minutes pour les deux oreilles (Hétu et Tran Quoc, 1994). Il peut donc être superflu de faire passer ce test à tous les individus qui se présenteraient en clinique audiologique.

BUT ET HYPOTHÈSE

Le présent projet vise à mettre au point un outil qui permettrait de sélectionner les candidats qui bénéficieraient d'une mesure quantitative de la sélectivité fréquentielle, telle que proposée par le GAUM, afin d'éviter l'utilisation massive de cette procédure exhaustive et coûteuse. Le développement d'un **questionnaire de dépistage** peut représenter une avenue intéressante à explorer en tant qu'outil de dépistage audiologique.

L'hypothèse à vérifier est la suivante: il existe une forte corrélation entre la mesure clinique des caractéristiques des filtres auditifs et la capacité de détection d'un signal sonore dans le bruit de fond identifiée à l'aide du questionnaire de dépistage.

MÉTHODOLOGIE

Le développement du questionnaire de dépistage a été réalisé à partir d'un répertoire exhaustif de questionnaires portant sur les capacités auditives, tels que SAC, HPI (Alpiner et Schow, 1993) et EMDA (GAUM et al.,1993). Parmi les questions portant sur les capacités auditives, seules les questions spécifiques à la sélectivité fréquentielle ont été choisies. Ces questions sélectionnées ont été parfois modifiées ou élaborées afin de former des questions plus spécifiques et explicites. Les questions de langue anglaise ont été traduites en français afin de mettre au point un questionnaire pour les francophones. Un certain nombre de questions ont été développées mais le construit et le contenu a été fortement influencé par des questions tirées de questionnaires validés. Enfin, le questionnaire est formé de questions, telles que "Vous êtes en automobile: vous écoutez la radio ou les passagers discutent entre eux. Pouvez-vous DÉTECTER la sirène de la police, de pompier ou de l'ambulance à proximité de vous?" et "Vous êtes au restaurant et il y a du bruit de fond (ex: musique, foule). Pouvez-vous COMPRENDRE le serveur s'il parle assez fort pour vous?"

Ce questionnaire de dépistage est formé de 22 questions et n'exige que 10 à 15 minutes pour y répondre. Le questionnaire est auto-administré, ce qui facilite l'usage sur une vaste échelle en clinique. La consigne écrite est claire et facile à comprendre. La forme de questions et de réponses est la plus uniforme que possible. L'échelle de score comprend 5 choix: jamais, parfois, souvent, toujours et non applicable. Le cinquième choix "non applicable" a été ajouté afin que tous puissent répondre à toutes les questions de façon la plus honnête et précise. Le score global est facile à utiliser.

En ce qui trait aux sujets expérimentaux, des travailleurs ayant été exposés au bruit d'une usine de pâte et papier ont

été choisis de façon à examiner les effets d'une perte induite par le bruit industriel sur la sélectivité fréquentielle. Puisque la fatigue auditive peut affecter la capacité auditive reliée à la sélectivité fréquentielle, des sujets n'étant plus exposés au bruit industriel ont été testés (Bergman, 1992). De façon à minimiser l'influence de l'âge sur les filtres auditifs, des sujets âgés entre 18 et 55 ans ont été invités à participer à la cueillette de données (Patterson, 1982). Des sujets présentant des seuils absolus supérieurs à 30 dB HL ont été sélectionnés puisque la sélectivité fréquentielle n'est généralement réduite que pour des seuils auditifs supérieurs à 30 dB HL (Laroche et al., 1992). Des sujets présentant des seuils absolus inférieurs à 65 dB HL ont été choisis puisque la procédure clinique de mesure des FRE se limite à des seuils absolus égaux ou inférieurs à 65 dB HL (Hétu et Tran Quoc, 1994).

Des auditeurs normaux ont été choisis comme sujets contrôles. Le groupe contrôle va permettre de valider le questionnaire. En effet, on s'attend à ce que ces sujets ne rapportent aucun problème au questionnaire si leurs filtres auditifs sont normaux. Par ailleurs, les résultats de ce groupe pourraient être comparés avec la base de données normatives établie par le GAUM afin de vérifier si les deux études sont compatibles. L'étude menée par le GAUM est la seule à avoir établi une base de données normatives. Nos résultats pourraient donc s'y ajouter.

Chacun des participants expérimentaux et contrôles seront soumis aux deux modalités d'évaluation de la capacité de sélectivité fréquentielle, à savoir la passation du questionnaire de dépistage et la mesure clinique des filtres auditifs.

ANALYSE DES DONNÉES

Les données recueillies à l'aide du questionnaire de dépistage serviront à constituer une base de données des incapacités auditives rapportées par les 15 sujets expérimentaux et 5 sujets contrôles. Ces données seront mises en relation avec les données issues des mesures de FRE de ces mêmes 20 sujets pour chaque fréquence discrète ou moyennes de fréquences (par exemple, 0.5 kHz, 1 kHz et 2 kHz). Les 20 sujets seront traités en tant qu'un continuum de données.

RETOMBÉES DU PROJET PROPOSÉ

Lors de la rédaction de cette article, la cueillette de données n'était pas finalisé. Les résultats du présent projet seront toutefois présentées lors du congrès de l'ACA.

L'hypothèse sera vérifiée si une forte corrélation entre le score obtenu au questionnaire et la valeur de la FRE est observée pour les sujets expérimentaux et contrôles. Si une forte corrélation est démontrée entre les deux mesures, le questionnaire pourrait servir d'outil de dépistage. Ce questionnaire de dépistage permettrait de sélectionner les candidats qui bénéficieraient d'une mesure quantitative de la sélectivité fréquentielle. Toutefois, une collecte de données plus exhaustive est nécessaire pour déterminer à partir de quel score un sujet pourra être référé en clinique audiologique.

Si une faible corrélation est démontrée entre les deux outils, ceci suggère que ces deux outils ne mesurent pas le même phénomène. Donc, le questionnaire ne permettrait pas de sélectionner les candidats qui bénéficieraient d'une mesure quantitative de la sélectivité fréquentielle.

Remerciements:
La réalisation de cette étude a été possible grâce à la collaboration du bureau de santé Porcupine, Spruce Falls Inc. et Régis Foré, technicien de laboratoire en audiologie.

Références:

ALPINER, J.G. ET SCHOW, R.L., (1993). Chap. 10. Rehabilitatitive Evaluation of Hearing-Impaired Adults. pp. 237-283. Dans: Rehabilitative Audiology Children and Adults, 2nd edition, ed by Alpiner, J.G. and McCarthy, P.A., Williams and Wilkins.

BERGMAN, M., NAJENSON, T., KORN, C., HAREL, N., ERENTHAL, P. & SACHARTOV, E., (1992). Frequency selectivity as a potential measure of noise damage susceptibility. British Journal of Audiology, **26**, 15-22.

FLORENTINE, M., BUUS, S. & ZWICKER, E., (1980). Frequency selectivity in normally-hearing and hearing-impaired observers. J. Speech Hear. Res., **23**, 646-669.

GAUM, NOBLE, W., & STEPHENS, D., (1993). Échelle de mesure de difficultés d'audition. Université de Montréal.

HÉTU, R., & TRAN QUOC, H., (1994). Étude de validité de la prédiction des capacités individuelles de détection des signaux sonores en milieu bruyant auprès des personnes atteintes de défience auditive neuro-sensorielle - Rapport final, Subvention IRSST PE-92-08.

HÉTU, R. & TRAN QUOC, H., (1992). Évaluation des capacités de détection auditive en milieu bruyant et intégration des personnes déficientes auditives en milieu de travail. Rapport final, Subvention IRSST PE-92-08.

LAROCHE, C., HÉTU, R., TRAN QUOC, H., JOSSERAND, B. & GLASBERG, B., (1992). Frequency selectivity in workers with noise-induced hearing loss. Hear. Res., **64**, 61-72.

PATTERSON, R.D., NIMMO-SMITH, L., WEBER, D.L. & MILROY, R., (1982). The deterioration of hearing with age: frequency selectivity, the critical ratio, the audiogram, and speech threshold. J. Acoust. Soc. Am., **72**(6), 1788-1803.

TRAN QUOC, H., HÉTU, R. & LAROCHE, C., (1991). Choix d'une procédure de mesure de la capacité de détection dans le bruit en vue de la mise au point d'une examen clinique. J. Speech Lang. Pathol. Audiol., **15**, 21-33.

ACTIVE NOISE CANCELLATION VS PASSIVE SOUND ATTENUATION: HELP OR HINDRANCE?

Sharon M. Abel and Deborah L. Spencer

Mount Sinai Hospital
600 University Ave., Room 843
Toronto, Ontario M5G 1X5

1.0 INTRODUCTION

Normal-hearing subjects show improved speech understanding when they wear conventional passive hearing protectors in noisy surroundings. In contrast, hearing-impaired subjects are at a disadvantage. Sound attenuation exacerbates the handicap from hearing loss (Abel et al., 1982). Level-dependent (active) hearing protectors which provide limited amplification of sounds below 85 dBA have the opposite effect. Normal-hearing listeners are at a disadvantage. In contrast, hearing-impaired listeners show some improvement in consonant discrimination and word recognition (Abel et al., 1993).

Unlike limited amplification, active noise reduction (ANR) appears to improve speech intelligibility in noise in normal-hearing listeners. However, it is unclear whether the benefits oberved with ANR are greater than those from passive attenuation (Gower and Casali, 1994; Nixon et al., 1992). The present study was designed to answer this question. The effect of muffs with active low-frequency noise cancellation was compared with the effects of conventional muffs and plugs with good low-frequency attenuation and plugs with minimal attenuation, in young and middle-aged normal-hearing subjects. Aging, apart from hearing loss, has been shown to affect speech discrimination ability (Bergman, 1980).

2.0 METHODS AND MATERIALS

2.1 Subjects

Two groups of 16 subjects with normal hearing, aged 21-36 yrs and 40-59 yrs participated in the study. Across individuals, free-field binaural hearing thresholds were equal to or less than 20 dB SPL in the range of 500 Hz to 4000 Hz. All were native English speakers. Some had participated previously in studies of hearing protectors.

2.2 Hearing Protective Devices

Each subject was tested with the ears unoccluded and fitted binaurally with E-A-R foam plugs, E-A-R HI-FI plugs, Bilsom Viking muffs and Peltor 7004 muffs without and with ANR operational. Based on the manufacturers' specifications, all but the E-A-R HI-FI plugs were Class A, as defined by CSA Standard Z94.2-94.

2.3 Psychoacoustic Measures

Two types of measurements were made within each of the six ear conditions: free-field binaural hearing thresholds for 1/3-octave noise bands centred at 250, 500, 1000, 2000, 3150, 4000, 6300 and 8000 Hz and word recognition for speech presented at 80 dB SPL. These measurement were made in quiet and in a background of continuous 75 dB SPL-cable swager noise. The noise was similar in sound to riveting. It had a repetition rate of 20 impulses/sec and a low-frequency bias.

2.4 Procedure

Each subject was tested individually in a sound proof semi-reverberant chanber that met the requirements of ANSI Standard S12.6-1984. Acoustic stimuli and noise were presented over a set of three Celestion DL10 three-way loudspeakers. The unoccluded condition was presented first, followed by the protected conditions, the order counterbalanced across subjects.

Hearing thresholds were obtained using a variation of Bekesy tracking (Giguère and Abel, 1990). One threshold determination was made for each of the eight frequencies within each ear by background condition. Word recognition was assessed using the SPIN test (Bilger et al., 1984). The test comprises eight alternative pre-recorded lists of 50 sentences. In half the sentences in each list, the final word is highly predicatable from the context, and in the remainder, poorly predicted. In the present study, one list was randomly selected for presentation in each ear by background condition within subject. The subject wrote down the final word in each sentence.

3.0 RESULTS AND DISCUSSION

The attenuation provided by each hearing protector was derived by subtracting the unoccluded from the protected hearing threshold for each of the eight frequencies. An analysis of variance performed on the data indicated that age of subjects was not a significant factor. The means for the two plugs were within 5 dB, and those for the muffs within 10 dB, of the manufacturers' specifications. The Bilsom Viking muff and the Peltor muff without ANR were virtually identical. With ANR, the Peltor muff provided an additional 10 dB of attenuation at 250 Hz.

The mean percentage of final words correctly recognized in sentences with good (high) and poor (low) contextual cues is shown in Fig. 1. Age was not significant and the two groups were collapsed. Overall, the presence of noise resulted in a significant decrement in score. In the quiet condition, a significantly lower mean score was observed for the E-A-R foam plug compared with the other ear conditions, given low contextual cues only. In noise, protected listening improved outcome relative to unoccluded listening for both types of speech materials. With high context, the mean score for the E-A-R foam plug was significantly lower than the scores for both the E-A-R HI-FI plug and Peltor muff with ANR operational. There was no difference due to device with low context.

4.0 CONCLUSIONS

The results support previous findings of a beneficial effect of conventional hearing protectors for speech intelligibility in noise, in normal listeners. Under the conditions of the present experiment, there was no clear improvement or decrement with active low-frequency noise cancellation.

Acknowledgements

Supported by a contract from the Directorate of Health Protection and Promotion, Dept. of National Defence, Canada, and a Scientist Award (SMA) from The Saul A. Silverman Family Foundation.

References

Abel, S.M., Alberti, P.W., Haythornthwaite, C. and Riko, K.(1982). "Speech intelligibility in noise: effects of fluency and hearing protector type." J. Acoust. Soc. Am. 71, 708-715.

Abel, S.M., Armstrong, N.M., and Giguère, C. (1993). "Auditory perception with level-dependent hearing protectors: the effects of age and hearing loss." Scand. Audiol. 22, 71-85.

ANSI S12.6-1984 (1984). "Method for the measurement of the real-ear attenuation of hearing protectors." American National Standards Institute, New York.

Bergman, M. (1980). Aging and the Perception of Speech. (University Park Press, Baltimore).

Bilger, R.C., Nuetzel, M.J., Rabinowitz, W.M. and Rzeczkowski, C. (1984). "Standardization of a test of speech perception in noise." J. Sp. Hear. Res. 27, 32-48.

CSA Z94.2-94 (1994). "Hearing protectors." Canadian Standards Association, Rexdale, Ont.

Giguère, C. and Abel, S.M. (1990). "A multi-purpose facility for research on hearing protection." App. Acous. 31, 295-311.

Gower, D.W.,Jr. and Casali, J.G. (1994). "Speech intelligibility and protective effectiveness of selected active noise reduction and conventional communications headsets." Hum. Factors 36(2), 350-367.

Nixon, C.W., McKinley, R.L., and Steuver, J.W. (1992). "Peformance of active noise reduction headsets," in Noise-Induced Hearing Loss, edited by A.L. Dancer, D. Henderson, R.J. Salvi, and R.P. Hamernick (Mosby, St. Louis), pp. 389-400.

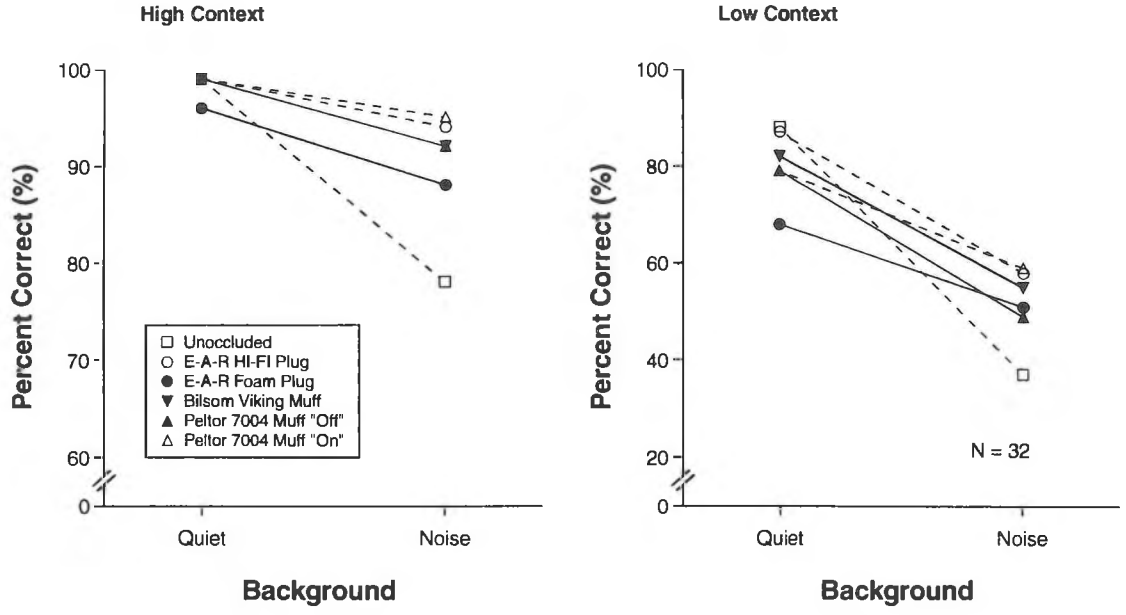

Fig. 1 Word recognition by normal-hearing listeners: Effects of background, hearing protector and context.

DISTORTION-PRODUCT OTOACOUSTIC EMISSIONS: COMPUTER MODELLING AND EXPERIMENTAL DATA

C. Giguère[a,b], H. Kunov[b] and P. Madsen[b]

[a)]Audiology/Speech-Language Pathology Program, University of Ottawa, 545 King Edward, Ottawa, K1N 6N5
[b)]Institute of Biomedical Engineering, University of Toronto, 4 Taddle Creek, Toronto, M5S 1A4

INTRODUCTION

This study concerns the computational modelling of auditory distortion products elicited by two closely-spaced stimulus tones f1 and f2. These distortion products can be perceived subjectively in psychoacoustic experiments as combination tones (CTs) and recorded objectively in the ear canal as distortion-product otoacoustic emissions (DPOAEs). Both phenomena are widely believed to have a common cochlear origin and appear to be closely related to the functioning of the outer hair cells (OHCs) [1].

In a recent article [2], we presented a computational model reproducing the essential properties of auditory distortion products. In particular, the model predicted a significant difference in the growth of the 2f1-f2 and 2f2-f1 DPOAEs with increasing level (L1=L2) of the stimulus tones. The current paper presents further computer simulations, and compares model results to corresponding experimental data. The purpose of this work is to help establish a stronger theoretical base from which to interpret clinical data.

MODEL

The model is described in detail in [2,3]. The input stimulus is equivalent to an acoustic pressure wave incident upon the head. It is processed through a series of cross-coupled concha/ear canal, middle ear and cochlear stages. The latter is a nonlinear 1-D transmission line approximation of basilar membrane (BM) motion, discretized into N=320 channels from base to apex. In each channel, a source $V_n^{ohc}(t)$ produces a nonlinear and saturating pressure, assumed to originate from the OHCs, as follows:

$$V_n^{ohc}(t) = G * (1 + |I_n(t)|/I_o)^{-0.5} * R_n * I_n(t) \qquad (1)$$

where R_n is the passive acoustic resistance of the cochlear partition, $I_n(t)$ is the BM volume velocity, I_o is a scaling constant (equivalent to a BM velocity of 3.6×10^{-3} cm/s), and G is the gain. Functionally, $V_n^{ohc}(t)$ reduces the damping of the BM at low levels and leads to level-dependent BM tuning curves. For G > 1.0, the damping of the BM can become negative (active case). The model is implemented numerically in the time domain and the sampling rate of operation is 71680 Hz. The DPOAE amplitudes are obtained from spectral analyses of the model output at the eardrum position.

Figure 1 shows the growth of the 2f1-f2 and 2f2-f1 DPOAEs in the model for increasing stimulus level (L1=L2) for f1 = 1400 Hz and f2/f1 = 1.20. The 2f1-f2 DPOAE levels increase monotonically with a slope of about 0.7 dB/dB. The levels are typically about 55-75 dB below that of the stimulus components f1 and f2. Increasing the gain G of the OHC pressure source from 0.99 (passive nonlinear case) to 1.01 and 1.02 (active nonlinear case) significantly increases the amplitude of the 2f1-f2 DPOAEs at low stimulus levels. An increase of about 15 dB is seen for L1 = L2 = 20 dB SPL. At higher levels, the saturation function in Equation (1) reduces the effective gain and prevents the BM from becoming active.

In contrast, the 2f2-f1 DPOAE levels are very small at low stimulus levels but they grow with a much steeper slope of about 2.0 dB/dB until they reach the size of the 2f1-f2 levels around L1 = L2 = 80 dB SPL. Increasing the gain G has no observable effect on the 2f2-f1 DPOAEs.

EXPERIMENTAL DATA

The measurements were collected in a quiet laboratory using a prototype distortion-product emission system under development at the Institute of Biomedical Engineering of the University of Toronto. The system consists of a virtual instrument installed on a PC equipped with a dual-channel signal generation and acquisition hardware, and an acoustic probe containing two independent miniature speakers and one miniature microphone. The system employs a special synchronous time-domain signal averaging to reduce the deleterious effect of noise on DPOAE measurements as described in [4]. The levels reported below are the average of three fit/refit of the acoustic probe. The standard deviation of the results is typically 0.5-1.0 dB. The subject (CG) was a 33-year old male with normal audiometric thresholds, tympanograms and acoustic reflexes.

Figure 2a shows the growth of the 2f1-f2 and 2f2-f1 DPOAEs for increasing stimulus level (L1=L2) in the left ear of the subject for f1 = 1378 Hz and f2/f1 = 1.25. The 2f1-f2 DPOAE levels increase monotonically with a slope of about 0.75 dB/dB, and are typically about 55-70 dB below that of the stimulus components f1 and f2. The 2f2-f1 DPOAE levels are much smaller than the 2f1-f2 levels at low stimulus levels. The gap decreases gradually with increasing stimulus level.

Figure 2b presents data for the right ear of the subject for the same stimulus parameters as in Figure 2a. Additionally, Figure 2c presents data for the left ear of the subject but for slightly different stimulus parameters f1 = 1470 Hz and

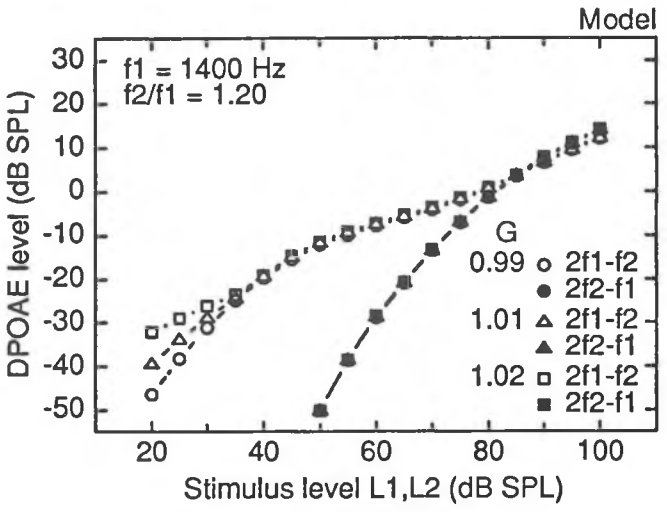

Figure 1: Model results

f2/f1 =1.20. Although the shapes and slopes of the curves in Figures 2a, 2b and 2c differ somewhat from one another, the main effect is that the difference between the 2f1-f2 and 2f2-f1 DPOAE levels decreases with stimulus level and approaches 0 dB around L1 = L2 = 75 dB SPL.

CONCLUSIONS

The model successfully predicts the general pattern of response observed for the 2f1-f2 and 2f2-f1 DPOAE amplitude versus stimulus levels (L1=L2). The best quantitative agreement between model and experimental data is obtained when the gain G of the OHC pressure source is sufficiently high to make the nonlinear cochlear model active. However, a non-active, but nonlinear, cochlear model seems sufficient to account for the experimental data at moderate and high stimulus levels.

REFERENCES

[1] Probst, R., Lonsbury-Martin, B.L., and Martin, G.K. (1991). "A review of otoacoustic emissions," J. Acoust. Soc. Am. 89: 2027-2067.

[2] Giguère, C., Kunov, H., and Smoorenburg, G.F. (1995). "Computational modelling of psychoacoustic combination tones and distortion-product emissions," Proc. of the 15th Int. Cong. on Acoustics, Trondheim (Norway), Vol. III, pp. 237-240.

[3] Giguère, C., and Woodland, P.C. (1994). "A computational model of the auditory periphery for speech and hearing research. I. Ascending path," J. Acoust. Soc. Am. 95: 331-342.

[4] Kulik, R.S., and Kunov, H. (1995). "Results of two types of averaging for distortion-product otoacoustic emission measurements," to appear in Proc. of the 17th Int. Conf. of the IEEE Eng. in Med. and Biol. Soc. & 21st Can. Med. and Biol. Conf., Montréal (Canada).

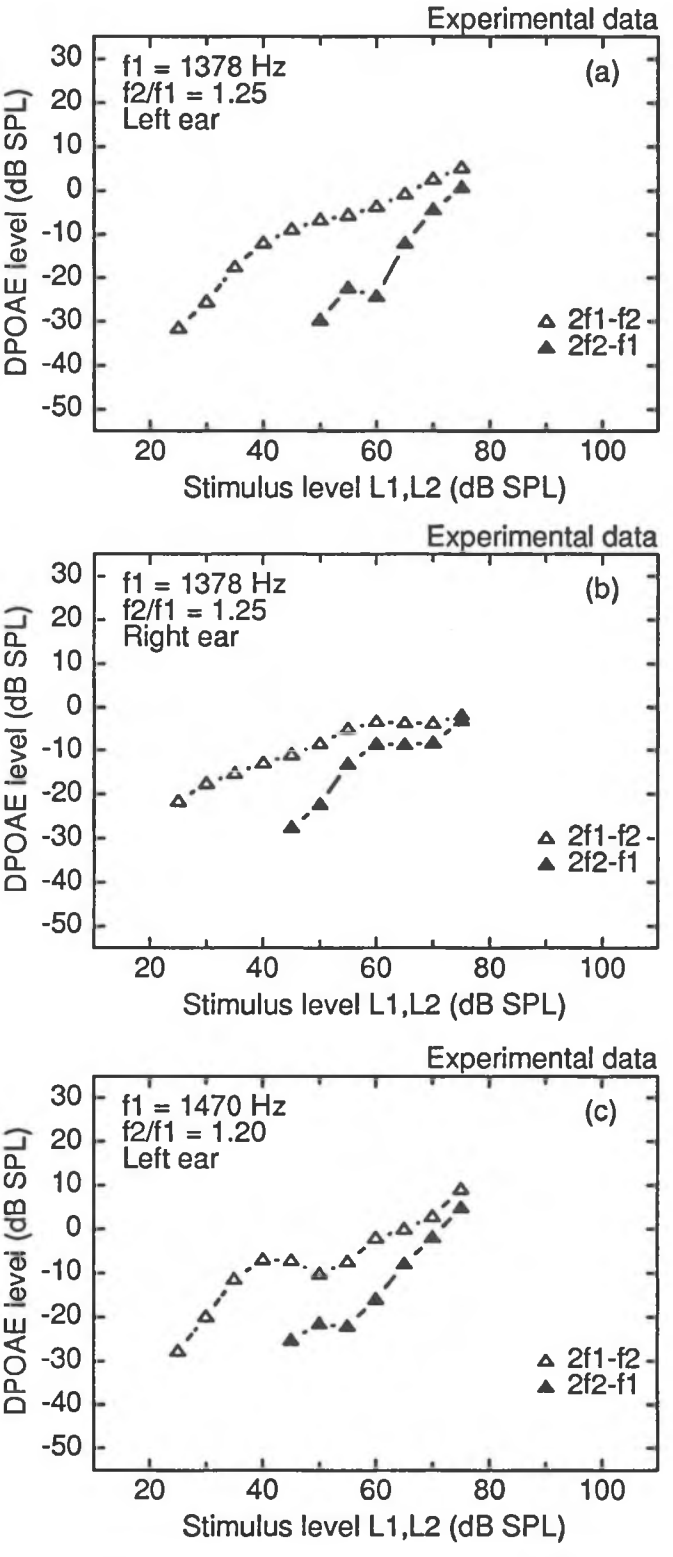

Figure 2: Experimental data for one subject

VACUUM ACTIVATED DAMPING PADS: A NEW, CLEAN AND MORE EFFICIENT TOOL TO CONTROL IMPACT NOISE AT THE SOURCE

Dr. M. Amram, Professor at École Polytechnique de Montréal
P.O.Box 6079, Station Centre-Ville, Montréal, Québec H3C 3A7

1- INTRODUCTION

Impact noise is very frequent in industries where operations are mostly performed on metallic parts. This type of noise is very damaging to the hearing and may permanently destroy the hairlike cells in the cochlea, leading to a permanent hearing loss. Over a long period of time, various solutions have been looked into in order to control this particular type of noise with very few success (discovery of non-ringing metallic materials such as incramute, which is good but expensive, vibrations damping by friction with the use of heavy metallic chains, and more commonly the use of damping pads, with or without a constrained layer, applied by gluing, bolting, soldering..., and dissipating vibrations, thus noise, by heat with extensional or shear mechanisms). Furthermore, most of those solutions were cumbersome or presented risks to spoil the structure on which they were applied, and they were discarded by the operators because they introduced delays in their production schedule. An original tool has been developed and patented at Bombardier/Canadair as a remedy to these noise problems in the aeronautic processes. It consists in vacuum applicated damping pads with a metal plate constrained viscoelastic layer. The originality of this device is the method of application giving rise to an important vibrations dissipation mechanism based on microslip at the friction interface and also the nature of the polyurethane used as the viscoelastic material. This device remains in place as long as the riveting operation (or other impacting operations) takes place. Further research has been sponsored at École Polytechnique de Montréal by the I.R.S.S.T. to optimise those "Vac Damp" devices and investigate their performances in other industries (trains, busses, boats, heat exchangers). Benches have been mounted with real parts of some of those structures in parallel with a more classical and well studied experiment, a simply supported thin metal plate to optimise this new impact noise control device on well controlled experiments. Part of the shear mechanism associated to well glued damping pads with constrained viscoelastic layer has been advantageously replaced (about 3 dBA better) by a partial slip (microslip) mechanism at the friction interface when applying the Vac Damps on each side of the impacted area. Furthermore, two important parameters in the radiated impact noise control (ringing noise as well as acceleration noise) seemed to be the fraction of the impacted structure covered and the thickness of the viscoelastic material selected, which can also compensate partially for a smaller fraction covered.

2- DESCRIPTION OF THE "VAC DAMP"AND OF THE SET UP FOR MEASUREMENTS AND OPTIMISATION

2.1 Vac Damp: Description and Advantages

The damper is constituted of a constraining plate (about 1/16" thick) made of very hard and rigid aluminum composite (type 75 T 6) on which a shock-resistant polyurethane called RhinoHyde (1/8" to 1/4" thick), and presenting good internal damping properties, has been bonded. The contour of the rectangular constraining plate (with rounded corners) was covered with a rubber gasket specially designed for best sealing but also for covering the sharp edges of the constraining plate in order to protect very expensive airplane structures. A hole has been drilled in the middle of the damping pad to enable the installation of the vacuum line and to exert with a vacuum pump a partial vacuum of about 28" of mercury (13.75 PSI) in the thin air volume between the Vac Damp and the impacted part. The device is reusable and applied temporarily during riveting without deforming the structure at all because the forces exerted by the atmospheric pressure are well balanced and, furthermore, those pads resist very well to the rough handling at the workplace.

2.2 Experimental Set Up Description

The mechanism of sound radiation associated to a random, repeated impact process is very dependent on the geometry, weight, rigidity and dimensions of the colliding object and of the receiving structure. We have, for the optimisation of the "Vac Damp", installed a very well documented (2) set up consisting of a small metal sphere colliding with a simply supported thin plate. The noise radiated is related to rapid surface deformation (acceleration noise), then with the ringing of the plate (reverberation or ringing noise). A pseudo-steady state process takes place with regularly spaced in time impacts (or triggering on those impacts) to obtain a statistically good average of impact noise measurement (about 30 consecutive blows are necessary to have a good standard deviation on the noise measurement average). The two parts of the impact noise (acceleration and ringing noises) have been separated by two methods in order to evaluate and compare their control successively with glued viscoelastic pads with an aluminum constraining layer, and the same simply applied by vacuum effect. The first one is a mechanical separation obtained by using a partial enclosure shaped like a quarter cylinder with acoustically absorbing foam inside in order to leave the impacting pendulum free and to measure only the ringing noise, the impact noise (mostly above 2 kHz) being stopped by this partial enclosure. The second one is an electronic separation in the time domain with a well adjusted rectangular window to separate in time the first peak associated to the acceleration noise from the rest related to the ringing noise. The two methods give very comparable results and validate each other. Measurements were taken for various partial coverages of the plate with three types of double damping pads (small, average and large) covering respectively 10 %, 16 % and 80 % of the free-base plate.

3- MECHANISM OF VIBRATIONS DISSIPATION

The response of the impacted plate will be monitored on the axis of the impacts independently of the fact that the sound radiated from the impact-excited plate may have directivity patterns with frequency dependance as shown in reference (2). This spot seems to be the most exposed to the combination of impact-radiated noise associated both to acceleration noise (maximum on axis of the impacts) and to the ringing noise, and this choice is related to the fact that the operators are situated in front of

the impacted area. The mathematical microslip model is presented in reference 3 for an elastic bar with an elastoplastic shear layer. In this model, it is assumed that the friction force is transmitted across an interface rather than through a point of contact (6) and that a distributed version of the Coulomb's law of friction determines which part of the contact surface slips.

Figure 15 of this same reference shows that for high relative normal loads and more rigid shear layer, yielding develops gradually giving rise to microslip of the joint. For a given load of the order of the atmospheric pressure, the presence of microslip diminishes significantly the peak responses of the atmospheric pressure. Experimental data, taken on the plate with two Vac Damps, also show that the trend is to increase the damping by microslip friction (replacing shear dissipation) with the increase of the rigidity of the viscoelastic layer (RhinoHyde instead of Dyad).

4- ANALYSIS OF THE RESULTS

Preliminary experiments, while riveting on real parts of a plane and of a bus (part of a fuselage and rear part of a bus), have shown that a hard polyurethane called RhinoHyde used as damping material on the Vac Damp gives its best performance to this device (up to 3 dBA better than other materials), and that, for large deformations associated to riveting. As described earlier, we have been using a simply supported thin plate excited by a metal ball suspended to a pendulum (small deformations) for a systematic optimisation of this device..

From the point of view of noise control, the total radiated energy is important. However, we need to separate in time the acceleration noise from the ringing noise in order to study the Vac Damp's performance on each component of the overall impact noise.

Thus, we have been measuring the radiated noise levels corresponding to the acceleration noise and to the ringing noise as a function of the type of material (the RhinoHyde is the hard one and the Dyad is the soft one), their thickness and the fraction of the plate covered by both Vac Damps successively with pads applied by the vacuum action, then by pads simply glued onto the base plate. The results of those experiments are presented on figure 1. It is shown for the ringing noise part of the impact noise that the RhinoHyde is the best viscoelastic material when 1/4" thick, mostly between 16 % and 80 % coverage of the base plate. We reach almost the same conclusion for the acceleration noise control, except that this material acts better with a thinner layer (1/8" instead of 1/4") for a larger surface covered (80 %). However, for the overall impact noise, the optimum attenuation for both components (acceleration and ringing) is obtained for the RhinoHyde 1/4" thick covering 80 % of the impacted base plate. By observation of this graph, it seems that the surface covered can be reduced if the thickness of the RhinoHyde is increased.

Finally, we did the same measurements in the same conditions for the total impact-radiated noise. The same trend occurs concerning the thickness of the rigid polyurethane versus its fraction of surface covered.

CONCLUSION

A new type of damping pad with constraining plate has been developed to control better the noise radiated by an impacted structure through the control at the source of the flexural vibrations. Its main feature consists in the fact that it is applied by vacuum action, but also that the viscoelastic material is a stiff layer of a polyurethane called RhinoHyde where the yielding develops gradually (under the shear forces provoked by the flexural vibrations associated to periodic impacts), giving rise to microslip of the joint. It has been shown that this type of dissipation process is more efficient (from one to five dBA depending on the surface covered and of the thickness of the RhinoHyde) than the one associated to shear effect only, when the damping pads are well glued to the impacted plate. The Vac Damps control the acceleration noise as well as the ringing noise parts of the impact noise mainly when they cover a large fraction of the impacted structure (about 80 %) and when their viscoeloastic layer is made of 1/4" thick RhinoHyde. These findings have been implemented with success on real structures such as bus panels, heat exchanger ducts and airplane fuselage parts, providing attenuations of the riveting, hammering and grinding noises of between 4 dBA and 12 dBA at the operator's ears.

REFERENCES

1. E.J. Richards, M.E. Westcott, R.K. Jeyapalan, "On the Prediction of Impact Noise II: Ringing Noise", J. Sound and Vibration, 65, 419-451 (1979).
2. D. Takahashi, "Frequency Analysis of Sound Radiation from Impact Excited Plate", JASA 91 (5), May 1992, p. 2708.
3. C.H. Menq, J.H. Griffin and J. Bielak, "The Influence of Microslip on Vibratory Response, Part 1: A New Microslip Model". Journal of Sound and Vibration (1986) 107 (2), pp. 279-293.
4. C.H. Menq, J.H. Griffin and J. Bielak, "The Influence of Microslip on Vibratory Response, Part II: A Comparison with Experimental Results". Journal of Sound and Vibration (1986) 107 (2), p. 295-307.

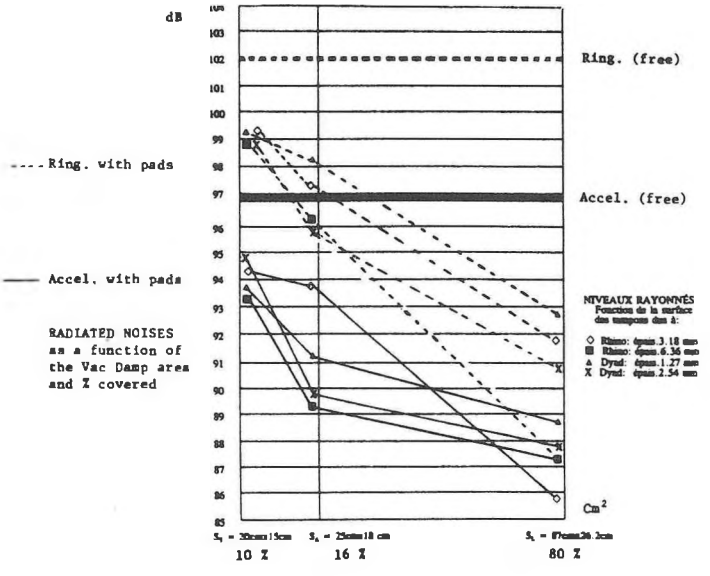

Recent Developments on the Optimization of Viscoelastic Coating

L. Cheng
Department of Mechanical Engineering, Université Laval, Québec, Canada G1K 7P4

Viscoelastic coating is widely used to attenuate both vibrations and acoustic radiation of vibrating structures. A non-exhausting number of papers have been published in the past to show the general performance of the technique. However, the effort made by manufacturers to build lighter and more powerful forces people to use the technique in an optimal manner. In fact, in many fields such as aerospace and aeronautics, the addition of extra weight due to the application of viscoelastic layers plays a critical role since it always drives to additional energy costs. Furthermore, the structures in these fields being frequently subject to a wide range of temperature and frequency variations, the optimization procedure should take these effects into account. In other more conventional industry applications, although the added weight is not necessarily a problem of primary concern, an overall layer setup may lead to the overheating of the machinery. This paper aims to illustrate such an issue using a simple vibrating structure.

The structure that is studied in the present paper is a rectangular thin plate covered symmetrically on both sides by rectangular sections of viscoelastic material (see Fig.1). For simplicity, The boundary conditions of the plate are supposed to be simply-supported along the edges. The Love-Kirchoff theory for thin plates under small displacements is used and its displacement along the z-axis is approximated according to the Rayleigh-Ritz method by a polynomial expansion over the x and y-axis. For sinusoidal excitations applied perpendicularly to the plate's surface, this formulation leads to a classic system of second-order linear differential equations. The response of the system as well as the damping factor of each mode can be easily solved by standard numerical methods.

Considerable research is being done in the area of analytical modeling on the stiffness and damping properties of viscoelasic materials. Several curve-fitting formulas derived directly from experiments made on commonly used viscoelastic sheets are available. These formulas give the storage modulus and the loss factor of the material as a function of temperature and frequency. In this work, the formulas for the viscoelastic layer of Soundcoat-D have been taken.

Depending on the thickness and the configuration of the viscoelastic material coverage, both the modal damping factors of the system and its response to external forces over a given frequency range will be optimized. To define the coverage configuration, the plate is first divided into a certain number of small sections and the components of a configuration vector $c(i,j)$ are assigned a value of 1 or 0, depending whether the corresponding section (i,j) is covered or not.

An optimization algorithm is applied to the system (see Fig. 2). The particularity of the problem is to avoid overlapping of the layers. Consequently, we have the layers' location as an optimization variable that is not a continuous quantity. To this end, a simple trivial routine is developed, which proceeds with a given percentage of the plate to cover and a fixed thickness of viscoelastic material. Two objective functions can be analyzed. The first one is the damping factor of a particular mode and the second one is the response of the system over a given frequency range. The algorithm starts off with a randomly chosen initial configuration and calculates the objective function. Then it makes a slight change in the configuration and compares the objective function obtained by this coverage with the previous one. If the result is better, the new configuration is kept. Otherwise, another change is made starting from the previous configuration. This routine is repeated until an optimum is reached. Note that a verification of the convergence of the solution has been made during its calculation to make sure that a global optimal solution was obtained.

A simply supported 30 cm by 45 cm by 3,175 mm aluminum plate is taken for the analysis. The response of the plate alone and the response of the plate entirely covered on both sides by a 1,5875 mm sheet of Soundcoat-D are presented in Fig.3. The response is in fact the mean quadratic velocity of the plate. Note the reduction of the vibration level and the shift of the resonance peaks to the left due to the effect of the added mass and stiffness to the system. This result is given for a room temperature. The so-called **gain** is defined as follows:

$$Gain = \frac{Undamped\ Area - Damped\ Area}{Undamped\ Area} \times 100\%$$

where the area is the area under the curve of mean quadratic velocity of the corresponding system (damped or undamped).

The optimization routine has been applied on the minimization of the mean quadratic velocity of the plate for forced vibration problems. A typical result is presented on Table 1. A force of 1 N was applied at x=0 cm and y=8,7 cm. Table 1 shows the results for three different frequency bands. For each frequency band of interest, the last column of the table gives the optimal configuration. Again the 1/4 coverage shows

itself more effective than the full coverage. The optimization process enhances even more the damping performance, reaching a damping increase varying from 78.0% to 88.3% compared to the bare plate, which is approximately twice the performance of the full coverage and about 50% higher than the non-optimized ones. It is interesting to note that, depending on the dominating mode involved for each frequency band and on the location of the exciting force, the obtained optimal arrangement is a combination of the ones previously obtained for each single mode.

To better illustrate the additional weight to the structure, the gain is expressed as a function of the percentage of weight added for the frequency range of 50 -300 Hz in Fig.4. The weight of the plate alone is used as the reference. Note that the maximal thickness of the coverage is limited to 3,175 mm (the thickness of the plate) since our model was made with the assumption of thin structures. Therefore, the results obtained in this range of thickness can be considered very accurate. For the same amount of viscoelastic material, the quarter coverage with optimal shape reaches a reduction of 78 % while the full coverage gives only a reduction of 42 %. To get the same reduction level, the full coverage requires an additional weight of 45 %, compared to 18 % for the quarter coverage. The half coverage gives an intermediate performance between the full coverage and the quarter coverage.

The aforementioned results related only to a certain number of selected configurations. As illustrated, the applied viscoelastic layers mainly bring three effects to the system (mass, stiffness and damping) to form a complex coupled system with the plate, so that an optimal result is a compromise based on these factors. Moreover, the details of the mechanical properties and applied excitations can also affect the optimization results. Generally speaking, modal damping optimization results seem to confirm the commonly used rule of applying the layers at the anti-nodal portion of the structure with optimally shaped arrangement. However, for the forced response, in addition to the variation of mechanical properties of the viscoelastic materials due to the temperature variation, the excitation position and the boundary conditions of the structures are the main factors affecting the energy partition over the structure. Consequently the optimization result on the response depends on a good knowledge of these factors. The methodology developed in this paper permits a systematic handling of the problem with all these factors taken into account. It should be pointed out that the formulation developed in the present work can be easily extended to treat more realistic structures in practical applications. A combination of the optimization procedure and the finite element method seems to be a reasonable way to tackle more complex systems.

Acknowledgment: The author wishes to thank Robby Lapointe for his contributions.

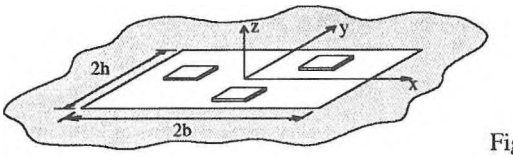

Fig.1

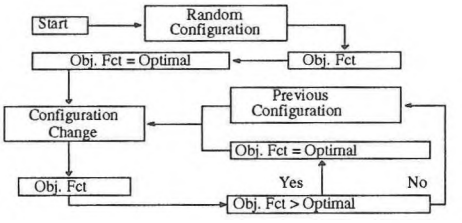

Fig.2

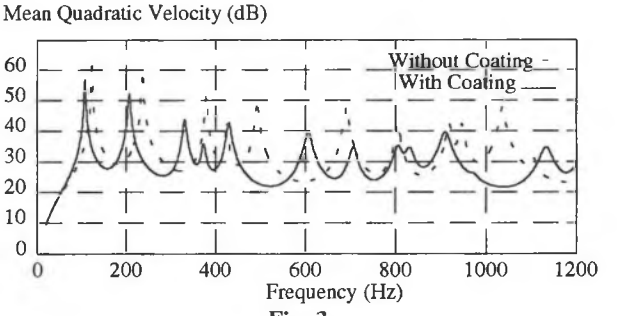

Fig. 3

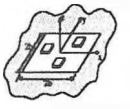	**Gain** (Bare Plate as Reference)		
Frequency Band	Full Coverage	1/4 Coverage	Optimized 1/4 Coverage
50 - 300 (Hz)	42,8 %	59,7 %	78,0 %
300 - 550 (Hz)	44,0 %	49,4 %	88,3 %
550 - 800 (Hz)	31.3 %	55,6 %	86,9 %

Table.1

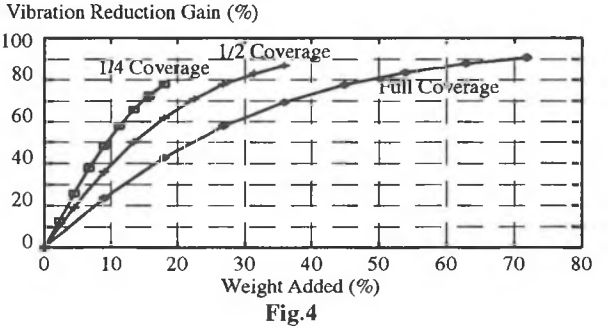

Fig.4

A Model on Self-Damping of Stranded Cables in Random Transverse Vibrations

A. Leblond[1], L. Cloutier[1], C. Hardy[2] and L. Cheng[1]
[1]Département de Génie Mécanique, Université Laval, Ste-Foy, Québec, G1K 7P4.
[2]Institut de Recherche d'Hydro-Québec, Varennes, Québec, J3X 1S1.

1. Introduction

Predicting the across-wind response of overhead conductors to alternating forces caused by vortex shedding mechanism (aeolian vibrations) requires knowledge of conductor self-damping characteristics. Conductor self-damping represents the capacity of the conductor to dissipate energy internally during motion. Energy dissipation is mainly related to frictional damping due to small relative movements between adjacent wires.

Methods of measurement of conductor self-damping have been described in a IEEE Guide [1]. Conductor self-damping is usually determined by means of a laboratory test span by measuring the energy dissipated by the conductor vibrating in a principal mode. However, such event involving a pure sinusoidal vibration is rarely observed on a test span excited by natural wind action [2]. Most recordings indicate a combination of two or more frequencies.

Conductor self-damping is a non-linear phenomenon since loss factor depends on the conductor vibration amplitude. Consequently, the energy dissipated is not so readily determined as the superposition principle cannot be used when several modes are excited in the conductor. This paper presents a model to evaluate the energy dissipated by the conductor undergoing sinusoidal as well as multi-modal vibrations.

2. Theoretical approach

The variation of conductor curvature plays a dominant role in the dissipation mechanism. It is proposed here to develop a model based on the conductor curvature and its time-wise variations.

Usually, the mean power dissipated by the conductor undergoing sinusoidal vibrations is expressed as a function of antinodal amplitude, frequency and mechanical tension, but not directly in terms of curvature. The present model assumes that the instantaneous power dP dissipated by any infinitesimal element dx of the conductor is related to its curvature $y''(x,t)$, the time rate of change of curvature $\dot{y}''(x,t)$ and the static longitudinal stress σ_{al} in the outer layer of the conductor according to the following equation:

$$dP = C\,|y''(x,t)|^{\alpha}\,|\dot{y}''(x,t)|^{\beta}\,\sigma_{al}^{\gamma}\,dx \qquad (1)$$

where C is a proportionality factor. Quantities α, β and γ are exponents to be determined experimentally. Absolute values of $y''(x,t)$ and $\dot{y}''(x,t)$ are used to make sure the instantaneous power dP is always positive. For sinusoidal vibrations, the energy dW dissipated per cycle in the element dx is given by:

$$dW = \int_0^T dP \qquad (2)$$

where T is the period of vibrations. Hence, the total energy W dissipated per cycle in a span of length L (neglecting end effects) is:

$$W = \int_0^L dW \qquad (3)$$

Introducing equations (1) and (2) in (3), one finds:

$$W = C\,\sigma_{al}^{\gamma} \int_0^L \int_0^T |y''(x,t)|^{\alpha}\,|\dot{y}''(x,t)|^{\beta}\,dt\,dx \qquad (4)$$

Equation (4) has been calibrated to the similarity laws of Noiseux [3] recently modified by Hardy and Leblond [4] to be applicable to sinusoidal vibrations of multi-layer electrical stranded conductors. On this basis, equation (1) can be expressed as:

$$dP = K\frac{EI}{\rho_{al}^{2.44}}\,|y''(x,t)|^{1.69}\,|\dot{y}''(x,t)|^{0.75}\,\sigma_{al}^{-0.32}\,dx \qquad (5)$$

where K is a proportionality factor, EI is flexural rigidity of the cable $\left(\cong EI_{max}/2\right)$ in Nm^2, ρ_{al} is aluminum density in kg/m^3, σ_{al} is expressed in Pa and, $y''(x,t)$ and $\dot{y}''(x,t)$ are expressed in m^{-1} and $m^{-1}s^{-1}$ respectively.

Figure 1 shows instantaneous power dP as a function of spatial coordinate x and time t for sinusoidal vibration of a half-wavelength of the conductor. Positions $x = 0$ and $x = \lambda/2$ correspond to nodes of vibration. Times $t = 0$ and $t = T/4$ correspond to zero and maximum displacements of the conductor respectively. One can see that dP is maximum at $x = \lambda/4$ which is the position of the antinode, somewhere between $t = 0$ and $t = T/4$. The value of t corresponding to this maximum is solution of the following equation:

$$\cos^2\left(\frac{2\pi t}{T}\right) = \frac{0.75}{1.69}\sin^2\left(\frac{2\pi t}{T}\right) \qquad (6)$$

which leads to $t = 0.156\,T$. The total volume included between surface dP and the x-t plane represents the energy dissipated in a half-wavelength of the conductor in a quarter cycle of vibration, as stated by the double integration in equation (4). At time t, the instantaneous power dP is zero at a vibration node. It is also zero at $t = 0$, corresponding to zero curvature of the conductor and at

$t = T/4$, which corresponds to zero time rate of change of conductor curvature.

Finally, if the displacement $y(x,t)$ of the conductor is known (one or more frequencies), it is possible to calculate the total energy W dissipated in the span between times 0 and t:

$$W = K \frac{EI}{\rho_{al}^{2.44}} \sigma_{al}^{-0.32} \int_0^L \int_0^t \left|y''(x,t)\right|^{1.69} \left|\dot{y}''(x,t)\right|^{0.75} dt\, dx \qquad (7)$$

3. Results

The integration time t in equation (7) is taken as the elapsed time for a traveling wave to move from one end of the span to the other, where it is reflected, and to return to the same point. Under this consideration, the relative phases between each vibrational mode excited in the conductor has negligible effect on the integral result. Integral in equation (7) is solved numerically using Monte Carlo method [5]. Had the self-damping phenomenon been linear, the total energy dissipated during the conductor motion would be the sum of the separate energies dissipated by each of the modes present. In this fictitious case, it has been verified that the results of the present model calibrated on this basis would be the same as those obtained through application of the superposition principle.

4. Conclusion

The present model permits the evaluation of the energy dissipated by the conductor undergoing general transverse vibrations. This model could be integrated in any computer program performing aeolian vibration calculations.

5. Acknowledgments

The authors gratefully acknowledge Dr. Denis Noiseux for many helpful discussions. This work has been supported by Hydro-Québec.

6. References

[1] "IEEE Guide on Conductor Self-Damping Measurements", IEEE Standard 563-1978.

[2] Transmission Line Reference Book, "Wind-Induced Conductor Motion", Electric Power Research Institute, Palo Alto, CA, 1980, Section 1.4.

[3] Noiseux, D.U., "Similarity Laws of the Internal Damping of Stranded Cables in Transverse Vibrations", Proc. of the 1991 IEEE PES, Trans. & Distr. Conf., Dallas, September 1991.

[4] Hardy, C., Leblond, A., Goudreau, S., Cloutier, L.J., "Review of Models on Self-Damping of Stranded Cables in Transverse Vibrations", To be presented to the International Symposium on Cable Dynamics, Liège (Belgium), 19-20 Oct. 1995.

[5] Press, W.H., Teukolsky, S.A., Vetterling, W.T., Flannery, B.P., "Numerical Recipes in Fortran: The Art of Scientific Computing", Second Edition, Cambridge University Press, 1992.

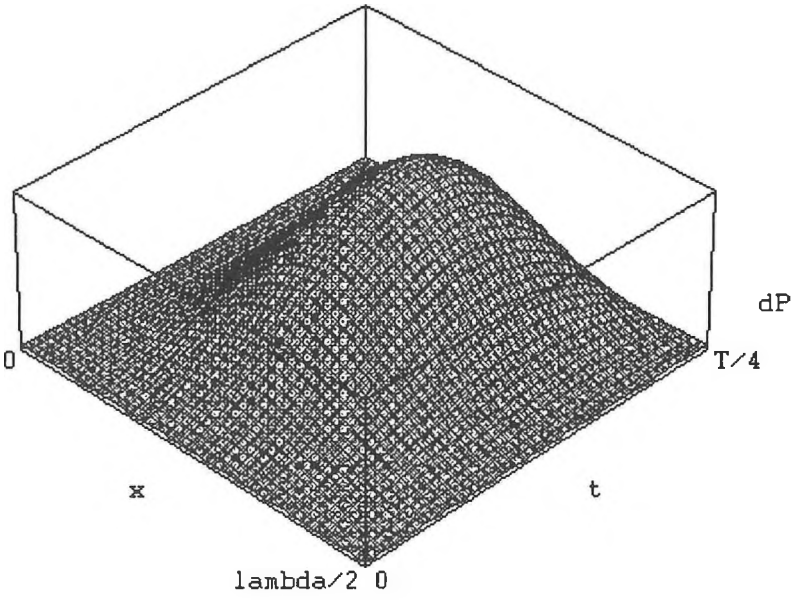

Figure 1: Instantaneous power dP dissipated in a half-wavelength of the conductor as a function of coordinate x and time t.

A simplified model for predicting vibrations of airplane fuselage

J. Missaoui and L. Cheng
Department of Mechanical Engineering
Laval University Quebec, Canada, G1K 7P4

1. Introduction

Several previous investigations were performed to study and to understand the airplane cabin's structural and acoustical responses. The aircraft fuselage was mostly modelled as a cylindrical shell with and without stringers. In the real case, the cylindrical model does not always warranty a good prediction of the vibration level other than permitting a general understanding of mechanism of noise transmission. The addition of a floor to the cylindrical shell seems to be more realistic. In ref. [1], the free vibration of a cylindrical shell with a floor partition has been studied by including the effect of several parameters. More recently, in ref. [2], he natural frequencies of a simply supported stiffened cylindrical with a floor partition have been calculated. In this work, fuselage is treated as a cylindrical shell coupled to a floor. A general formulation is presented to study the structural influence of the cabin floor on the modal characteristics and the vibration level.

2. Analytical approach

The analytical formulation is based on the application of Hamilton's principle where the energies of the whole system shown in Figure 1 is minimized. The structural coupling between the floor and the cylindrical structure is investigated by introducing a set of uniform distributed artificial springs as dynamic element [3]. The coupled modal equations of motion are developped [4] using a physical modal basis with a *shear diaphragm* condition. The in-plane motion and the transversal bending of the floor are included to the model. Furthermore, the external dynamic loadings are considered to be a punctual forces directly applied on the external surface of the shell. Finally, an average quadratic radial velocity is used to characterize the vibration level of the coupled system.

3. Numerical results

The developed model is validated with available results in the literature. Moreover, a Finite Element Analysis using a commercial code is also performed. The agreement is good except for the fundamental mode reported in ref. [1] where the error increased with increasing the floor angle. The mode shapes are also examined and analysed showing three controlled regions in the modal behavior of the coupled structure. In Figure 2, a physical observation of the mode shapes shows that the lowest frequency corresponds to a mode which is basically dominated by a floor motion. The second mode is a strongly coupled one in which the the substructures vibrate with a comparable level. The third mode is a shell-controlled mode , in which one notice a slight deformation of the floor and a strong motion of the shell.
The effect of the in-plane motion of the floor on the combined system is also discussed. The analysis shows that at low frequency region, the in-plane motion has no effect on symmetric modes but a visible effect is observed for the antisymmetric modes. So, at least rigid motion of the floor in the horizontal direction must be considered in the simulation at this region. It is also pointed out that the longitudinal motion has no visible effect on the modal behavior of the combined system.
This section study the structural response under a point excitation, the procedure consists on comparing first the vibration levels of the shell with and without the floor, and second, the floor behavior compared to the shell when the system is structurally coupled. The vibration level is calculated by considering the radial quadratic velocity. It can be seen from figure 3 that the inclusion of the floor into the model does not basically change the general trend of the overall vibration level of shell. A detailed examination of the two curves shows that the floor has a visible effect on the shell response. More specifically, due to the coupling introduced by the floor, resonance peaks are shifted. Moreover, additional resonances dominated by the floor motion can be clearly identified. Figure 4 illustrates the vibration levels for both substructures. It can be seen that at low and mid-

dle frequency regions, a strong coupling between the shell and the floor exists. But at a high frequency region, the shell which is directly excited is more active than the floor. Combining the two figures, one can notice that from the dynamic analysis point of view, the single shell model seems to be sufficient to estimate the global vibration of an airplane fuselage. This justifies the common use of a single shell model in numerous papers. From the noise prediction point of view, due to the strong structural coupling at low and middle frequency regions, the floor could be considered as a sound radiator in noise prediction.

4. Conclusion

The fundamental structural influence of the cabin floor has been discussed using analytical approach. The structural coupling was found to be strong at low and frequency regions. However, from acoustical view point, the floor may change significantly the internal pressure level.

References

[1] M.R. Peterson and D.E. Boyd 1978 *JSV* **60**, 45–62. Free vibrations of circular cylinders with longitudinal, interior partitions.

[2] R.S. Langley 1992 *JSV* **156**(3), 521–540. A dynamic stiffness technique for the vibration analysis of stiffened shell structures.

[3] L. Cheng and J. Nicolas 1992 *JSV* **155**(2), 231–247. Free vibration analysis of a cylindrical shell-circular plate system with general coupling and various boundary conditions.

[4] J. Missaoui, L. Cheng and M. J. Richard: Free and forced vibration of a cylindrical shell with a floor partition. To appear in *JSV*.

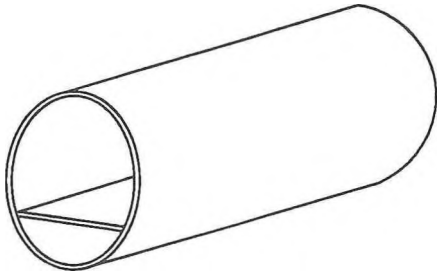

Figure 1: Cylindrical shell with a floor partition

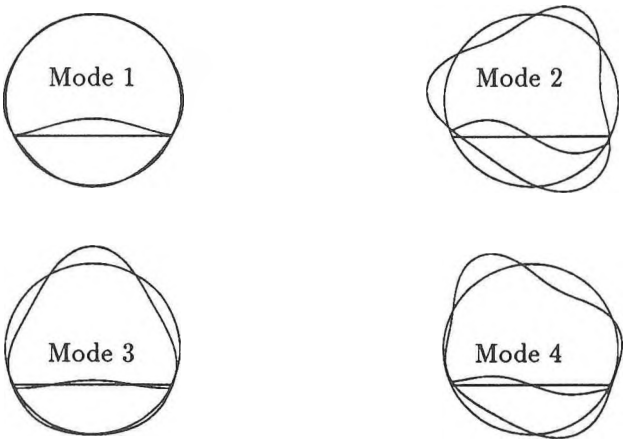

Figure 2: Mode shapes of the partitioned structure

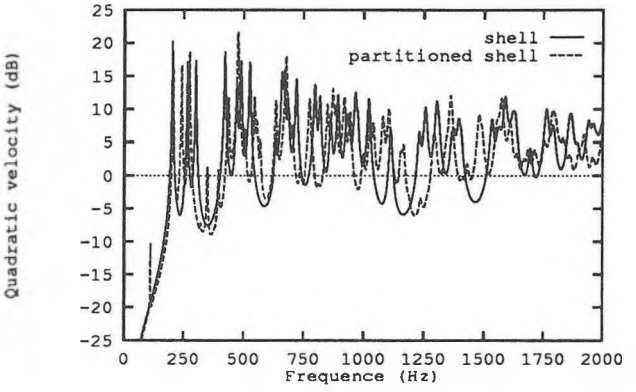

Figure 3: Vibration level of the cylindrical structure

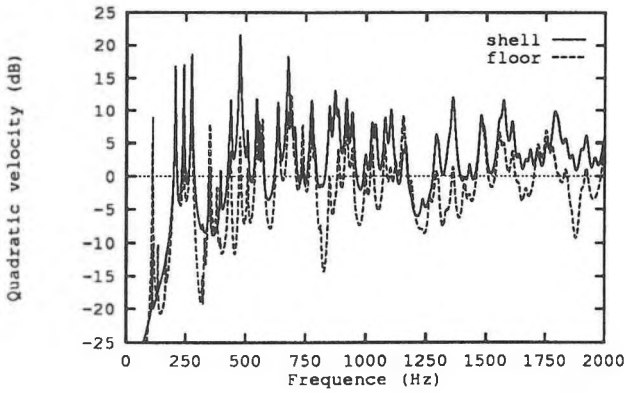

Figure 4: Vibration level of the combined structure

A Hybrid Approach for Vibrational Analysis of Coupled Structures

M. Hatam, L. Cheng, D. Rancourt

Department of Mechanical Engineering, Laval University, Quebec, Canada G1K 7P4

1) Introduction

Mechanical coupling of structures along continuous boundaries induces serious difficulties for vibrational analysis. Analytical, numerical or experimental methods alone are not efficient enough to tackle the problem.

There are a vast amount of methods that use theoretical or experimental methods to predict the vibrational behavior of coupled systems. Statistical methods (e.g. SEA) are often used to calculate power flows between coupled structural elements and the vibration levels of each element of the system when the modal density is high [1]. Deterministic theoretical solutions have also been presented for different combinations of academic structures such as beams, plates and shells. The majority of these methods are based on a substructure synthesis approach which divide the whole structure into different substructures and try to obtain a general solution of the whole structure using solutions of all substructures [2]. The classical modal analysis CMA [3] and mobility power flow [4] are other proposed methods in the literature. CMA is based on the modal analysis of the global structure and no assumption is made about either the nature of the coupling or the excitation type. The main objective of the mobility power flow method is to develop the appropriate expressions for the vibrational power flow through coupled substructures by means of structural mobility functions. Finite element method is a general method which can be used for all types of complex structures. The method is however too expensive when applied to three dimensional problems and/or high frequency domains.

This paper presents a hybrid method that combines analytical, numerical and experimental methods to derive the dynamic response of a complex structure. A complex coupled structure is divided into two categories: a master structure and auxiliary substructures. In general, one is interested in the behavior of the master structure while the influence of each auxiliary structure is introduced by the compliance functions at the junction. This approach allows one to change the characteristics of one or more elements of the system or to add or eliminate elements, without discarding measurements or calculations which have been done for other elements of the system.

2) Line coupling

In a general three dimensional problem, after dividing the whole structure into main and auxiliary structures, there exist six components of load for each contact point. The substructure compliance matrix at contact point defines the relations between each component of the deformation vector to each component of the load vector. The problem is more complicated in the case of a line or surface contact between two or more structures. As shown in figure 1, a linear junction can however be presented as a combination of separate coupling points. Therefore each component of the substructure compliance matrix is a square matrix with dimension N_p, and each component of the load or deformation vector is a vector of dimension N_p, where N_p is the number of contact points.

$$\begin{Bmatrix} D_j^1 \\ D_j^2 \\ .. \\ .. \\ D_j^N \end{Bmatrix} = \begin{bmatrix} \beta_{11}^{ij} & \beta_{21}^{ij} & .. & .. & \beta_{N1}^{ij} \\ \beta_{12}^{ij} & \beta_{22}^{ij} & .. & .. & \beta_{N2}^{ij} \\ .. & .. & .. & .. & .. \\ .. & .. & .. & .. & .. \\ \beta_{1N}^{ij} & \beta_{2N}^{ij} & .. & .. & \beta_{NN}^{ij} \end{bmatrix} \begin{Bmatrix} F_i^1 \\ F_i^2 \\ .. \\ .. \\ F_i^N \end{Bmatrix} \tag{1}$$

where $i, j = 1, N_p$ and N=6 for a general three dimensional problem. The compliance matrix β can be defined as:

$$\beta_{ij}^{km} = \frac{D_j^m}{F_i^k} \qquad , \qquad [\eta] = [\beta]^{-1} \tag{2}$$

where F_i^k is the excitation at point "i" in the direction of "k" and D_j^m is the measured deformation at point "j" in the direction "m".

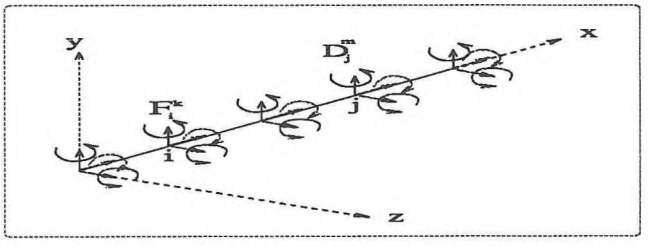

Figure 1: Distribution of forces and moments due to coupling along a common edge.

In reality, there are many problems that can be treated more easily. As an example, let's analyze the force vibration of an L-shape plate with simply supported edges. After dividing the L-shape plate into main and auxiliary structures, one is able to study the auxiliary structure by applying a distributed moment M_x at its junction. It is the only coupling load because of the pinned joint between two plates that avoids the in-plane wave transmission. By applying a moment M_x at point "i" and measuring or calculating the rotations θ_x of all points along the junction, one can write $\beta_{ij}^{R_x} = \theta_j / M_i$. Hence

$$\theta_j = \sum_i \beta_{ij}^{R_x} M_i \qquad\qquad M_j = \sum_i \eta_{ij}^{R_x} \theta_i \tag{3}$$

A variational formulation of a rectangular thin plate using Rayleigh-Ritz approach has been performed to study the main structure. A polynomial decomposition for lateral displacement of the plate is considered and artificial springs connected at the edges allow one to define different types of boundary conditions. The potential and kinetic energies as well as the potential energy due to boundaries are derived and the energy terms due to work done by external forces and

moments are included. The only new term to be considered, is the effect of the auxiliary structure. This energy term can be defined as

$$E_{cp} = \int_{-b}^{b} M_x \theta_x dx \tag{4}$$

where

$$\theta_x = \frac{\partial W}{\partial y} \quad and \quad W = \sum_{i,j} a_{ij} \left(\frac{x}{b}\right)^i \left(\frac{y}{h}\right)^j \tag{5}$$

with "b" is half the width of the plate along the x axis, and "h" is half the length along the y axis. The line of junction is x=[-b,b]. Replacing the moment distribution by rotational deformations in equation 4 and using the second equation in 3 , E_{cp} is easily obtained. Experimentally , it is easier to measure the β matrix and E_{cp} can be derived by inverting β. This however leads to two problems: Firstly, by increasing the number of contact points, β matrix approaches singularity; secondly, the nature of the η matrix is such that the regression analysis is not permitted. It is simply due to the fact that the value of the compliance at a single point will change with the number of contact points chosen. Figure 2 shows the variations of the central line of β and η matrices. For the β matrix, it means that the rotational moment is applied at point x=0 and the responses are measured at different contact points along the junction. The dashed and solid lines are used for 5 and 9 contact points respectively. It is clear that by increasing the number of contact points, the inversion process complexifies and the regression analysis on η matrix leads to incorrect estimation of η at other points. To avoid β matrix inversion, a polynomial decomposition is considered for the moment distribution along the junction:

$$M_x(x, y_0) = \sum_i \sum_j b_{ij} \left(\frac{x}{b}\right)^i \left(\frac{y_0}{h}\right)^j \tag{6}$$

where y_0 indicates the y coordinate of the junction which, for simplicity, is taken parallel to the x axis. The matrix β can be transformed to a two dimensional function $\beta(x, \zeta)$ using a polynomial regression technique

$$\beta(x, \zeta) = \sum_k \sum_l C_{kl} x^k \zeta^l \tag{7}$$

where x and ζ indicate the excitation and the observation points respectively. Using equations 3 ,5 ,6 ,7 and some mathematical operations, one obtains a matrix relation between coefficients a_{ij} and b_{ij}. The dynamic energy due to the auxiliary structure can then be computed by equation 4 . The other kinetic and potential energy terms are all related to the main structure and can be simply derived.

3) Results

As a practical application, the force vibrations of a system composed of two coupled perpendicular thin plates has been studied. Both plates have same dimensions and material properties. The excitation is a unit lateral load. Figure 3 indicates the variation of lateral displacement amplitude *vs* frequency. The substructure compliance matrix has been obtained by the same variational procedure as the main structure using 9 contact points. For more complex structures, the compliance matrix can either be calculated by numerical methods or measured experimentally. The results are compared by a finite element solution using the IDEAS package with 12 and 24 vibrational modes. It is clear that at higher frequencies, higher number of modes must be used to obtain valuable results. A sensibility analysis has been performed regarding possible errors in measuring or calculating compliance components of the substructures. It is however out of the scope of this brief report. Also, an analysis has been conducted to investigate the role of the number of measurement points and the suitable degree of regression in different frequency ranges. It will help to minimize the measurement and calculation time and cost to obtain a desired precision.

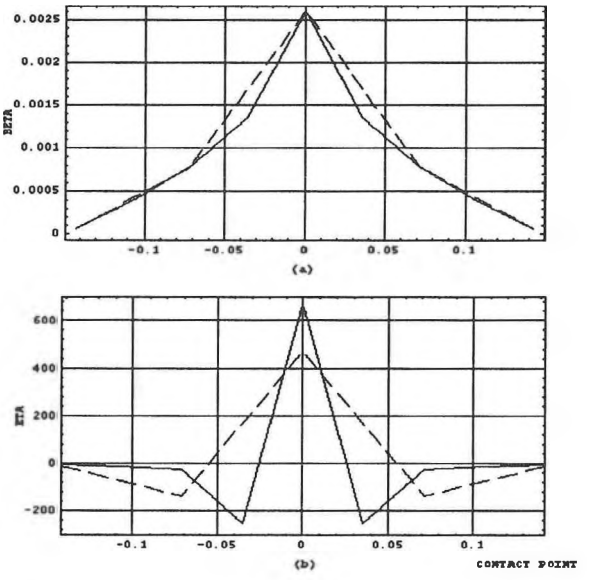

Figure 2: Compliance variation and its inverse along the junction with 5 and 9 contact points

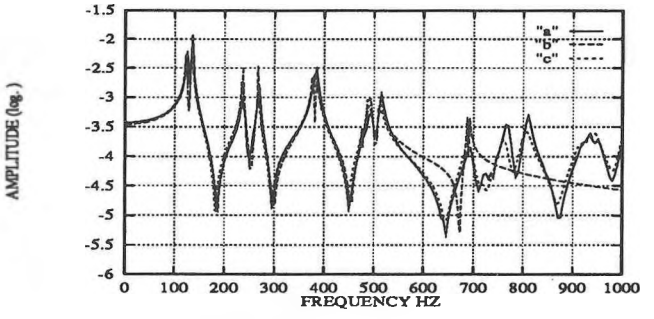

Figure 3: Lateral vibration of two coupled perpendicular plates a) Hybrid method b) Finite element using first 12 modes c) Finite element using first 24 modes.

References

[1] Lyon R.H. and Maidanik G. : "Power flow between linearly coupled oscillators.", J.acoust.soc.am. 34(5) 623-639, 1962.

[2] Hale A.L. and Meirovitch L. : "A general substructure synthesis method for the dynamic simulation of complex structures", J.S.V (1980) 69(2) 309-326.

[3] Guyader J.L., Boisson C. and Lesueur C. : "Energy transmission in finite coupled plates, Part(I,II)",J.S.V (1982) 81(1) 81-105.

[4] Cushieri J.M.: "Structural power flow analysis using a mobility approach of an L-shaped plate.", J.acoust.soc.am. 87(3), March 1990.

PRIMARY CALIBRATION OF ACCELEROMETERS BY LASER INTERFEROMETRY AT THE NATIONAL RESEARCH COUNCIL

George S. K. Wong, Anil K. Agarwal and Lixue Wu

Acoustical Standards
Institute for National Measurement Standards
National Research Council Canada, Ottawa, Ontario, K1A 0R6

Abstract

This paper describes the absolute accelerometer calibration system developed at the Institute for National Measurement Standards, NRC. Details of the calibration procedure and the associated equipment are described. The system, based on laser interferometry, operates from 20 Hz to 5000 Hz, with an estimated uncertainty of less than 0.5% at a confidence level of 95%.

Introduction

Advances in the design of structures and machines over recent years have created stringent demands for investigation into vibration problems. Accurate measurements of vibration have become important with more research efforts devoted to the design of better transducers. As a result, accurate calibrations of accelerometers are necessary to verify design parameters and performance characteristics.

Calibration Arrangement

A standard absolute accelerometer calibration procedure [1] and the principles of operation [2, 3] have been described. The measurement set-up is shown in Figure 1. It consists of a Michelson interferometer with associated equipment as shown. For frequencies up to 800 Hz the number of fringes R_f per vibration period is counted. It can be shown that the displacement amplitude D of the vibration is given by

$$D = R_f \frac{\lambda}{8}$$

where λ is the wavelength of the laser. For a sinusoidal vibration at frequency f, the acceleration amplitude A is given by

$$A = 4\pi^2 f^2 R_f \frac{\lambda}{8}$$

For frequency ranges from 800 Hz to 5000 Hz the output signal of the detector is filtered with a bandbass filter. According to the standard procedure [1], the filtered signal has a number of minimum points at various accelerometer displacements. For a helium-neon laser with a wavelength of 0.6328 μm, the acceleration, in ms^{-2}, is given by

$$A = 39.478 \times 10^{-6} d f^2$$

where d is the displacement amplitude in micrometres, and f is the frequency of the shaker in hertz.

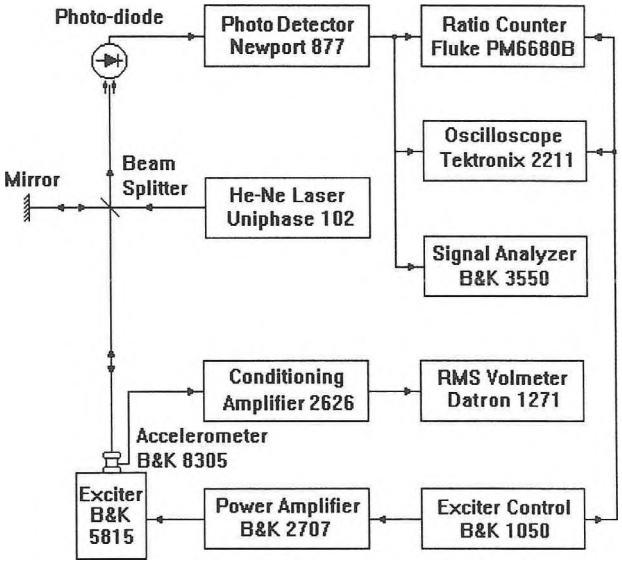

Figure 1 *Accelerometer calibration set-up*

Implementation Considerations

External vibrational noise is one of the most serious problems encountered in measuring small displacements. In the arrangement used at INMS, the entire system is mounted on a heavy 5 cm thick steel bench supported by a 10 cm thick granite table that is resting on air-pads (Micro-g air table, Technical Manufacturing Co.). The interferometer is mounted on top of the shaker supported by four box-shaped columns, and isolated by a second air-pad system, as shown in Figure 2. Other disturbances, such as airborne noise may be reduced by performing the calibrations in the evening or overnight.

Thermal air currents generated by the cooling fans of the equipment can cause random fluctuations in the refractive index of air. This leads to random changes in beam intensities. The effect can be effectively eliminated by shielding the beam path.

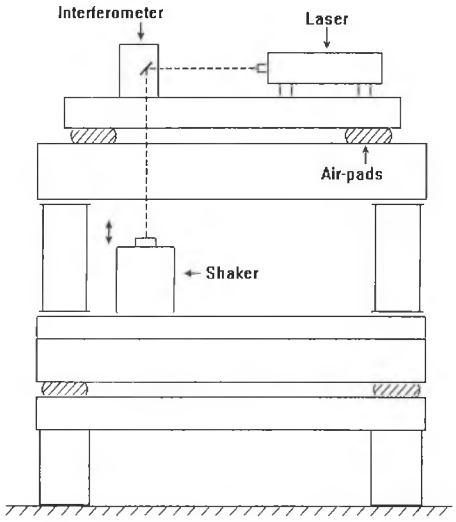

Figure 2 *Accelerometer calibration*

Uncertainties

The calculation of the absolute uncertainty for the calibration is governed by international standard [1]. The uncertainty audit of the absolute calibration at a frequency 160 Hz is listed in Table 1. The uncertainties of the frequency ratio counter, charge amplifier and voltmeter are estimated based on manufacturers' specifications. The estimated uncertainties due to tilting (orthogonality), transverse vibration and waveform distortion are determined experimentally. The overall uncertainty calculated according to Annex A in [1] is less than 0.5% at 95% confidence level.

Table 1 *Uncertainty contributions for a B & K type 8305 standard reference transducer calibrated at a frequency 160 Hz with an acceleration 10 ms* $^{-2}$

Error source	Uncertainty
Voltmeter & charge amp.	±0.08%
Frequency counter × 2	±0.002%
Ratio counter	±0.2%
Distortion	±0.5%
Tilting	±0.1%
Transverse vibration	±0.06%
Temperature	±0.1%
Estimated standard deviation (3 measurements)	±0.04%

Conclusions

The absolute accelerometer calibration system developed at INMS has an uncertainty of less than 0.5% at 95% confidence level. Future investigation related to orthogonal movements of the shaker-head may reduce the uncertainty.

References

[1] *ISO 5347 -1*, 1993: "Methods of calibration of vibration and shock pick-ups"

[2] H. A. Deferrari, R. A. Darby and F. A. Andrews, "Vibrational displacement and mode-shape measurement by a laser interferometer," *J. Acoust. Sco. Am.*, Vol. 42, pp. 982-990, 1967.

[3] S. M. van Netten, "Laser interferometer microscope for the measurement of nanometer vibrational displacements of a light-scattering microscopic object", *J. Acoust. Sco. Am.*, Vol. 83, pp. 1667-1674, 1988.

[4] J. T. Verdeyen, *Laser Electronics*, Englewood Cliffs: Prentice-Hall, 1981.

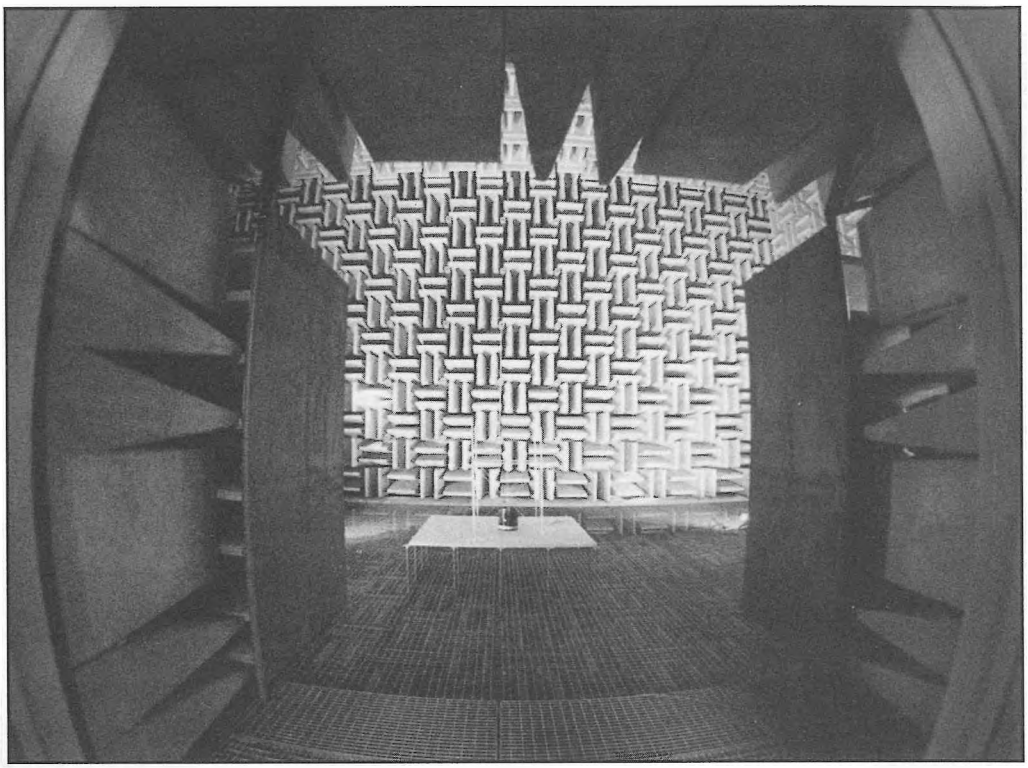

GRANDE SALLE ANÉCHOÏDE

DU BUREAU DE LA RADIOPROTECTION DE SANTÉ CANADA DISPONIBLE CONTRE PAIEMENT À L'ACTE

Cette installation est dotée d'un vaste espace, calme, anéchoïde et souple permettant de produire et de caractériser des champs sonores. Sans être conçue pour remplacer les salles anéchoïdes commerciales, elle convient à une vaste gamme d'applications pertinentes en génie et en recherche et développement, qui pourraient intéresser le secteur privé, les universités, de même que les ministères et organismes gouvernementaux.

La disponibilité de la salle anéchoïde sera établie selon les exigences du programme de protection contre le bruit du Bureau.

Nous vous invitons à nous communiquer vos besoins en vous adressant à :

Stephen Bly, Santé Canada
Pièce 228A, 775 chemin Brookfield
Ottawa (Ontario) K1A 1C1
Tél. : (613) 954-03080
Téléc. : (613) 941-1734
c. élec. : sbly@hpb.hwc.ca

Il nous fera plaisir de vous communiquer plus de détails, y compris l'estimation des coûts, le calendrier et la disponibilité de l'équipement.

Caractéristiques :

- 12,7 x 8,7 x 7,8 m (l x l x h) d'une pointe de coin à l'autre
- anéchoïde de 50 à 20 000 Hz
- bruit de fond inaudible

Options :

- robot de positionnement des microphones
- milieu hémi-anéchoïde pour charges réparties jusqu'à 1200 kg/m^2

Quelques applications :

- systèmes actifs de réduction du bruit
- moyens techniques de réduction du bruit
- systèmes de divertissement audio
- psychoacoustique

Blachford

"The ABC's of noise control"

H.L. Blachford's Comprehensive Material Choices

Noise treatments can be categorized into three basic elements: Vibration Damping, Sound Absorption and Sound Barriers.

Vibration Damping

It is well known that noise is emitted from vibrating structures or substrates. The amount of noise can be drastically reduced by the application of a layer of a vibration damping compound to the surface. The damping compound causes the vibrational energy to be converted into heat energy. Blachford's superior damping material is called ANTIVIBE and is available either in a liquid or a sheet form.

ANTIVIBE DL is a liquid damping material that can be applied with conventional spray equipment or troweled for smaller/thicker application.

It is water-based, non-toxic and provides economical and highly effective noise reduction from vibration.

ANTIVIBE DS is an effective form of damping material provided in sheet form for direct application to your product.

Sound Barriers

Sound Barriers are uniquely designed for insulating and blocking airborne noise. The reduction in the transmission of sound (transmission loss or "TL") is accomplished by the use of a material possessing such characteristics as high mass, limpness, and impermeability to air flow. Sound barriers can be a very effective and economical method of noise reduction.

Blachford Sound Barrier materials:

BARYMAT

Limp, high specific gravity, plastic sheets or die cut parts. Can be layered with other materials such as acoustical foam, protective and decorative facings to achieve the desired TL for individual applications.

Sound Absorption

Blachford's CONASORB materials provide a maximum reduction of airborne noise through absorption in the frequency ranges associated with most products that produce objectionable noise. Examples: Engine compartments, computer and printer casings, construction equipment, cabs,...etc.

Available with a wide variety of surface treatments for protection or esthetics. Material is available in sheets, rolls and die-cut parts – designed to meet your specific application.

Suggest Specific Material or Design

Working with data supplied by you, H.L. Blachford will make recommendations or treatment methods which may include specific material proposals, design ideas, or modifications to components.

A Quality Supplier

The complete integration of:

- Experience
- Quality-oriented manufacturing technology
- Research and development
- Problem solving approach to noise control

Our Mississauga Plant is ISO-9001 CERTIFIED

Result in:

Comprehensive Noise Control Solutions

MISSISSAUGA (905) 823-3200
MONTREAL (514) 938-9775
VANCOUVER (604) 263-1561

STATISTICAL ENERGY ANALYSIS APPLIED TO LIGHTWEIGHT CONSTRUCTIONS PART 1: SOUND TRANSMISSION THROUGH FLOORS

T.R.T. Nightingale Institute for Research in Construction, National Research Council, Ottawa, Ontario, Canada K1A OR6
Robert J.M. Craik Heriot Watt University, Dept. of Building Engineering and Surveying,, Riccarton Edinburgh UK EH14 4AS
John A. Steel Heriot Watt University, Dept. of Mechanical Engineering, Riccarton Edinburgh UK EH14 4AS

This is the first of three papers on the application of statistical energy analysis (SEA) to a lightweight wood frame construction. In this paper the basic theory behind SEA will be presented by examining a simple model for sound propagation through the floor/ceiling assembly shown in Figure 1.

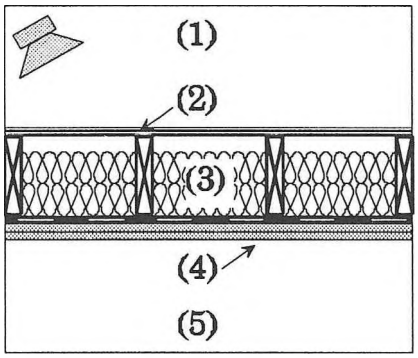

Figure 1: Sketch of the floor/ceiling assembly. (1): source room, (2): 15.9 mm OSB decking, (3): 235 mm deep cavity with two layers of 89 mm batt insulation, (4): 2 layers 12.7 mm type X gypsum board mounted on resilient channels, (5): receive room.

SEA enables the prediction of energy contained in individual elements (or sub-systems) of a complete system when power is input in one or more of the sub-systems. The basic principle of SEA requires that the power, W, into a sub-system is equal to the power lost either through transmission, radiation, or internal losses.

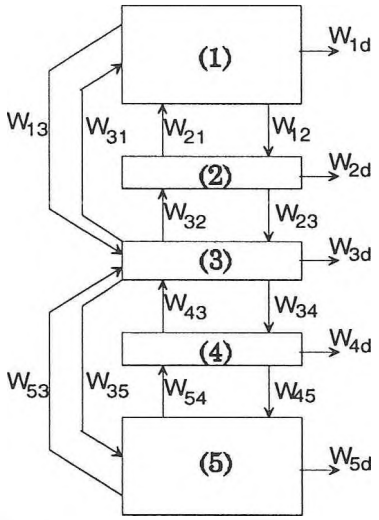

Figure 2: Sub-system diagram for the SEA model of the modelled floor/ceiling assembly.

Figure 2 shows a sub-system diagram with the paths of power flow illustrated by the arrows. It has been assumed that the resilient channels remove any coupling between the floor decking and the gypsum board ceiling via the joists. There are arrows showing power flow directly from room to cavity or via versa apparently without involving the floor decking or the gypsum board ceiling. These represent the non-resonant paths of energy transport that are essentially independent of the damping of the element through which energy passes.

The following set of equations can be written describing the partition of energy between the sub-systems,

$$\begin{bmatrix} -\eta_1 & \eta_{21} & \eta_{31} & 0 & 0 \\ \eta_{12} & -\eta_2 & \eta_{32} & 0 & 0 \\ \eta_{13} & \eta_{23} & -\eta_3 & \eta_{43} & \eta_{53} \\ 0 & 0 & \eta_{34} & -\eta_4 & \eta_{54} \\ 0 & 0 & \eta_{35} & \eta_{45} & -\eta_5 \end{bmatrix} \bullet \begin{bmatrix} E_1 \\ E_2 \\ E_3 \\ E_4 \\ E_5 \end{bmatrix} = \begin{bmatrix} -W_1/\omega \\ 0 \\ 0 \\ 0 \\ 0 \end{bmatrix} \quad [1]$$

where the power flow between sub-systems i and j is given by

$$W_{ij} = E_i \omega \eta_{ij}, \quad [2]$$

E_i is the energy stored in i, ω is the angular frequency, and η_{ij} is the coupling loss factor (CLF) between i and j. The CLF is defined as the fraction of energy transmitted in one radian cycle. Also, the concept of a total loss factor (TLF) was introduced to simplify the set of equations,

$$\eta_i = \eta_{id} + \sum_j \eta_{ij}, \quad [3]$$

where j indicates the sub-systems to which i is connected and η_{id} is the internal loss factor. The TLF is the faction of energy transmitted, lost due heat and radiation. The TLF is easily measured as it is a simple function of the reverberation time, T, and frequency, f,

$$\eta_i = \frac{2.2}{fT_i} \quad [4]$$

Thus the energy in any one of the sub-systems can be found by solving a set of equations involving CLF's and TLF's.

CLF's

The CLF will depend on i and j and how they are coupled. It is beyond the scope of this paper to derive the individual CLF equations but rather they will just be presented to indicate their dependencies. Craik has previously provided a detailed examination[1].

Resonant transmission from a room volume to a plate (i.e., (1) to (2) and (5) to (4)) is given by,

$$\eta_{12} = \frac{5556 S_2 f_{c2} \sigma_2}{V_1 \rho_{s2} f^3}, \quad [5]$$

where S_2 is the surface area of the decking, f_{c2} is its critical frequency, ρ_{s2} is its surface density, and f is the frequency. The radiation factor, σ, can be calculated from various equations[2] depending on the accuracy required.

Resonant transmission from a plate to a room (i.e., (2) to (3), and (4) to (5)) is given by,

$$\eta_{45} = \frac{66\sigma_4}{\rho_{s4} f}. \quad [6]$$

If the method of energy transport between rooms/cavities is non-resonant transmission then the coupling loss factor can be determined from the non-resonant transmission coefficient, τ_{ij}, for the element separating the rooms or cavities. For example, the CLF between the source room (1) and the floor cavity (3) for non-resonant transmission is,

$$\eta_{13} = \frac{13.7 S_3 \tau_{13}}{f V_1}, \quad [7]$$

where τ_{13} is the transmission coefficient of the floor decking.

CLF's associated with joints occur commonly when modelling complete building assemblies,

$$\eta_{ij} = 0.1365 \left(\frac{h C_{Li}}{f} \right)^{\frac{1}{2}} \frac{L}{S_i} \tau_{ij} \quad [8]$$

where C_{Li} is longitudinal wave speed for sub-system i, L is the length of the joint, S_i is the surface area of the sub-system i, and τ_{ij} is the power transmission coefficient between i and j.

The CLF between two sub-systems can be measured using the power balance between the two sub-systems,

$$\eta_{12} = \frac{E_2 \eta_2}{E_1}, \quad [9]$$

where η is the loss factor. In writing this equation it has been assumed that the power input into sub-system 2 from all other subsystems other than 1 can be ignored. The estimates of the energy contained in a plate can be obtained from the measured space-time averaged surface velocity $\langle v^2 \rangle$ given,

$$E_{plate} = \langle v^2 \rangle \rho_s S, \quad [10]$$

where ρ_s is the surface density, and S is surface area. Alternately, if the sub-system is a room or cavity then the energy can be estimated from the space-time average sound pressure $\langle p^2 \rangle$ given,

$$E_{room/cavity} = \frac{\langle p^2 \rangle V}{\rho_o c_o^2}, \quad [11]$$

where V is the room volume, ρ_o is the density of air, and c_o is the speed of sound in air.

Transmission through the floor cavity

The model of Price and Crocker[3] was used to predict the transmission through cavity. It assumes that transmission from a room into the cavity of a partition wall or floor is the same as transmission into a small room from a much larger room. Both resonant and non-resonant transmission are possible. Transmission out of the partition cavity into the receive room then follows from the consistency relationship,

$$n_{room} \eta_{room,cavity} = n_{cavity} \eta_{cavity,room} \quad [12]$$

where n is the modal density.

Measured and Predicted Results

Often it is easier, and even more accurate, to use the measured TLF for a similar or nominally identical sub-system in a similar construction than it is to assume that the TLF is the sum of the CLF's. Given in Table 1 are the measured regression fit equations for the total loss factors of some common lightweight building elements,

Sub-system	Density (kg/m^3)	Total loss factor
Gypsum board of a wood stud wall	751	$0.5 f^{-0.37}$
16 mm OSB floor decking	451	$0.4 f^{-0.37}$
Wood joist floor cavity 1/2 to 3/4 full of absorption	n/a	$3.0 f^{-0.34}$

Table 1: Computed TLF's from measured data for some common building elements. Values will vary depending on specific factors such as joint types amount and type of cavity absorption, etc.

The five sub-system model shown in Figure 1 represents a very simplified model for the floor ceiling assembly. The effect of the joists have been ignored, and it is assumed that the resilient channel prevents structure borne transmission from the decking to the gypsum board ceiling. The measured TLF's listed in Table 1 were used in the model. All CLF's were calculated according the equations given. Figure 3 shows that despite the very simple model the measured and predicted results are in good agreement.

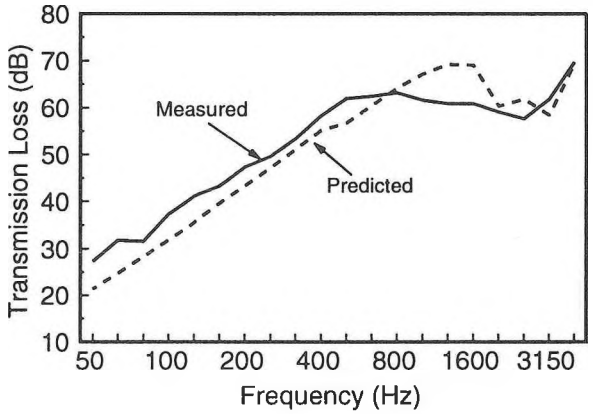

Figure 3: Measured and predicted transmission loss.

The SEA prediction tends to overestimate the efficiency of the coupling between the room/cavities and the wall surfaces, thus underestimating the transmission loss. This is especially true at the critical frequencies (2000 and 3000 Hz). More accurate models of the radiation efficiency which controls the degree of coupling can be used but with significantly more computation time.

Conclusions

The predicted transmission loss of the simplified model agrees well with measured results despite the many assumptions (the resilient channels remove any physical coupling from floor decking to the gypsum board ceiling via the joists, and the joists have no effect). The model showed that transmission through a cavity can be modelled using the method of Price and Crocker.

---

[1] Craik, R.J.M., "The noise reduction of flanking paths," Applied Acoustics, Vol. 22, pp. 163-175, 1987.

[2] Leppington, F.G., Broadbent, E.G., Heron, K.H., "Acoustic radiation from rectangular panels with constrained edges," Proc. Royal. Soc., A393, pp. 67-84. 1984.

[3] Price, A.J., Crocker, M.J., "Sound transmission through double partitions using statistical energy analysis," JASA, No 47, pp. 683-693, 1970.

STATISTICAL ENERGY ANALYSIS APPLIED TO LIGHTWEIGHT CONSTRUCTIONS PART 2: JOINTS BETWEEN FLOORS AND PARTY WALLS

T.R.T. Nightingale Institute for Research in Construction, National Research Council, Ottawa, Ontario, K1A 0R6
John A. Steel Heriot Watt University, Dept. of Mechanical Engineering, Riccarton Edinburgh UK EH14 4AS

This is the second of three papers on the application of statistical energy analysis (SEA) to a lightweight wood frame construction. This paper considers methods of modelling the joint that is formed when a load bearing party wall is added to the floor/ceiling assembly considered in Part 1[1] of this series. As in Part 1, the SEA model will use assumptions to keep the model as simple as possible. They are: there is no significant coupling between the floor decking and the gypsum board ceiling, the studs of the walls can be ignored, and the joists of the floor/ceiling assembly can be ignored. The simplified assembly and the sub-systems are shown in Figure 1.

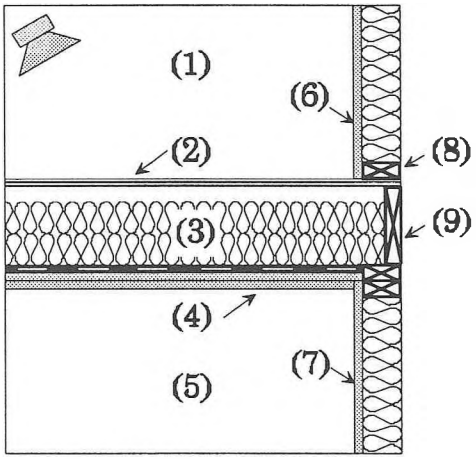

Figure 1: Section through the floor and load-bearing party walls. (1): source room, (2): 15.9 mm OSB decking, (3): 235 mm deep cavity with two layers of 89 mm batt insulation, (4): 2 layers 12.7 mm type X gypsum board mounted on resilient channels, (5): receive room, (6) and (7): 15.9 mm type X gypsum board, (8): 38x89 mm sole plate, (9): 38x235 mm joist header.

The material properties of sub-systems are given in Table 1.

Sub-system	length (m)	width (m)	height (m)	density (kg/m^3)	f_c (Hz)
2	4.5	4.6	n/a	451	2000
4	4.5	4.6	n/a	751	3000
6	4.5	n/a	2.4	751	2500
7	4.5	n/a	2.0	751	2500
8	4.5	0.089	0.038	451	n/a
9	4.5	0.038	0.235	451	n/a

Table 1: Material properties of the sub-systems.

From Figure 1, which shows the sub-systems of the simplified model SEA model, it can be seen that the load bearing party wall introduces a series of flanking paths: 1-6-7-5, 1-2-7-5, 1-2-6-7-5, etc. It is assumed that the gypsum board ceiling (sub-system (4)) is not involved in any of the flanking paths since it is mounted on resilient channels and is only very weakly connected to the head of the lower party wall.

In order to model the flanking paths, the joint between the walls and the floor/ceiling assembly must be modelled. A series of different models for the joint are now presented and their accuracy discussed.

Simple Tee Joint

A tee formed by the intersection of the gypsum board party wall (sub-systems (6) and (7)) by the OSB floor decking (sub-system (2)) is the simplest representation of the joint. It is assumed that the plates are rigidly connected and that the beams (sub-systems (8) and (9)) at the joint can be ignored. In Figures 2, 3 and 4 the predicted velocity level differences (VLD's) are shown and labeled as 'Simple "Tee"'. Measured data is also shown for comparison. The simple tee joint model completely fails to predict the VLD's (as calculated from Equation 10[1]) for the paths 2-7 shown in Figure 3 and 6-7 shown in Figure 4. The prediction for path 2-6 is perhaps the best of the three predictions; showing the general trend for frequencies greater than 400 Hz. It is clear from the measured data that the type of coupling between the floor decking (2) and the upper party wall (6) is different than that to the lower party wall (7). A more complex model is required which does not have the symmetry suggested by the simple tee joint.

Tee Joint with a Beam

The upper and lower party walls are of nominally identical construction so it is likely that the differences in the measured VLD's between the two paths 3-5 and 3-6 will be due to different coupling mechanisms for each path. Figure 1 suggests that the joist header might be involved in the coupling between the floor decking and the lower party wall. Similarly, the upper party wall might be viewed as also being connected to the joist header. In this representation the head plates of the lower party wall are taken to be an extension of the joist header thereby making an equivalent beam of dimension 38x311 mm. The model of Steel[2] was used to calculate the joint transmission coefficients and using Equation 10[1] the VLD's were computed. In Figures 2, 3 and 4 the predictions are labeled '"Tee" with Beam' and show that including a joist header did not improve the accuracy of the predictions for any of the paths. This suggests that the joint may not behave as a "Tee".

Examining the measured data, it can be seen that the VLD for the path 6-7 is close to the sum of the VLD's for the paths 2-6 and 2-7. This might suggest that the joint should be modelled as two corner joints sharing a common plate; the floor decking (sub-system (2)).

Two corner joints sharing a common plate

In this representation, the joint is modelled as being two corner joints sharing a common plate, the floor decking. The first corner joint will be between the floor decking (2) and the gypsum board of the upper party wall (6). The 38x89 mm sole plate (8) common to both (2) and (6) is included. The second corner joint will be between the floor decking (2) and the lower party wall (7). The 38x235 mm joist header (9) common to both is included. The predicted VLD's for the three paths are labeled "2 Corner

Joints" and are shown in Figures 2, 3 and 4. For all three paths there is reasonably good agreement between measured and predicted results for the frequency range 400-4000 Hz. However, below 400 Hz the predictions are quite poor. The VLD's are underestimated and in all cases the wrong trend is indicated.

Discussion

For most ribbed panels there is a transition between behaving as a single plate and a series of independent sub-panels defined by the ribs. The 400 Hz third octave marks the cut-on of cross modes in the sub-panels and a corresponding increase in modal density as shown in Table 2.

1/3 Octave Band (Hz)	Number of Modes	Angular range (degrees)
Less than 100	0	n/a
100	5	$5 \leq \theta \leq 23$
125	3	$27 \leq \theta \leq 35$
160	3	$38 \leq \theta \leq 44$
200	2	$46 \leq \theta \leq 49$
250	3	$51 \leq \theta \leq 54$
315	3	$56 \leq \theta \leq 59$
400	13	$5 \leq \theta \leq 62$

Table 2: Number of modes and angular range for the OSB floor decking sub-panels (0.4x4.6 m dimension).

Below about 400 Hz the floor may behave as a single plate or a series of independent sub-panels. As sub-panels, there are only a very small number of modes in any one of the third octaves below 400 Hz. The angular range of the modes within each third octave band is quite narrow. This does not satisfy the requirent of SEA that there be a diffuse field.

To investigate the behaviour of the sub-panels, all the modes were computed along with their angle of incidence on the joint. The joint transmission coefficients for each mode were computed using the "two corner joints sharing a common plate" model and band averaged to compute the VLD's in the usual way. The results are shown in the Figures and labeled as "2 Corner Joints + Modes". Improvement in the predictions for all paths are shown for frequencies above about 315 Hz. This suggests that the sub-panel model is the most accurate once the cross modes have cut-on. For paths 2-6 and 2-7 the sub-panel model apparently improved results for frequencies below 315 Hz. However, this was not the case for 6-7.

Conclusions

Measured and predicted results for sound transmission along flanking paths have been shown. Best agreement is found with predictions which allow for separate joints. The first is between floor deck and upper party wall with the sole plate included. The second is between the floor deck and lower party wall with the joist header included. Modelling the system using two joints assumes that there is no direct coupling mechanism between the sole plate and the joist header. In measured specimen, the sole plate was nailed to the floor decking and not the joist header.

The model gives very good agreement with measured results at frequencies above 400 Hz with measured and predicted transmission reducing with increasing frequency. It is in this range of very good agreement where flanking paths involving the joint may become significant. At lower frequencies where flanking via the joints will not be important, the measured transmission is much weaker than predicted.

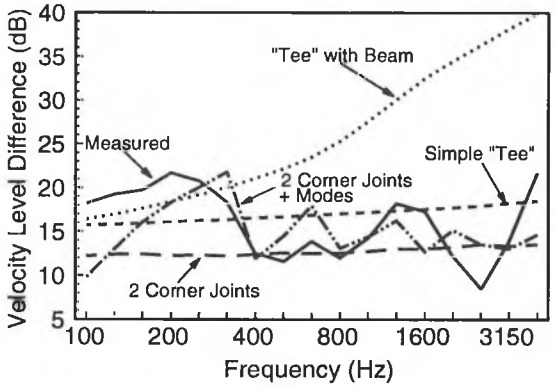

Figure 2: Measured and predicted velocity level differences for transmission from floor decking (2) to upper party wall (6).

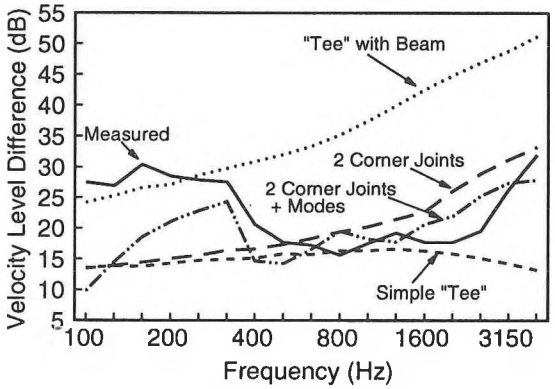

Figure 3: Measured and predicted velocity level differences for transmission from floor decking (2) to lower party wall (7).

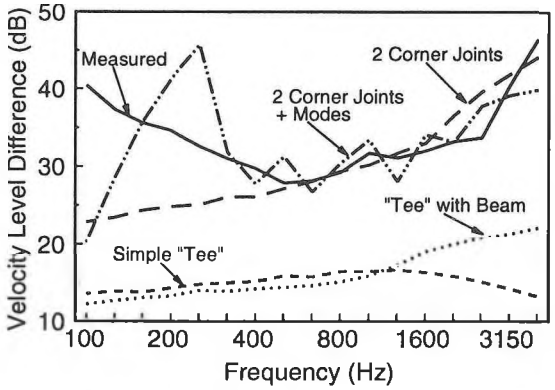

Figure 4: Measured and predicted velocity level differences for transmission from the upper party wall (6) to the lower party wall (7).

[1] Nightingale, Craik, Steel, "Statistical energy analysis applied to lightweight constructions Part 1: sound transmission through floors," Canadian Acoustics, Vol. 23, No. 3, 1995.

[2] Steel, John, A., "Sound transmission between plates in framed structures," Journal of Sound and Vibration, Vol. 178, No. 3, pp. 379-394, 1994

STATISTICAL ENERGY ANALYSIS APPLIED TO LIGHTWEIGHT CONSTRUCTIONS PART 3: MEASUREMENTS AND PREDICTIONS OF FLANKING TRANSMISSION

T.R.T. Nightingale Institute for Research in Construction, National Research Council, Ottawa, Ontario, Canada K1A OR6
John A. Steel Heriot Watt University, Dept. of Mechanical Engineering, Riccarton Edinburgh UK EH14 4AS
Robert J.M. Craik Heriot Watt University, Dept. of Building Engineering and Surveying,, Riccarton Edinburgh UK EH14 4AS

This is the third of three papers on the application of statistical energy analysis (SEA) to a lightweight wood frame construction. This paper takes the basic model for direct transmission presented in Part 1[1] and uses the 'two corner joints sharing a common plate' model developed in Part 2[2] to describe the coupling to the load bearing party walls. The model will be used to reveal the dominant flanking paths and to investigate the potential effectiveness of two retrofits.

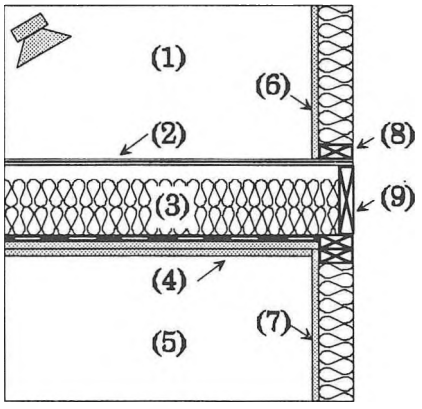

Figure 1: Sketch the floor/ceiling assembly and the load bearing party walls that are modelled. The sub-systems are (1): source room, (2): 15.9 mm OSB decking, (3): 235 mm deep cavity with two layers of 89 mm batt insulation, (4): 2 layers 12.7 mm type X gypsum board mounted on resilient channels, (5): receive room, (6) and (7): 15.9 mm type X gypsum board.

As in Part 1, the SEA model will use assumptions to keep the model as simple as possible. They are: there is no significant coupling between the floor decking and the gypsum board ceiling, the studs of the walls can be ignored, and the joists of the floor/ceiling assembly can be ignored. The SEA sub-system diagram for the complete model is shown in Figure 2.

Measured and predicted net transmission loss

Figure 3 shows the measured and predicted net transmission loss (TL) for the assembly shown in Figure 1. The predicted results indicate the correct trends in the measured transmission loss, but the SEA model tends to underestimate the transmission loss. This underestimation of the TL was also present in the SEA prediction for the floor/ceiling assembly without any flanking paths given in Part 1. This suggests that the basic model for the transmission through the floor/ceiling assembly is biased toward underestimating the transmission loss (i.e., overestimating the coupling between sub-systems).

In the low frequencies 50-200 Hz, differences may be due to incorrectly estimating the total loss factor of the floor cavity, and/or incorrectly estimating the coupling between the surfaces forming the cavity (i.e., the OSB floor decking and the gypsum board ceiling). It should also be realized that the low modal density of the small source and receive rooms (volumes, source: 50 m^3 and receive: 40 m^3) will tend to increase uncertainty in the transmission loss measurements in the low frequencies.

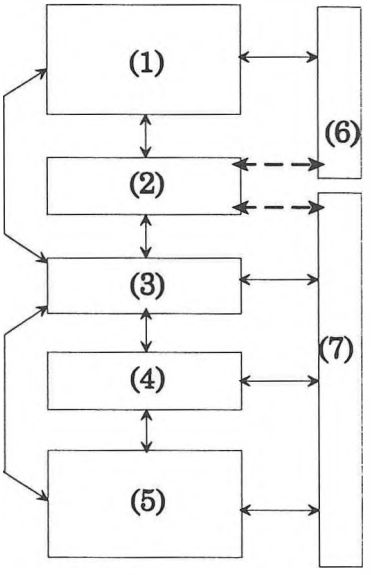

Figure 2: SEA sub-system model used to describe the direct and flanking paths for the floor/ceiling assembly. Paths via the joints are indicated by the wide dashed lines.

In the mid-frequencies, 250-1600 Hz the model has good agreement with measured results. A significant portion of this range, above 315 Hz, is controlled by flanking transmission, indicating that when both the transmission through the joint and the coupling between the room and its surfaces can be modelled accurately, there is good agreement with measured results.

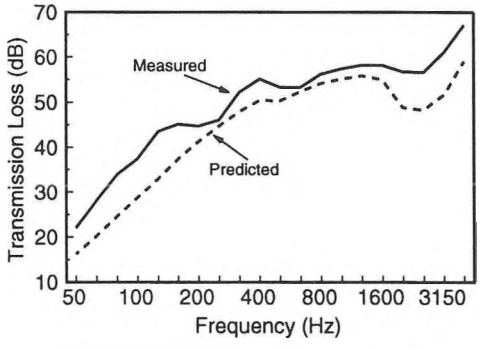

Figure 3: Measured and predicted net transmission loss (including flanking paths) for the floor ceiling assembly.

In the high frequencies 2000-4000 Hz flanking transmission completely controls the sound isolation and the SEA model underestimates the transmission loss. The underestimation is most likely due to the fact that the coupling between the flanking surfaces and the room volume is overestimated at the critical frequencies of the flanking surfaces (floor decking: 2000 Hz, party walls: 2500 Hz, and ceiling: 3000 Hz). A more exact method for computing the radiation efficiency could have been used.

Noise reduction as a function of flanking path

SEA lends itself to the prediction of noise reduction for a particular flanking path. The noise reduction for room to room transmission is given in terms of the computed counpling and total loss factors for the sub-systems in the path and, V, the volumes of the source and receive rooms,

$$NR_{1-2-3-4\ldots n} = 10\log\left[\frac{\eta_{12}\eta_{23}\eta_{34}\ldots\eta_{n-1,n}V_n}{\eta_2\eta_3\eta_4\ldots\eta_n V_1}\right] \qquad [1]$$

Figure 4 shows the predicted noise reduction for the three most important flanking paths 1-2-7-5, 1-6-2-7-5 and 1-6-2-3-4-5.

It is clear that the path 1-2-7-5 is the dominant flanking path, controlling the net sound reduction for all frequencies greater than 315 Hz. The path 1-6-2-7-5 is the next important, but has typically 10 dB greater noise reduction than path 1-2-7-5. Of almost negligible importance is the path 1-6-2-3-4-5. From the path analysis it can be seen that the two flanking paths offering the least noise reduction are those involving the party wall (sub-system (7)) in the lower room. In both cases, because of the joint model chosen, the energy must travel through the floor decking (sub-system (2)) and the joist header (sub-system (9)) to get to the party wall of the receive room.

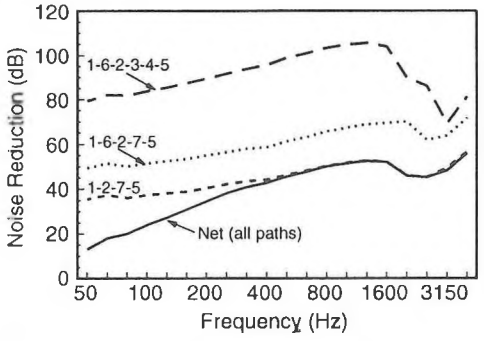

Figure 4: Predicted noise reduction (or sound pressure level difference) between the source room (sub-system (9)) and the receive room (sub-system (10)) as a function of the flanking path.

Treatments to improve the sound isolation

The path analysis indicates that the most important path is 1-2-7-5. Sound transmission along this path can only be reduced by treating sub-systems 2, 7 or redesigning the joint that connects them. If sub-system 2 is treated, then sound isolation of both the direct and flanking paths can be improved, and there is the greatest potential for improvement to the sound isolation.

A possible treatment for new or existing constructions might be to add a concrete topping to the floor decking. Figure 5 shows the predicted transmission loss for the assembly with and without a 38 mm thick concrete topping (91 kg/m^2). (In the prediction it was assumed that the bending stiffness of the topping and the OSB would be about that of the concrete topping alone.) The predictions indicate that there should be a significant increase in the sound isolation in the low frequencies where the mass of the topping helps to control the direct transmission through the floor/ceiling assembly. Differences between the bending stiffness of the concrete topping and the gypsum board of the walls tends to reduce transmission through the joints for high frequencies. With the topping, the predicted sound isolation is STC 64, a 12-point improvement from the STC 53 without the treatment.

Alternatively, one could place the gypsum board of the upper and lower party walls on resilient channels. This should effectively remove the structural coupling between the finish gypsum board surfaces and the frame work. This will remove all the flanking paths. Figure 5 shows that a significant improvement only occurs for frequencies above about 400 Hz. In terms of a single number rating, the sound isolation would be STC 58 with the treatment, a 5-point improvement.

Redesigning the joint is an option for new constructions. Further work needs to be done in this area. It was shown in Part 2 that including the joist header in the model reduced joint transmission in the high frequencies. Thus, using a double joist header may help to reduce transmission through the joint.

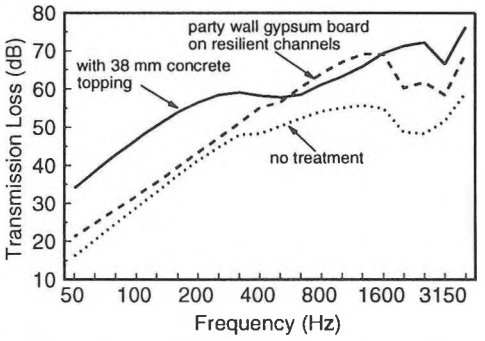

Figure 5: Predicted transmission loss for various treatments to improve the sound isolation between the two rooms. It has been assumed that the joint model developed in part 2 is still valid for the case when the OSB is covered with a concrete topping.

General conclusions Parts 1, 2, and 3

Part 1 in the series showed that the direct sound transmission through a floor/ceiling assembly can be modelled with good accuracy using the method of Price and Crocker. This method requires that the total loss factor of the cavity be accurately known. The assumption that the joists could be ignored and that resilient channel in the ceiling removed any structural paths from the decking to the ceiling was reasonable for direct transmission.

Part 2 showed that the joint between the floor/ceiling assembly and the load bearing party wall was complex, having to be treated as two corner joints sharing a common plate. Including the sole plate and joist header in the model were necessary if the joint transmission was to be accurately predicted in the high frequencies. The results suggest that greater accuracy can be attained by computing the joint transmission coefficients at each modal frequency of the sub-panels. This had the largest effect for frequencies below the first cross mode of the sub-panels.

Part 3 showed that flanking paths controlled the net transmission loss for frequencies greater than about 400 Hz. The most dominant flanking path was from the floor decking through the joist header and into the party wall below. Predictions also showed that adding a concrete topping to the floor decking would be an effective way of increasing the net sound isolation.

---

[1] Nightingale, T.R.T., Craik, Robert J.M., Steel, John .A., "Statistical energy analysis applied to lightweight constructions Part 1: sound transmission through floors," Canadian Acoustics, Vol. 23, No. 3, 1995.

[2] Nightingale, T.R.T., Steel, John A., "Statistical energy analysis applied to lightweight constructions:Part 2: joints between floors and party walls," Canadian Acoustics, Vol. 23, No. 3, 1995.

SOUND TRANSMISSION THROUGH GYPSUM BOARD WALLS

A.C.C. Warnock and J.D. Quirt

National Research Council of Canada, M27 Montreal Road, Ottawa, Ontario, Canada, K1A 0R6

INTRODUCTION.

This paper describes additional findings from a project to study sound transmission through cavity walls constructed from gypsum board using industry-standard details and carefully selected materials[1]. The project was initiated because of increased sound insulation requirements in the 1990 National Building Code of Canada, the removal minimum weight requirements for gypsum board in Standard CAN/CSA-A82.27-M91, and the realization that much of existing published data is obsolete or unsuitable. By making all measurements in a single laboratory, differences among laboratories were avoided and details of specimen construction could be controlled closely. The full report of the study[2], in terms of STC only, provides for builders and regulators a reliable and consistent assembly of sound transmission class (STC) data. About 400 wall systems were tested to examine many parameters but only a few issues can be discussed in this paper. A more detailed report is in preparation.

MATERIALS AND STRUCTURES.

Stud systems tested included a single row of 90 mm wood studs (with and without 13 mm resilient metal channels), 65, 90 and 150 mm non-load-bearing steel studs, staggered 90 mm wood studs, a double row of 90 mm wood studs, double rows of 40 and 65 mm steel studs and load-bearing steel studs with 13 mm resilient metal channels. Average properties of the seven sound absorbing materials used are listed in Table 1. In some walls two thicknesses of batts were used. The thickness of sprayed-on cellulose insulation varied with the type of structure being measured.

Type X fire-rated and conventional gypsum board with thicknesses of 12.7 and 15.9 mm were used. Board density (Mg) ranged from 7.3 to 11.5 kg/m^2. The average value of Young's modulus was 2.3 x 10^9 N/m^2.

DEPENDENCE OF STC AND R'$_W$ ON MATERIALS AND STRUCTURE.

The major factors that control sound transmission through walls have long been known. This project revealed the significance of other factors that had not been considered very important. To provide an overview, multiple regression analyses were made for the single number ratings STC[3] and R'$_w$[4] as dependent variables and factors such as mass, cavity depth, airflow resistance as independent variables. Only 360 walls, those with a single cavity containing sound absorbing material and having the two layers of gypsum board independent or resiliently connected, were included in the analyses. For STC and R'$_w$ the regression equations found were

$$STC = -69.8 + 33.5\log_{10} M_g + 32.2\log_{10} d - 7\times10^{-4} R + 0.017 S_{oc},\ r^2 = .903$$

and

$$R'_w = -60.3 + 29.5\log_{10} M_g + 32.2\log_{10} d - 2.1\times10^{-4} R + 9.2\times10^{-3} S_{oc},\ r^2 = 0.924$$

Here M_g is the total mass per unit area of the gypsum board layers (kg/m^2), d is the cavity depth (mm), R is the flow resistance of the sound absorbing material (mks rayls), and S_{oc} is the stud spacing (mm). The standard errors of the estimates are 2.0 and 1.6 dB respectively. Below 500 Hz, these factors accounted for most of the variance. Above 500 Hz, stud spacing was not significant. Simple multiple correlation with these variables failed at higher frequencies because of gypsum board stiffness effects and other factors. This is of little importance if only STC or R'$_w$ are considered. Transmission loss (TL) contours for common cavity walls using lightweight materials are such that ratings are usually controlled by TLs at frequencies below 500 Hz.

Dependence of TL on weight and cavity depth were expected. Some dependence on stud spacing, discussed in the next section, was also expected from the earlier work in this project where pronounced resonances were seen when gypsum board was directly attached to wood studs. What is surprising in the equations above, is the negative dependence on the flow resistance of the sound-absorbing material. For a 90 mm material thickness, using the minimum and maximum values of flow resistance in Table 1, the expected change in STC is about 3; for R'$_w$, it is about 1. The reason for this is discussed below.

Table 1: Properties of sound absorbing materials. G and M denote glass and mineral fibre batt materials. C denotes cellulose which was sprayed on to one surface or blown into the cavity.

Code	Thickness mm	Density kg/m^3	Airflow Resistivity mks rayls/m
G1	90	12.2	4800
G1	65	11.7	3600
G1	150	11.2	4300
G2	90	16.4	7900
M1	90	32.6	12700
M1	65	36.7	11400
M2	75	44.2	16600
M2	40	51.9	15000
M3	83	98.1	58800
C1	wet spray	56.3	—
C2	90 (blown)	49.3	33000

EFFECTS OF STUD SPACING.

Attaching gypsum board to studs creates smaller sub-panels with a width determined by the stud spacing. The edge conditions and the effective radiating area for these sub-panels will depend on stud properties and the spacing of the screws attaching the gypsum board. Figure 1 shows improvements for three systems with different combinations of 16 mm gypsum board on each face. The curve labeled SS90 shows the mean improvement for 90 mm steel stud walls when the stud spacing is changed from 400 to 600 mm. The curve labeled DWS shows the improvement with double wood stud walls for the same change in stud spacing. The curve labeled WS&RC shows the improvement when both wood stud and resilient metal channel spacings are changed from 400 to 600 mm. Resonance effects are pronounced around 125 and at 200 Hz. Similar results were found for other types of gypsum board. STC and R'$_w$ are often controlled by TL values around 125 Hz, so increased stud and channel spacings can lead to dramatic rating increases. In general, the greater the distance between studs or resilient metal channels, the greater the TL at the lower frequencies. Even with resilient steel studs and double wood studs, there is a benefit to having larger stud separations.

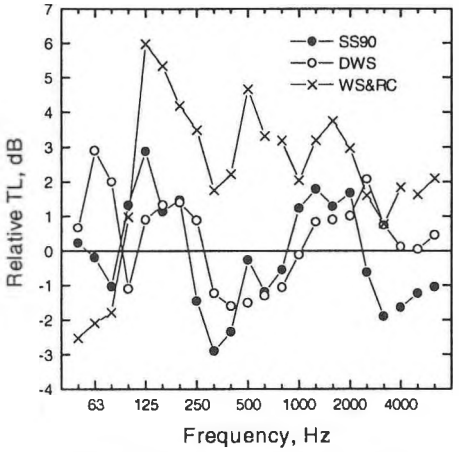

Figure 1: Improvements in transmission loss due to changes in stud or resilient metal channel spacing.

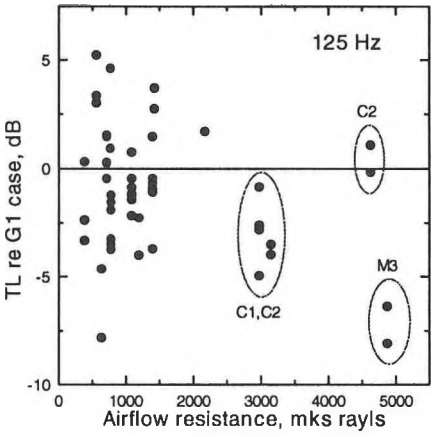

Figure 2: Transmission loss at 125 Hz relative to a cavity containing 90 mm of G1.

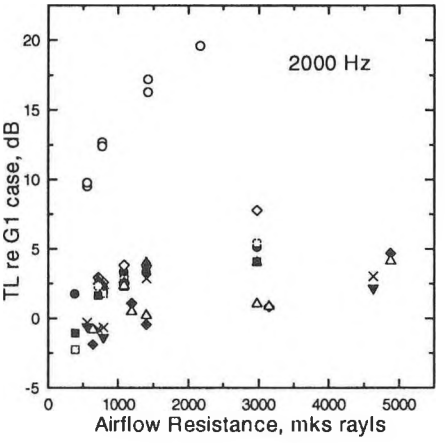

Figure 3: Transmission loss at 2000 Hz relative to a cavity containing 90 mm of G1.

EFFECTS OF SOUND ABSORBING MATERIAL.

The previous paper[1] reported a positive correlation between airflow resistance and TL from 500 to 2000 Hz. The reason for the negative correlation found here between STC and R'_w and airflow resistance can be found by examining Figures 2 and 3. The plots show differences in TL as a function of airflow resistance relative to the case where the cavity contained 90 mm of sound absorbing material G1. A set of differences was calculated for a single stud and gypsum board arrangement with different sound absorbing materials. The figures combine several sets of differences. By referring to a standard absorption condition for each construction type, differences in TL should be due only to the sound absorbing material. Reference to Table 1 shows that different locations on the flow resistance axis correspond to different materials, especially at the right hand side of the plots. Clumps of points are identified in Figure 2 for mineral fibre and cellulose fibre. Figure 2 shows that the mineral fibre and cellulose fibre materials tend to give lower TL values at 125 Hz. Similar relationships are found for other low frequencies. This leads to lower STC and R'_w ratings. For some of these materials as flow resistance increased, so did density and rigidity and there might well have been transmission through the structure of the material, especially for blown-in cellulose (C2) material. The very dense M3 material, which was tightly fitted between the studs, might have increased the effective rigidity of the non-load-bearing steel studs.

At higher frequencies transmission loss increases with increasing flow resistance as found in the previous work[1]. Figure 3, for 2 kHz, marks sets of differences with different symbols and shows some outliers (open circles) in the upper left corner. These outliers come from measurements made on double wood stud systems and show clear, consistent trends at the higher frequencies with improvements due to increasing airflow resistance significantly higher than for other systems. Double wood stud systems are physically connected only around the edges of the specimen through the mounting frame. In all other wall systems, there is coupling through resilient metal studs or channels. These paths may allow significant sound energy to bypass the airborne path through the sound absorbing material and reduce its effectiveness. This needs further investigation.

SUMMARY

While the most important factors controlling TL in cavity walls constructed with isolated or resiliently coupled leaves are the gypsum board mass and the depth of the cavity, there are some important gains to be made at the lower frequencies by carefully selecting stud spacing and the type of sound absorbing material. The benefits available from using sound absorbing materials with higher flow resistivity and density are evident at the higher frequencies but not at the low frequencies that determine STC and R'_w. The sound absorbing materials tested were selected from commercial materials sold for use in wall and floor cavities. The data presented here suggest that there are factors other than airflow resistance to be considered.

REFERENCES

1 J.D. Quirt and A.C.C. Warnock, INCE 93, p. 971, 1993.

2 "Sound transmission through gypsum board walls - sound transmission results", National Research Council Canada Report No. IRC-IR-693, 1995.

3 ASTM E413

4 ISO 717

LA SONORISATION DES ESPACES PUBLICS, CHOIX ET DISPOSITION DES HAUT-PARLEURS EN PLAFOND ET INTELLIGIBILITÉ

MIGNERON, Jean-Gabriel, *Laboratoire d'acoustique, Faculté d'aménagement et d'architecture, Université Laval, 1 Côte de la Fabrique, Québec, Qué., G1K 7P4*

ABSTRACT: When a sound-reinforcement system is used for communication, information or security, its intelligibility firstly depends on the ambiant noise level, expressed by the signal to noise ratio, and on the initial part of the reverberation (EDT), that is susceptible to affect each syllabe given to ear. A short early decay time depends on the normal reverberation time of the room (RT60) and on the distance of the listeners (located or not in the acoustical radius). The resulting intelligibility depends on the frequency response of the selected speakers, on their directivity following the disposition in the ceiling, the model of the grid and on the density of the speakers (average distance). Acoustical tests have been performed concerning different models of speakers, specially designed for suspended ceilings. These experiments have been done on frequency response, pressure level for 1W and 1m of distance, directivity angle at -6 dB, for a speaker positioned in the middle of a plan baffle, intelligibility index in relation with reverberation time and distance to the listening point and, finally, on a critical listening of female voices. Some interesting conclusions and practical recommandations resulted from these tests.

INTRODUCTION

Indépendamment de la qualité des équipements, de leur réponse en fréquence et de leur niveau de bruit propre, l'intelligibilité des messages distribués par un système de publi-diffusion peut être affectée par deux paramètres acoustiques:

- le niveau de bruit de fond, dépendant de l'achalandage des locaux sonorisés,
- et le temps de réverbération initial susceptible d'affecter le signal entre la source et le receveur. Ce temps de réverbération initial (EDT) dépend globalement du temps de réverbération RT-60 et, plus localement, des conditions de proximité et de directivité de la source.

Comme la décroissance totale du signal entre chaque syllabe prononcée dépend du niveau de bruit de fond et de la vitesse de décroissance de l'énergie acoustique, ces deux paramètres peuvent réduire la dynamique du signal donné à entendre, de ce fait, ils sont souvent exprimés en termes de rapport signal sur bruit, c'est d'ailleurs sous cette forme que l'on peut convertir les pertes de modulation correspondantes en pourcentage d'intelligibilité (exemple de la procédure RASTI) [1].

Le bruit ambiant qui règne dans des locaux publics peut être constitué des bruits techniques toujours présents, auxquels viennent s'ajouter les bruits résultants des activités humaines. Ce bruit vient masquer les messages et en réduire la dynamique, donc l'intelligibilité. Il est généralement admis, indépendamment de l'influence de la réverbération, que, lorsque le niveau de bruit de fond atteint le niveau moyen du signal donné à entendre, l'intelligibilité est réduite à 50%. Or il serait souhaitable que l'intelligibilité reste supérieure à 60%, voire même 65% et plus lorsque la sécurité du public est en jeux. Le niveau de reproduction moyen des messages est d'environ 72 à 75 dB(A) dans les espaces publics sonorisés, alors que le niveau de bruit de fond dépasse souvent 65 dB(A) (dépendant également du temps de réverbération du local). Il convient à certains moments d'élever le niveau du signal, de manière à rétablir une bonne intelligibilité (réglage automatique dans les systèmes les plus modernes). Le temps de réverbération initial, qui peut affecter la vitesse de décroissance du niveau de pression acoustique de chaque syllabe, dépend d'abord du temps de réverbération RT-60. Par exemple, si un local présente un temps de réverbération de 0,25 s à 1kHz, la dynamique du signal permise entre deux syllabes distantes de 50 ms sera de 12 dB, alors que si le temps de réverbération est de 1 s, cette même dynamique tombe à 3 dB. On constate ainsi une réduction significative du niveau de modulation du signal donné à entendre et donc de l'intelligibilité. Le temps de réverbération initial dépend ensuite de la proximité de la source et de sa directivité, ce dernier paramètre affectant la longueur du rayon acoustique dans toute les directions autour de la source. Au voisinage d'un haut-parleur, le temps de réverbération initial peut être relativement plus court que RT-60, ce surtout dans les grands locaux réverbérants.

MARQUE	*MODELE*	*Diam nomi.*	*Puiss. nomi.*	*Niv. 1W/ 1m à 1kHz*	*500 Hz*	*1kHz*	*2kHz*	*4kHz*
Altec	309-8A	8"	16W	95,4	114°	104°	53°	54°
Altec	538-4A	8"	16W	95,9	116°	104°	58°	50°
Altec	409-8E	8"	16W	94,7	115°	95°	62°	46°
Amscott	CO 810	8"	16W	91,8	115°	108°	69°	49°
Bose	32	4"	32W	92,4	112°	116°	84°	81°
Bose	102	4"	25W	94,6	132°	117°	84°	54°
JBL	8140	8"	40W	93,1	115°	97°	73°	49°
JBL	2152	12"	150W	103,3	100°	92°	47°	32°
JBL	P100	4"	40W	91,0	87°	88°	106°	62°
Mc Bride	8LS813-FY5	8"	16W	93,5	114°	104°	73°	53°
Sammisound	CX801 (mod.)	8"	20W	92,0	115°	108°	85°	57°
Sammisound	CX 802	8"	40W	93,1	116°	119°	81°	58°
Sammisound	SPM 602	6"	20W	88,2	115°	61°	90°	103°
Soundolier	CP 802	8"	16W	91,1	116°	134°	79°	40°
Soundolier	C 803	8"	16W	94,2	115°	102°	84°	51°
Soundolier	CF 883	8"	30W	88,0	116°	88°	33°	112°
Soundolier	EQ 818	8"	50W	88,0	100°	65°	83°	40°
Tannoy	ICT 165mm	6"	100W	94,5	100°	100°	90°	50°
Toa	F-120C	5"	20W	95,0	122°	121°	110°	38°
University	CS 815	8"	16W	95,3	115°	104°	58°	58°
MOYENNES				93,0	115°	99°	81°	61°

Tableau Nº1: Description des différents échantillons de HPs.

RÉPONSE EN FRÉQUENCE DES HAUT-PARLEURS

Avec la mise en oeuvre des nouvelles technologies pour le traitement digital du signal audio, on peut considérer que ce

signal peut être amplifié et distribué de façon quasiment parfaite. Pour une voix claire et agréable, il reste donc la qualité de reproduction des haut-parleurs. La réponse en fréquence des haut-parleurs de plafond utilisés pour les systèmes de publi-diffusion est souvent irrégulière. Même, si un haut-parleur présente une réponse dans l'axe pratiquement linéaire, ce n'est pas une garantie d'une écoute agréable de la voix ou de la musique dans toutes les directions.

Lorsque la réponse d'un modèle de haut-parleur installé dans toute une même zone n'est pas complètement satisfaisante, on peut introduire une correction spectrale du signal destiné à cette zone (certains modèles de haut-parleurs sont d'ailleurs distribués avec un contrôleur électronique adéquat). Il n'est pas nécessaire de reproduire à un trop grand niveau les fréquences les plus basses de la voix, qui seront de toute façon perturbées par la réverbération. On peut valoriser les bandes d'octave de 2 et 4 kHz, importantes pour l'intelligibilité, cependant on risque de tomber dans un autre piège, soit que, d'une part, le son devienne nasillard et désagréable et que, d'autre part, la directivité des haut-parleurs pour ces fréquences soit trop prononcée, provoquant ainsi une irrégularité spatiale de l'intelligibilité. Il convient, le plus souvent, pour valoriser l'intelligibilité de la voix perturbée par un certain niveau de bruit de fond, sans affecter par ailleurs son équilibre et sa répartition spatiale, de relever légèrement les fréquences médianes du spectre.

Distance et directivité des haut-parleurs

La directivité d'un haut-parleur varie de façon importante avec la fréquence, elle s'exprime globalement par l'indice de directivité en dB (avec I = 10 logQ), cet indice correspondant à la proportion d'énergie radiée dans l'axe du haut-parleur, dans un bande de fréquence donnée [2]. Un haut-parleur monté en plafond peut être considéré comme sur un baffle plan infini; pour les basses fréquences, la radiation est donc plutôt hémisphérique (la membrane étant beaucoup plus petite que la longueur d'onde, I =3 dB); alors que pour les hautes fréquences, la membrane agit plutôt comme un piston plan et produit une onde plane plus ou moins diffractée, le facteur de directivité peut donc atteindre des valeurs relativement élevées.

Mais l'indice de directivité ne concerne qu'une bande de fréquence précise et il n'est donné que dans l'axe du haut-parleur. Pour un haut-parleur rond, il est plus aisé d'employer l'angle d'ouverture totale à -6 dB, c'est-à-dire l'angle de dispersion pour une fréquence donnée, jusqu'à une atténuation de -6 dB du niveau de pression par rapport au niveau dans l'axe. Les haut-parleurs vérifiés ont, en moyenne, avec leur grille, des angles de dispersion de 115°, 99°, 81° et 61° (500 Hz, 1, 2 et 4 kHz).

Pour la distance entre les haut-parleurs, il est généralement admis que les cônes de dispersion à -6 dB doivent se croiser à la hauteur des oreilles du public, même pour les bandes d'octave de 2 et surtout 4 kHz, si importantes pour l'intelligibilité (atténuation résultante entre deux haut-parleurs d'au maximum 3 dB). La hauteur du plafond a donc également une influence directe sur la distance à respecter entre les haut-parleurs. Sinclair recommande une distance de 1,4 fois la hauteur effective au-dessus des têtes (à 1,8 m du plancher ou bien 1,2m, suivant que le public est debout ou assis) [3].

Tests sur différents haut-parleurs

Un total de 23 haut-parleurs différents ont été testés. Ces tests ne prétendent pas couvrir l'ensemble des produits disponibles, néanmoins, ils donnent un bon aperçu du comportement de ce genre de haut-parleurs destinés aux plafonds suspendus.

Tous les échantillons ont été vérifiés en chambre anéchoïque, ils ont été installés dans leur propre coffret ou bien dans un coffret avec traitement absorbant de 10,6 dm^3, avec un baffle plan de 1,22 x 1,22 m en gypse pour simuler l'effet du plafond et avec une grille conventionnelle en tôle perforée à 33% d'ouverture. Dans la plupart des cas, les haut-parleurs ont été branchés sur une ligne 70V (constamment mesurée par bandes au tiers d'octave), à l'aide d'un tranformateur d'impédance, réglé de manière à obtenir une puissance nominale de 1W RMS dans 8 Ω.

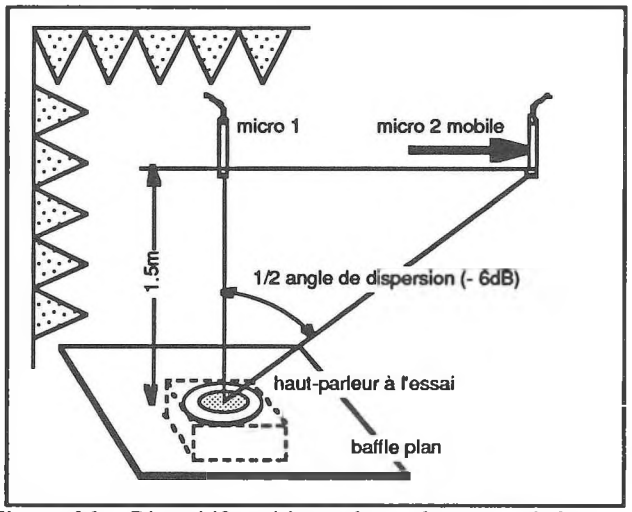

Figure nº 1: Dispositif expérimental pour la mesure de la directivité et du rendement

Les mesures acoustiques ont porté sur les points suivants:

- réponse en fréquence par bandes au tiers d'octave,
- réponse en fréquence par bandes au douzième d'octave,
- niveau de pression en dB(A) dans l'axe du haut parleur, à 1m de distance, à 1W RMS dans 8 Ω,
- niveau de pression en dB à 1m, avec signal sinus à 1kHz,
- angle de dispersion à -6 dB mesuré dans un plan à 1,5 m de distance de la grille du haut-parleur, pour les fréquences sinus de 500 Hz, 1, 2 et 4kHz (voir figure nº 2),
- intelligbilité selon l'indice RASTI en 6 points, selon trois conditions de réverbération (RT-60 = 0,08, 1,0 et 2,7 s).

Complémentairement, une écoute subjective, surtout consacrée à la parole et plus spécifiquement à la voix féminine, a également été mise en oeuvre.

Le tableau nº1 fait état des principales caractéristiques des modèles de haut-parleurs vérifiés, il indique leurs dimensions et leurs puissances nominales, ainsi que divers résultats. La figure nº 1 illustre, à titre d'exemple, le dispositif expérimental utilisé pour les mesures de directivité et de rendement. Les principaux résultats relatifs à la réponse en fréquence, à la dipersion et à l'intelligibilité feront l'objet de la communication orale.

Conclusion

Au plan pratique, il faut s'assurer que toutes les personnes ne se trouvent pas trop éloignées d'un haut-parleur, de manière à rester le plus possible dans le champ direct. En plus d'une puissance suffisante et d'une bonne réponse en fréquence, il importe de choisir la directivité d'un haut-parleur en fonction de la hauteur du plafond et, dans une moindre mesure, en fonction de la réverbération du local. Dans des locaux bruyants aux plafonds les plus bas, on peut éviter par exemple de rapprocher trop les haut-parleurs en choisissant un modèle plus dispersif.

Références

[1] Houtgast, T. and Steeneken, H.J. M.: "The modulation transfer function in room acoustics", pp. 3-13, in B. & K. Technical Review, nov. 1985.

[2] Beranek, L.: Acoustical Measurements-Tests for Loudspeakers, pp.668-672, Pub. for the Acoust. Soc. of Am., 1988.

[3] Sinclair, R: Journal of the Audio Eng. Soc., dec. 1982.

FLANKING IN WAREHOUSE TO RESIDENTIAL CONVERSIONS

D.B. Larson and R.A. Strachan
Brown Strachan Associates
Two Yaletown Square
1290 Homer Street
Vancouver, B.C., Canada. V6B 2Y5

1. Introduction

Brown Strachan Associates have been working on an increasing number of warehouse conversion projects over the past few years. In these projects, warehouses built in the early 1900's are being converted to artist live/work studios or condominiums. The units range from rental units for low-income tenants to luxury condominiums.

The warehouse original construction typically has floors of full cut wood studs on edge (2 x 4 or 2 x 6). Hardwood or fir floor finishes are common. Heavy wood beams and columns form the basic supporting structure. Exterior walls are generally brick. Developers generally wish to retain the wood floor and to expose the wood ceilings.

Structural cross-bracing is required for seismic upgrading in most of the buildings. Both square hollow structural sections and steel cable tension elements have been used for this purpose. These often run continuously between dwelling units.

Several flanking paths have been identified in these projects. The most significant path has been through the continuous wood floors where the wood studs are oriented perpendicular to party walls. This path is particularly noticeable in top floors with a continuous wood roof where the studs are lighter. Flanking through structural cross-bracing and air leaks between studs and at structural penetrations have severely limited the isolation.

The wood stud roofs provide limited isolation from roof decks to top floor suites. Both impact noise and airborne transmission are concerns.

Treatment recommendations have included a concrete topping and isolated drywall ceiling. Partial cuts in the continuous wood floors were investigated where existing wood floor were required for architectural reasons. Generally, drywall ceilings are required to meet the STC 50 Code requirement between spaces in buildings. The Code Section 9.11 "Sound Control" does not cover roof decks.

2. Preliminary Measurements

2.1 Site #1

This project was a conversion to artist live/work studios. The floor construction was full cut 2 x 6 wood studs on edge running perpendicular to the party wall, with maple decking and plaster on the underside. The proposed wall construction was 3 1/2", 25 ga. steel studs, with two layers of 1/2" drywall on each side and 3 1/2" Fiberglas insulation in the cavity. Test data indicated STC 51 and STC 54 for this construction. A test suite was constructed to evaluate the floor and other flanking transmission paths.

Testing indicated that the floor isolation was NIC 30 with low frequency deficiencies between 160 Hz and 250 Hz. The measured wall isolation was NIC 35. Mid frequency deficiencies between 250 Hz and 1000 Hz were attributed to air leaks between the wall and adjacent columns.Vibration measurements indicated that flanking in the continuous floor and roof accounted for the low frequency deficiencies.

Later tests between rooms with an exposed wood roof of full cut 2 x 4's on edge perpendicular to the party wall indicated NIC 35. The isolation at 250 Hz to 300 Hz was only 25 decibels, which is characteristic of coincidence in 2 x 4's. Where the wood studs were parallel to the party wall, NIC 39 was measured, with 32 decibels at 250 Hz to 300 Hz. While these tests were affected at high frequencies by air leaks, they indicate the severe limitation of continuity in 2 x 4's oriented perpendicular to a wall.

2.2 Site #2

Flanking in a continuous wood roof constructed of 2 x 3's on edge was measured in a condominium conversion project. Double stud party walls were used and floors had 2" (nominal) concrete topping. The measured isolation between adjacent suites was NIC 43. High frequency isolation was limited by air leaks while reduced low and mid-frequency performance was attributed to continuity in the roof. Flanking was also present in structural cross-bracing which penetrated the party wall.

A further limitation of the lightweight wood roof was poor isolation from a common roof deck above the suite. The measured noise reduction between the deck and the test suite was NIC 32. High frequency flanking was also present (through exhaust ductwork) but the major limitation was the lightweight construction.

Impact Isolation Class (IIC) tests were not carried out but footstep impacts were clearly audible in the suite below.

2.3 Site #3

Site #3 had a floor construction of full cut 2 x 6's on edge (parallel to the party wall) with a fir finish. The wall plates were supported directly by the 2 x 6's. The party wall construction was a double row of 2 1/2" steel studs separated by a 1" airspace, batt insulation and two layers of 1/2" drywall on each side. Tests indicated that the isolation through the party wall with floor joists oriented parallel to the wall was FSTC 50 and 52. The isolation through the floor was FSTC 34, with deficiencies from 250 Hz to 2000 Hz.

3. Treatment Options

Air leaks were typically sealed with silicone caulking and careful attention to detail.

The transmission loss of the floors was improved to meet the Code STC 50 using a suspended drywall ceiling. The suspended ceiling construction at site #1 (without a concrete topping) was two layers of 1/2" drywall with a nominal 6" air gap. The metal framing was rigidly attached to the existing (12" deep) perimeter beams and the cavity was insulated with R12 home insulation. A central neoprene isolator support was provided on larger spans (15 ft.). The measured isolation was FSTC 52. A concrete topping alone generally increases the rating to about STC 46 and a concrete topping with a single drywall ceiling to about STC 54.

An initial treatment to reduce lateral flanking in the continuous floors was to use a concrete topping. Because of other flanking paths, the effect has not been determined. Provided the concrete is broken at the party wall line, the predicted isolation is about FSTC 50 with a separate stud wall (STC 55).

When a concrete floor topping was considered unacceptable at site #1, a 50% cut in the floor joists was recommended to reduce the bending stiffness to 1/8. A limitation in the cut depth was the (seismic) floor plate integrity. Allowing for a 3 decibel build-up in floor vibration resulting from changed boundary conditions, an improvement of 15 decibels was anticipated in the lateral floor transmission (NIC 35 to NIC 50). Beranek predicts a minimal reduction in reflection losses for a 50% cut based on considerations of the transversal forces, the transversal velocities, the moments and angular velocities on both sides of the junction. After minimizing airborne flanking, NIC 47 was eventually achieved. The difference

between theory and measured results is attributed to the support beam minimizing vertical (shear) motion at the cut but more work is required in this area.

A 100% cut in the floor joists has been recommended at site #3 where the joists run perpendicular to party walls. To maintain the integrity of the floor as a horizontal shear plate, the structural consultant has accepted steel angles between the underside of the floor and the heavy timber beams. This detail has not been tested but experience indicates STC 50 should be achieved.

At site #2, a suspended ceiling in the top floor units was not an acceptable treatment to control footstep noise from the rooftop patios. As an original attempt to control impact noise into the roof, the patios had been built as a 2 x 6 frame spanning between shims located above the existing structural beams, about 15' o.c. The finish was 2 x 4's on the flat. The roof had 3" of styrofoam insulation and the shims were resting on 24" x 24" pavers to spread the load over the insulation. The calculated resonant frequency of the assembly was about 500 Hz due to the very light dead load and high insulation stiffness.

Concrete pavers (24" x 24" x 1 1/2") were investigated as a means of lowering the resonance. Tests were conducted with the blocks directly on the existing deck and isolated from the deck by SCE 41 neoprene strips. The concrete blocks alone reduced footstep peaks above 315 Hz by 3-5 dB. Isolating the pavers with neoprene reduced peak levels by about 10 dB (approximately to background levels), including low frequencies. Eventually, this treatment was considered impracticable.

Airborne flanking through the structural cross-bracing was attenuated by sealing the open ends of the hollow structural sections with drywall and caulking. This treatment also controlled dust migration from the basement. It was suggested that the cross-bracing be filled with sand to provide damping of structure-borne noise. This treatment was not evaluated (because of the volume of sand required in the top floor suite).

4. Conclusions

The most difficult flanking path to treat is lateral flanking through continuous wood joists, where the joists are oriented perpendicular to party walls. Isolation is reduced to about NIC 35 in some cases. A 1 1/2" concrete topping appears to be an effective treatment. Where it is necessary to preserve the existing wood finish, a significant floor cut is necessary acoustically but may not be acceptable structurally. A 100% cut with steel angles attaching the floor to the beams may be an option. This treatment is relatively expensive and requires testing but is justified when considered against the cost of a downtown condominium in a heritage building.

Suspended drywall ceilings have proven very effective to meet STC 50 and may be applied between the existing wood beams to minimize the impact on the heritage look. However, a concrete topping is considered the best fundamental treatment to minimize impact noise and floor "squeaks" in an old building.

Careful attention must be paid to sealing air leaks, particularly where partitions meet structural elements. Flanking paths should be identified and corrected before occupancy to minimize negative reaction from residents.

5. References

DuPree, R. B. (1981), *Catalog of STC and IIC Ratings for Wall and Floor/Ceiling Assemblies With TL and ISPL Data Plots*, Office of Noise Control, California Department of Health Services, California

United States Gypsum Company (1984), *Design Data for Acousticians*

Beranek, L.L. (1971), *Noise and Vibration Control*, McGraw-Hill Inc., New York.

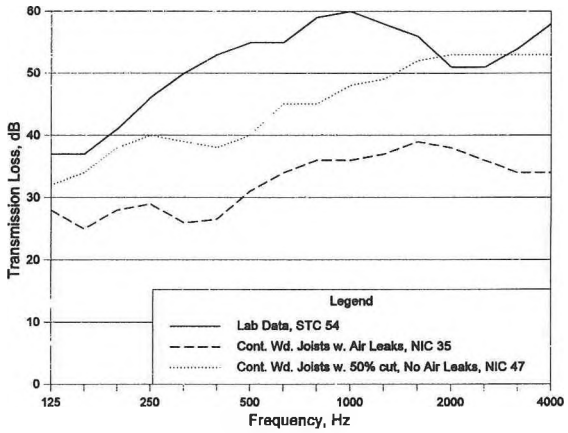

Figure 1: Effect of Flanking on Party Wall Performance

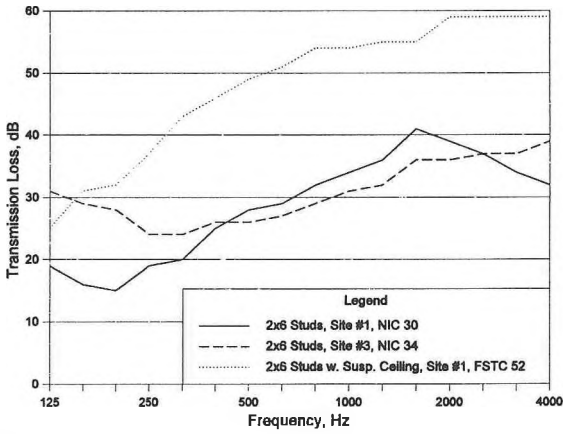

Figure 2: Effect of Suspended Ceiling Treatment

NUMERICAL MODELLING OF FIRE STOPS AT THE INTERSECTION OF FLOORS AND LOAD BEARING PARTY WALLS

T.R.T. Nightingale
Acoustics Laboratory, Institute for Research in Construction, National Research Council Canada, Ottawa Ontario K1A 0R6

Introduction

This is a companion paper to a previously published paper[1] which presented a numerical model for the transmission via a fire stop that coupled two corner joints. The present paper expands upon the previous work allowing for the modelling of transmission via a fire stop coupling two 'tee' joints. The three plates of the 'tee' joints could then be the floor, upper and lower load bearing party walls. The fire stop could be formed by running the floor decking under the upper load bearing party walls. Figure 1 shows a mechanical representation of the system as applied to a double wood stud construction.

Joint Equations

In this paper we will restrict ourselves to a model of simple bending waves and the effects of beams at the joint (in the form of joist headers, sole and head plates) will be ignored. Such a model will tend to predict stronger transmission than would a more complete model, especially at high frequencies. However, the simplified model will enable us to rank order fire stops of various stiffness and to examine the effectiveness of various treatments to the plates.

In deriving the equations for the joint it is assumed that each 'tee' is pinned (i.e., there is no translational motion) and the fire stop that couples the 'tee' joints has only stiffness. If the plates of the 'tee' joints are rigidly connected the following equations of motion can be written,

$$\phi_1 = \phi_2,\ \phi_2 = -\phi_4,\ \phi_3 = -\phi_5, \text{ and } \phi_5 = -\phi_6 \quad [1a]$$

$$M_1 - M_2 - M_4 - M_f = 0 \text{ and}$$

$$M_3 - M_5 - M_6 + M_f = 0, \quad [1b]$$

where φ is the angular rotation, and M is the moment. The subscript indicates the arm of the joint (as per Figure 1) while the subscript 'f' refers to the fire stop material that connects the two 'tee' joints. If the bending wave enters the joint from plate 1 then the following equations define the transverse displacement, ξ, in each arm,

$$\xi_1 = \left(e^{-ik_1 x\cos\theta_1} + T_1 e^{+ik_1 x\cos\theta_1} + T_{n1} e^{+k_{n1}x}\right) e^{-ik_1 y\sin\theta_1}, \quad [2a]$$

$$\xi_2 = T_2 e^{-ik_2 z\cos\theta_2} + T_{n2} e^{-k_{n2}z}, \quad [2b]$$

$$\xi_3 = T_3 e^{-ik_3 x\cos\theta_3} + T_{n3} e^{-k_{n3}x}, \quad [2c]$$

$$\xi_4 = T_4 e^{ik_4 z\cos\theta_4} + T_{n4} e^{k_{n4}z}, \quad [2d]$$

$$\xi_5 = T_5 e^{-ik_5 z\cos\theta_5} + T_{n5} e^{-k_{n5}z}, \quad [2e]$$

$$\xi_6 = T_6 e^{ik_6 z\cos\theta_6} + T_{n6} e^{k_{n6}z}, \quad [2f]$$

where T is the amplitude of the bending wave on the plate indicated by the subscript, the 'n' of the subscript indicates the near field or evanescent wave, k is the wave number for traveling waves, k_n is the wave number for the evanescent waves and θ is the angle of propagation. The displacements given in Equation[2] are related to Equation[1] by,

$$\phi_1 = \frac{d\xi_1}{dx} \text{ and } M_1 = -B_1\left[\frac{d^2\xi_1}{dx^2} + \mu\frac{d^2\xi_1}{dy^2}\right], \quad [3]$$

where B is the bending stiffness of the plate and μ is Poisson's ratio. Equations[1], [2] and [3] represent a set of six simultaneous equations involving the twelve unknown coefficients. Six additional equations are obtained by using the following boundary conditions for pure rotation at the pinned 'tee' joints:

$$T_1 + T_{n1} = -1,\ T_2 + T_{n2} = 0,\ T_3 + T_{n3} = 0,$$
$$T_4 + T_{n4} = 0,\ T_5 + T_{n5} = 0, \text{ and } T_6 + T_{n6} = 0 \quad [4]$$

Now a set of six simultaneous equations can be created to describe the amplitude of the bending waves in each of the six plates. For practical application normal incidence will be considered as a closed-form solution can be obtained. It was shown in a previous study[2] that the normal incidence results for this type of joint over estimate the transmission by about 1.8 dB. We will also assume that plates 2, 4, 5 and 6 are similar (i.e., constructed of the same material). While plates 1 and 3 are similar. Thus the following simplifications can be made,

$$k_2 = k_{n2} = k_4 = k_{n4} = k_5 = k_{n5} = k_6 = k_{n6}, \text{ and}$$
$$k_1 = k_{n1} = k_3 = k_{n3}, \text{ also}$$
$$B_2 = B_4 = B_5 = B_6, \text{ and } B_1 = B_3. \quad [5]$$

Using the general relationship between the joint transmission coefficient and the amplitude,

$$\tau_{12} = \chi^2\psi\left|T_{12}\right|^2 \quad [6]$$

where,

$$k_2 = k_1\chi, \text{ and } B_2k_2 = \psi B_1k_1 \quad [7]$$

one obtains Equations [8], [9], and [10] for the joint transmission coefficient where,

$$\delta = \frac{B_f}{B_1k_1}. \quad [11]$$

The joint transmission loss, R, for the path from plate i to plate j though the fire stop joint is given by,

$$R_{ij} = 10\log\frac{1}{\tau_{ij}} \quad [12]$$

In the special case that all the plates are made of the same material (both χ and ψ are unity) and it can be seen that in the limit that the fire stop is infinitely stiff, the joint transmission loss from plate 1 to all other plates is 12.6 dB. As the stiffness of the fire stop tends to zero, the joint transmission loss from plate 1 to plates 3, 5, and 6 tends to infinity, while the joint transmission

loss to plates 2 and 4 tends to 9.5 dB (i.e., exactly that for a 'tee' joint).

Fire Stop Modelling

The effective bending stiffness of the fire stop material is given by,

$$B_f = \frac{Et^3}{(1-\mu^2)}\frac{1}{d} \qquad [13]$$

where E is Young's Modulus, μ is Poisson's ratio, and *d* is the span of the fire stop. (Typically this is about 25 mm since this is the distance between plates in a double stud wall.)

By examining equations [8], [9],[10], [11] and [13] it can be seen that the transmission across the fire stop can be minimized by,

1. Reducing the apparent stiffness of the fire stop. This can be done by using a thin material, increasing the span, d, between the sole plates, and using a material that has a low Young's Modulus (E);
2. Increasing the bending stiffness of the source plate. (For the case shown this is plate 1. Plate 3 received the same treatment for symmetry.)

Reducing the apparent stiffness of the fire stop may not be practical if the assembly has already been built. However, it is possible to increase the bending stiffness of plates 1 and 3 by adding a concrete topping directly to the exposed floor decking.

To illustrate the potential improvement to the sound isolation Figure 2 shows the predicted joint transmission loss, R in dB, before and after plates 1 and 3 receive a 38 mm thick concrete topping (surface density 91 kg/m^3).

Plates 1 and 3 (floor decking) are 16 mm thick oriented strand board (OSB), plates 2, 4, 5, 6 (party walls) are 16 mm gypsum board. Before the topping the maximum attenuation from one dwelling to the next across the fire stop was between 10 and 15 dB (over the normal building acoustics range 100-4000 Hz). This would most certainly represent a serious flanking path especially if the party walls offer a high degree of sound isolation potential (i.e. double stud construction).

However, the model indicates that increasing the bending stiffness of the source plate by adding a topping can greatly reduce transmission across the fire stop from plate 1. The joint transmission reduced by at least 15 dB, and at least 20 dB for frequencies where the flanking surfaces can efficiently radiate.

Conclusions

The simple model for transmission across a fire stop connecting two 'tee' joints has shown that fire stops should not be formed from continuous surfaces. However, structural requirements may force connections between dwellings by continuous surfaces. In such cases, greatly increasing the bending stiffness of the exposed surfaces can significantly improve sound isolation. This may be a practical solution for both new constructions and retro-fit situations.

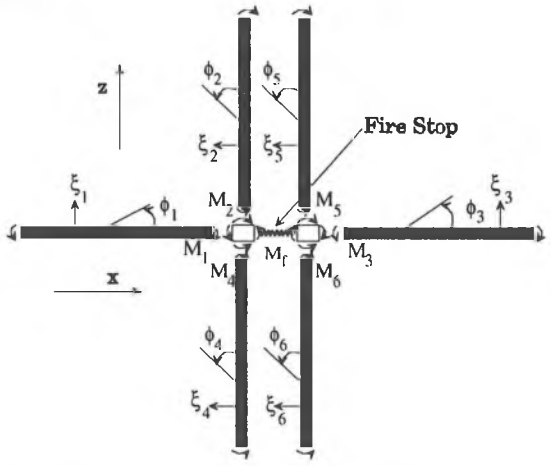

Figure 1: Mechanical representation of the joint.

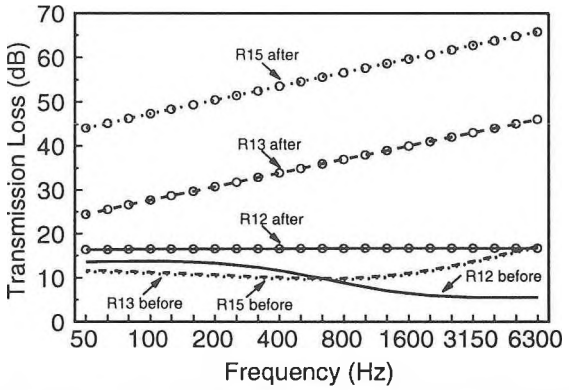

Figure 2: Predicted transmission loss for the various plates with and without a 38 mm thick concrete topping applied to the OSB floor decking.

$$\frac{1}{\tau_{12}} = \frac{1}{\tau_{14}} = \frac{2\psi\left(\delta^2 - 2\delta\psi - 4\delta + 2\psi^2 + 8\right)}{\left(8 + 9\delta^2\psi^2 + 8\psi^4 + 40\psi^3 + 66\psi^2 + 40\psi + 9\delta^2 + 18\delta^2\psi - 12\delta - 12\delta\psi^3 - 42\delta\psi^2 - 42\delta\psi\right)} \qquad [8]$$

$$\frac{1}{\tau_{15}} = \frac{1}{\tau_{16}} = \frac{2\psi\delta^2}{\left(8 + 9\delta^2\psi^2 + 8\psi^4 + 40\psi^3 + 66\psi^2 + 40\psi + 9\delta^2 + 18\delta^2\psi - 12\delta - 12\delta\psi^3 - 42\delta\psi^2 - 42\delta\psi\right)} \qquad [9]$$

$$\frac{1}{\tau_{13}} = \frac{2\delta^2}{\left(8 + 9\delta^2\psi^2 + 8\psi^4 + 40\psi^3 + 66\psi^2 + 40\psi + 9\delta^2 + 18\delta^2\psi - 12\delta - 12\delta\psi^3 - 42\delta\psi^2 - 42\delta\psi\right)} \qquad [10]$$

[1] Nightingale, T.R.T., Craik, R.J.M., "Numerical modelling of wood frame joints having fire stops," Canadian Acoustics, Vol. 29 No. 3, pp. 29-30. 1994.

[2] "Sound transmission through framed buildings", Internal Report IRC-IR-672, Institute for Research in Construction, National Research Council Canada, May 1995.

DEGRADATION OF WOOD STUD WALL SOUND ISOLATION BY ELECTRICAL BOXES

T.R.T. Nightingale, J.D. Quirt

Institute for Research in Construction, National Research Council, Ottawa, Ontario, K1A 0R6.

This paper presents a brief summary of a recent study that examined how sound isolation of wood stud walls was degraded due to penetrations formed by electrical outlet boxes. The walls included double wood stud, staggered stud, and single stud constructions. For this brief summary paper, we restrict ourselves to results for double wood stud walls and only STC ratings are reported. This summary further focuses on the main factors affecting the sound isolation: box location, box type, cavity absorption and baffles. Other factors, such as modification of the electrical boxes and the effect of outlets in other types of walls will be presented in a subsequent report.

Test Specimens and Test Method

The basic walls (i.e. without penetrations) provided a sound isolation greater than STC 50, and also have a one-hour fire resistance rating. The electrical boxes were positioned with the bottom of each box approximately 300 mm from the bottom of the wall. Outlets were wired to simulate normal field installation. The sound isolation tests were conducted in accordance with the requirements of ASTM E90-1990 and the single number STC rating was obtained using ASTM E413.

There are several electrical box locations depending on the framing of the wall. The wall details, the box locations, and the nomenclature to identify box locations are given in Figures 1(a) through 1(c).

Test Procedure

For each type of framing, a "base case" wall specimen was constructed with no penetrations and the measured sound isolation was compared to previously tested walls of nominally identical construction. Good agreement was obtained in all cases. Then the gypsum board was removed and saved for later re-installation.

The electrical outlet boxes and associated wiring were installed in accordance with the Canadian Electrical Code. Holes were cut in the gypsum board to accommodate the electrical boxes, and the gypsum board was re-installed. The openings in the gypsum board for each outlet were masked with heavy covers, and the sound transmission was re-tested. In all cases, the difference between the result with all outlets masked and that with no penetrations was less than the known repeatability associated with removing and replacing a layer or layers of gypsum board.

Electrical outlets and normal cover plates were then installed and tested for each outlet configuration in turn, with the other outlet positions masked.

When comparing the measured sound isolation performance of two assemblies expressend in terms of STC, it is important to realize that due to errors in repeatability and the round-off of the individual TL data in calculating the STC rating, a difference of one STC point should not be considered significant. A difference of two is probably significant, while three or more is a clear indication of different sound isolation performance.

Effect of Box Type

Two types of boxes were investigated: standard metal boxes and plastic air-barrier boxes. The two are fundamentally different by design. The plastic air-barrier box has few penetrations and those that exist (for electrical cables) have a closed-cell foam gasket. The plastic box also has a flange and gasket designed to form an airtight seal with the back face of the gypsum board.

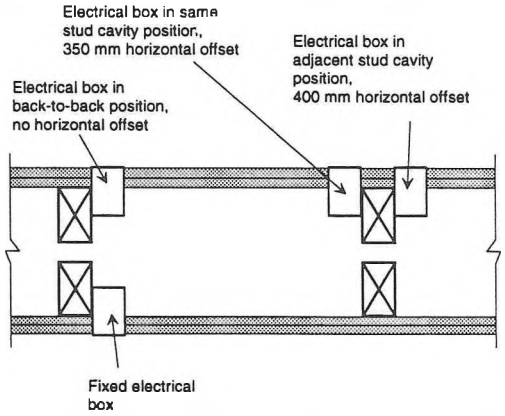

Figure 1(a): Positions of the electrical boxes in the double stud wall having double wood studs 400 mm o.c., separate head and sole plates separated by 25 mm, two layers 12.7 mm regular gypsum board on either side.

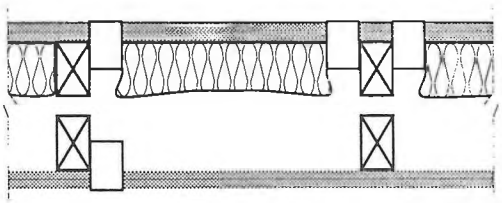

Figure 1(b): This construction was the same as in Figure 1(a), but with 90 mm glass fibre batt displaced around the electrical boxes in the stud cavity.

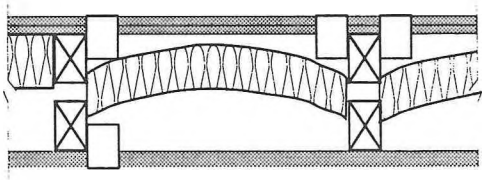

Figure 1(c): This construction was the same as in Figure 1(b), but with 90 mm glass fibre batts installed against the studs and covering the backs of the outlet boxes

Table 1 shows the measured sound isolation for a double wood stud wall as a function of the two box types for the two extreme

locations. The plastic air-barrier provided consistently better sound isolation than the untreated metal boxes, especially in the back-to-back configuration. The results indicate that if the boxes are airtight then there is negligible sound transmission through the boxes, and placement is not critical. Similar performance was obtained when the standard metal boxes were treated to make them air tight, (as will be presented in a subsequent detailed report).

COMPARISON OF BOX TYPE		Electrical Box Location	
Box Type	Base Case	Back to Back No offset	Adjacent Cavity 400 mm offset
Metal	55	51	53
Plastic	55	55	55

Table 1: Measured Sound Transmission Class (STC) for standard metal boxes and plastic air-barrier boxes in a double wood stud wall without cavity absorption. See Figure 1(a).

Box Placement and Cavity Absorption

Table 2 shows the change in sound isolation relative to the base case for various locations of the untreated metal boxes. From the table it is immediately obvious that the effect of electrical boxes on the sound isolation of a party wall can be large — degradations of up to 6 STC points were experienced for poorly located boxes.

The reduction in the sound isolation depends on several factors: the separation (horizontal offset) of the electrical boxes and the location of absorptive material.

METAL ELECTRICAL BOXES		Electrical Box Location		
Cavity Absorption	Base Case	Back to Back (no offset)	Same Cavity (offset 350 mm)	Adjacent Cavity (offset 400 mm)
None	STC 55	- 4	- 6	- 2
90 mm displaced	STC 61	- 6	-1	- 0
90 mm	STC 62	- 1	- 1	- 1

Table 2: Wall sound isolation (expressed as STC or change in STC relative to the base case) for walls with untreated metal boxes at various locations.

The greatest reduction of the STC occurred when there was a short unimpeded path between boxes — that is, the sound did not have to travel through the cavity absorption or through the narrow gap between studs into the next cavity. However, when the sound must travel through the absorption (i.e., all other absorption cases), the impact of box location is greatly reduced.

Very little reduction of the STC was evident for walls that have the electrical box in the adjacent stud cavity position (at least 400 mm from the fixed box) when there was absorption in the cavity. The combination of absorptive material and a horizontal offset greater than the stud separation ensures the outlets have minimal effect. The trend of increased sound isolation with increased separation may not hold true if there is no cavity absorption and standing waves can form in the cavity.

Table 2 shows the change in sound isolation for the double stud wall with cavity absorption installed in two ways: displaced around the side of the box (Figure 1(b)) or placed completely over the back of the box (Figure 1(c)). The table shows that for boxes located in back-to-back positions, having the layer of insulation between them greatly reduces the impact on the STC.

Cavity absorption reduces the effect that poorly placed electrical boxes have on the sound isolation of a party wall especially if the absorption is placed so it covers the backs of the boxes.

Gypsum Board Baffle

Often 'better building practice guides' recommend the use of gypsum board baffles to improve both the fire and sound resistance of wall assemblies having penetrations. Figure 2 shows a possible installation. In the specimen tested the gypsum board baffle extended from the sole plate to a height 300 mm above the box.

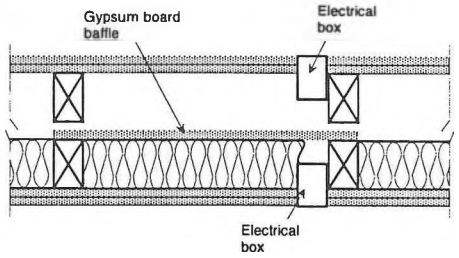

Figure 2: Sketch of a baffle for a double stud wall. Note that the structural isolation between the two faces is preserved.

Table 3 shows that the acoustical effectiveness of the baffle depends on the the presence of cavity absorption. This is to be expected since the cavity absorption controlls the reverberant field in the cavity and a baffle will only be effective if the reverberant energy is much less than that travelling directly between the two outlets. Consequently, reducing the direct component with the use of a baffle will only provide marginal improvement without absorption.

METAL ELECTRICAL BOXES		Back-to-Back Box Location	
Cavity Absorption	Base Case	No Treatment	Baffle
None	55	51	52
90 mm displaced	61	55	62

Table 3: Wall sound isolation (expressed as STC) with and without the gypsum board baffle shown in Figure 2.

Conclusions

Well-sealed electrical boxes offer better sound isolation performance than standard metal boxes. Where possible, electrical boxes should be suitably offset, preferably by at least 400 mm. Cavity absorption can be very effectively used to reduce any impact, especially if the absorption is placed so that it covers the backs of the boxes.

A SUMMARY OF THE CEN DRAFT BUILDING ACOUSTICS MODEL APPLIED TO A LIGHTWEIGHT DOUBLE LEAF CONSTRUCTION

T.R.T Nightingale
Institute for Research in Construction, National Research Council, Ottawa, Ontario, K1A 0R6.

Introduction

This paper is a summary of an existing paper1 illustrating how the draft CEN Building acoustics model, Estimation of acoustic performance of buildings from the performance of products; Part 1: Airborne sound isolation between rooms2, might be applied to the lightweight multi-leaf constructions of North America.

The CEN model, originating in Europe, was designed to be applied to buildings formed from heavy monolithic concrete or masonry elements. It allowed for the description of transmission via flanking paths in terms of the transmission loss of the individual building elements (either measured or predicted) and a simple expression for the joint. The CEN model defines the flanking sound reduction for path ij as R_{ij} ,

$$R_{ij} = \frac{(R_i + R_j)}{2} + K_{ij,situ} + 10\log\frac{S_o}{L_{ij}L_o} \qquad [1]$$

where

$$K_{ij,situ} = \frac{D_{ij} + D_{ji}}{2} + 10\log\frac{L_{ij}L_o}{\sqrt{S_i S_j}} \qquad [2]$$

where R_i and R_j are the resonant transmission losses of building element i in the source room and element j in the receive room. K_{ij} is the joint factor, D_{ij} and D_{ji} are the velocity level differences, S_o is the area of the nominally separating element, S_i and S_j are surface areas of the elements in the flanking path, L_{ij} is length of the joint, and L_o.is 1 metre.

Application to a flanking path

In this paper the CEN model will be applied to the lightweight multi-leaf construction shown in Figure 1. The dominant flanking path involves propagation from the source room 'A' to the receive room 'B' entirely via the side or flanking wall. Since this is a double wood stud wall there are two possible paths. Using the CEN nomenclature for flanking paths, there are Ff and F'f'. By inspection the path F'f' is considerably more direct than Ff, especially if the path of energy transport is the gypsum board cladding. Equation [1] would indicate that an idea of the relative importance can be obtained by considering the sound reduction of the elements F and F' which are shown in Figure 2. Clearly the path Ff is of negligible importance compared to F'f'. There is also a possible path involving the cavity, but since the cavity was completely full of absorption offering no direct line-of-sight, this path is not considered important.

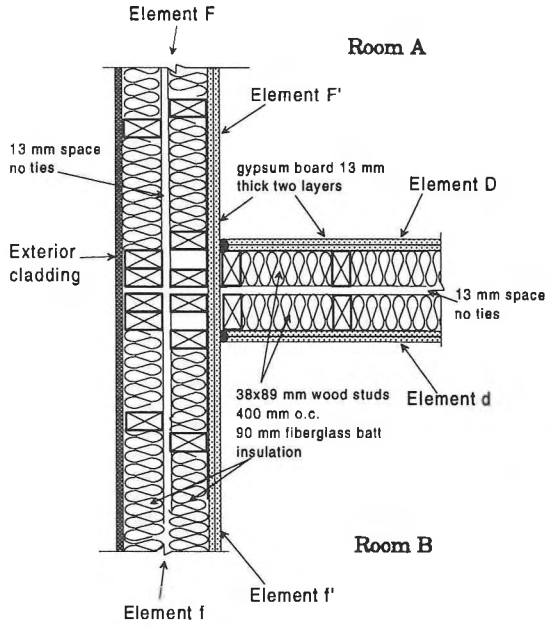

Figure 1: Plan section through the party and flanking walls.

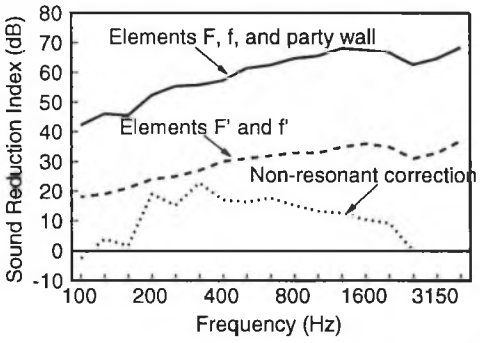

Figure 2: Measured sound reductions (using ISO 140) for the elements and the non-resonant correction for F' and f'.

Joint factor $K_{F'f'}$ for path F'f'

The effect of the 'tee' joint between the flanking and party wall must be considered. In order to use the joint equations given in Annex E[2] one must decide the type joint model that best suits the case at hand and the effective masses of the elements. If path F'f' is the dominant flanking path then, by examining Figure 1, the following can be written,

$$m_d = 2m_{F'} = 2m_{f'} \qquad [3]$$

where m is the surface density of the element indicated by the subscript. Figure 3 shows the CEN prediction for the joint factor K_{ij} for the two types of joints and the joint factor calculated from measured velocity level differences using equation [2]. The CEN

joint factor for the intersection of two double leaf walls (equation E7[2] agrees well with the measured if the mass of the flanking wall is taken to be half that of the party wall (equation [3]). Treating the joint as the intersection of a double leaf wall and a homogeneous wall (equation E6[2]) underestimates the joint factor.

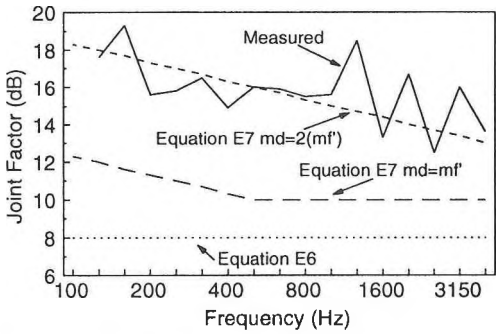

Figure 3: Measured and predicted joint factor K_{ij} using Annex E[1] and relationship given in Equation [3].

Sound reduction for the path F'f'

Having obtained a suitable model for the joint, the sound reduction for the flanking path F'f' can be determined using equation [1] and the measured sound reduction shown in Figure 2. Figure 4 shows the measured, SRI_{Meas}, and predicted sound reduction, SRI_{CEN1}, for the flanking path F'f'. The figure shows that the CEN model grossly underestimated the SRI for the path F'f' for frequencies less than the critical frequency (f_c=2900 Hz). The underestimation occurs because the SRI of the standard test methods is the sum of two transmission types: resonant and non-resonant. (Greatly simplified, resonant transmission dominates for frequencies above the critical frequency while non-resonant transmission dominates below the critical frequency.) Since, flanking transmission occurs through resonant transmission, the non-resonant component present in the standard test method SRI data represents a fictitious source of energy for frequencies below the critical frequency.

Figure 4 shows, that for lightweight constructions where the critical frequency is likely to occur in the middle of the building acoustics range, it is necessary to remove the non-resonant component from the input SRI data. Currently, there is no analytic method for obtaining the resonant transmission of a lightweight multiple leaf assembly. The closest might be SEA.

Determining the sound reduction for path F'f'

Providing details on obtaining the resonant component from measured data is beyond the scope of this summary paper and the reader is referred to a previous publication[1]. Figure 2 shows the non-resonant correction that must be added to the sound reduction data obtained from standard test methods for the elements F' and f' in order to give an estimate of the resonant SRI. The computed resonant SRI, the calculated joint factor K_{ij}, and equation [1] were used to estimate the SRI for the path F'f'. The results are shown as labeled as SRI_{CEN2} in Figure 4. When a reasonable estimate of the resonant SRI is used, the predictions are in quite good agreement with measured results. Differences between measured and predicted are likely due to experimental uncertainties and assumptions made in determining the resonant correction.

Net sound reduction

The net sound reduction between rooms A and B is given by summing the transmission coefficients of the direct path and all the flanking paths. For this case the paths are: Dd, F'f', F'd, and Df'. Figure 5 shows the two predictions, SRI_{CEN1} and SRI_{CEN2}. The measured data SRI_{meas} is included for comparison. The CEN prediction that made use of the non-resonant correction, SRI_{CEN2}, is in good agreement with measured results throughout most of the frequency range. However, the prediction that did not make use of the non-resonant correction, SRI_{CEN1}, consistently under estimates the net SRI for frequencies less than the critical frequency.

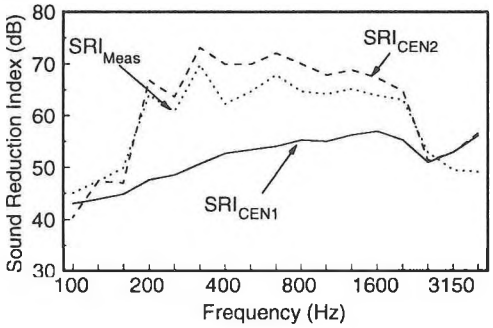

Figure 4: SRI for path F'f'. Measured: SRI_{Meas}, CEN prediction using standard test method SRI data: SRI_{CEN1}, CEN prediction using computed resonant SRI data: SR_{ICEN2}.

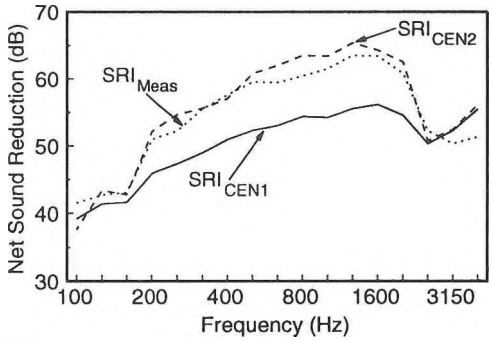

Figure 5: Net SRI between Rooms A and B. Measured: SRI_{Meas}, CEN prediction using standard test method SRI data: SRI_{CEN1}, CEN prediction using computed resonant SRI data: SRI_{CEN2}.

Conclusions

The accuracy of the CEN model to predict either the flanking or the net sound reduction depends on the ability of the user to identify the dominant flanking paths, select the best joint model, and obtain a reasonable estimate of the resonant sound reduction for the flanking elements.

---

[1] T.R.T. Nightingale, "Application of the CEN draft building acoustics model to a lightweight double leaf construction," accepted Applied Acoustics.

[2] CEN/TC126/WG2 N96, "Estimation of acoustic performance of buildings from the performance of products; Part 1: Airborne sound isolation between rooms," Sixth working draft, 1993.

ACOUSTIC DESIGN OF THE NEW FORD THEATRE, VANCOUVER

John C. Swallow
John Swallow Associates
250 Galaxy Boulevard
Etobicoke, Ontario
M9W 5R8

1.0 INTRODUCTION

The new Ford Theatre, Vancouver, is an 1800 seat venue intended for musical theatre - Broadway shows. The building is being built by Live Entertainment Corporation of Canada, designed by Moshe Safdie and Downs Archambault- project manager Kofman Engineering, and will open in November 1995 with "Show Boat". The auditorium has a dress circle and balcony both of which wrap around the sides. The stage is rectangular with a large proscenium and the orchestra pit is designed for 80 players.

2.0 THEATRE FUNCTION

As a musical theatre it is intended for live music, song and drama with voice and music being of approximately equal importance. All shows will be either reinforced or amplified with a sound system being provided by the show. Consequently a very low background sound level is not necessary because the reinforcement easily allows for adequate signal - to - noise ratio. As voice and music are approximately of equal acoustical importance the reverberation time would be a compromise between the shorter times required for the voice speech intelligibility and the longer times desirable for music. It would also be possible to design for a short reverb time for speech and use electronics to provide the longer reverb times when desired. However, it is the preference of all associated with the venue and the show to use the acoustics of the room to provide the longer reverb time and, so, the design of the auditorium reflects this.

Similarly a house sound system could provide surround sound - lateral reflections, colour etc. However, shows usually do not want to use a house system but would rather provide their own systems: usually stage-mounted speakers right and left, and possibly a central cluster, effects speakers on walls and rear and under-balcony infill. Again the theatre has been designed to use the acoustics of the room as much as possible and consequently reflecting surfaces have been set up to aid voices from on stage and music from the orchestra pit.

Finally, several potential problems were dealt with by the architectural team in a way that not only solved the problem but provided desirable features.

3.0 THEATRE DESIGN

The auditorium is 29m wide at the rear, narrowing at the front to 27m with gently curved side walls. The furthest seat is 27m from the stage apron. The dress circle and balcony both wrap around the sides of the auditorium and are narrow with only 7 rows of seats at the rear and two at the sides. The dress circle rear seats are 6.3m from the balcony edge while the opening is 3.8m deep. The proscenium opening is 9 x 15.3m]. The proscenium opens gradually to the auditorium using two sets of angled reflectors. The reflectors are 3.050 and 2.750m wide respectively and extend to the full height of the proscenium. They are nominally 18 and 21m apart opening out into the room which is 27m wide at the front. Similarly two reflectors are located in the front of the proscenium at the ceiling making a gentle transition between the proscenium arch and the ceiling surface. The stage is 32m wide x 16m deep and is clear to allow complete flexibility in the use of flown and moving sets.

4.0 EXTERIOR NOISE

Exterior noise such as traffic, distant aircraft and even rainfall have been dealt with by providing a double shell construction. The stage house is double wythe concrete block construction while the auditorium side walls are poured concrete. The exit stairwells are outside of this concrete providing a large space between the concrete and exterior cladding. Above the exit stairwells is concrete block with exterior cladding. The roof is metal over insulation and concrete. Extra insulation has been added between the metal and concrete to deal with rainfall impact noise. The ceiling below is suspended providing some additional transmission loss but does contain openings. Lobbies separate the rear of the auditorium from the street while tandem doors separate the auditorium from the lobby.

5.0 REVERBERATION

The deliberately long reverberation time implies less sound absorbing material and more concentrated placement. Consequently sound absorption of the seating and carpet has been somewhat reduced, with upholstered seats and backs, but hard seat back panels and reduced carpet absorption. The ceiling is comprised of panels but lighting openings have been left open to the ceiling plenum. Sound absorbing material has been deliberately placed on the side walls at the rear. The rear side walls are treated with panels with large slots and deep batt insulation covered by open cloth. Soffits have been treated with single layer gypsum board in order to provide more low frequency absorption and spectral balance. Provision has been made in the rear wall for the additional sound panels (if needed for future shows) on well-defined flat surfaces. However, no sound absorption is included in the present design.

6.0 REFLECTIONS AND DIFFUSION

The large proscenium side surfaces incorporate two panel reflectors to direct stage sound from loud speakers and voice more towards centre and rear audience. The panels are each about 3m deep and full height, although openings are provided for lighting. The proscenium arch panel reflectors, also each 3m deep and full width, are placed to direct centre stage voice and orchestra pit sound to the rear orchestra and dress circle seating.

For structural reasons the ceiling is inherently a longitudinal barrel vault. The entire suspended ceiling is comprised of individual panels following the line of the barrel vault. The panels are sloped as reverse splays to direct sound down more to the front to the centre orchestra seating.

All of the above panels have been curved to distribute the reflected sound, to provide multiple reflections at each of the seats and to promote diffusion within the reverberant field. Curving the ceiling panels (about a transverse axis) removes the focus of the barrel vault and diffuses ceiling reflections.

The rear wall follows the natural curve of the seating arranged to face the stage. To avoid the focusing and provide future locations for sound panels the profile has been made saw-toothed. The balcony and dress circle soffits have been given a gentle concave curve, not enough to focus on the seating, but which tends to take rear wall reflections and direct them down to the seating below.

7.0 DESIGN EVOLUTION

The ceiling reflector panels provide an example of how an acoustic difficulty combined with an architectural need evolved into a desirable feature for the venue. The original smooth barrel vault ceiling was seen as a problem for focusing while the architect wished to introduce some texture into the ceiling surface. The structure above is transverse arches. The architect also liked the ideal of downstanding ribs which would tie together architecturally the false columns on the sides. The suggestion of suspended panels allowed the architect to put the panels between the downstanding ribs thus giving texture. Of course, the downstanding ribs where kept short. The panels where then sloped downwards to the rear to provide improved reflections and curved to give more texture and diffuse reflections. To pick up on other aspects of the design the architect wished to make the panels "S" shaped with half of the panel concave. It was possible to accommodate this acoustically by moving the inflection point forward to the quarter point so that the impression of an "S" curve is maintained but the actual amount of concave surface is minimal. Further, the concave surface is almost entirely shadowed regarding sound originating from the stage by the downstanding rib. The use of panels made it easy to provide openings for HVAC diffusers, house and stage lighting and these openings, in turn, are treated as part of the acoustic absorption of the room.

8.0 THE NEW FORD THEATRE

The New Ford Theatre will be an extremely valuable addition to the cultural and entertainment environment in Vancouver. The owners and operators prefer natural acoustics and have worked closely with the acoustic consultant to achieve this goal.

SCALE-MODEL EVALUATION OF THE EFFECTIVENESS OF NOVEL ABSORBER TREATMENTS FOR INDUSTRIAL NOISE CONTROL

Murray Hodgson

Occupational Hygiene Programme and Department of Mechanical Engineering,
University of British Columbia,
2324 Main Mall, Vancouver, BC V6T 1Z4.

1. Introduction

Sound fields in industrial buildings are often controlled by the installation of arrays of baffles suspended from the building roof. The performance of baffle arrays covering the complete ceiling area has recently been evaluated using scale-modeling and ray-tracing techniques [1]. It is clear that such baffle arrays can reduce steady-state sound pressure levels and reverberation times (RT) significantly. Unfortunately, the treatments are also often expensive, since large areas of ceiling are covered. Furthermore, the effectiveness may be reduced by the fact that the ceiling baffles are located a long way from sources and receivers on the floor. This report summarizes the results of further scale-model tests aimed at evaluating novel local-absorber treatments, which are less extensive and expensive and, thus, potentially more cost-effective than traditional treatments.

2. Scale model

The 1:8 scale model of an idealized typical industrial workroom was built. It had a length of 30 mFS (FS = full-scale equivalent value), a width of 15 mFS and variable height (5 or 10 mFS). The floor of the model was made of painted concrete. Its walls were made of varnished 12 mm plywood. Its flat roof was of varnished 3 mm plywood. The average absorption coefficient of these surfaces was about 0.06 at all test frequencies, values typical of real factories at all but the lowest frequencies. The model was fitted with 12, 2mFS-cube varnished wooden boxes located randomly over the floor area.

3. Measurements made

Measurements were made of sound decay / RT and of sound propagation (SP - the variation with distance of the difference between the sound pressure level and the source sound power level) in third-octave bands from 800-20000 Hz (100-2500 HzFS). The sound source was a 75-mm-diameter tweeter loudspeaker. A rigid cone narrowing from 75 mm to 3 mm was attached to the tweeter. This resulted in a compact source which was omnidirectional even at the highest test frequencies. Its constant output sound power was measured in an anechoic chamber. A B+K 4135 1/4" microphone was used as the receiver. In each test, sound decays were measured at 4 source/receiver positions and the results averaged. For SP testing the source was located 5 mFS from one end wall, at half width and at a height of 1 mFS. The receiver was at half width and at a height of 1.5 mFS; sound pressure levels were measured at source/receiver distances of 1, 2, 5, 10, 15, 20, 25 mFS. Octave-band SP levels were derived from the third-octave results. Measurements were made using a Nortronics 830 real-time analyser. Air absorption was not scaled and was, therefore, excessive at higher frequencies.

4. Treatment test configurations

Test absorbent treatments were made from 6-mm-thick glass fibre. The diffuse-field absorption coefficient of a large sample of the material located against a hard backing was measured to vary from 0.27-0.78 over the test frequency range. The following configurations were tested:

a. Variable-height baffles - roof heights of 5 / 10 mFS; full-coverage baffle array suspended from the roof at various heights. The aim was to see if full-coverage baffle arrays are more effective if suspended closer to sources and receivers on the floor;

b. Ceiling baffles vs wall absorption - roof heights of 5 / 10 mFS; no absorption / full-height, full-coverage baffle array (168 mFS^2 of absorbent material) / absorbent material fully-covering the side walls (300 and 600 mFS^2 of absorbent material) / both ceiling baffles and wall absorption. The aim was to see if wall or ceiling absorption is most effective;

c. Full vs partial wall coverage - 10 mFS roof height; with / without full-coverage ceiling baffles; with full- / partial- (50% - in a checkerboard pattern) coverage wall absorption. The aim was to see if absorbent patches are particularly cost-effective;

d. Partial-coverage ceiling baffles - 10 mFS roof height; full-height ceiling baffles extending full width but covering only 50 / 75 / 100% of the ceiling, starting at the source end. The aim was to see if, in the case of sources located at one end of a workroom, not applying ceiling treatments at the other end is cost effective;

e. Flat local suspended absorbers - 10 mFS roof height; as shown in Figure 1, flat, square absorbers, with / without rigid backing, with dimension 2 / 3 / 4 mFS and heights of 2 / 3 / 4 mFS located directly above the source. In some tests 1-mFS-high sound-reflecting barriers were located around and 1-mFS away from the source in an attempt to reflect sound into the absorbent material, making it more effective;

f. Novel local suspended absorbers - 10 mFS roof height; a number of configurations of novel local suspended absorbers, located directly above the source with bottoms at 2 mFS. As shown in Figure 1, these consisted of partial boxes — with / without internal absorbent dividers — and pyramids, and inverted cones and pyramids, made of absorbent material. In some tests 1-mFS-high sound-reflecting barriers were introduced, as above.

5. Results and conclusions

In general results were different for SP and for RT. SP results depended on source/receiver distance. Trends were difficult to discern at short distances, and at lower frequencies - presumably due to wave effects.

a. Variable-height baffles - the height of a full-coverage baffle array had negligable effect on both SP and RT;

b. Ceiling baffles vs wall absorption - Combined ceiling and wall absorption gave lower SP levels than did ceiling baffles, which gave lower levels than (5 mFS height), or similar levels to (10 mFS height), wall absorption. Given the relative treatment areas, the ceiling treatment was generally most cost-effective. In both cases, the RT decreased in proportion to the amount of absorbent material introduced;

c. Full vs partial wall coverage - SP levels were lower with ceiling baffles and full wall absorption. Again, the RT decreased in proportion to the amount of absorbent material introduced. Applying absorbent material in patches is not particularly cost effective;

d. Partial-coverage ceiling baffles - SP levels at all distances decreased significantly with introduction of 50% coverage, then further decreased slightly with increased coverage. Again, RTs decreased in proportion to the amount of absorbent material introduced. Smaller coverages are more cost-effective at reducing SP levels, but not RTs;

e. Flat local suspended absorbers - Decreased height, increased lateral extent and the presence of reflecting barriers reduced SP levels slightly. The presence of a rigid backing increased levels near the source. Generally the treatments were ineffective at reducing RT;

f. Novel local suspended absorbers - These absorbers were generally more effective than flat absorbers. Partial boxes with absorbent dividers were most effective at reducing SP levels. Generally the treatments were only marginally effective at reducing RT.

Figure 2a compares 1000-Hz SPs measured in the model workroom with no absorption / local flat absorber / full-height, full-coverage ceiling baffles / local divided box. At short distances, the local absorbers were more effective than ceiling baffles - the divided-box configuration was much more effective than the flat one. At large distances the divided-box and the full ceiling baffles were most effective.

Figure 2b compares RTs measured in the model workroom with no absorption / full-height, full-coverage ceiling baffles / flat local absorber and reflecting barriers / open pyramid with reflecting barriers. At all frequencies full baffles were more effective than local absorbers. The open pyramid was more effective than the flat absorber.

References

[1] M. R. Hodgson, M. V. Eldada and L.- P. Simard, "Evaluation of the performance of suspended baffle arrays in typical industrial sound fields - Part I: Scale-model experiment. Part II: Prediction", *J. Acoust. Soc. Am.* **97** (1), 339-354 (1995).

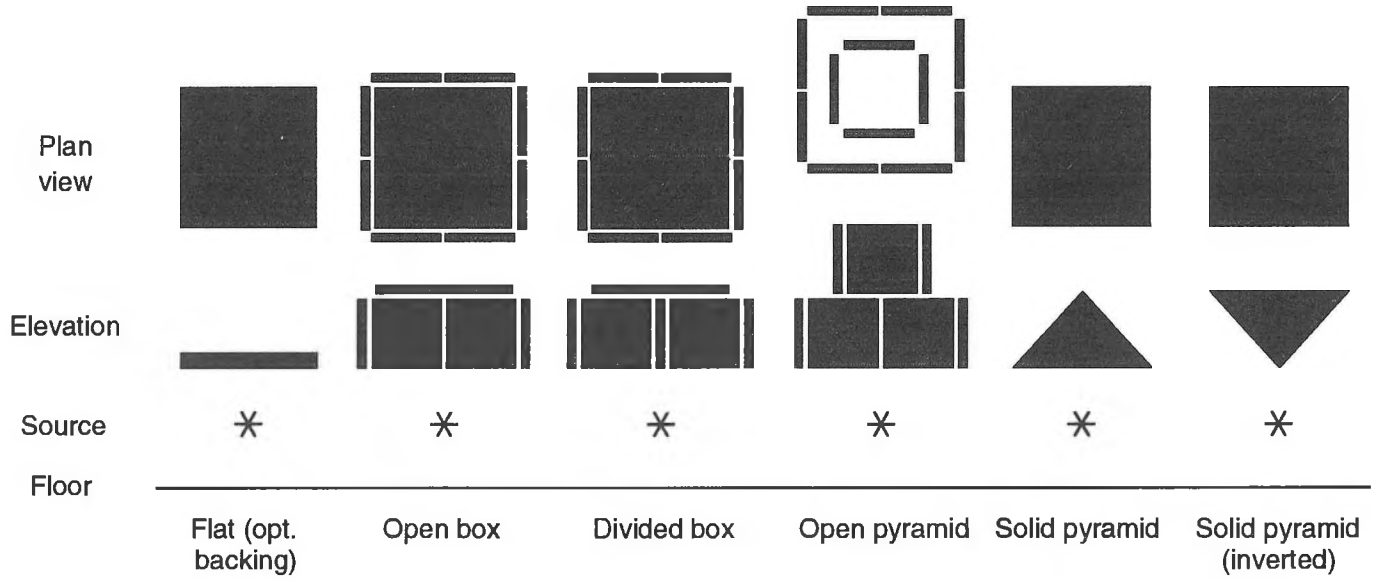

Figure 1. Illustration of the flat and novel local absorbers.

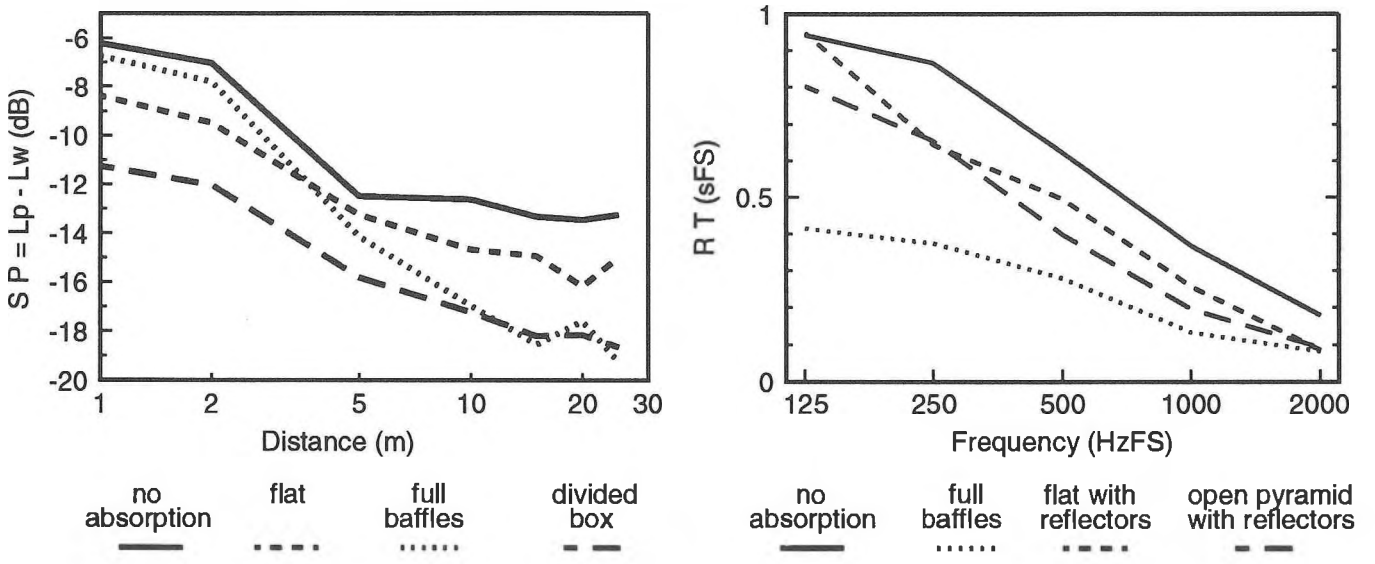

Figure 2. Results of measurements in the fitted 10-mFS-high scale-model workroom without and with absorbent treatments as shown above: a) 1000-HzFS SP; (b) third-octave-band RT.

INCREDIBLE VERSATILITY

At Only 2.2 lbs.

RION

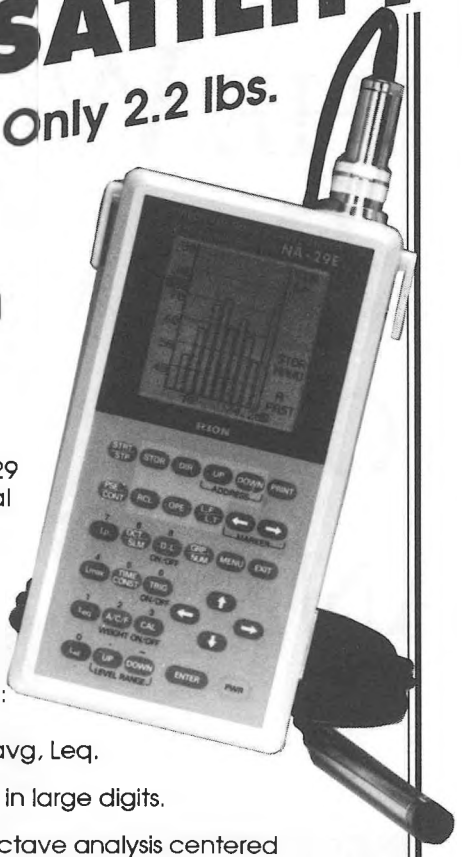

Rion's new NA-29 provides unusual capabilities for a pocket-size acoustical analyzer weighing only 2.2 lbs. It's displays include:

- ❑ Lmax, Ln, Lavg, Leq.
- ❑ Sound level in large digits.
- ❑ Real-time octave analysis centered 31.5 Hz. through 8000 Hz.
- ❑ Level vs. time, each frequency band.
- ❑ 1500 stored levels or spectra.
- ❑ Spectrum comparisons.

It also features external triggering, AC/DC outputs, and RS-232C I/O port. A preset processor adds additional versatility for room acoustics and HVAC applications. To minimize external note taking, users can input pertinent comments for each data address. Specify the NA-29E for Type 1 performance or the NA-29 for Type 2.

Our combined distribution of Norwegian Electronics and Rion Company enables us to serve you with the broadest line of microphones, sound and vibration meters, RTAs, FFTs, graphic recorders, sound sources, spectrum shapers, multiplexers, and room acoustics analyzers, plus specialized software for architectural, industrial and environmental acoustics. You'll also receive *full* service, warranty and application engineering support. Prepare for the '90s.

Call today. (301) 495-7738

SCANTEK INC.

916 Gist Avenue • Silver Spring, MD 20910

PALM SIZE FFT

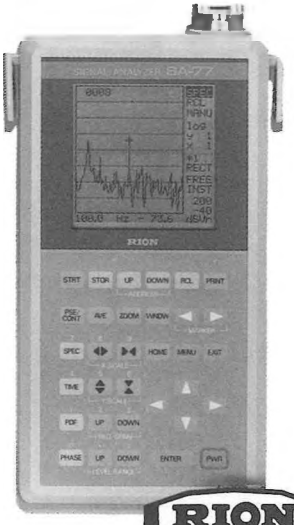

RION

Amazingly smaller and lighter than a lap-top

Our new SA-77 FFT Analyzer is a true miniature. Yet it is very big in capability.

- 0 – 1 Hz to 0 – 50 kHz.
- Zooms to 800 lines.
- FFT, phase and PDF analysis and time waveform.
- External sampling for order analysis.
- Stores 150 screen displays plus 30K samples of time data.
- Single/double integration or differentiation.
- Arithmetic/exponential averaging or peak-hold.
- Built-in RS-232C.
- $8\frac{1}{4}$ X $4\frac{3}{8}$ X $1\frac{1}{2}$ inches.
- 23 ounces.

Call today. Discover how much noise, vibration and general signal analysis capability you can hold in the palm of your hand. And at how reasonable a cost.

SCANTEK INC.

916 Gist Avenue, Silver Spring, MD. USA 20910 • (301) 495-7738

HOLD THE SOUND OF THE WORLD IN THE PALM OF YOUR HAND

Bruel & Kjaer has introduced
a sound level analyzer
which is the most advanced
in the world and yet is so compact
that it can be held
in the palm of your hand

The Type 2260

- **REAL TIME ANALYSIS**
- **2 channel capability with 80 dB dynamic range**
- **Fully programmable due to DSP design**
- **Uses New Type 4189 microphone**
- **PCMCIA Technology**
- **Spectral statistics**
- **Back-Lit LCD display**
- **Multi-Language**
- **1.3 Kg weight**

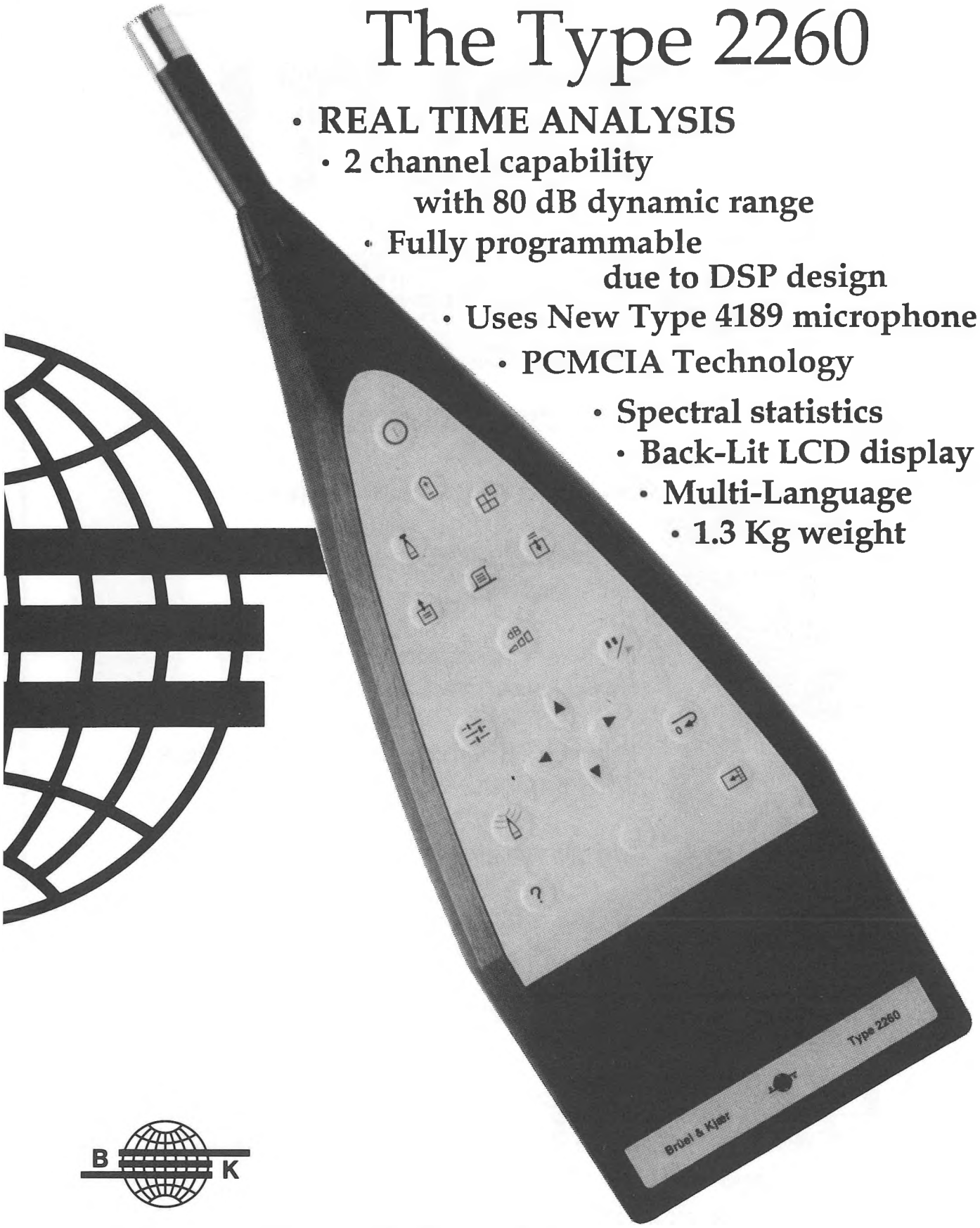

B K

BRÜEL & KJAER CANADA LTD
90 Leacock Road, Pointe Claire, Quebec H9R 1H1
Tel.: (514) 695-8225 Fax: (514) 695-4808

The TRUTH!

FOR NOISE MEASUREMENTS, LARSON DAVIS IS THE SMART CHOICE

The 700 and 800 series of sound level meters and dosimeters...

Adaptable to a variety of measurement applications.

Completely configurable to meet any legislation you need to comply with.

Built-in report generation for down loading directly to a wide range of printers.

High speed serial interface for transfer of data to a computer or directly to a printer.

Large internal memory for logging your noise measurements.

WINDOWS and DOS based software for data retrieval, analysis, reporting and archiving.

Reliable instruments backed with a two year warranty.

Dalimar Instruments Inc.

193, Joseph Carrier
Vaudreuil-Dorion, Québec J7V 5V5

Tel. : (514) 424-0033 Toronto: (905) 508-8345
Fax: (514) 424-0030 Fax: (905) 508-8344

HI-TECH PRODUCTS, HI-TOUCH SERVICE

A Reference Specimen for Air Flow Resistance Measurements.

Wing T. Chu
Acoustics Laboratory, Institute For Research in Construction
National Research Council of Canada, Ottawa, Ontario, K1A 0R6.

1. Introduction

For quality assurance purposes, it is necessary to design and fabricate a reference specimen for periodic checking of the entire measurement system. Presumably properties of the reference specimen should remain stable for at least a number of years. Two different types of materials are currently being tested and monitored at the Acoustics Laboratory of IRC/NRC. This report covers some of the preliminary results gathered up to the present.

2. Measurement System

Figure 1 shows a schematic drawing of the apparatus used for the test according to the ASTM C522 standard[1]. It consists of a 15.24 x 15.24 x 15.24 cm plexi-glass pressure equalization chamber and a specimen holder of the same cross-section locked onto it with latches on four sides. The joint is sealed by an "o" ring and high vacuum grease. For this particular test, the reference specimen formed an integral part of the sample holder.

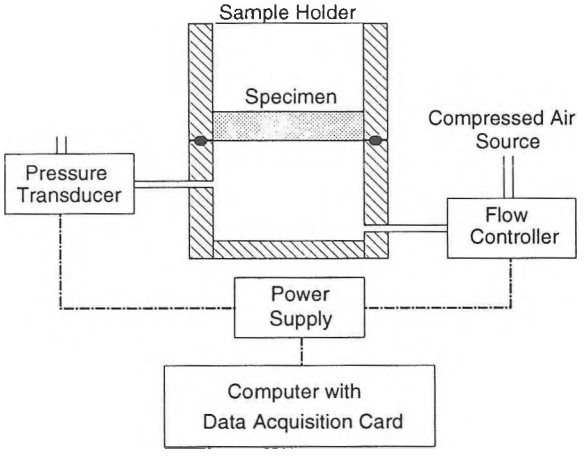

Fig. 1 Schematic diagram of airflow apparatus.

The air flow is provided by the building's compressed air line. A pressure regulator maintains an overpressure at the "upstream" side of the system. The downstream side from the specimen is vented to atmospheric pressure. The air flow is controlled by an MKS flow controller (1259B). The constant pressure drop across the specimen is measured with an MKS 223B differential pressure transducer. An MKS 246 power supply/readout package is used to power both the flow controller and the pressure transducer.

The outputs from the MKS 246 are sampled by the A/D converter of a data acquisition card (DAC) installed in a personal computer (PC). The MKS flow controller receives commands from the PC through the I/O ports of the DAC. Using different volume flow rates through the specimen and measuring the corresponding pressure drops, the airflow resistance can be deduced if laminar flow is maintained[1].

The test is automated using computer software developed in-house.

3. Description of Specimens

Potential reference specimens using two different types of material were tested. The first specimen consists of small glass beads designated as A090 'Highway Beads' by Potter Industries. The diameter of these beads is approximately 1 mm. 924.6 grams of them were packed between two 100 mesh (100 wires per inch) screens exactly 25.4 mm apart. The screens were held in place by two heavy wire-grid supports. The specimen was built into the sample holder as shown in Fig. 2. Two samples having the same weights were tested using two similar sample holders.

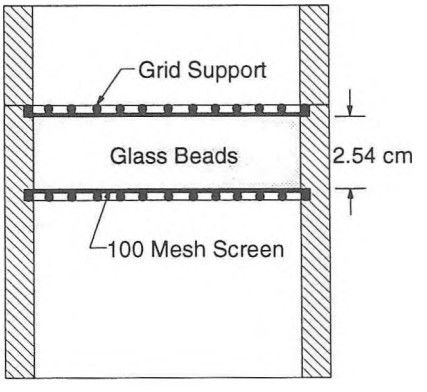

Fig. 2 Schematic diagram of sample holder with the glass-beads specimen.

The second specimen is a 3 mm thick sintered aluminum. Two samples were tested using the same sample holder.

4. Results and discussions

Figure 3 shows the pressure drops across the specimens as a function of the volume velocity of airflow through the specimen. Linear relationships are obtained for both specimens indicating that they passed the first requirement of a reference specimen.

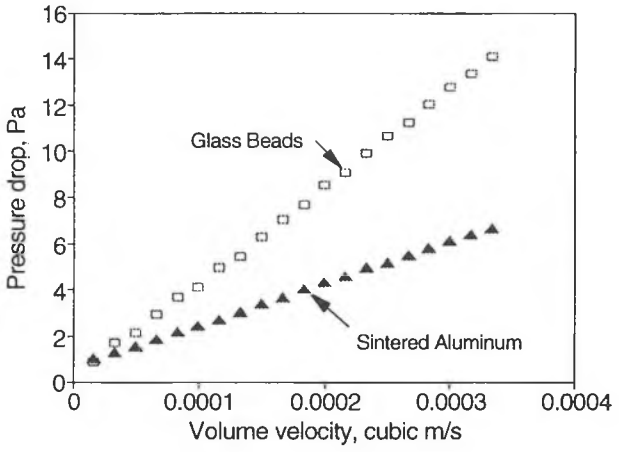

Fig. 3 Pressure drop vs. volume velocity plots for the two specimens.

Further tests showed that it is necessary to pack the glass-beads specimen properly. This was done by shaking the specimen on a shaker table. The following table shows the airflow resistivity of the glass-beads specimen at different stages of packing. There was a 11% change in the airflow resistivity between loosely filled and properly packed conditions.

Condition	Airflow Resistivity (mks rayl/m)
Loosely filled	32757
After tapping	34766
After shaking	36461
8 days later	36213

For each specimen, the same test was repeated ten times over a period of several days without any rearrangement of the sample and equipment. These tests were carried out in an ordinary room without any environmental control. Averages and normalized standard deviations were computed and they are shown in the following table.

Specimen	Average Airflow Resistivity (mks rayl/m)	Normalized Standard Deviation
Glass Beads #1	39144	0.010
Glass Beads #2	36425	0.010
Sintered Aluminum #2	123664	0.005
Sintered Aluminum #3	140502	0.007

The low values of the normalized standard deviation indicate that the specimens are not sensitive to environmental changes and that they have good short term stability. However, both types of specimens lack good homogeneity. There was a 7 % change in the average airflow resistivities of the glass-bead samples and a 12% change for the sintered aluminum samples. For the glass-beads samples, a portion of the change could be due to the non-uniformity of the 100 mesh screens which form part of the sample. Additional tests are required to confirm this assertion.

5. Conclusions

Preliminary tests show that both the glass beads and the sintered aluminum specimens have fairly good short term stability. However, the glass-beads specimen required proper packing. This could be done with a shaker table. Their long term behavior is currently being monitored. Because of the lack of homogeneity, these specimens might not be suitable for round robin tests between laboratories

6. References

1. 'Standard Test Method for Airflow Resistance of Acoustical Materials', ASTM C 522 - 87 (Reapproved 1993).

A Unified Approach for the two ASTM Standards for Impedance Tube Measurements.

Wing T. Chu
Acoustics Laboratory, Institute For Research in Construction
National Research Council of Canada, Ottawa, Ontario, K1A 0R6.

1. Introduction

At present, there are two ASTM standards for impedance tube measurements, the ASTM C384 and the ASTM E1050. The former standard relies on measuring the standing-wave ratios at different discrete frequencies whereas the latter relies on measuring the broad-band transfer function at two positions with a pair of phase matched microphones. The two standards specify two different types of tubes and measurement equipment. This is not necessary. The essential requirements of the two standards can be met with a single impedance tube with a traversing probe-tube microphone. The measurements can be performed inexpensively with a PC computer and a 12 bit data acquisition board that has two A/D inputs and one D/A output.

In this report, a description of the combined setup will be presented together with results obtained by the new procedures.

2. Theoretical Background

According to the ASTM C384[1], the magnitude of the reflection coefficient R is determined by the standing -wave ratio of p_{max} and p_{min}. The phase angle, ϕ, of R is determined by the position of first minimum and the tube attenuation is accounted for by an extrapolation scheme. However, the procedure can be implemented more accurately using an exact formulation based on the plane wave analysis of the standing wave pattern in the tube. According to Ref. 2, the ratio of p_{min} and p_x at any other point can be written as,

$$\frac{|p_{min}|^2}{|p_x|^2} = \frac{e^{2ad} + |R|^2 e^{-2ad} + 2|R|\cos(2kd - \phi)}{e^{2ax} + |R|^2 e^{-2ax} + 2|R|\cos(2kx - \phi)} \qquad (1)$$

and

$$\phi = -(2n+1)\pi + 2kd + \varepsilon \qquad (2)$$

where $\varepsilon = \sin^{-1}[(a/2k|R|)(e^{2ad} - |R|^2 e^{-2ad})]$,

a is the tube attenuation constant, k is the wavenumber and d is position of the nth pressure minimum. Assuming a is known, the reflection coefficient can be determined from Equations 1 and 2 by an iteration process based on two pressure magnitude measurements. Measurements are to be taken one frequency at a time.

For the ASTM E1050[3], two complex pressure measurements are required. The reflection coefficient is calculated according to

$$R = \left[\left(H_{12} - e^{-\gamma S} \right) \left(e^{\gamma S} - H_{12} \right)^{-1} \right] e^{2\gamma L} \qquad (3)$$

where $\gamma = ik + a$, $H_{12} = p_2 / p_1$ is the complex transfer function, S is the microphone separation, and L is the distance of the first microphone from the sample according to the convention of Ref. 3. Fixed positions for two phase matched microphones are specified in the standard. However, more accurate results can be obtained using different microphone positions for different frequencies[4]. Although broad-band measurements can be made with this procedure, more accurate results are obtained with single frequency measurements[5].

3. Proposed Test Procedures

When broad-band random noise is used in the ASTM E1050 test, p_2 and p_1 have to be measured simultaneously. But, if a deterministic type of signal is used, such as a pure tone or a maximum length sequence (m-sequence), the two pressures can be measured sequentially[6]. Recently, Chu has demonstrated that very accurate magnitude and phase measurements can be made using deterministic types of periodic signal and FFT[7]. Thus, a single set of equipment can be used to perform tests according to either one of the standards. The following schematic shows a simple setup of the equipment.

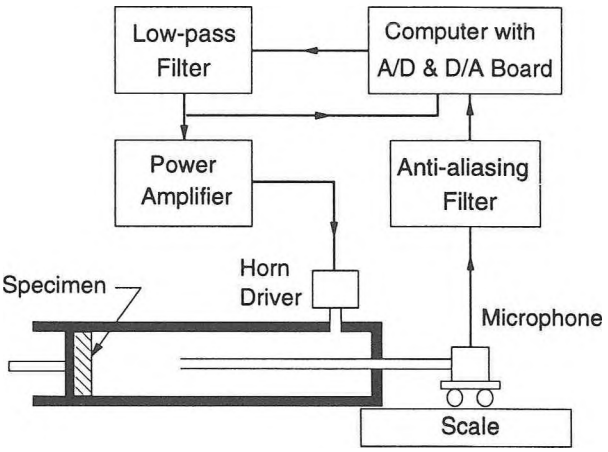

Fig. 1 Schematic drawing of experimental equipment.

Pure tone or deterministic broad-band m-sequence signals are generated mathematically by software and output through the D/A converter. A low-pass filter is used to generate a smooth analog signal before it is fed to a power amplifier which drives the horn driver. A traversing probe microphone is used to sample the acoustic pressure inside the tube at two locations. Both the driving and the microphone signals are digitized simultaneously by a two channels A/D converter. The magnitude and phase of the acoustic signal referenced to the driving signal are computed by a fast Fourier transform program (FFT). Since the signals are periodic, exact multiple periods have to be used to avoid leakage problem and special non-power of 2 FFT routine has to be used. The Glassman's general n points FFT[8] is used in this study.

A common data acquisition program can be used for both the ASTM C384 and ASTM E1050 tests. Only the sections on computing the reflection coefficient are different for the two tests.

4. Experimental Results

The procedures have been used to determine the complex reflection coefficients of a special reference sample used previously in a round robin test[9]. Pure tones at the third-octave band center frequencies from 100 to 2500 Hz were used for both the C384 and E1050 tests. The sampling frequency used was 16 kHz and the number of points used was 3200. This combination provided the exact frequency bins of the FFT for all the frequencies of interest. The results are compared with those obtained for the round robin test[9] using the two-point transfer function method. Previously, the pure tones were generated by an accurate frequency synthesizer and the magnitude and phase were determined with a lock-in amplifier. Both Figures 2 and 3 show good agreement between the two procedures and previous results.

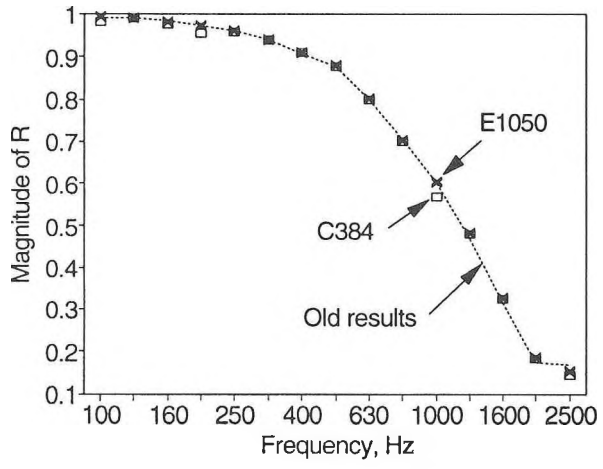

Fig. 2 Comparison of the magnitude of R obtained by the two procedures with that obtained in a round robin test.

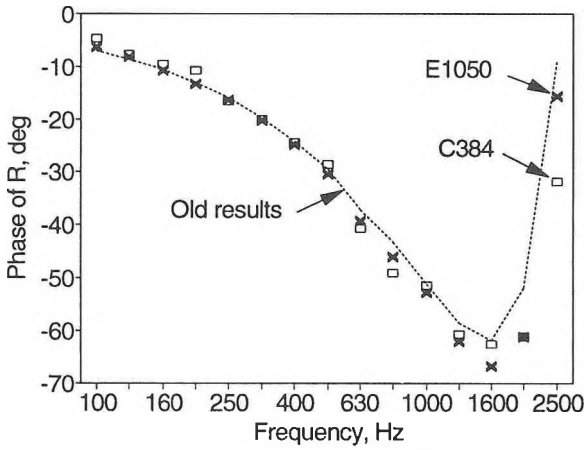

Fig. 3 Comparison of the phase of R obtained by the two procedures with that obtained in a round robin test.

5. Conclusion

It has been demonstrated that a unified approach for the two ASTM standards is possible with a single set of apparatus and equipment.

6. References

1. "Standard Test Method for Impedance and Absorption of Acoustical Materials by the Impedance Tube Method," ASTM C384-90a.
2. W. T. Chu, "An Improved Tube Method for Acoustic Measurement," DBR, National Research Council of Canada, BRN No. 113, (1977)
3. "Standard Test Method for Impedance and Absorption of Acoustical Materials Using a Tube, Two Microphones, and a Digital Frequency Analysis System," ASTM E1050-90.
4. W. T. Chu, "Further Experimental Studies on the Transfer-Function Technique for Impedance Tube Measurements," JASA, 83 (6), (1988).
5. W. T. Chu, "Impedance Tube Measurements-a Comparative Study of Current Practices," Noise Control Engineering Journal, 37 (1), (1991).
6. W. T Chu, "Single Microphone Transfer Function Method for Measuring Impedance and Absorption in an Impedance Tube," JASA, 80 (2), (1986).
7. W. T. Chu, "On Response Measurements using Deterministic Types of Periodic Signal and FFT," Canadian Acoustics, 22 (3), 1994.
8. Warren E. Ferguson, Jr., MRC Tech. Summary Report #2029, Math. Research Center, Univ. of Wisconsin, Dec. 1979.
9. ASTM Committee E33 on Environmental Acoustics, Research Report # RR:E33-1006 on Standing Wave and two-Microphone Impedance Tube Round-Robin Test Program.

Experimental Characterization of the Noise Generation Mechanism of Percussion Drill Steel Rods under Laboratory Controlled Conditions

Claude LESAGE, Rémy ODDO and Yvan CHAMPOUX,
G.A.U.S., Dept. of Mechanical Engineering,
Université de Sherbrooke, Sherbrooke QC J1K 2R1

1 Introduction

Percussion drills are the source of the most serious noise problems in mining activities, because of their extremely high noise levels and widespread use [1]. The exhaust air is the primary noise source on pneumatic rock drills. Manufacturers now offer mufflers that can reduce the exhaust noise at a level at which the drill rod vibrations become the dominant noise source [2]. The noise levels remain high, future efforts should concentrate on reducing the drill rod noise.

Works by Hawkes *et al.* [2, 3] for the U. S. Bureau of Mines provide the most complete description on the noise and vibration of percussion drill rods. The two most important types of elastic waves generated in drill rods are longitudinal and bending waves. Only the longitudinal waves make contribution to the drilling rate. The bending waves are caused by non-centralized impacts, drill rod curvature and non-uniform bit/rock interface. Drill rod noise is generated by Poisson's ratio expansions and contractions of the rod as the longitudinal waves travel up and down it and by transverse rod motions induced by bending waves. The radiation efficiency is much higher for bending waves than for longitudinal waves. As expected, most of the impact energy is transformed into longitudinal waves. It is generally assumed that flexural waves are the main noise source on drill rods. However, measurements up to now have been somewhat contradictory and researchers are still unable to state with certainty that this is indeed the case [4].

In this paper, the relative contribution of longitudinal and flexural waves is investigated experimentally on a laboratory test fixture designed to simulate a percussion drill.

2 Test fixture and procedure

The test fixture (figure 1) was built around a 2.44 m long rod. The outer and inner diameters were respectively 38 mm and 14 mm. The lower end of the rod was equipped with a bit in contact with a concrete block. The 10.5 kg hammer was accelerated by a spring under compression over a 8 cm course. The spring was compressed by pulling a cable attached to the hammer. A clamping system was used to hold the hammer in its armed position. The system allowed to be rapidly released with very few moving parts. The rod was guided at its upper extremity to avoid a random impact point. A fork lift was used to thrust the rod with a static load of 7 000 N, this load is representative of percussion drills in operating conditions. To avoid acoustic perturbation by the contact noise between the hammer and the rod, an enclosure was mounted around the hammer system. The drilling bit was also enclosed.

The rod was instrumented with four full bridge strain gauges transducers, two of them measuring longitudinal waves and the two others measuring flexural waves. To be sensitive to longitudinal waves, strain gauges were mounted on opposite sides of the rod and coupled in series. To measure bending waves, the gauges were again mounted on opposite sides and connected to the bridge to estimate the strain difference between the two sides. Full bridges were composed of two stacked rosettes. See figure 2 for the instrumentation layout.

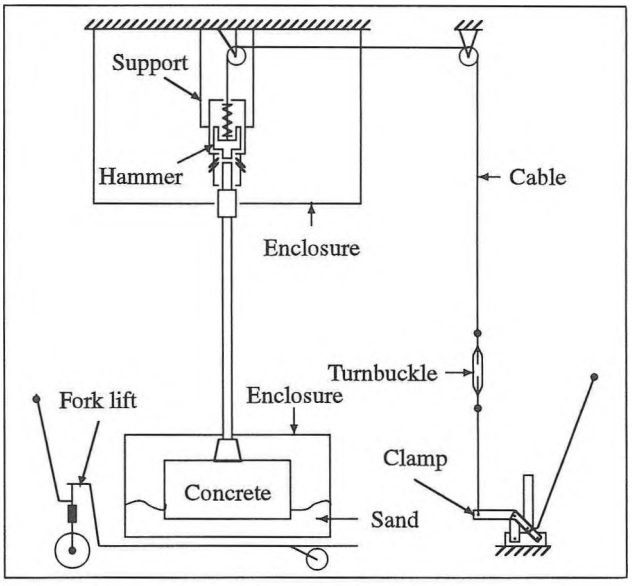

Figure 1: Test fixture schematic

The acoustic measurements were made with a circular antenna which can be positioned everywhere on the vertical axis. The antenna was equipped with eight microphones to adequately characterize the directional behaviour of the bending waves. The microphones were at 40 cm of the rod.

A Brüel & Kjær type 8309 impact accelerometer fixed on the hammer was used to quantify the impact force.

Two Sony multi-channel DAT recorders were used to store the measurements for future processing. The recorders allowed a 10 kHz bandwidth for 16 channels.

A strict procedure was adopted to take the measurements. Five impacts were recorded for each of the ten measurement stations. This important number of measurement points was needed because of the non-uniform sound field. After each impact, the drilled hole was cleaned and the rod was turned to present a new surface to the bit.

Signal processing and analysis were achieved using LabVIEW software running on a personal computer. Acoustic and vibration signals were windowed from the moment the hammer touched the rod to the moment the hammer fell back on it after the rebound. The windowed signals were about 100 ms long, enough for the signals to be damped out. The signals were zero padded to 4096 samples (171 ms) to increase the frequency resolution of spectrums. A Fourier transform was performed on each impact.

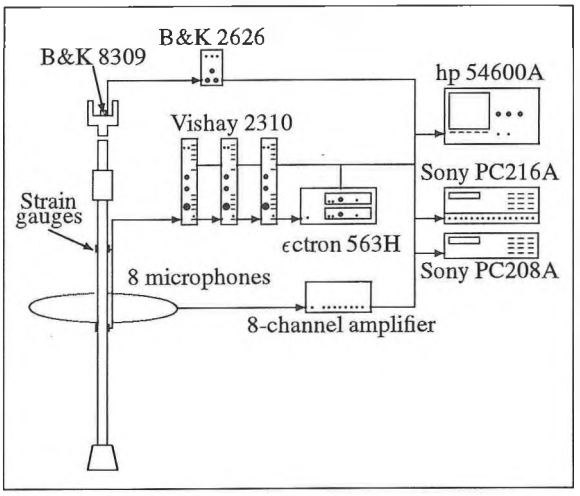

Figure 2: Measurement and recording instrumentation

3 Results

3.1 Test fixture versus percussion drill

In order to evaluate if the test fixture is representative of a percussion drill, vibroacoustic measurements were conducted on a running hydraulic drill. These measurements showed that between two successive impacts the amplitude dies out due to strong damping. Therefore, the one by one impact generation mechanism of the test fixture is not a significative limitation.

Figure 3 compares the axial stress measured on the test fixture and on a percussion drill. The same instrumented rod was used for both tests. The traces show many similarities but differ by peak stress amplitude and damping rate. The peak stress produced by the percussion drill is about twice the one produced by the test fixture. The piston velocity explains the difference. Although the peak stress was lower, the level is high enough to drill in a concrete block. On a drill in real operating conditions, the longitudinal vibrations amplitudes are more damped.

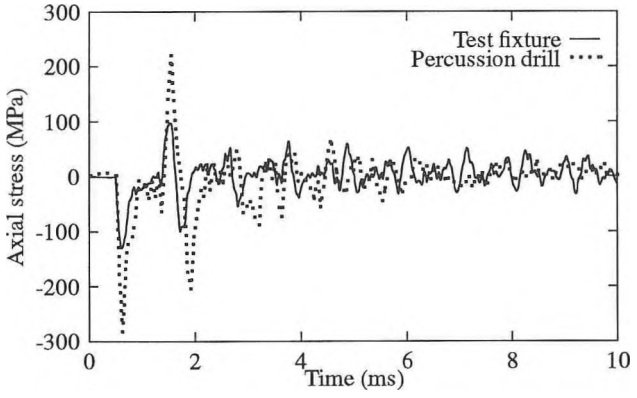

Figure 3: Axial stress time domain traces compared for the test fixture and a percussion drill

3.2 Noise radiation

Figure 4 shows the influence of the alignment of the rod with the hammer on the sound pressure levels. When the rod is aligned with the hammer, the axial modes sound radiation levels are comparable with those from flexural modes. Since spectral density is higher for flexural modes despite all the efforts to avoid the flexural modes excitation, the flexural modes still contribute more to the sound level than axial modes. When the rod is out of alignment by 2 degrees, flexural modes sound radiation gained up to 8 dBs. Vibration measurements showed that only the flexural vibrations were affected significantly when the alignment was changed.

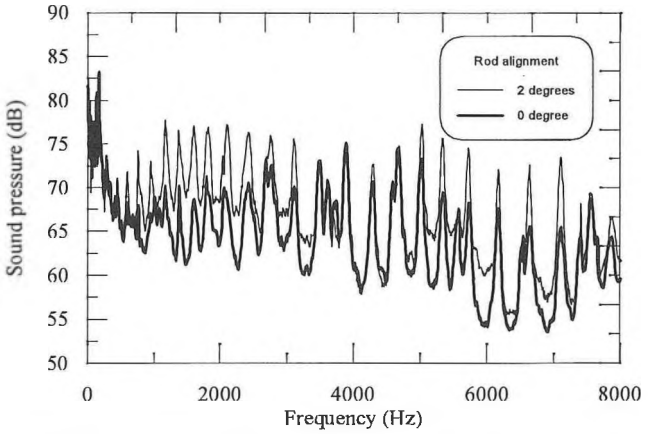

Figure 4: Comparison of sound levels for two rod alignments

Other measurements (not presented here) demonstrated that when the bit is not enclosed, the contribution of longitudinal modes to the sound radiation increased to a level at which the longitudinal modes become the dominant noise source. Sound pressure at frequencies corresponding to longitudinal modes increased by up to 15 dBs.

4 Conclusion

It is possible to reduce the drill rod noise of percussion drills by reducing only the flexural vibrations. However, the noise caused by axial vibrations will soon become dominant. Furthermore, we shall be concerned by the bit noise at the beginning of holes which is related to the axial vibrations.

The test fixture developed will be used to study potential solutions to the noise problem. The fixture was found to be adequate to simulate a percussion drill behaviour in many aspects.

5 Acknowledgement

This work was supported by a grant from the Institut de Recherche en Santé et en Sécurité du Travail (IRSST).

References

[1] Roy C. Bartholomae and Robert R. Stein. Noise reducing technologies for newly designed mining percussion drills. In *Proceedings Noise-Con 88*, pages 123–128, 1988.

[2] I. Hawkes and J. A. Burks. Investigation of noise and vibration in percussive drill rods. *Int. J. Rock Mech. Min. Sci. & Geomech. Abstr.*, 16:363–376, 1979.

[3] Ivor Hawkes et al. Development of a quiet rock drill volume 2: Sources of drill rod noise. Technical Report 77-2, U. S. Bureau of Mines, November 1977.

[4] D. Lednik, N. C. Perkins, et al. On the noise from percussive drill rods. In *Proceedings Inter-Noise 88*, pages 687–690, 1988.

EXPERIMENTAL INVESTIGATIONS OF RIVETED PLATES IN THE LOW, MID AND HIGH FREQUENCY RANGE

Hédi Kaffel, Olivier Beslin, Jean Nicolas,
G. A. U. S., Mechanical Engineering Department,
Université de Sherbrooke,
Sherbrooke, Québec, J1K 2R1, Canada

1 - INTRODUCTION

The simulation of the vibration and acoustic response of canonical structures such as beam, plate and shells is now well under control. However, even buy using finite element or boundary element method, practical simulations are still not well understood: This is the case about joints such as riveting. In this paper a riveted plate is compared to an homogeneous one based on measurement data in term of quadratic velocity and natural mode shape, eigenfrequency and damping. It is shown that the rivets line induced a weakening in stiffness for modes having high bending moments in the rivets line area, and additional damping related to the relative "in plane" motion of the plates in the zone of the rivets line.

2 - EXPERIMENTAL SETUP OF A SIMPLY SUPPORTED RIVETED PLATE

The experimental setup (figure 1) which was used is composed of two plates joint by three rivets (two rivets near the plate edges and one rivet in the middle), the joint has been designed in order to keep a constant thickness, and the same mass per unit area than the homogeneous plate.
The plate was excited by a shaker and normal plate velocities have been measured using a laser vibrometer. Then, quadratic velocity was calculated (cf fig. 2) and Natural modes shapes, eigenfrequencies and dampings were calculated (using SMS STAR*Struct* software[2] (cf fig. 4 to 7).

3 - EFFECT OF THE RIVETS LINE ON THE PLATE STIFFNESS

Natural frequencies of the riveted plate are compared with the natural frequencies of an homogeneous plate which are reported in figure 3. It can be seen that, as expected, the general tendency is a decrease in eigenfrequencies. This decrease is induced by the weakening of the plate bending stiffness on the rivets line. However, this weakening do not affect all the modes with the same proportions, and some of them are even unaffected. It can be seen that mode (2,1) have a 7% decrease in natural frequency. Natural shapes of mode (2,1) is reported in figures 5. It can be observed that this shapes present a slope discontinuity in the rivets line area, due to a weakening in bending stiffness. For the corresponding homogeneous plate mode (2,1), the line coinciding with the rivets line corresponds to a zone containing high bending moments. These high level bending moments cannot be transmitted by the rivets line. Then these riveted plate modes are less stressed than the corresponding full plate modes. that is why eigenfrequencies of these kind of modes are greatly decreased.

4 - EFFECT OF THE RIVETS LINE ON THE PLATE DAMPING

Damping of the 11 first modes of the riveted and homogeneous plates are plotted in figure 4. Damping relative to the riveted plate mode (3,1) and (1,3) must be disregarded as it was very difficult to extract their modal parameters because both modes have very closed eigenfrequencies. It can be seen that the general tendency induced by the rivets line is increase in damping. However, like for eigenfrequencies, modes are not affected in the same proportions. Looking at figure 4, it can be observed that dampings of riveted plate modes (2,1) is multiplied by 6 comparatively to the homogeneous plate modes, while dampings of riveted plate mode (1,2) is just slightly increased. After observing carefully several modes shapes like those given in this paper, it can be stated that the main source of damping is the slip damping which occurs between the two plates in the rivets line area. This slip damping

is directly related to the differential "in plane" motion between the two plates in the rivets line zone. These conclusions on the origin of damping are in agreement with previous papers treating of damping in joints [3].

SUMMARY

The influence of rivets has been studied, based on experimental data. Physical tendencies were found which will allow to know what assumptions can be made when theoretically predicting the effects of a rivets line. In term of stiffness, the rivets line can be taken into account by a punctual weakening of bending stiffness. In term of damping, it was shown that in plane motion of the plates must be taken into account as damping depends on it.

REFERENCES

[1] N. Atalla, J. Nicolas, O. Foin, user's guide of ADNR, internal report, GAUS Sherbrooke University, January 95.

[2] Structural Measurement Systems, 510 Cottonwood Drive, Milpitas, CA 95035 (408) 432-8600.

[3] "Structural Damping by slip in joints", L. Jézéquel, *Journal of Vibration, Acoustic, Stress, and Reliability in Design*, 105, 497-504 (1983)

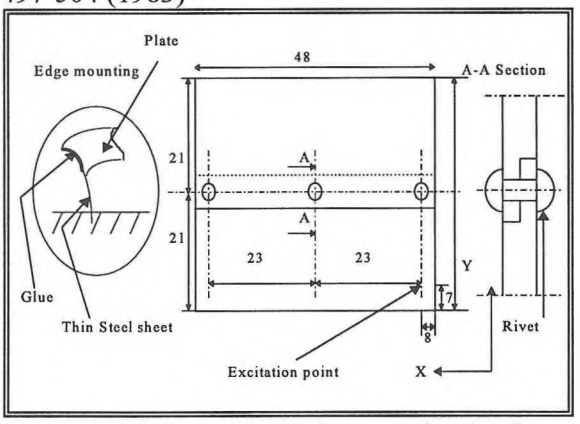

Figure 1: Experimental setup of a simply supported riveted plate (Unit lenght=cm).

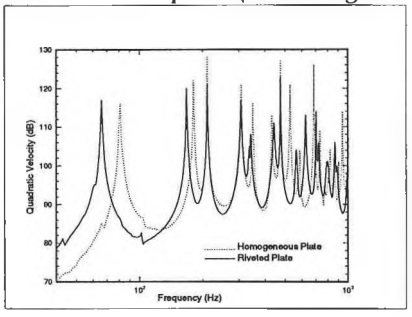

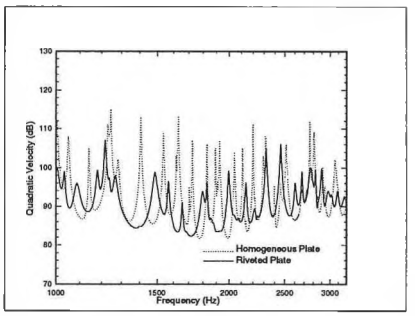

Figure 2: Experimental quadratic velocity of an homogeneous and riveted plate submitted to a point excitation force.

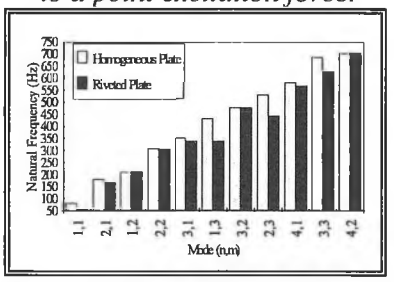

Figure 3: Natural frequencies of riveted/homogeneous plates modes

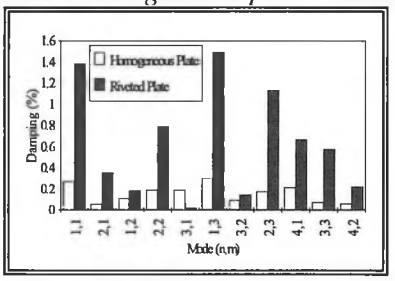

Figure 4: Damping factors of riveted/homogeneous plates modes

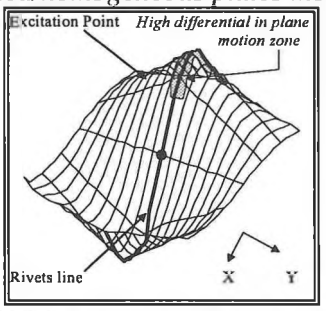

Figure 5: Riveted plate mode (2,1)

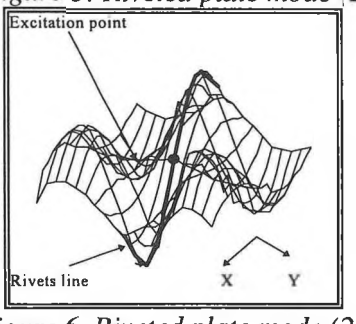

Figure 6 Riveted plate mode (2,3)

SOUND FROM RESONANCES IN SPORTS EQUIPMENT: CAN IT BE USED TO EVALUATE ATHLETIC PERFORMANCE ?

David G. Browning[1], Robert H. Mellen[2], Melissa A. Jarrell[3]

1. Browning Biotech, 139 Old North Road, Kingston, RI 02881 USA
2. Kildare Corporation, 95 Trumbull Street, New London, CT 06320
3. Head Softball Coach, Univ. of Rhode Island, Kingston, RI 02881

1. INTRODUCTION

Physicists have conducted extensive analyses of various sports such as tennis(1) and baseball(2) using many measurement techniques. However, only timing devices, whether a stop-watch for track or a radar gun for baseball, are presently available to provide real-time non-obtrusive performance evaluation. It is proposed that with the advent of sophisticated hand-held analyzes (7), acoustics, specifically the sound generated by resonances in sports equipment, may provide a valuable tool for real-time analysis of athletic performance.

2. SOUND FROM INFLATED SPORT BALLS

Volleyball, soccer, football and basketball all use an air inflated ball, which when struck such as "spiking" a volleyball and kicking a football or soccer ball, produces a significant level of sound with stable characteristics. This is caused by the excitation of the fundamental "breathing" mode as shown in Figure 1 for a "spiked" volleyball(3).

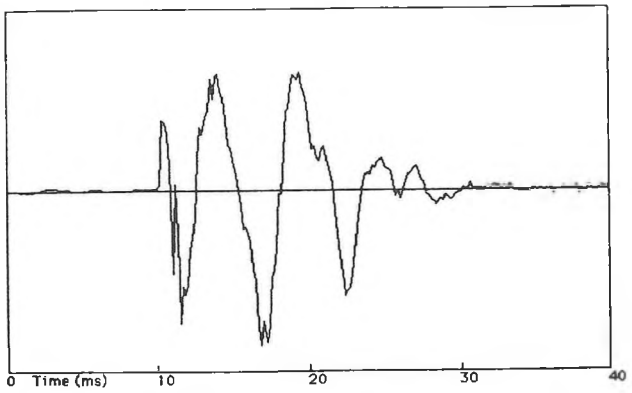

Figure 1. Sound from "spike".

The fundamental frequency was found to be approximately 150 Hz. The corresponding frequency spectrum for the volleyball "spike" is shown in Figure 2. Similar results were obtained from "dribbled" basketballs and kicked footballs(3) and were in agreement with the theory of Morse and Feshbach(4).

3. ALUMINUM SOFTBALL BATS

Perhaps an even more striking example is the sound from an aluminum softball bat. With the commonly used "Bottle Bat" design The hitting area is a uniform cylinder with a minimum wall thickness to increase the "trampoline" effect. Hitting a softball excites a rich set of modal vibrations in the bat. Figure 3. shows the acoustic signature from an aluminum softball bat struck lightly near the outward end of the cylinder. the corresponding acoustic spectrum is shown in Figure 4.

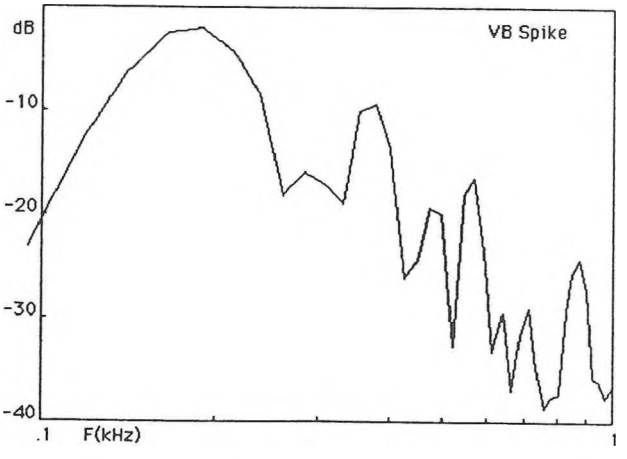

Figure 2. Acoustic spectrum of "spiked" volleyball.

4. ANALYSIS

For the inflated sport balls it was found(3) that the amplitude of the acoustic signal could be used to straightforwardly determine a "good"from a "poor" hit. In addition, the most efficient coupling from the initial impact on the ball (the hand slap when "spiking" a volleyball, for example) to the larger amplitude of the ball resonance determined the"sweetest" hit and could be easily detected acoustically.

The aluminum softball bat with its multi-mode excitation provides an even greater potential for analysis. For example, it was easily demonstrated that the location of the ball impact on the bat could be determined from the frequency spectrum of the sound produced.

5. CONCLUSIONS

In many sports acoustics appear to have the potential to be a valuable tool for the in situ analysis of athletic performance. The further development of hand-held analyzers to include replica-correlation and other processing techniques should ehance this unique capability.

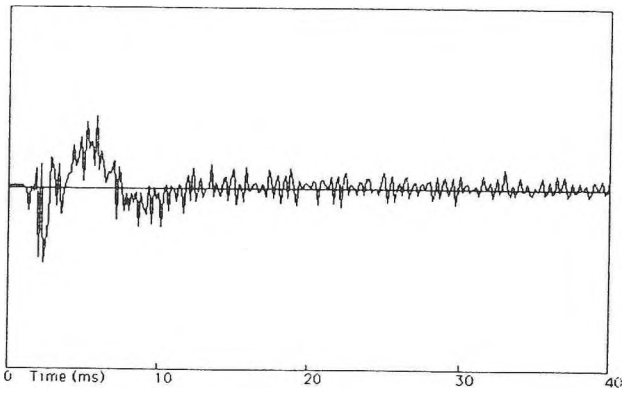

Figure 3. Sound from aluminum softball bat struck near outward end of cylinder.

REFERENCES

1. Brody, H.,"How Would a Physicist Design a Tennis Racket?" PHYSICS TODAY, 48(3), March 1995, pp.26-31.

2. Adair, R.K.; "The Physics of Baseball", PHYSICS TODAY, 48(5), May 1995, pp.26-31.

3. Browning, D.G., Mellen, R.H., Schneck, R.J., and Milbradt, S.; "Spiked Volleyballs, Dribbled Basketballs, and Kicked Footballs: Excitation of the Fundamental Breathing Mode in Inflated Sport Balls", J. Acoust. Soc. Am. 97(5), Pt.2, May 1995, p.3399(A).

4. Morse, P.M., and Feshbach, H., Methods of Theoretical Physics, McGraw-Hill, New York, 1953, pp.1469.

5. Van Zandt, L.L., "The Dynamical Theory of the Baseball Bat", Am. J. Phys. 60(2), February 1992, pp. 172-181.

6. Collier, R.D., "The Crack of the Bat", ECHOES 2(1), Spring 1992, pp. 1-4.

7. Bruel & Kjar Canada Ltd,

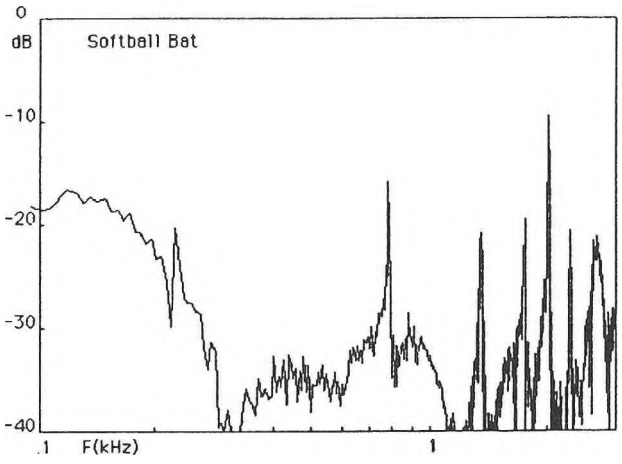

Figure 4. Acoustic spectrum of aluminum softball bat. Hit near end.

ACOUSTIC BACKSCATTER CHARACTERIZATION OF IN-VITRO FETAL LUNGS: DETERMINATION OF ALVEOLAR SACS SIZE

Souheil Hakim, Kenneth L. Watkin
Department of Biomedical Engineering
McGill University, Montreal (Quebec), Canada
E-mail: souheil@rvhob2.lan.mcgill.ca

INTRODUCTION

One of the major causes of newborn mortality is pulmonary immaturity. Fetal lung maturation is determined by biochemical analysis of the amniotic fluid phospholipids. This is an invasive procedure that is potentially harmful to the mother and fetus. Anatomical changes in the lung co-occur with biochemical changes [1]. The developing alveolus has a central cavity containing fluid. During maturation, as the wall of the alveolus becomes thinner (cf. Figure 1), the ratio of the volume of the central cavity to the total volume of the alveolus increases resulting in an increase in the percent fluid content per alveolus [2]. B-mode acoustic scattering techniques have been utilized to determine lung tissue structural properties [2][3]. Scattering from the fetal lung as a function of maturity has been attempted by analysing qualitatively and semi-quantitatively B-mode images of commercial US equipment. Although these scattering techniques have provided encouraging results with regard to assessing lung maturation, they remain highly dependent on the equipment used, and are subjective to the evaluation of the sonographer.

Therefore, to advance our knowledge of fetal lung development, there is a need to 1) seperate the acoustic scattering properties of fetal lung tissue from the properties of the measuring equipment using standardized tissue characterization methods 2) verify the validity of these methods to characterize the lung tissue by using standard phantoms, and 3) apply these methods to characterize fetal lung tissue, i.e., correlate acoustic measurement with tissue properties using quantitative techniques. These issues can be addressed using A-mode US which provides the means for quantitative, equipment independent, signal analysis of raw radio frequency (RF) data to yield a measure of acoustic scattering over a wide frequency range and with sufficient linearity.

The aim of this research is to examine the potential of A-mode US to accurately determine the size of alveolar sacs which is fundamental to the eventual determination of fetal lung development.

METHODS

SIZE ESTIMATION

The backscatter power spectrum of a signal reflected from a volume containing small randomly suspended scatterers was used to estimate average size. The rationale for the estimation of scatterer size from a tissue phantom containing small scatterers has been described elsewhere [4].

INSTRUMENTATION

The basic instrumentation is diagrammed in Figure 2. It consisted of a transmitter and a receiver (6.2 MHz, 12.7 mm diameter spherically focused at 50.8 mm) both driven by a Matec SR9000 pulser/receiver circuit. The received analog signal was digitized (Tektronix) and analyzed using a specially developed software that permitted setting the sampling frequency, and gating only a segment of interest in the signal.

CALIBRATION

For a valid tissue characterization experiment it is necessary to use a known tissue medium for instrument calibration, and henceforth, use this calibrated equipment to characterize the unknown lung tissue. A Tissue mimicking (TM) material (prepared at the Department of Medical Phyics and Engineering, University of Wisconsin, Madison) containing 4 mg/cm^3 microspherical glass scatterers of 45-53 μm in diameter with equal concentrations and spread homogeniously throughout the material was used for calibration. The mean spherical scatter diameter across the frequency range 2-8 MHz was equal to 43 ± 5 μm. Assuming the TM contains spheres of a mean diameter equal to 49 μm (average diameter of 45 and 53 μm spheres), the correlation coefficient between the estimated spherical scatterer diameter and the average diameter contained in the TM was equal to 0.97 (P value < 0.00024).

PROCEDURE

7 preterm lamb lungs (gestational age 134-141 days; mean age = 137 days, standard deviation = 3 days) obtained from pregnant ewes, were inflated (pressure = 18 ± 2 mmHg) and fixed with 10% formaldehyde. Samples representing only alveolar regions were cored from the upper, middle, and lower lobes of each lung for scattering measurements. 30 independent signals from each lung were obtained by translating the transducer perpendicular to beam direction and were analyzed in 3 μs time gates located in the focal zone of the insonifying transducer. To remove system effects on the reflected signals, echo signals were normalized with a plane perfect reflector. The same lung samples were used for histological analysis to verify the accuracy of the size estimation technique. 10 light microscopic images (256 256 pixels, 1.538 μm per horizontal pixel, 1.274 μm per vertical pixel) were digitized from each lobe in such a way to include only alveolar structures. Larger structures were excluded in order to measure only the mean alveolar sac surface area. Based on Weibel [5], software was developed to compute the mean alveolar sac surface area by dividing the total alveolar surface area over the total number of alveolar sacs inside the image sample.

RESULTS

Scatterer dimensions clustered in three size ranges; 1) a small size range, 20-150 μm, 2) a medium range, 150-250 μm, and 3) a large range 250-400 μm. The large and medium scatter sizes are believed to arise from bronchioli, respiratory and terminal bronchioli. Results from morphometric analysis were compared to the *small size* scattering range obtained from acoustic scattering. The effective scatterer diameter acoustically estimated and averaged over the 7 lambs data was 81.6 ±1.5 μm when only scatterers at high frequencies (small size scatterers) were considered. The mean alveolar sac size, histologically determined, was 87.0 ± 3.0 μm.

DISCUSSION AND CONCLUSION

The close values between the mean effective scatterer diameter and the mean alveolar sac size suggested that the primary sources of scattering were the collagen rich septal walls of the alveoli which makeup the alveolar sacs. Therefore, A-mode US can provide accurate structural information about the fetal lung. Further research will examine the sensitivity of A-mode US to structural changes within different regions of the lung and throughout gestation in-vitro and in-vivo.

REFERENCES

[1] Brumley GW, Chernick V, Hodson WA, Normand C, Fenner A, Avery ME, "Correlations of Mechanical Stability, Morphology, Pulmonary Surfactant, And Phospholipid Content In The Developing Lamb Lung," *Journal of Clinical Investigation*, 46(5):863-73, 1967.

[2] Thieme G, Banjavic R, Johnson M, Meyer C, Silvers W, Herron D, Carson P, "Sonographic Identification of Lung Maturation in the Fetal Lamb," *Invest. Radiol.*, 18:18-26, 1983.

[3] Feingold M, Scollins J, Cetrulo C, Koza D, "Fetal Lung to Liver Reflectivity Ratio and Lung Maturity," *J. Clin. Ultras.*, 15:384-7, 1987.

[4] Insana F, Wagner RF, Brown DG, Hall TJ, "Describing Small-Scale Structure in Random Media Using Pulse-Echo Ultrasound," *J. Acoust. Soc. Am.*, 87(1), 1990.

[5] Weibel ER, "A simplified Morphometric Method for Estimating Diffusing Capacity in Normal and Emphysematous Human Lungs," *American Review of Respiratory Disease*, 107(4):579-87, 1973.

ACKNOWLEDGEMENTS

The authors wish to thank Drs., Moy Fung Chen, James Zagzebski, Edmond Quillen Jr., and Bahij Nuwayhid for counsel and valuable support.

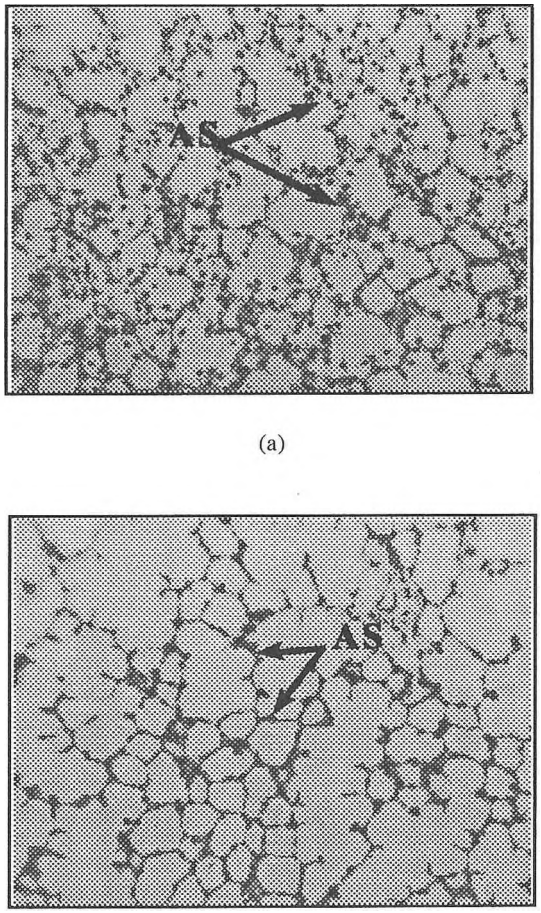

(a)

(b)

Figure 1. Alveolar Sac (AS) septal walls appear to be thicker at 134 days of gestation (a) than those at 141 days of gestation (b) in the sheep fetal lamb.

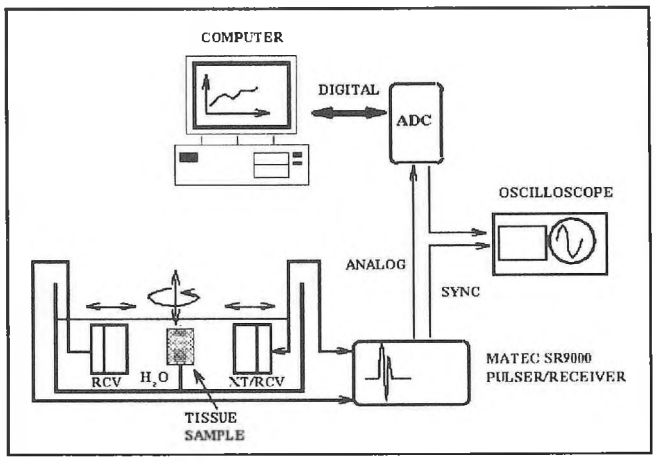

Figure 2. Basic Instrumentation.

Maximum Likelihood Deconvolution of Ultrasonic Signals for Biological Tissue Classification

I. Diouf, K. L. Watkin

Departments of Obstetrics and Gynecology and Biomedical Engineering
McGill University

Introduction- A model for the backscattered signal consists of a convolution of components representing the contributions of a measuring system impulse response, the input signal and the medium or structure to be classified [3]. In order to perform such a classification, the impulse response of the medium needs to be extracted. Techniques such as homomorphic processing [4], fourier deconvolution [2], have been used to perform this task. Homomorphic processing is computationally expensive, it involves two fourier transforms and a filtering operation. The fourier deconvolution technique is unstable when zero's are present in the system transfer function. Whereas the result of the maximum likelihood deconvolution method (MLD) is an efficient estimator of the tissue impulse response in the Cramer-Rao sens. The purpose of this work was to develop a robust and efficient estimator of the insonified tissue structure in order to achieve a good classification in the presence of noise. The classification problem was to identify the tissue type based on the observation data $r_1, r_2, ..., r_N$ where N is the number of samples in one insonification experiment. We have assumed stationarity of the backscattered signal. It was also assumed that under hypothesis H_i the observation sample was the sum of the true underlying nonrandom sample value and a noise term. Thus, all observations were corrupted with an additive zero-mean white Gaussian noise with variance σ_n^2. The noise samples at various instants were independent random variables and were independent of the source output.

Deconvolution Method-The return echo from a target medium can be represented as a convolution of the impulse response $h_s[n]$ of the measuring system, the input signal $i[n]$ and the impulse response $M_i[n]$ due to the structure of the medium as shown in equation (1). The contributions of the impulse response of the measuring system as well as that of the input signal were fixed throughout the experiment.

$$y_i[n] = i[n] * h_s[n] * M_i[n] = s[n] * M_i[n] \quad (1)$$

$$r_i[n] = y_i[n] + noise[n] \quad (2)$$

where i represents the tissue under investigation and n represents the time index of the window used as the analysis frame for each insonification experiment. In order to perform the deconvolution, the received waveform $\mathbf{r}$ was passed through a filter matched to the system response $\mathbf{s}$ to give a set of numbers $a[k]$. The measuring system autocorrelation coefficients $b[k]$ and the noise at the matched filter output $ns[k]$ were computed:

$$a[k] = \sum_{n=1}^{N} r[n]s[n-k] \quad k = 1, 2...N \quad (3)$$

$$b[k] = \sum_{n=1}^{N} s[n]s[n-k] \quad k = 1, 2...N \quad (4)$$

$$ns[k] = \sum_{n=1}^{N} noise[n]s[n-k] \quad k = 1, 2...N \quad (5)$$

The $a[k]$'s form a set of sufficient statistics in the estimation of the M_i's. Values of $s[n-k]$ outside the window of analysis were padded with zero's. The problem was reduced to an estimation of the $M_i[k]$'s given a set of relations:

$$a[k] = \sum_{n=1}^{N} M_i[j]b[k-j] + ns[k] \quad k = 1, 2...N \quad (6)$$

Using suitable notation, the solution of the above equation can be written in matrix form as:

$$\mathbf{a} = \mathbf{B} \times \mathbf{M_i} + \mathbf{ns} \quad (7)$$

where $\mathbf{B}$ is a symmetric non singular NxN matrix formed by the autocorrelation coefficients $b[k]$'s.

Classification Method-The classification method was treated as a M-hypotheses testing problem. We hypothesized that different structures will generate different trends in the signal and consequently similar media or structures will influence the signal the same way. For each tissue class, a vector formed by the MLD estimate for each insonification position was computed. The power spectrum pow_i of this MLD vector $\mathbf{M_i}$ was then computed. This was repeated for different insonification positions for each class of tissue. Within any given tissue class, there is a degree of variability. This variability was modelled as an additive white Gaussian noise. Therefore the computed power spectrum was composed of the true underlying power spectrum representing a given class and an additive zero-mean white Gaussian noise term with variance σ_n^2. A general Gaussian problem formulation is then used together with the Bayes criterion with cost $C_{ij} = 0$ if $i = j$ and $C_{ij} \neq 0$ otherwise to perform the classification [5]. The test reduces to choosing H_i for:

$$P_i P(R|H_i) \geq P_j P(R|H_j) \quad \forall j \quad (8)$$

where R is a random vector computed in the same way as pow_i from an unknown tissue to be identified and H_i is an hypothesis representing a given tissue type. The equivalent test was to compute $P_i P(R|H_i)$ for all H_i and choose the largest. Since log is a monotonically increasing function of its argument, taking the log of each likelihood and eliminating the constant term yields the sufficient statistic:

$$l_i(R) = logP_i - 1/2log|K_i| - 1/2(R^T - m_i^T)K_i^{-1}(R - m_i) \quad (9)$$
$$K_i = E[(R - m_i)(R^T - m_i^T)|H_i)] \quad (10)$$

where m_i is the expected value of the random variable pow_i and K_i is the covariance matrix. E is the expectation operator. In order to simplify equation 9, we represent R in a new coordinate system in which the components are statistically independent random variables. The new coordinate system is computed by the Gram-Schmidt orthogonalization method using the set of power spectrum vectors formed from each class of tissue as the initial coordinate system [1]. It was assumed that all the hypotheses have equal *a priori* probabilities and that the statistics of the observations were only due to the statistics of the additive white Gaussian noise. Thus we have $K_i = \sigma_n^2 I$ in the new coordinate system. After eliminating constant terms, the sufficient statistic reduces to :

$$l_i'(R) = (-1/2\sigma_n^2)(R'^T - m_i'^T)(R' - m_i') = (-1/2\sigma_n^2)d^2 \quad (11)$$

The largest of $l_i'(R)$ corresponds to the minimum of distance d. Therefore, the processor of the classification is a minimum-distance decision rule.

Computer generated data simulating the backscattered ultrasonic signal were used to test the reliability of the MLD and the classification algorithms. The probability of correct decision was found to be influenced by the following factors: the data size and the noise variance. As the number of sample points was increased so was the correct decision percentage. It was also possible to increase arbitrarily the level of the noise variance. Such increases caused the performance of the classifier to degrade to the point where it was unable to extract any information from the data.

In-Vitro Experiments and Results with Biological Tissues-The classification technique was used to identify 3 tissues types: liver, kidney and pancreas. The experiments were conducted using a Panametrics broadband transducer with 5 MHz center frequency and a 3-dB bandwidth of 2.75 MHz. A Matec pulser and receiver were also used to excite the transducer and receive the backscattered echo signal. A Tektronix digital oscilloscope was used to digitize the echo signal with a sampling rate of 25 MHz.

The maximum likelihood estimate vector of the underlying signature of a tissue at a given position was computed from 60 A-scans data. The power spectrum of the MLD vector was then computed. A set of 20 power spectrum vectors was computed for a given tissue at different positions. Half of the set was used to construct the minimum distance processor and the remaining 10 vectors were used for the classification test. Figure 1 shows

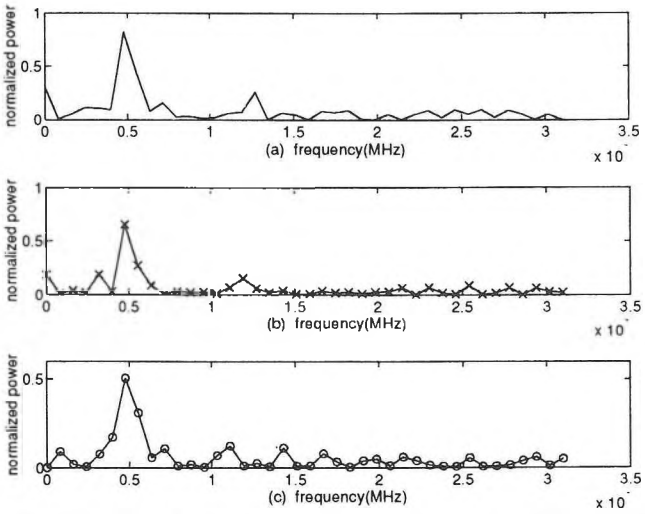

Figure 1: Power spectrum samples of the 3 tissue types: (a) liver, (b) kidney, (b) pancreas.

power spectrum vectors for each class of tissue. The result of the classification yielded a percentage of correct decision of 90%.

Conclusion-We implemented a backscattered echo signal classifier using a minimum distance processor. The decision was based of the nearest neighbor rule. Results obtained from both computer simulation and in-vitro biological tissue resulted in a probability of correct classification of about 90%. Further improvement can be achieved by applying this technique at different scales and combining the results of all the scales into one probability of correct decision.

References

[1] E. Oja,"Subspace Methods of Pattern Recognition," Research Studies Press, New York: John Wiley, 1983.

[2] L. L. Lizzi. E. Feleppa, N. Jaremko, D. King, and P. Wai, "Liver-Tissue Characterization by Digital Spectrum and Cepstrum Analysis," in Proc. 1981 Ultrason. Symp., pp 575-578.

[3] J. Saniee, N. M. Bilgutay, "Statistical Evaluation of Backscattered Ultrasonic Grain Signals," J. Acoust. Soc. Amer., Vol. 84. pp. 400-407, July 1988.

[4] j. Saniee, T. Wang, N. M. Bilgutay, "Analysis of Homomorphic Processing for Ultrasonic Grain Signal Characterization," IEEE Trans. Ultrason. Ferroelec. Freq. Contr., Vol 36. No 3, May 1989.

[5] H. L. Van Trees, "Detection, Estimation, and Modulation Theory", New York: John Wiley, New York, 1968.

Acoustic localization using ice-mounted geophones in the Canadian high Arctic

S. E. Dosso, Capt. R. W. Van Der Pryt and R. I. Verrall

Defence Research Establishment Atlantic

Esquimalt Defence Research Detachment, FMO Victoria B.C. V0S 1B0

INTRODUCTION

The direction to an acoustic source in the open ocean is typically determined by applying beamforming techniques to acoustic pressure fields as measured at an array of hydrophones, or by employing directional hydrophones. In the Arctic, however, deploying hydrophones through the sea ice cover is a laborious task which is difficult to automate or carry out remotely (e.g., from an aircraft). Geophones coupled to the surface of the ice are much more easily deployed and have proven to be sensitive to ocean acoustic fields [1]. However, to date, little work has been reported regarding the capability of ice-mounted geophones to determine source direction (bearing). In theory, a three-component geophone or an array of vertical-component geophones can provide enough information to resolve source direction. In practice, however, the interpretation may be confused by multiple arrivals, by scattering in the rough, inhomogeneous ice layer, and by shear waves in the ice.

EXPERIMENT

To investigate the effectiveness of acoustic localization using ice-mounted geophones, an experiment was carried out on the polar pack ice north of Ellesmere Island, NWT. A linear array of five geophones (three 3-component, two vertical-component), each separated by 20 m, was deployed on the surface of the ice. A simple continuous-wave (CW) source was fashioned by bolting a flexible 6-m metal tube to the exhaust pipe of a diesel generator engine (muffler removed) and lowering the tube into the water through a hole in the ice. A multi-channel digital seismograph was used to record 40-s time series (sampling rate: 500 Hz) when the source was deployed at ranges of 200 m, 500 m and (nominally) 1000 m along lines at 0°, 30°, 60°, and 90° with respect to the array orientation (endfire). The experiment site was characterized by smooth, flat annual ice, approximately 2 m thick; the water depth varied from 18–105 m.

An example of the recorded data is given in Fig. 1 which shows the acoustic power as a function of time and frequency for the source at 855-m range and 90° bearing. Spectral lines are evident at 30 Hz (the cylinder-firing rate of the engine) and 60 Hz, with higher-order harmonics at 30-Hz intervals. The dispersive arrivals at frequencies less than 30 Hz are identified as ambient noise events (plate waves in the ice due to thermal ice cracking or distant pressure-ridge building [2]).

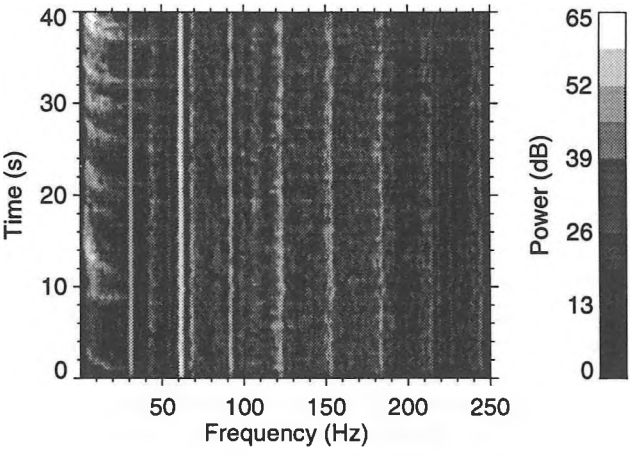

Fig. 1. Time-frequency representation of acoustic power (arbitrary decibels) for the CW source.

ANALYSIS

In this paper, two methods are considered for determining source bearing: principal-component analysis of the horizontal particle motion, and array beamforming of the vertical-component measurements. If the direct (unscattered) compressional wave is the dominate arrival at a 3-component geophone, the particle motion in the horizontal plane should be polarized along a line from source to receiver, providing an indication of the source direction. However, compressional waves that have been scattered at the rough underside of the ice or within the inhomogeneous ice layer and shear waves in the ice produce particle motion that is not polarized in the source direction and degrades the bearing estimate. Principal component analysis [3] provides an optimal method of determining the principal (symmetry) axis of the particle motion. Fig. 2 shows an example of the particle motion in the horizontal plane for a source at 60° and 200 m. The dashed line indicates the principal axis of the particle motion. The principal axis is at an angle of 58° and provides a good estimate of the true source bearing (dotted line). Fig. 3 shows the estimated bearing angles for all source locations. In each case, the recorded 40-s time series were divided into ten 4-s samples which were analysed individually to provide a mean bearing estimate and a standard deviation about the mean. Fig. 3 shows that reasonably good bearing estimates are obtained at a 200-m range;

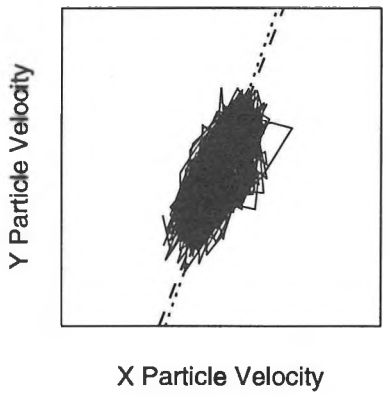

Fig. 2. Horizontal particle motion for a source at 60° and 200 m. Dashed line indicates the principal axis; dotted line is the true bearing.

however, the estimates degrade rapidly with range.

A second approach to determining source direction is to apply plane-wave array beamforming techniques [4] to the vertical-component recordings. The smallest acoustic wavelength that is not spatially aliased in beamforming analysis is given by twice the sensor separation: for the 20-m sensor spacing used here, this corresponds to frequencies <35 Hz. Fig. 4 shows the results of frequency-domain beamforming at 30 Hz for the acoustic source at 500 and 1000 m (the results for the source at 200 m were poor, due to violation of the plane-wave assumption for this short range). Good estimates for source bearing are obtained at 90° and 60° for both ranges, with the main lobe approximately 5 dB above the side lobes (the symmetry about 0° results from using a linear array). At 30° and 0° the beamforming results indicate a source bearing in the interval ±30°, reflecting the decrease in beam resolution with angle and the interpretation of the vertical grazing angle as a horizontal angle near endfire. Considering the small array and short propagation ranges of the experiment, the beamforming results indicate that determining source direction using an ice-mounted geophone array is a promising approach.

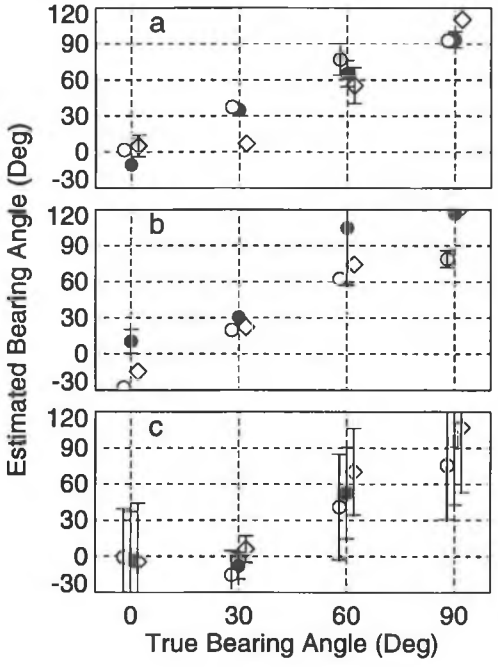

Fig. 3. Bearing angle estimates from principal-component analysis for sources at: (a) 200 m, (b) 500 m and (c) 1000 m. Different symbols indicate estimates for the three 3-component geophones. Error bars (plotted when larger than the symbol) indicate standard deviations.

REFERENCES

[1] S. E. Dosso, R. J. Stockermans and R. I. Verrall. Ice-buoy Arctic field trials during Iceshelf 94, *DREA Tech. Memo.*, Defence Research Establishment Atlantic, Halifax NS, 1995.

[2] M. V. Greening. A two-component Arctic ambient noise model, *Ph.D. thesis*, University of British Columbia, Vancouver BC, 1993.

[3] W. R. Dillon and M. Goldstein. *Multivariate analysis: Methods and applications*, Wiley and Sons, New York, 1984.

[4] W. S. Burdic. *Underwater acoustic system analysis*, Prentice Hall, Englewood Cliffs NJ, 1991.

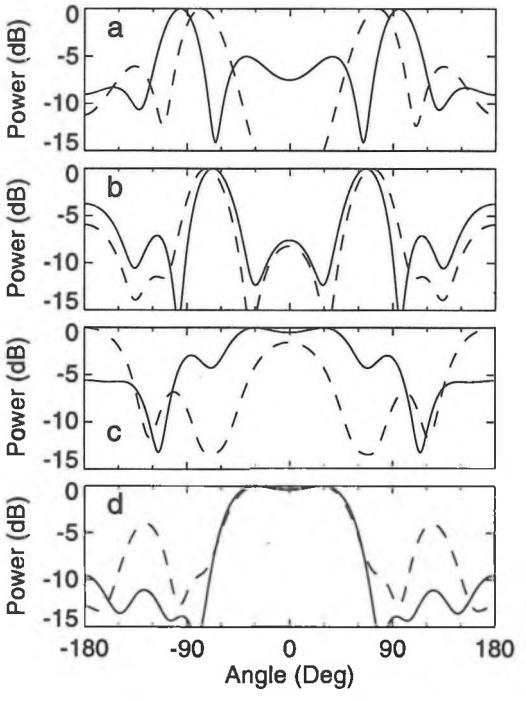

Fig. 4. Beamforming results for source at 500-m range (dashed line) and 1000-m range (solid line) and bearings of: (a) 90°, (b) 60°, (c) 30° and (d) 0°.

NOISE AND VIBRATION SOURCES OF HANDHELD GRINDERS

Jean-Luc Wojtowicki & Jean Nicolas
Acoustic and Vibration Group
Mechanical engineering dept.
University of Sherbrooke
Sherbrooke (Quebec)
J1K 2R1

I- INTRODUCTION

Noise and vibration of handheld grinders is one of the most important health and safety problems at work in metal workshops, shipbuilding, ... The sound pressure levels of the grinding process are much higher than 90 dB(A) at the operator and the generated handarm vibrations (HAV) can cause serious diseases like "vibration white fingers".
The aim of this study is to characterize noise and vibration sources of portable grinders and grinding wheels and to define the ways to reduce them.

II- GRINDING FORCE

The grinding force is generated by the grinding wheel rotating at high speed on the grinded metal. This force excites both the grinding wheel and the grinded metal which can generate noise and vibrations.

A classical hypothesis was that the grinding force depends on the coarseness of abrasive grains and the hardness of the bounding. Actually, this is not true. Experiments clearly showed that the grinding force is mainly due to the buckling of the grinding wheel. This buckling can be very important, it exceeds 1 mm in some cases. Because of the buckling and the high rotation speed, the grinding is not in continuous contact with the metal work piece. The grinding force is generated when the wheel meets the work piece.

Figure 1 features a power spectrum of the grinding force measured in the axis of the wheel. The "distance" between two peaks is 100 Hz, which is the frequency of rotation in that case.

The plot of the grinding force versus time is a periodic signal (see figure 2). This signal can be divided in two components: a carrier frequency at the frequency of rotation and a random superposed oscillation. Each component has its own origin depending on buckling. The carrier frequency is due to the general or averaged buckling, and the oscillation is due to the surface roughness of the wheel.

Figure 3 presents the plot of the grinding force versus time after machining the grinding wheel to decrease the surface roughness. The machining has eliminated the surface roughness but not the general buckling: the oscillation has disappeared on the plot of the grinding force. Other experiments showed that the carrier frequency can de reduced in the same manner when eliminating the general buckling of the wheel.

Experiments also showed that the noise and vibrations can be significantly reduced when decreasing the buckling of the wheel. The noise has been experimentally reduced up to 5 dB(A) and vibrations up to 6 dB with a general buckling of less than 0.1 mm.

III- THE GRINDING WHEEL

Noise:

Figure 4 presents a typical sound power spectrum of the grinding wheel. It can be seen that the shape of this spectrum is similar to the grinding force power spectrum

A classical way of reducing the noise of vibrating objets is to add damping in the structure [1]. The modal analysis of grinding wheels has shown that the structural damping is very important. Damping is nearly 1% (and 5% in the case of specially designed grinding wheels). The damping required to obtain less than 90 dB(A) sound pressure level at the operator was calculated [2] and was found to be 15%. In practice, it is impossible to increase the damping so much, because the initial damping is already very high.

Vibrations:

The unbalance is the major source of vibrations when the grinder is running free. Experiments showed that there is a strong relationship between vibrations and unbalance of the wheel. Figure 5 presents the vibration levels measured at the handgrip versus the specific unbalance of grinding wheels.

For safe operation, vibration levels should not exceed 137 dB. This value is obtained for a specific unbalance of 250 g.mm/kg. Then, classical values of unbalance of grinding wheels is 600 g.mm/kg and higher. It must be mentioned that this unbalance is well above the norm according to the ISO 1940 standard [3]. Recommended unbalance should not exceed 63 g.mm/kg. Thus, the vibration reduction of free running grinders requires a better control of the unbalance of the wheel. This can be done setting tighter machining tolerances on grinding wheel runout and balancing with a maximum unbalance of 250 g.mm/kg which is still higher than the ISO 1940 requirements.

IV- THE GRINDER

The obvious source of noise of pneumatic grinders is the motor. The noise is generated by air discharge at the exhaust. The exhaust noise is a pure tone noise whose fundamental frequency is the frequency of rotation multiplied by the number of rotor blades. This noise can be reduced using a muffler. But this solution can generate other problems like a decrease in motor efficiency or ice buildup.

A survey study of manufacturers showed that this noise source can be eliminated by choosing the right technology for the pneumatic motor. It appears that air turbines (a new type a pneumatic motors) could advantageously replace pneumatic motors with blades. Using air turbines makes the pneumatic motor an unsignificant source of noise of in grinding process. Measurements on one grinder equiped with an air turbine reveals sound pressure levels

V- CONCLUSION

Noise and vibration reductions of the handheld grinders can be achieved by tighter control on the fabrication of grinding wheels and a better choice for the motor technology.

A decrease in the wheel buckling and runout brings about a reduction of the grinding force, thus a reduction of noise and vibrations. In the case of a grinding wheel, there is no obvious solution to reduce vibration generated noise using damping materials. The control of wheels unbalance leads to the reduction of the free running vibrations. And finally, the pneumatic motor becomes an insignificant source of noise when using an air turbine instead of a bladed rotor.

VI- REFERENCES

[1]: J-L. Wojtowicki, O. Beslin, J Nicolas,"Design of circular saw blade for quiet operation", *Proceeding of Canadian Acoustics 1994*, Vol. 22, No. 3, 1994, pp. 105-106

[2]: A. Côté, N. Attala, J. Nicolas, "Forced vibration of a thick rotating annular plate", submitted to *JVA*

[3]: ISO 1940 standard, "Qualité d'équilibrage des corps en rotation"

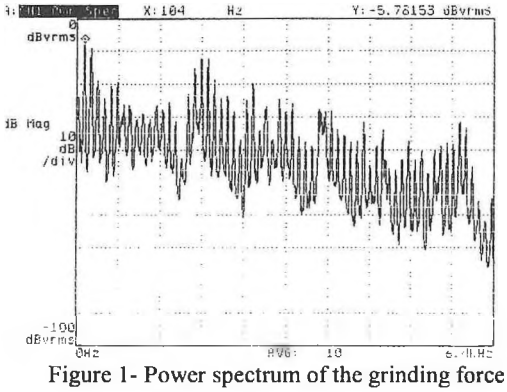

Figure 1- Power spectrum of the grinding force

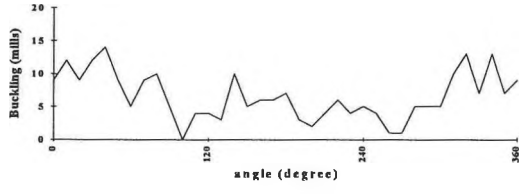

(a)

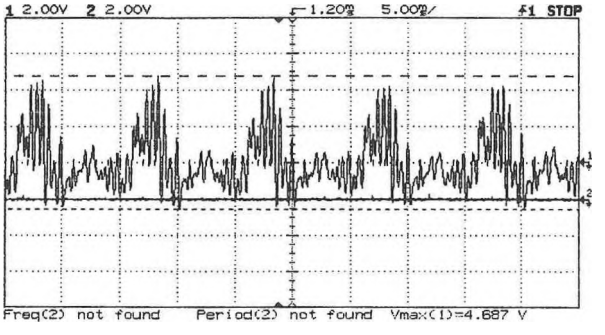

(b)

Figure 2- Buckling (a) and grinding force (b)

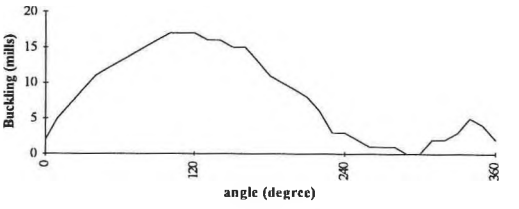

(a)

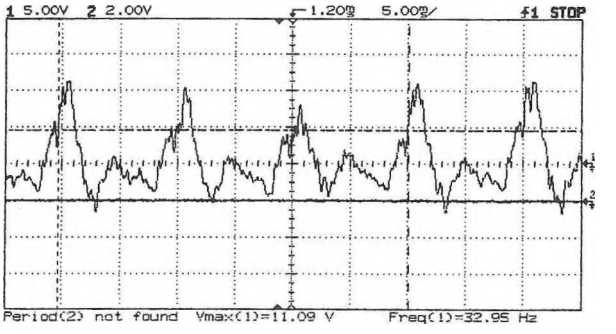

(b)

Figure 3- Buckling (a) and grinding force (b) after machining

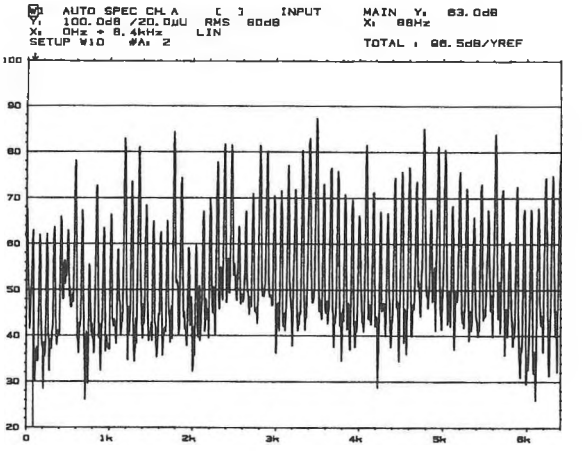

Figure 4- Typical sound power spectrum generated by grinding wheels

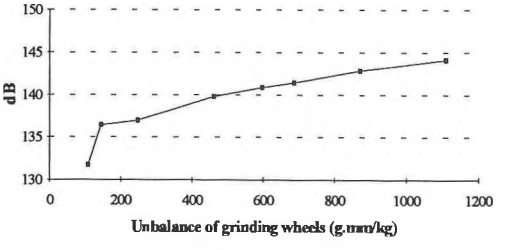

Figure 5- Vibration levels *vs* specific unbalance

VIBRATORY MEASUREMENTS TO ESTIMATE MECHANICAL PROPERTIES OF COMPOSITE MATERIALS

Bertrand Mercier, André l'Espérance, Jean Nicolas
GAUS, Université de Sherbrooke
Sherbrooke, Qc, J1K 2R1

July 1995

1- INTRODUCTION

In practice, engineers frequently work with materials of unknown mechanical properties. However, pratically every aspect of the acoustic domain require the knowlegde of the elastic modulii, density and structural damping of material. These properties are easy to quantify for classical materials such as steel and aluminium. On the other hand, when we have to deal with composite materials, they may be more difficult to estimate. The purpose of this paper is to demonstrate that it is possible to find the mechanical properties of a composite material with the help of vibratory measurements.

2- EXPERIMENTAL METHOD

We have chosen to run our experiment with a fiberglass/polyester composite material. The sample tested was handcrafted using a wet layup and a chopper process. The mechanical properties found in the literature generally concern glass/epoxy composite materials with a particuliar fiber orientation [1]. However, very few publications concern glass/polyester materials[2]. Moreover, it is a known fact that the properties of a composite material vary a lot with the fiber/resin ratio which is difficult to quantify.

To begin our experiment, we designed a 0.48 m x 0.42 m x 6.86 mm simply supported rectangular plate. Since the plate's thickness varied (6.35 mm to 7.87 mm), we considered the tickness mean for our simulations. A shaker located at 8 cm and 7 cm from a corner was used to produced a pseudo-random excitation. Using a force-transducer and laser vibrometer, which mesured the displacement for a precise point, it was possible to mesure the frequency response (H1) between the imposed force and the plate's displacement. The frequency response has been mesured for 361 points on the surface of the plate with a span of 0 to 2400 Hz. Using all the frequency responses and a simple algorithm, we calculated the mean square velocity of the plate. Figure 1 shows the setup used in the experimentation.

3- IMPULSE EXCITATION

Since the results could not be analysed directly on site, we made sure that our measurements were accurate. In this way, we made some impulse excitation tests to verify if the frequencies found by impulse excitation corresponded to the one obtained with the mean square velocity. Table 1 shows the first five modal frequencies of the plate (f_{mn}).

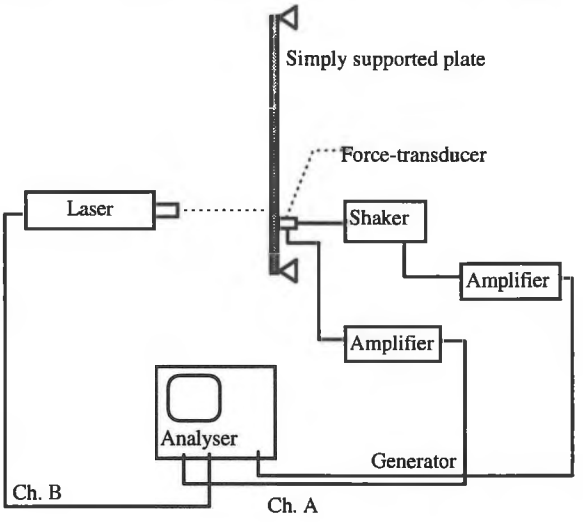

Figure 1: Schematic experimental setup.

Table 1

Comparison of the first five modal frequencies obtained by impulse excitation and mean square velocity

f_{mn} with impulse excitation (Hz)	f_{mn} with mean square velocity (Hz)
80.5	81.0
183.0	183.0
210.0	212.0
310.0	314.0
350.0	350.0

4- RESULTS

Knowing the frequency corresponding to the first experimental mode and the expression of the modal resonance frequencies of a simply supported isotropic

panel (eq.1), it is possible to find a rough estimate for the elastic modulii.

$$\omega_{mn} = \sqrt{\frac{D}{\rho h}}\left[\left(\frac{m\pi}{a}\right)^2 + \left(\frac{n\pi}{b}\right)^2\right] \text{ (rad / s)} \qquad (1)$$

where $D = \frac{Eh^3}{12\left(1-\nu^2\right)}$

a and b are the dimension of the plate
m,n = 1,2,3,...

With the use of a program called ADNR [3] developed at GAUS, which give us the opportunity to simulate the vibroacoustic behavior of a simply supported plate, we tried to obtained, by iteration, the same theorical mean square velocity as found in our experiment.

Figure 2 compares the experimental mean square velocity to the one simulated by ADNR. As can be seen, the vibratory levels and the position of the peaks are very similar. The properties used in ADNR to obtained this curve correspond to the real properties of the composite material or are very close.

Contrary to all expectations, the composite material used behaved like an isotropic material with the following properties:

E = 8.3 GPa $\rho = 1450$ kg/m^3
$\nu = 0.26$ $\mu = 10^{-2}$

If we look attentively at the experimental curve, we note a few irregularities in the mode definition. Those irregularities are mainly due to the fact that the plate is not perfectly homogeneous and has a small variation in thickness. This fact also introduces the same modeat two frequencies, therefore doubling the mode. This phenomenon can be seen at 530 Hz and 1400 Hz. In general, this method gives very good results.

4- CONCLUSION

We have presented a method that gives the opportunity to quantify the mechanical properties of materials by using vibratory measurements. This method consists in correlating the theorical mean square velocity of a simply supported plate to the one obtained experimentally. We applied this method to a composite fibreglass/polyester material and we obtained very good results. It is then possible to predict precisely the acoustic power radiated by such material.

5- ACKNOWLEDGMENTS

The authors would like to thank M. Hedi Kaffel, M. Rémy Oddo and M. Olivier Foin for their scientifical support as well as their help during this study as well as BOMBARDIER for supplying the composite material.

6- REFERENCES

[1] LOUIS A. Roussos, C.A. Powel, F.W. Grosveld, and L.R. Koval, *"Noise transmission characteristics of advanced composite structural materials,"* J. Aircraft, **21** (7), july1984, p 528-535.

[2] E.O. Ayorinde, R.F. Gibson, *"Improved method for in-situ elastic constant of isotropic and orthotropic composite materials using plates modal data with trimodal and hexamodal Rayleigh formulations,"* Journal of Sound and Vibration and Acoustics, Transactions of the ASME, **117**,april 1995, p 62-69.

[3] O. Foin, *" Étude du comportement vibro-acoustique de plaques multicouches, "* M. Sc. A , Université de Sherbrooke, Québec, Canada, mars 1995.

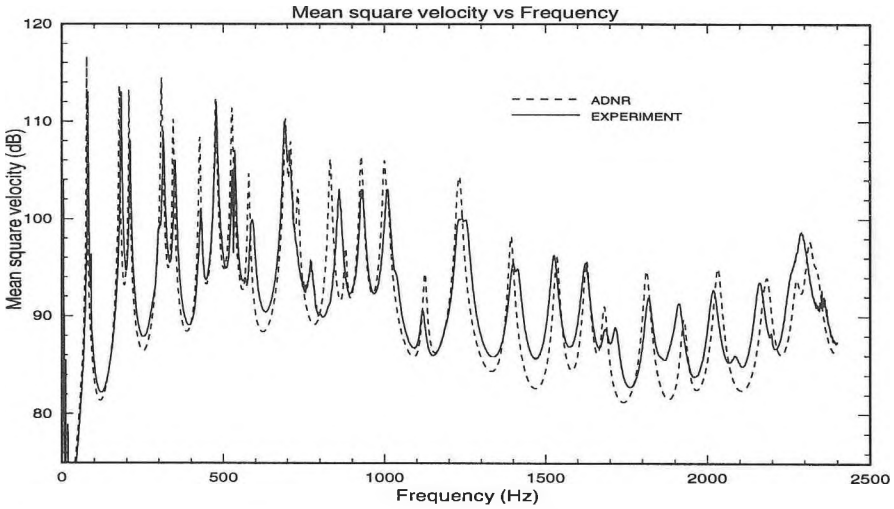

Figure 2 : Comparaison of the experimental and theorical mean square velocity.

RAYONNEMENT ACOUSTIQUE PRODUIT LORS DU CHOC INÉLASTIQUE ENTRE UNE SPHÈRE ET UNE PLAQUE MINCE RECTANGULAIRE.

P. TROCCAZ, R. WOODCOCK, F. LAVILLE
École de technologie supérieure
Département de Génie Mécanique
4750, avenue Henri-Julien, Montréal, QC H2T 2C8

INTRODUCTION

L'impact entre deux structures est une cause importante de bruit dans l'industrie mécanique. Cependant, d'un point de vue théorique, c'est un phénomène peu connu.

Les modèles disponibles dans la littérature utilisent des plaques infinies ou des plaques finies circulaires et la force à l'impact est souvent approximée par une fonction trigonométrique. Dans le modèle développé, la plaque est rectangulaire sur appuis simples, et la force à l'impact sera calculée.

I - CALCUL DE LA FORCE A L'IMPACT

Le calcul de la force à l'impact est effectué par résolution numérique du système de trois équations [1]:

La première équation est obtenue à partir de la loi de Newton :

$$\frac{d^2}{dt^2}\left(u(t)+w(t)\right)+\frac{1}{m}F(t)=0$$

La deuxième équation donne la réponse de la plaque :

$$w(t)=\int_0^t F(t).M(t-\tau)d\tau$$

où M(t) est la mobilité impulsionnelle de la plaque, u(t) le déplacement de la bille, w(t) le déplacement de la plaque, m la masse de la bille et F(t) la force à l'impact. (Voir schéma du dispositif en figure 1.)

La troisième équation est determinée par la relation entre la force de contact et le déplacement. Si on considère que l'impact est élastique, la force est donnée par la loi de Hertz [2]:

$$F(t)=K.u(t)^{3/2}$$

La loi de Hertz a été étendue au cas de déformations plastiques en combinant plusieurs modèles théoriques ([3], [4]), car ce type de déformation est très courant lors des chocs (par exemple dans le procédé de rivetage). La phase de contact est alors divisée en trois zones :

- Déformation élastique: $F(t)=K.u(t)^{3/2}$
- Déformation purement plastique, dès que la contrainte sur la surface de contact devient supérieure à P_0, limite élastique dynamique du matériau. L'expression de la force est alors $F(t)=2\pi RP_0u(t)$. Cette phase se termine lorsque la force atteint sa valeur maximale F_{max}.
- Déformation élastique lors du rebond:

$F(t)=F_{max}\cdot\left(\frac{u(t)-u_r}{u_m-u_r}\right)^{3/2}$ où u_r est le déplacement résiduel (plastique) et u_m le déplacement maximal (plastique et élastique).

II - CALCUL DE LA PRESSION ACOUSTIQUE

Connaissant F(t), la pression acoustique dans le domaine temporel est obtenue à partir de l'intégrale de Rayleigh. Le cas de la bille, qui conduit à une forme analytique, ne sera pas présenté dans cette communication. Le cas présenté sera celui, plus complexe, de la plaque, qui nécessite une intégration numérique où chaque élément de surface est considéré comme une source ponctuelle.

La solution générale de l'équation du mouvement d'une plaque rectangulaire finie de dimensions a et b et d'épaisseur h soumise à la force ponctuelle F(t) est [5]:

$$w(t)=\frac{4}{\rho hab}\sum_i\sum_j\frac{H_{ij}(x,y)H_{ij}(x_0,y_0)}{\omega^*_{ij}}\cdot\int_0^t F(t)e^{-\xi\omega_{ij}(t-\tau)}\sin\left[\omega^*_{ij}(t-\tau)\right]d\tau$$

avec

$$H_{ij}(x,y)=\sin\left(\frac{i\pi}{a}x\right)\sin\left(\frac{j\pi}{b}y\right)$$

$$\omega_{ij}=\sqrt{\frac{D}{\rho h}\left[\left(\frac{i\pi}{a}\right)^2+\left(\frac{j\pi}{b}\right)^2\right]}$$

$$\omega^*_{ij}=\omega_{ij}\sqrt{1-\xi^2},\ D=\frac{Eh^3}{12(1-\nu^2)}$$

ξ rapport d'amortissement
(x_0,y_0) coordonnées du point d'impact

La pression acoustique en un point M de l'espace de coordonnées (r,θ,φ) est alors obtenue en calculant numériquement l'intégrale

$$p(r,\theta,\varphi,t)=\frac{\rho_0}{2\pi}\int_S\frac{\ddot{w}\left(x,y,t-\frac{d}{c}\right)}{d}dS$$

où d est la distance entre l'élément de surface considéré et le point de mesure.

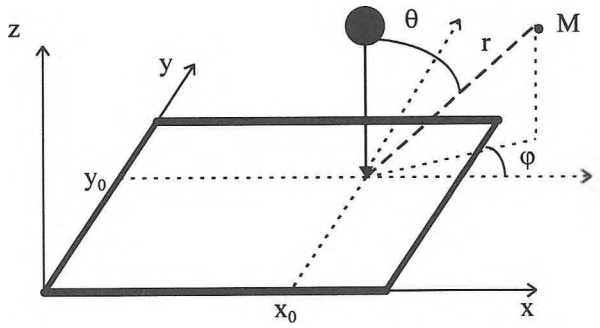

Figure 1

III - RÉSULTATS

1- Force à l'impact:

La figure 2 montre que la prise en compte des déformations plastiques diminue la valeur maximale de la force et déplace ce maximum dans le temps (par rapport au cas purement élastique).

Les résultats présentés concernent un choc entre une sphère en acier de diamètre 7,8 mm et une plaque en aluminium de dimensions 405×325×3 mm. La vitesse initiale de la bille est 1,40 m/s et l'impact a lieu au centre de la plaque.

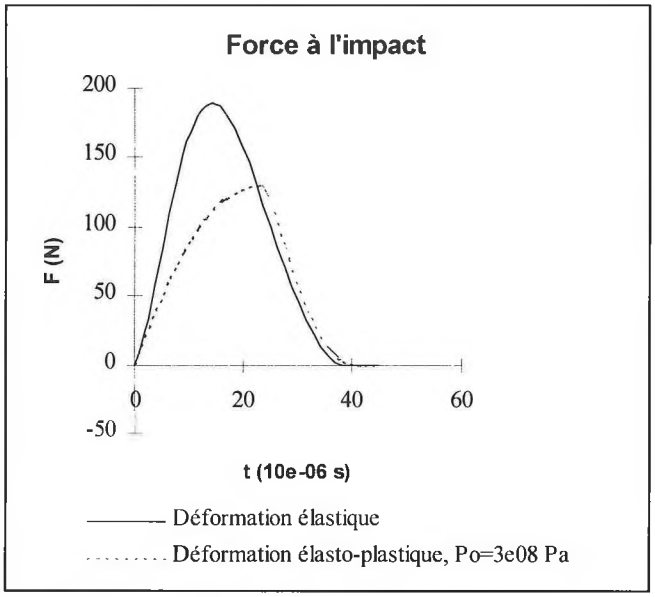

Figure 2

2 - Pression acoustique:

Les courbes de pression acoustique obtenues comportent trois zones distinctes. Premièrement, un pic correspondant à la déformation initiale de la plaque au point d'impact (régime "transitoire"), deuxièmement, une zone de pression faible ou nulle correspondant à la propagation des ondes de déformation jusqu'au bord de la plaque (cette zone existe si le point de mesure est situé près de la normale à la plaque au point d'impact car le rayonnement acoustique des ondes qui s'éloignent du point d'impact ne l'atteint pas en premier), et, troisièmement, une zone correspondant au passage des ondes de déformation réfléchies par les bords de la plaque (régime "pseudo-permanent").

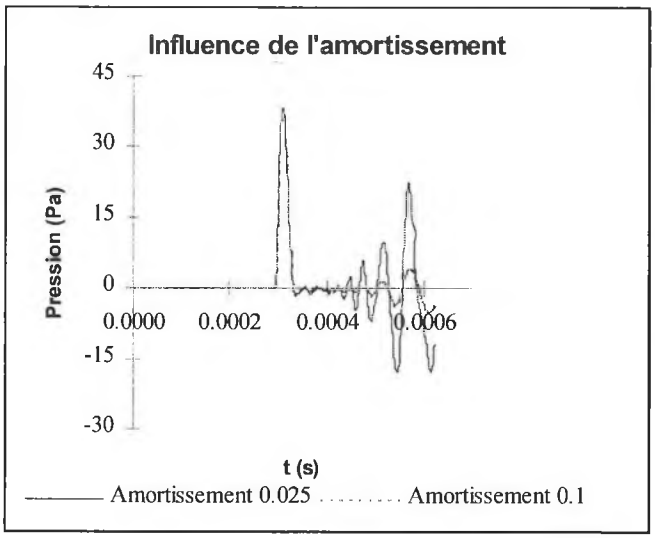

Figure 3

Le modèle est alors utilisé pour déterminer la contribution aux différentes parties du bruit d'impact de paramètres caractérisant les deux structures intervenant dans le choc. Les deux résultats suivants concernent un point de mesure situé à 10 cm de la plaque au-dessous du point d'impact, tel que $\theta = \varphi = 0$.

Le premier résultat montre que l'amortissement n'a une influence que sur le régime pseudo-permanent (voir figure 3).

Le deuxième résultat montre que par contre, le fait de changer le matériau de la plaque pour un matériau plus plastique permet de réduire le bruit rayonné dans toutes les zones (voir figure 4).

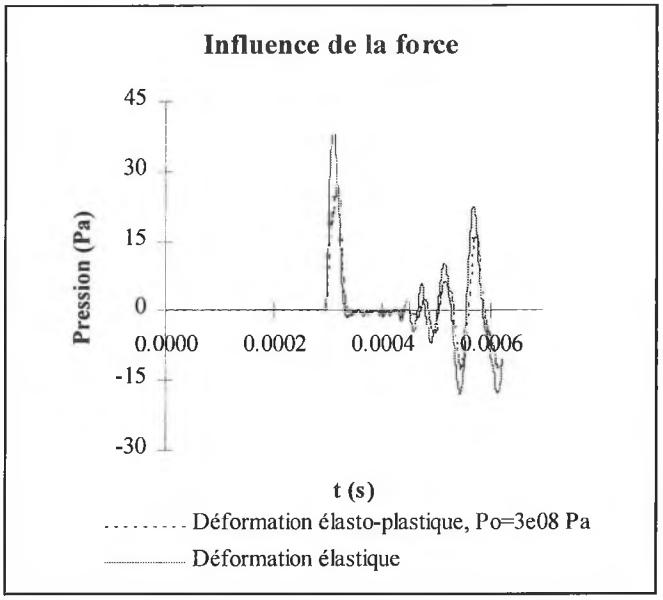

Figure 4

CONCLUSION

Le modèle développé a permis de mettre en évidence les différentes composantes du bruit dû à l'impact entre une sphère et une plaque mince rectangulaire, ainsi que de voir par quels moyens on peut arriver à réduire ce bruit.

Son utilisation pour la conception optimale de systèmes mécaniques dont le fonctionnement comporte un impact a été illustrée par une étude paramétrique sur l'amortissement et sur la plasticité du matériau de la plaque.

RÉFÉRENCES

[1] F.Laville, D.Trentin, "Impact noise modeling with application to noise control at the source in the case of a plastic granulator", *Inter - Noise 92*, 607-609.

[2] W.Goldsmith, *Impact*, Edward Arnold Publishers, London, 1960.

[3] D.Tabor, *The Hardness of Metals*, Oxford, The Clarendon Press, 1951.

[4] S.Chattopadhyay, "Permanent indentation effects on the impact response of elastic plates", *Journal of the Acoustical Society of America*, 82(2):493-497, 1987.

[5] M.Tokunaga, A. Ackay and M. Latcha, "A theoretical analysis of transient sound radiation from a clamped circular plate", *Journal of Applied Mechanics*, 51:41-46, 1984.

NOISE REDUCTION IN A FACTORY WORKPLACE USING RAY TRACING METHOD

Jean-Luc Wojtowicki & Jean Nicolas
Acoustic and Vibration Group
Mechanical engineering dept.
University of Sherbrooke
Sherbrooke (Quebec)
J1K 2R1
CANADA

I- INTRODUCTION

This paper presents the results of a noise control study using the RAYSCAD+ software based on the ray tracing method developed by INRS [1].

The aim of this study is to test the efficiency and the accuracy of the ray tracing method applied to factory noise predictions. The originality of the work lies in the complete validation of the method on a real factory workplace instead of a well controlled laboratory case.

II- DESCRIPTION OF THE FACTORY HALL

The factory is 60 meters long, 29 meters wide and 6 meters high. It is separated in three areas: the fabrication area, the delivery area and the assembly lines (figure 1).

The noise sources (punch presses, cutting presses, ...) are located in the fabrication area. The broadband noise generated by impacts propagates through the factory hall from the fabrication area to the assembly lines as well as across the separating wall to the delivery area.

The problem in this study was to protect the workers on the assembly lines and in the delivery area from the fabrication area noise.

III- MODELING THE FACTORY HALL AND PRELIMINARY MEASUREMENTS

Because punch presses generate noise with a strong variability, the sound field in the factory has been characterized using a well controlled sound source.

Sound propagation decay and sound pressure level distribution have been measured and calculated using the RAYSCAD+ software. As a example, figure 2 presents calculated and measured sound propagation decay for the 1 kHz octave band. The comparison of the two curves demonstrate a very good agreement between calculated and experimental results. The difference is less than 2 dB at any distance from the source.

IV- DESCRIPTION OF THE STUDIED ACOUSTICAL TREATMENTS

The advantage of the RAYSCAD+ software lies in the possibility to make assessments of various scenarios of acoustical treatments.

It has been used to find the most promising ideas of treatments. It appears that the noise in the delivery area could be easily reduced raising a wall between the delivery area and the fabrication area (figure 3). The noise of the noisiest punching machines could be reduced with a partial enclosure (acoustical screens) around the machines (figure 4). And the best solution to decrease the sound propagation from fabrication area to the assembly lines was to use acoustical baffles hanging from ceiling.

V- MODELING THE ACOUSTICAL TREATMENT AND VALIDATION MEASUREMENTS

The modeling of the acoustical treatments has been made modifying the initial model. Absorbing planes were added to simulate the partial enclosure, the separating wall and the baffles.

The RAYSCAD+ software has been used to study several configurations of screens and baffles to obtain the highest reduction with the minimum absorbing material quantity. Parametric studies have been performed to optimize baffles (number, spacing, size, ...) and screen positioning.

The predicted reductions are given in table 1. These calculated results were presented to the company executives and engineers. The decision of settling up the acoustical treatment could have been taken knowing both the involved reduction and the cost.

The actual baffles were made of a sandwich of two 2.5 cm acoustic tiles separated by an air gap and supported by a light steel frame. The screens are made with 1.2 cm plywood boards, absorbing material in the inner face of the partial enclosure and protected by a perforated steel sheet. The separating wall is made of two corrugated steel sheets separated by an air gap and thermo-acoustic material (figure 6).

Figure 5 shows the sound propagation decay at 1 kHz. One can see that the agreement is good from 0 to 15 meters from the source and the calculated sound pressure levels are a bit overestimated from 15 to 25 meters. The measured reductions are given in table 1. The comparison of the calculated and measured reductions proves the efficiency of the method to predict reliable noise abatements. The main objectives of noise reduction in the factory were reached in the delivery area and in the assembly lines.

VI- CONCLUSION

The RAYSCAD+ software has proven its ability to guide decisions when an acoustical treatment is needed in a factory workplace. The main advantage is the possibility to associate predicted reduction and costs to various scenarios of acoustical treatments.

Actually there are several local discrepancies between calculations and measurements. Those errors are due to the calculation hypothesis of the ray tracing method which neglects phenomena like wave diffraction on the edge of screens. But for industrial

applications where no detailed precision is needed, the method gives a good estimate on the sound field in a room.

VI- ACKNOWLEDGMENTS

The authors would like to thank the Venmar Company for its technical and financial support during this study.

VII- REFERENCES

[1]: A-M. Ondet and J-L. Barbry, "Modelling of sound propagation in fitted workshops using ray tracing", *J. Acoust. Soc. Am.I* **82**(2), 787-796 (1989).

[2]: M. Hodgson, "Case history: Factory prediction using ray tracing - Experimental validation and the effectiveness of noise control measures", *Noise Control Engineering Journal*, **33**(3), 97-104 (1989).

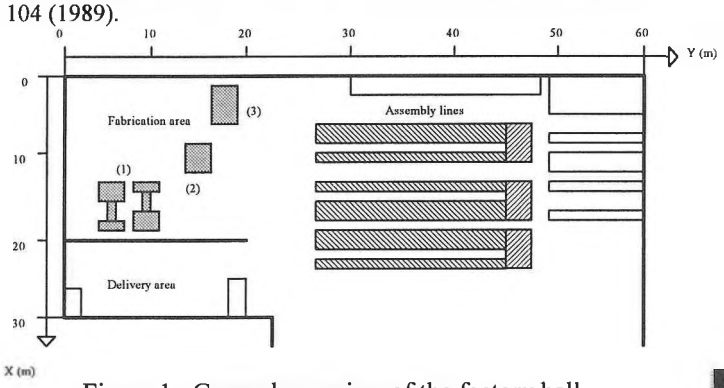

Figure 1. General overview of the factory hall

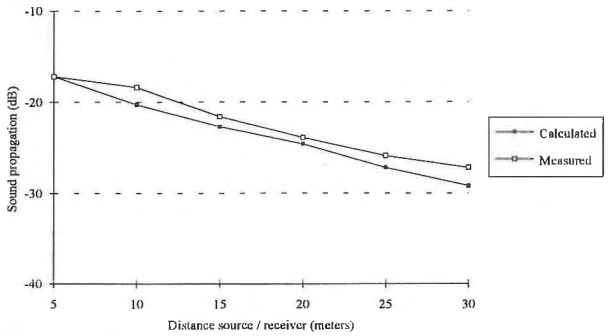

Figure 2. Sound propagation decay at 1 kHz before treatment

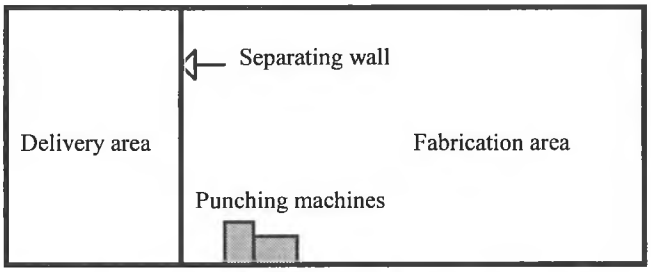

Figure 3. Separation wall between fabrication and delivery areas

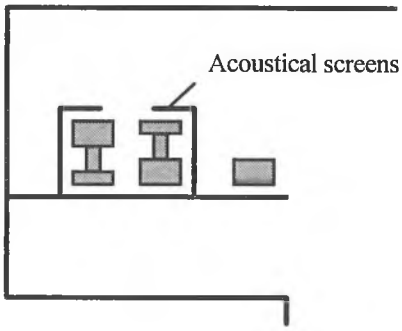

Figure 4. Acoustical screens around the pair of punching machines

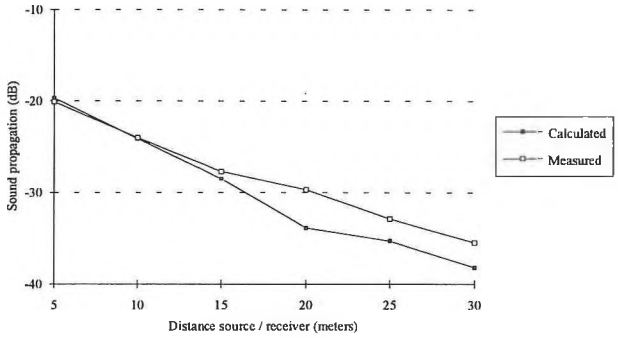

Figure 5. Sound propagation decay at 1 kHz after treatment

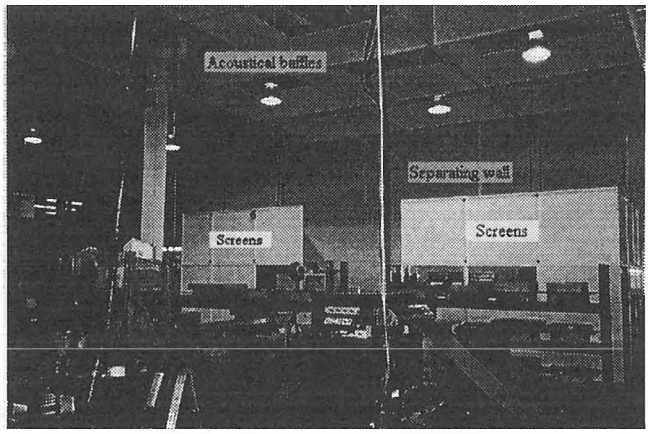

Figure 6. Actual acoustical treatment

	Calculated reduction	Measured reduction
Fabrication area	6 dB	5.5 dB
Assembly lines	8 - 12 dB	7 - 10 dB
Delivery area	12 dB	13.5 dB

Table 1. Predicted and measured reduction at 1 kHz

THE EFFECTS OF FIRING PATTERNS, METEOROLOGY AND TERRAIN ON COMMUNITY NOISE EXPOSURES FROM A MILITARY RIFLE RANGE

Clair W. Wakefield, M.A.Sc., P.Eng.
Wakefield Acoustics Ltd.,
618 Yates Street, Victoria, B.C., V8W 1K9

BACKGROUND

Heals Range in Central Saanich, B.C., has been an active military small arms range since before WWI. Semi-rural residential development has gradually encroached on the range and this, combined with its then upcoming use during the 1994 Commonwealth Games, led to calls from some elements of the community for restriction or termination of its use, due to excessive noise impacts. In response, the DND retained ***Wakefield Acoustics Ltd.*** to study the shooting noise and how it was influenced by firing patterns/positions, meteorology and terrain features.

SHOOTING NOISE MEASUREMENTS

Heals Range is located in a semi-agricultural valley bounded by forested hillsides. On several occasions during 1992-93, C7 rifle noise measurements (A-weighted Impulse levels - dBAI) were made at ten mostly residential locations around the range (source-receiver distances varied from 150 to 1650 m) under a variety of light-wind and windless conditions. Both normal multiple-shooter military practices or "serials" (at 25 to 300 m firing ranges) and controlled individual-round shooting (at 25 to 1000 m firing ranges) were measured.

At distant valley floor receivers, single C7 round noise levels varied by up to 30 dBAI (e.g. 45 to 75 dBAI) depending largely on meteorological conditions. Nearer the range along the valley sides, this variation was more like 10 to 15 dBAI (e.g. 65 to 80 dBAI).

SINGLE-ROUND NOISE MODEL

An empirical model was developed to predict single-round noise levels as a function of firing range and firing posture (prone, kneeling, standing) and to define the probable limits of shooting noise at the various receiver locations. The model generated three separate results: 1. upper-limit or "worst-case" noise levels accompanying either a significant "source-to-receiver" wind or a strong temperature inversion, 2. "with excess attenuation" noise levels (one for each firing posture) occurring under near-neutral atmospheric conditions when ground effect attenuation and/or terrain/forest shielding are fully active, 3. lower-limit "near maximum sound shadow" values accompanying either a "receiver to source" wind or a strong temperature lapse condition. The single-round model (derived from components of U.S. CERL, Swiss and Swedish military rifle noise models) was as follows:

$$L_{AI} = 141 + 7(1+\cos\theta) - (24 + \cos\theta)\log_{10}D - 40\,(1-e^{-D/400})/(h_{av}+0.5) - 10\log_{10}(3+59\Delta PL) - 5(W_F/100) \quad \text{(dBAI)} \qquad \text{(Eqtn.1)}$$

where:

L_{AI} = A-weighted impulse response sound level,
141 = reference impulse sound level at 1 m,
θ = source to receiver bearing angle (degrees),
D = source to receiver distance (m),
h_{av} = aver. height sound path above ground (m),
ΔPL = increase in sound path length due to terrain shielding,
W_F = width of forest belt(s) encountered along sound path (m), to maximum of 200 m.

Under "worst-case" conditions (only geometric spreading and atmospheric absorption present), just the first three terms of Eqtn. 1 were used. However, where terrain features and/or forest belts were so close to the source and/or receiver that their shielding would not likely be fully overridden by down-wind or thermal inversion effects, extra shielding effects of from -1 to -10 dBAI were applied to the "worst case" shooting noise levels. Under "with excess attenuation" conditions all six terms were used. Under "near maximum sound shadow" conditions, a sound shadow attenuation term (-30 to -35 dBAI depending on source-to-receiver distance) was applied to the worst case noise levels.

The model was applied to each of the nine residential measurement locations around the range. As an example, Figure 1. below illustrates the model's output, with

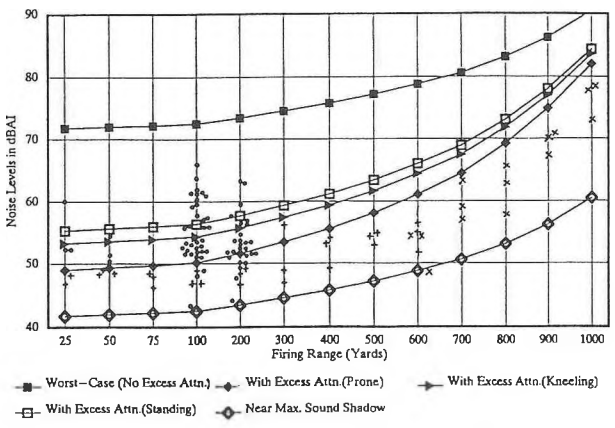

Figure 1: Single-Round C7 Rifle Noise Levels (dBAI) at Foxtrot Site as a Function of Firing Range

measured single round data plotted, for "Foxtrot Site" (located on the eastern edge of the valley floor about 150 m southeast of the 1000 m firing position and about 1125 m from the 25 m firing position). Typically during the noise measurements, "Foxtrot" site was upwind of the range and therefore appears to have generally benefited from ground effect attenuation as well as some sound shadow attenuation.

Heals Range is surrounded on three sides by residences so that certain firing positions are favourable for certain residences and unfavourable for others. To indicate which firing ranges could be expected to produce the least overall noise impact, community average "worst case" single round noise levels were computed for each firing range. The shortest ranges (from 25 to 200 m) were projected to create average community noise exposures from 4 to 5 dBAI lower than the longest ranges (700 to 1000 m). This was fortunate since most military rifle practices are from ranges of 200 m or less.

EFFECTS OF FIRING PATTERNS

During a given military practice serial, up to 20 shooters may fire more or less concurrently. The firing rate (rounds/sec) varies considerably with type of serial. With 20 shooters, the total firing rate of the group can range from about 1 rnd/s for the more deliberate serials (zeroing, application and grouping) to 20 rnd/s for the "snap" and "rapid" serials. Sustained firing within the semi-reverberant environment of Heals Range (decay rates induced by the surrounding forested hillsides were measured at 15 to 60 dB/s), can produce substantial amplification of shooting noise levels. Differences of 5 to 7 dBA were observed between 20-shooter "rapid" and 20-shooter "application" serial).

The following expression was developed to predict this sustained fire, reverberant build-up effect:

$$L_{sust} = 10\log \sum_{n=1}^{N} 10^{[L_0-(n-1)D_R/F_R]/10} - L_0 \quad \text{(dBAI)} \qquad \text{(Eqtn. 2)}$$

where:

L_{sust} = sustained-fire reverberant noise level build-up (dBAI),
L_0 = single round impulse noise level (dBAI),
D_R = reverberant decay rate (dB/s),
F_R = total firing rate (rnds/s),
$N = tF_R$ = total number rounds fired in time "t".

For conditions at Heal Range, this expression predicted reverberant build-up effects of between 0 to 7 dBAI.

LOCAL METEROLOGICAL PATTERNS

A meteorological station (Davis Weather Monitor II) was set up at Heals range to monitor the wind velocity, relative humidity and temperature at two heights (0.9 and 7.25 m) above ground allowing temperature inversion or lapse conditions to be detected. Data was continuously sampled and stored in the system's digital memory and periodically down-loaded via modem. Data acquired from summer 1993 to early 1994 was used to generate monthly summary plots of wind velocity and temperature gradient versus time of day. These could be used to select practice times which, on a statistical basis, would minimize the potential for disturbance in the surrounding community by avoiding periods of likely temperature lapse or of downwind propagation towards residential areas of greatest concern.

CONCLUSIONS

Through a combination of noise measurement, empirical propagation model development and monitoring of local meteorology, it has been found that appreciable variations in community noise exposures around Heals Range can result from the selection of firing range, firing patterns and firing postures. However, much more significant fluctuations can be attributed to local meteorology, which, at least during the more critical warm weather months, exhibits fairly consistent diurnal patterns.

These investigations have then provided the DND with the information necessary to permit, over time, minimization of community noise exposures from Heals Range primarily through the selection of practice times and firing ranges that take best advantage of natural sound attenuating mechanisms available in the range's valley bottom setting.

LONG RANGE OUTDOOR SOUND PROPAGATION MODEL

Alex Boudreau[1], André L'Espérance[1], Jean Nicolas[1] and Gilles Daigle[2]

1) Faculty of Applied Sciences, Université de Sherbrooke, Sherbrooke (Qué) Canada, J1K 2R1

2) Institute of Microstructural Sciences, National Research Council of Canada, Ottawa Canada, K1A 0R6

Introduction

In the case of medium and long ranges outdoor sound propagation, refraction due to temperature and wind gradients may increase (or decrease) the sound pressure due to a point source[1,2]. To fulfill the needs of practical outdoor sound propagation studies, it appears to be necessary to develop practical and reliable software for engineering purposes to predict outdoor sound propagation under general meteorological conditions. This paper present the software *LORAP* developed to reach that goal.

1.0 Theoretical background

This software included an acoustical propagation model and a meteorological model. Those theoretical model are based on the research done in the past 10 years on the effect of ground and of the atmospheric conditions on outdoor sound propagation.

The acoustical model is based on an extension of the classical ray-theory[3]. This heuristic model assume a linear sound speed gradient 'a' .) to consider the effect of the atmospheric refraction. This hypothesis allows an analytical determination of the curved ray path parameters (travel time, angle of reflection on ground, path length etc.). The effect of the atmospheric turbulence can also be included by considering the lost of coherence between rays. Various comparisons with other acoustical models and with experimental results done in the recent years have shown the efficiency of this model[3-4].

The meteorological model estimates the sound speed profile (SSP) between a source and a receiver and the fluctuating index of refraction according to input meteorological data. This (SSP) is calculated using the temperature and wind profiles. The exact determination of the wind and temperature profiles from general meteorological conditions is done using the surface-layer similarity scaling theory[5]. The data needed to estimated these SSP will be mentionned in the following section.

Using this SSP, the algorithm then calculated the linear sound speed gradient a necessary to the acoustical model to evaluate the effect of the atmospheric refraction. The linear sound speed gradient a used in the acoustical model is determined based on a method used in radio communications[5]. This method assumed that between a source and a receiver, the zone of space concerned with the propagation process is mostly defined by the first Fresnel ellipsoïd. The equivalent linear sound speed gradient is obtained by considering the mean of the real sound speed profile in the first Fresnel zone. Because the wide of the Fresnel ellipsoid is function of the distance and of the frequency, the linear sound speed gradient a depends not only on the heights of the source and receiver, but also on the frequency and on the heights of the source and of the receiver.

2.0 Data input

The software has been developed with the window standards and the main panel has 6 menus: *Fichier, Météo, Balayage, Géometrie, Options, Calcul and Résultats.*

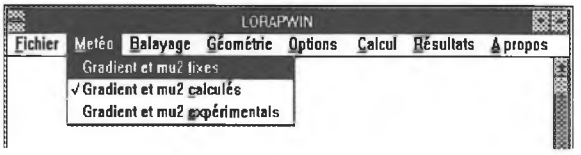

The *Fichier* (*File*) menu is used to input old data files or store new data file and results. The option Météo is used to set the values of the sound speed gradient a and the index of turbulence$<\mu^2.>$. These values can be either fixed, calculated from meteorological conditions, or be experimental values. If the user want to calculated a from the meteorological conditions (the second choice), then a sub-menu asking for the wind speed and direction, the temperature, cloud cover, azimuth of the sun, and roughness of the ground will be presented, in which the user can change any parameters.

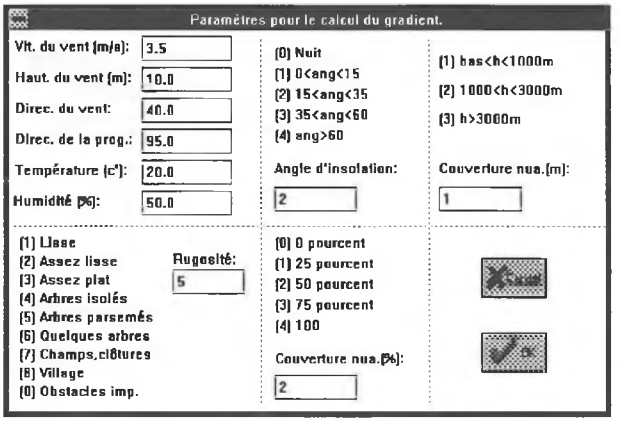

The menu *Balayage* (sweeping) allows to the user to calculated the sound pressure as a function of the frequency, or the distance, or the height of the source, of the receiver etc. In each case, the minimum and the maximum values and the step could be choose by the users.

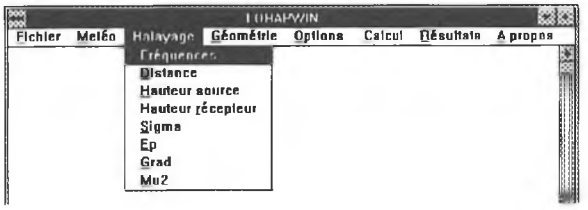

The data related to the geometrical configuration to study (height of the source and of the receiver, distance source to receiver, type of ground and sound power spectra of the source), are input using the geometry menu.

The *Options* menu allows to the user to modify some aspects of the theoretical calculation. For example, the maximum number of rays between a source and a receiver can limited. This option thus allows to the user to see the effects of additional rays in presence of a positive sound speed profiles. The effect of the atmospheric absorption can also be considered or not. The maximum height that a ray can reach can also be limited to a certain value, which can be usefull to simulate, for exemple the effects of a double linear sound speed gradient etc.

The *Calcul* menu start the calculation. For standard cases, the calculation time is couple seconds, even at high frequencies and long distances. When the sound speed gradient is important and/or when the number of calculation points increases (which depend on the value of the *step* choose in the *Balayage* menu), the computation time will increase, but in general it will be lower then a minute. It should be mentioned at this point that the heuristic acoustical model used in this software required very low computation time compared to other method like PE[6] or FFP[7] methods that could required hours of computation at long distances and high frequencies.

3.0 Results

After the calculation, numerical value or graphics of the results could be obtained with the *Resultats* menu.

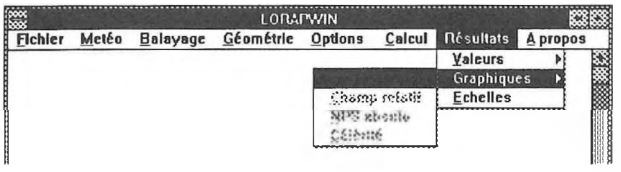

Numerical values or graphics of the results can be obtained on the screen, and/or transfer on a Excel file. The results available are the excess attenuation (attenuation compared to the level at 1m), the relative sound pressure level (attenuation compared to the level in free field without atmospheric effects), and the absolute sound pressure level (which depend on the sound power of the source input in the *Geometrical* menu). Figure 1 give as an example the results of the benchmark case published in a recent paper[4]. Note that the sound speed profile calculated according to the meteorological data can also be visualized by choosing the *celerité* sub-option.

Figure 1 Excess attenuation at 100 Hz in the case of a linear gradient of 0.00295 m^{-1} source height 5 m, receiver height:1 m.

4.0 Conclusions

A practical software to predict outdoor sound propagation under general meteorological conditions have been developed. This software, presented on a friendly window environment, included a meteorological model and an acoustical propagation model. The results obtained are the absolute sound pressure level, the sound pressure level relative to free field and/or the excess attenuation. A second version of this software is now under development in order to calculate a mapping of the overall sound pressure level created by a different number of sources over a surface.

References

1. P.H. Parkin et al., "The horizontal propagation of sound from a jet engine close to the ground at hatfield", J. Sound Vib. 2, 4, pp. 353-374 (1965).
2. L'Esperance A. et al., Sound propagation in the atmospheric surface layer: comparison of experiment with FFP predictions", Applied Acoustics, (40) p. 325-346, 1993
3. L'Espérance A. et al.. "Heuristic model for outdoor sound propagation based on an extension of the geometrical ray theory in the case of a linear sound speed profile" Applied Acoustics, 37 p.111-139 (1992)
4. K. Attenborough,..., A. L'Espérance and others, "Benchmark cases for outdoor sound propagtion models", J. Acoust. Soc. Am., (97), 1, p.173-191 (1995)..
5. a. L'Espérance, G. Daigle « Effect meteorological conditions on outdoor sound propagation: modelisation and analysis of practical cases »,NATO-CCMS Symposium on Aircraft Noise Receiver Technology », Baltimore, Maryland, 16-20 May 1994.
6. K.E. Gilbert and X. Di " A fast Green's function method for one-way sound propagation in the atmosphere", J.Acoust. Soc. Am. 94 pp. 2343-2352 (1993).
7. S.W. Lee et al., "Impedance formulation of the Fast-Field program for acoustic wave propagation in the atmosphere", J. Acoust. Soc. of Am., **79** pp. 628-634 (1986).

Development of Perceptual Distinction between Phonemic Contrasts in a First and Second Language

Elzbieta B. Slawinski,
Psychology Department, The University of Calgary
2500 University Dr. Calgary, Alberta T2N 1N4

In order to perceive a contrast between phonemes of a particular language a child has to develop an appropriate phonological system. Such a phonological system includes a phoneme inventory imposed on a multidimensional phonetic space that is divided into a set of classes. These classes differ by distinctive features along one or more dimensions.

It has become increasingly apparent that there are developmental influences on the categorical perception of the [r], [w], and [l] phonemes; however, the exact nature of these influences has not been determined. Specifically, it has not been definitively found whether the attainment of adult perceptual capabilities is a gradual process or whether it occurs more abruptly.

Phonemic perception is a product of processes that occur at sensory (auditory) and cognitive (interpretive) levels. Phoneme discrimination during infancy is based on acoustical differences between phonemes and is thus performed on the sensory level [1]. During the process of language acquisition in a particular linguistic environment, a child seems to engage her/his attentional system in the interpretation of the sensory level output [1]. This system seems to have the capacity to modify its use of environmental information to arrive at an interpretation of phonemic contrast appropriate for the language to be acquired. Such a modification might include enhancement or suppression of auditory information depending on its relevance in the language. Children, while acquiring the phonology of a language, learn to classify phonemes along the relevant dimensions of the phonetic space. Thus, the development of a phonemic contrast might correspond to an improvement in the ability to reject irrelevant information and accept relevant information which constitute the distinctive features of the language being acquired. At the same time children are also gaining proficiency in the integration of these distinctive features in order to arrive at the phoneme percept. It has been demonstrated that such improvement in the integration of distinctive cues is associated with a diminished range of uncertainty [2], and is reflected by steeper slopes of identification functions and more prominent peaks in discrimination functions of facilitating two-cue comparison pairs [4].

In order to assess the course of development of perceptual distinction between initial prevocalic [w], [r], and [l], performance of children of various ages was examined on identification and discrimination tasks.

Three age groups of English children (three, four, and five years old) and adults were recruited as participants in a study of the perceptual development of the [r-w] contrast. The experimental paradigm involved a two-alternative forced choice identification task. The stimuli employed in the identification task were acoustic tokens of a [r-w] synthetic continuum ranging from 'red' to 'wed' and varying in F_2 and F_3 onset frequencies (spectral acoustical cue) and F_2 and F_3 transition durations (temporal acoustical cue). Percent identification data was computed and transformed to yield measures of phonemic boundaries. The significant shifting in phonemic boundaries ($F(3,36) = 4.61$; $p < .01$) and increasing steepness of the identification function ($F(3,36) = 3.2$; $p < .01$) as a function of age supports the hypothesized progressive development in phonemic perception (Figure 1).

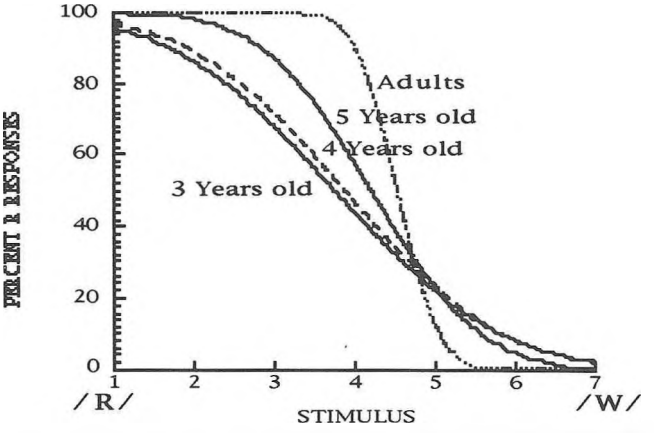

Figure 1.Identification of 'red' and 'wed' by 3, 4, and 5 year old children and adults. Steepness of the curves increases with increased age of participants.

The development of the incorporation of spectral and temporal acoustical features in the perception of the phonemic contrast between [r] and [l] sounds in the initial prevocalic position for English and Japanese children and adults with different exposure to English was also examined. Integration of both spectral and temporal information enables English listeners to efficiently discriminate between [r] and [l] sounds in the initial prevocalic position. Furthermore, adult English listeners discriminate facilitating two-cue comparisons pairs better than conflicting two-cue comparisons pairs [4]. This corresponds to a perceptual equivalence of temporal and spectral cues, and is the result of a language-specific phonemic categorization process and as such should be a gradual process.

Four groups of monolingual English children in the range of 3-6 years of age, and four groups of Japanese children in the range of 3-7 years of age, and two groups of Japanese adults with different exposure to English participated in the aforementioned study. A set of oddity discrimination tasks differing in the relation between spectral and temporal acoustical cues was administered to participants. Out of two continua that varied spectrally from F2 and F3 onsets characteristic of 'rake' to those of 'lake', but had different temporal patterns, two-cue facilitating and conflicting oddity discrimination tasks were prepared.

Separated repeated measures analyses of variance (ANOVA) were performed for English and Japanese children as well as adults. There were significant main effects for age as well as language exposure, condition (two-cue facilitating and conflicting), and for comparison pairs. The pooled discrimination functions for the two-cue facilitating condition are displayed in Figure 2 for English children, in Figure 3 for Japanese children, and for English and Japanese adults in Figure 4. There is a significant change among English children in the ability to integrate spectral and temporal acoustical cues during perceptual distinction of the [r-l] contrast as a function of age. Thus, with increasing age, children rely more on phonemic similarities

than on acoustic dissimilarities, as they are showing improved discrimination between the middle range of comparison pairs as compared to those closer to phonemic templates (Figure 2).

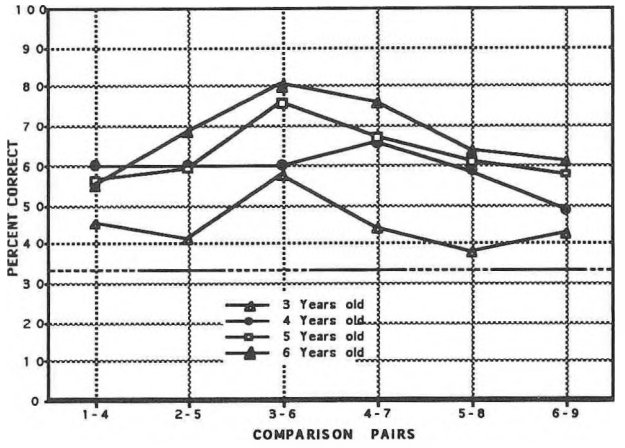

Figure 2. Discrimination curves for four age groups of English children. Percent of correct responses increases with increased age of children group.

Perceptual distinction of [r-l] by Japanese children (Figure 3) shows a different picture: 3, 4, and 5 year old children seem to rely on detection and classification of acoustical differences only. However, the discrimination accuracy of [r] and [l] sounds by 7-year old Japanese is based on the process of attending to patterns of acoustical cues which differentiate this phonemic contrast, and subsequently comparing them to the multidimensional representation of the phonemic percept. The difference obtaining between English and Japanese children in the course of acquisition of the [r-l] phonemic contrast is likely due to a difference in the duration and intensity of exposure to English. The Japanese children were first exposed to English 3-4 years later than English children.

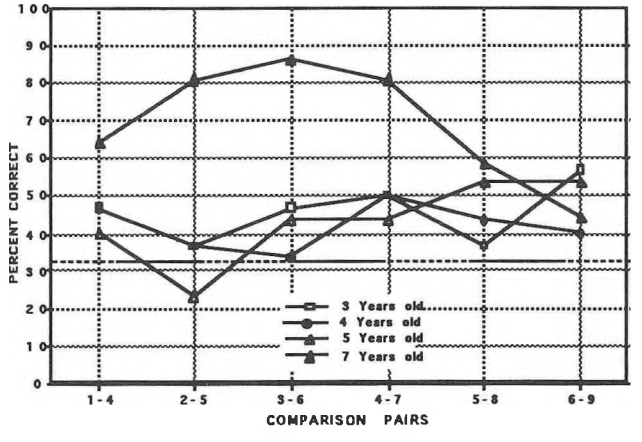

Figure 3. Discrimination curves for four age groups of Japanese children. The performance of three younger age groups is very poor. Only the oldest age group demonstrates high scores on discrimination.

A similar effect of the exposure to English on discrimination performance can be observed in results obtained for English and Japanese adults (Figure 4) [3].

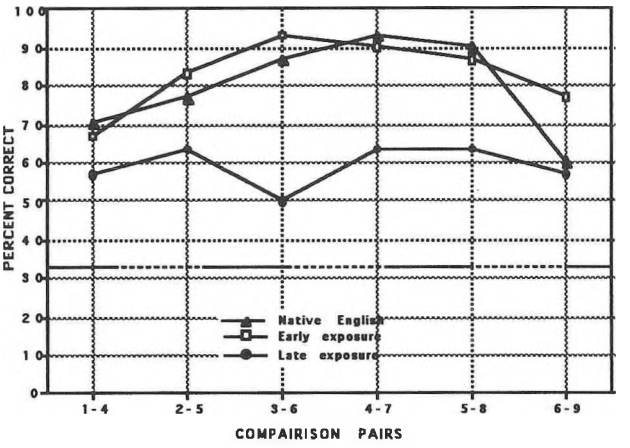

Figure 4. Discrimination curves for three groups of adults with different exposure to English. Native English and Japanese with intensive exposure demonstrate very high performance scores. Japanese listeners with limited exposure demonstrate much poorer discrimination.

In conclusion, it has been found that English and Japanese children, and Japanese adults with different degrees of exposure to English, did not rely in the same manner on the available acoustical cues needed for prevocalic [r], [w], and [l] discrimination. While discrimination or identification by older English and Japanese children, and Japanese adults with an early and intensive exposure to English, was strongly based on similarity or dissimilarity between percepts derived from the integrated information of spectral and temporal cues, the performance of younger English and Japanese children and Japanese adults with a late and less intensive exposure to English relied to a lesser degree on the perceptual configuration of acoustical cues and was probably more influenced by the acoustical dissimilarities. The observation that there is a significant improvement in the ability to integrate acoustical cues with increasing age supports the hypothesis that the attainment of perceptual distinction between phonemic contrasts is a gradual and progressive development in the proficiency of categorical perception [5].

References

1. R. Aslin and D. Pisoni (1980) Some developmental processes in speech perception In G.M. Yeni-Kosmshian, J.F. Kavanagh and C.A. Ferguson, (eds.) Child Phonology v.2. pp. 67-96.

2. R.N. Ohde, K.L. Haley, H.K. Voperian, and C.W. McMahon (1995). A developmental study of the perception of onset spectra for stop consonants in different vowel environments. J.A.S.A. ,94, pp. 3800-3812.

3. E.B. Slawinski and J.F. MacNeil (1994). The relationship between perceptual and productive discriminations of English [r] and [l] sounds by Japanese speakers. International Journal of Psycholinguistics, 10, 1-23.

4. M. Underbakke, L. Polka, J. Gottfried and W. Strange (1988). Trading relations in the perception of /r/-/l/ by Japanese learners of English. J. A.S. A. 84, 90-100.

5. M. Zlatin and R.A. Koenigsknecht (1975). Development of the voicing contrast: perception of stop consonants. J.S.H.R., 28, pp. 541-553.

Acknowledgment: The research was supported by Toronto Hospital for Sick Children Foundation.

PERCEPTION OF A FRICATIVE-STOP CONTINUUM BY ADULTS AND CHILDREN

Karen M. Krueger, Megan M. Hodge and Terrance M. Nearey
University of Alberta, Edmonton, Alberta

1. INTRODUCTION

The purpose of this study was to determine if there are differences between the identification functions of normally articulating children and adults for perception of a consonant manner contrast, in this case, a continuum of synthesized alveolar fricative and stop "like" sounds. Based on previous research addressing age differences in categorical perception [1, 2], the following hypotheses were made. Compared to adults, children will exhibit: (1) Less enhanced discriminability at category boundaries than adults, i.e., wider category boundaries, (2) A greater range in the shape of their individual response functions, and (3) Less stability in their internal representation of the fricative-stop manner contrast, as reflected by greater internal and external response variability scores. In addition, a misarticulating child, who substituted alveolar stops for fricatives, provided an opportunity to explore the hypothesis that: (4) Misarticulating children who do not produce a perceptually differentiated alveolar fricative-stop contrast will exhibit less stability of their internal representation of the fricative-stop contrast than normally articulating children.

2. METHOD

2.1 Subjects

Three men and 3 women, 25 - 28 years of age (subjects A1 - A6), formed the adult group. Three boys and 3 girls, ages 4 years 2 months to 5 years 8 months (subjects C1 - C6), formed the child group. All these subjects had age appropriate articulation skills and produced age-appropriate, clearly distinguishable /s/ and /t/ sounds. One additional 5 year-old girl was included who misarticulated several sounds and used an alveolar stop for fricative substitution pattern (subject MC). All subjects passed a hearing screening, had age-appropriate receptive language ability, had English as a first language, and had never received speech or language therapy.

2.2 Stimuli

The Computerized Speech Research Environment (CSRE) software [3] was used to generate the experimental stimuli, following the parameters described in [4]. A continuum of seven "alveolar-like" consonant segments (C) was synthesized that represented a range in manner from fricative to stop. These segments were each combined with a synthesized vowel-consonant syllable, (VC) /ip/, to form CVC stimuli /Cip/. The VC portion remained constant across the seven point continuum, i.e., Stimulus 1 through 7. The initial consonant segment was varied by manipulating the slope of the rise time of the prevocalic noise source (frication) and as a consequence, noise duration. Frication duration included the noise rise time and a 25 ms segment of steady-state noise at 60 dB. Amplitude of frication increased from 20 dB at onset to 60 dB at onset of the steady state noise segment. The C segment of Stimulus 1 had a rise time of 120 ms. Noise rise time decreased in 20 ms decrements for consecutive stimuli, with a 19 ms decrement between Stimuli 6 and 7, giving Stimulus 7 a noise rise time of 1 ms. All other parameters remained constant across the stimuli. An additional CVC, "Pip", was synthesized for subject training procedures. The Experimental Control System of CSRE randomized the presentation of the stimuli for each subject and recorded the subjects' responses.

2.3 Procedures

Each subject completed a practice listening task to ensure that he or she understood what was expected and could respond reliably. The listening stimuli were then presented using a two-option, forced choice, picture identification paradigm. The presentation of training items and experimental stimuli followed procedures described in [2] with the exception that 8, rather than 16 tokens of each stimulus were presented to accommodate the shorter attention spans of the child subjects. Once training was completed, the subject was presented with the seven experimental stimuli, four times each, in random order. After presentation of these 28 tokens, the subject took a short break. The training tasks and presentation of the experimental stimuli were then repeated. Thus, each subject heard 8 presentations of each of the seven stimulus items on the continuum.

3. RESULTS

Identification functions obtained for the adults, children and for MC are shown in Figures 1, 2 and 3, respectively. Phoneme boundaries (50% crossover point) are indicated by the horizontal dashed lines. The width of phoneme boundary zones, i.e., the number of stimuli for which identifications were not categorical, was also determined using the following criterion. Six out of eight assignments of a stimulus to one of the categories meant that the stimulus was perceived categorically ($p < 0.10$ in binomial distribution). Phoneme boundaries for the adults ranged from Stimulus 2 to between Stimuli 5 and 6 (M=3.67). Results for the children were less well defined as subjects C3 and C4 did not have a boundary. For the other four children, boundaries ranged from Stimulus 1 to between Stimuli 6 and 7 (M=2.83). The phoneme boundary zone is also referred to as the "zone of uncertainty", corresponding to the number of stimuli that are identified at chance levels. This zone covered a range of five stimuli for the child group (Stimuli 1 through 5) and only one stimulus for the adult group (Stimulus 4). MC had a four stimuli "zone of uncertainty" (greater than any other adult or child subject).

Analysis of the subjects' responses to the two end point stimuli on the continuum revealed that the adults identified Stimulus 1 as "sip" more frequently than the normally articulating children ($X^2(1, N=48)-4.47, p<.05$). Both groups identified Stimulus 7 as "tip" for 100% of their responses. It is evident that the range of response patterns for the children's identification functions is greater than the adults'. MC's function has the majority of stimuli in the "zone of uncertainty", including Stimulus 7. This differed from all other subjects who identified Stimulus 7 unequivocally as "tip".

Response variability scores were determined using the procedures described in [1]. The internal response variability score was calculated with respect to the particular subject's phoneme boundary while the external response variability score was calculated with respect to the adult groups' mean boundary.

Internal response variability scores ranged from 3 to 24 for the adult group (Mean=12.3; SD=7.6) and from 1 to 17 for the child group (Mean=11.0; SD=7.3) External response variability scores ranged from 3 to 21 for the adult group (Mean=10.2; SD=7.5) and from 2 to 20 for the child group (Mean=11.8; SD=6.2). While means and standard deviations were similar for each group for both external and internal variability scores, the

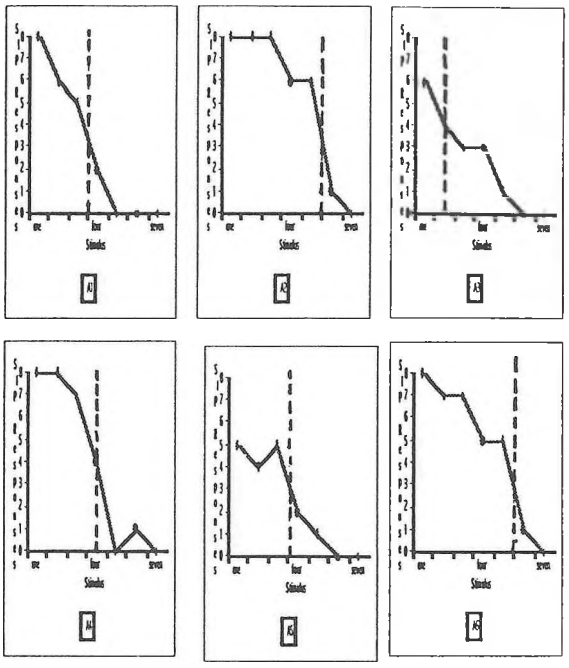

Figure 1. Adult "sip" identification functions.

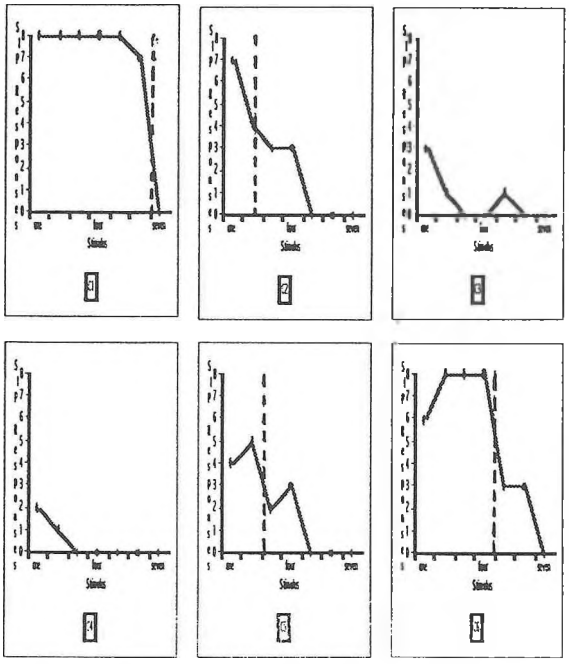

Figure 2. Child "sip" identification functions.

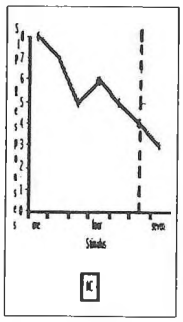

Figure 3. Misarticulating child "sip" identification function.

children's mean internal variability score does not include subjects C3 and C4 because they did not have a phoneme boundary. MC's internal response variability score of 23 was the second highest, and her external response variability score of 25 was the highest of all subjects.

4. CONCLUSIONS

(1) As predicted, the child group had wider boundaries, i.e., they exhibited less enhanced discriminability for fricative versus stop manner categories on this seven step synthetic continuum than the adult group.

(2) As predicted, the child subject group exhibited a greater range in their response patterns than the adult group: phoneme boundaries could not be calculated for two of the children and the children responded significantly differently to Stimulus 1.

(3) Contrary to what was predicted, the normally articulating adult and child subjects showed similar group mean and standard deviations in their internal and external response variability scores, suggesting that they were similar in the stability of their internal representation of the fricative-stop contrast represented by this seven step continuum varying in noise rise time and corresponding noise duration. A greater number of subjects would provide a more robust test to support or refute this finding.

(4) MC had the widest "zone of uncertainty" (including Stimulus 7) and the highest external response variability score of any adult or child subject. This suggests that her internal representation of the fricative-stop contrast was less stable than the normally articulating subjects. Future research considerations include testing these hypotheses for a group of misarticulating subjects who use a stop for fricative substitution, and investigating the effect of perceptual training on a fricative-stop continuum (vis a vis [2]) on these subjects' stop and fricative productions.

5. REFERENCES

[1] Raymaakers, E. & Crul, T. (1988). Production and perception of the final /s-ts/ contrast in Dutch by misarticulating children. JSHD. 53, 262-270.

[2] Rvachew, S. & Jamieson, D. (1989). Perception of voiceless fricatives by children with a functional articulation disorder. JSHD. 54, 193-208.

[3] Computerized Speech Research Environment. CSRE (1994). AVAAZ Innovations, Inc., London, ON.

[4] Klatt, D. (1980). Software for a cascade-parallel formant synthesizer. JASA. 67, 971-995.

Perceptions of Dialect Change in the Speech of Adult Canadians Living in Alabama*

Murray J. Munro
Department of Linguistics
Simon Fraser University

Tracey M. Derwing
Department of Educational Psychology
University of Alberta

Introduction

Evidence indicates that speakers of a particular dialect may modify their speech when they move to a new dialect region. Chambers (1992), for instance, observed changes in choices of lexical items and in the pronunciation of certain words in the speech of adolescent immigrants. However, relatively little is known about phonetic changes in the speech of adults. It might be expected that adjustments to the segmental and prosodic features of adult immigrants' speech would be comparable to those seen in adult second language (L2) learners. Considerable research indicates that adult L2 learners almost never learn to pronounce their second language like native speakers, even after years of immersion in the L2 environment (see e.g., Flege, Munro, & Mackay, 1995), though they do often show evidence of phonetic learning (Munro, Flege, & Mackay, in press). Similarly, adult learners of a second dialect might be unlikely to develop pronunciation patterns identical to native speakers of their new dialect, while nonetheless exhibiting a tendency to "approximate" the phonetic norms of the new dialect (see Flege, 1980).

In this study we addressed the issue of dialect change in adults by examining listeners' ratings of the speech of Canadians who had immigrated to Birmingham, Alabama. Although several different dialects (defined often along racial and socio-economic lines) are spoken in metropolitan Birmingham, the white, middle-class speech to which the speakers in the study were almost certainly exposed has a number of distinctive properties, including the use of the monophthong [ɑ] for the Canadian English diphthong [aj], the neutralization or near-neutralization of the distinction between [æ] and [ɛ], distinctive vowel-colouring before [ɹ], and the frequent use of rising final intonation in statements. Of course, Canadian English also differs from Birmingham English in its use of the "raised" diphthongs [ʌj] and [ʌw] before voiceless consonants (Chambers, 1973).

Our hypotheses were 1) that adult speakers of Canadian English living in Alabama would eventually adopt some of the segmental and prosodic pronunciations of the speakers in their new dialect area; 2) that these changes would be noticeable to phonetically untrained Canadian speakers who had not moved to a new dialect area; and 3) that the speakers would tend to approximate rather than fully adopt the new dialect.

Methods

In order to test the three hypotheses proposed above, we used a listening task in which native Canadian listeners rated the "Americanness" of the speech of Canadians, Alabamians, and Canadians living in Alabama.

Recordings. Speech samples were elicited from three groups of ten speakers (5 female, 5 male) each. Group CE consisted of adult native speakers of Canadian English living in Edmonton. Group AB consisted of residents of Birmingham, Alabama, who had been raised in the American South. Group CB consisted of speakers of Canadian English who had taken up residence in Birmingham after the age of 18 years. The mean length of time spent in the US was 7.7 years, with a range of 1 to 23 years. Five of the participants from Group CB had lived in other US cities besides Birmingham (in Illinois, Indiana, Missouri, Oregon, and Tennessee).

Individual recordings were made with high fidelity audio equipment in a sound booth. Participants were presented with a series of cartoons (without dialogue) depicting an amusing story about a hunting trip. The speakers were asked to describe the story in a short narrative, providing as much detail as they wished.

Despite a careful examination of the 30 speech samples, we were able to find only marginal indications that any specific lexical items or grammatical structures might have betrayed the place of origin of any of the speakers. Rather the differences in the speakers' productions seemed to be confined mainly to pronunciation in both the segmental and the prosodic domains.

Listening Task. To facilitate random presentation of the speech samples to the listeners, the narratives were digitized on a Macintosh computer and saved as audio files. An excerpt of 10 - 14 sec from each speaker's narrative was selected from the beginning to be used as a stimulus in the listening task. A stimulus tape was then prepared. Four example tokens (narratives from speakers whose voices were not used in the study) were recorded first, to be used as a practice set for the listeners. Next, 8 randomly-selected tokens from the actual stimulus set were recorded to allow the listeners to "warm up." The listeners were not informed of this, however, and the ratings of these tokens were excluded from the subsequent analyses. Finally, the actual randomized stimulus set, consisting of two tokens of each narrative, was recorded.

The listeners were 22 native speakers of Canadian English living in Edmonton at the time of the experiment. During a listening session conducted in a quiet room, they were instructed to rate how "American" each speech sample sounded by circling a number on a response sheet from 1 to 9 where 1 = "Very Canadian" and 9 = "Very American." They were told that they would be hearing speech from Canadians, Southern

Americans, and Canadians living in the American South. They had no prior knowledge, however, of the place of origin of any specific speakers.

Results

The distribution of all 1320 ratings according to speaker group is illustrated in Figure 1. The ratings of the CE speakers tended to cluster near the left side of the scale: more than half were ratings of 1. Very few ratings higher than 4 were assigned to this group, and none of the ratings was higher than 7. In sharp contrast, the modal rating category for the AB group was 9, and very few ratings lower than 6 were assigned. The ratings of the CB group's productions showed much less of a tendency to fall at the extremes of the continuum. The mean ratings assigned to the three groups are given in Table 1.

Table 1: Mean Ratings by Speaker Group

Group	Mean	Range
CE	2.1	1.3 - 3.5
CB	4.0	2.1 - 6.7
AB	7.6	5.4 - 8.9

The CB group was assigned a mean rating intermediate to that of the other 2 groups. A repeated measures of Analysis of Variance on the mean scores assigned by each of the 22 listeners to the three groups (pooled over talkers) revealed a significant effect of speaker group [$F(2, 42) = 514.46$, $p<0.001$]. Post hoc (Tukey HSD) tests indicated that all three groups differed significantly from each other $p<0.01$). In short, the CE group was rated as most Canadian-sounding and the AB group was rated as most American-sounding. The CB group received an intermediate rating that differed significantly from the ratings assigned to the other groups. Furthermore, every listener showed the same ordering of mean ratings (CE < CB < AB).

An examination of the data for the individual speakers yielded similar results. A one-way ANOVA on the scores from the 10 speakers in each group revealed a significant effect of speaker group [$F(2, 27) = 61.44$, $p<0.001$]. Tukey HSD tests indicated that the mean score assigned to every group differed significantly from the mean for every other group ($p<0.01$). As can be seen from Table 1, the ranges of mean scores assigned to individual speakers overlapped somewhat. Some of the CB speakers were heard as more American-sounding than others. Moreover, some received mean ratings comparable to those assigned to members of the CE group, while others were rated as American-sounding as some of the AB speakers.

Conclusions

With respect to the three hypotheses offered above, the first two were clearly confirmed. The adult Canadians who had immigrated to the United States showed evidence of American pronunciation patterns that were clearly noticeable to the Canadian listeners.

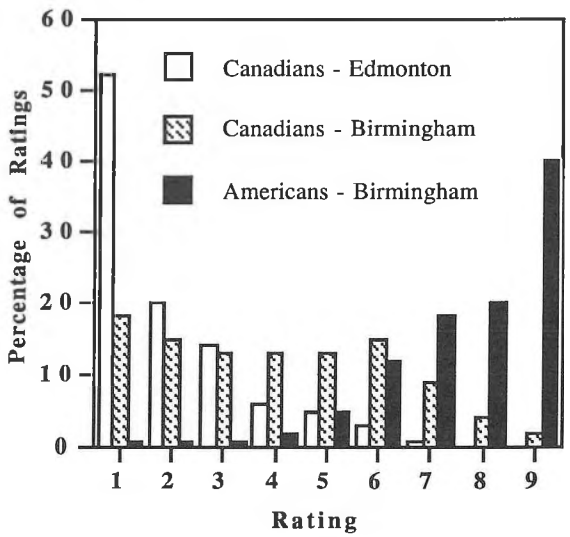

Figure 1: Distribution of Ratings by Group

The listeners had very little difficulty distinguishing the CE from the AB speakers, and they tended to rate the CB speakers as having an intermediate degree of American-sounding speech. Further analysis of the speech samples used in this study may reveal more about the segmental and prosodic cues that were available to the listeners when they made their judgements.

The data also generally support the third hypothesis, that the CB group would approximate, rather than fully adopt, the new dialect. However, some of the CB speakers were judged to be just as American-sounding as some of the AB speakers. While this may mean that some CB speakers had indeed become indistinguishable from Alabamians, firm conclusions are not possible here, given the short speech samples that were used. A full evaluation of this hypothesis would, of course, require an analysis of judgements from native Alabamians in order to determine whether they too would perceive some members of the CB group as indistinguishable from other Alabamians.

References

Chambers, J. (1992). Dialect acquisition. *Language,* **68**, 673-705.

Chambers, J. (1973). Canadian raising. *Canadian Journal of Linguistics*, **18**, 113-135,

Flege, J. (1980). Phonetic approximation in second language acquisition. *Language Learning*, **30**, 117-134.

Flege, J., Munro, M., & Mackay, I. (1995). Factors affecting strength of perceived foreign accent in a second language. *Journal of the Acoustical Society of America,* **97**, 3125-3134.

Munro, M., Flege, J., & Mackay, I. (in press). The effects of age of second-language learning on the production of English vowels. *Applied Psycholinguistics.*

*Research supported by the University of Alberta and SSHRC. The authors are grateful to J. Flege, A. Schmidt, and H. Southwood for their comments and assistance in the completion of this study.

PERCEPTUAL CHANGE IN ADULTS: ACOUSTIC FACTORS AFFECTING THE IDENTIFICATION OF ENGLISH /r-l/ BY JAPANESE LISTENERS

John S. Logan, Kathy BharrathSingh
Department of Psychology, Carleton University, Ottawa

1. INTRODUCTION

Perception of the English phonemes /r/ and /l/ by Japanese listeners can serve as a model system to explore some of the factors underlying the capacity for perceptual change in adult listeners. Japanese listeners generally have difficulty perceiving the /r/ - /l/ distinction in English, especially when these phonemes are in word-initial positions (MacKain, Best, & Strange, 1981; Mochizuki, 1981). Logan, Lively, and Pisoni (1991) and Lively, Logan, and Pisoni (1993) demonstrated that Japanese listeners can learn to identify /r/ and /l/ more accurately after completion of a laboratory training procedure, indicating that adult listeners can redirect their attention to novel acoustic cues. However, many questions remain about how Japanese listeners learn to direct their attention to the acoustic cues necessary to identify /r/ and /l/.

A critical factor in the perception of /r/ and /l/ by Japanese listeners is phonetic context (Mochizuki, 1981; Sheldon & Strange, 1982). Performance is better when the phonemes are located in word-final positions than in word-initial positions. Acoustic analyses suggested that this effect is due to differences in the duration of /r/ and /l/ in these two contexts (Dissosway-Huff, Port, & Pisoni, 1982; Sheldon & Strange, 1982): /r-l/ segments located in word-final positions tend to be longer in duration than in word-initial positions. This explanation for the effects of phonetic context in the perception of /r/ and /l/ by Japanese listeners is referred to as the duration hypothesis.

Several factors, however, mitigate against the complete acceptance of the duration hypothesis. First, the evidence for it is primarily correlational and somewhat equivocal (i.e., /r-l/ duration does not account for all of the variation in perception by listeners). Second, Cantonese listeners, who also have difficulty perceiving the /r-l/ contrast show a positional asymmetry that is opposite to that observed in Japanese listeners (i.e., Cantonese listeners perceive /r-l/ in word-initial position more accurately than in word-final position).

Logan and BharrathSingh (1994) sought to directly evaluate the role of duration in the perception of /r/ and /l/ by Japanese listeners. A group of Canadian English (CE) and Japanese listeners were presented a series of naturally produced English words contrasting /r/ and /l/. The /r-l/ segments were either shortened or lengthened using a waveform editor. Results indicated that the duration manipulation did not have any effect on the identification performance for either group of listeners. Moreover, rating data from the CE listeners suggested that the quality of the stimuli may have been compromised by the waveform editing procedure. Accordingly, the null result that was obtained for the duration manipulation was not interpreted as indicating the duration hypothesis was incorrect but instead that the experiment did not provide an adequate test of the hypothesis.

The present experiment was designed to address some of the problems associated with using naturally-produced stimuli. Synthesized speech was used to permit the manipulation of /r-l/ duration without the difficulties inherent in modifying natural speech. In addition, it enabled a more fine-grained manipulation of the acoustic cues underlying duration by enabling the independent* variation of /r-l/ steady duration and /r-l/ formant transition duration in order to determine whether one aspect of duration was more salient to listeners than another.

As well, the present experiment utilized an additional group of listeners. In addition to CE and Japanese listeners, Cantonese listeners were also tested. The inclusion of the Cantonese listeners provided an extra control group for comparison with the Japanese listeners. Moreover, because the Cantonese listeners also have difficulty perceiving /r/ and /l/, albeit in another phonetic context, they serve to demonstrate the potential interaction between acoustic information and the listener's phonological system.

2. METHOD

Stimulus preparation and experimental control utilized CSRE software (Jamieson, Ramji, Neary, & Baxter, 1990). RIGHT and LIGHT stimuli were synthesized using the Klatt software synthesizer (Klatt, 1980) as implemented in CSRE. Parameters for these stimuli were derived from a combination of Klatt's parameters and measurements from natural tokens. Each synthesized /t/ segment also included a naturally-produced burst.

Additional stimuli were constructed by varying two parameters in the original RIGHT and LIGHT stimuli: 1) the duration of the steady-state portion of the /r-l/ segments (referred to as the steady-state manipulation) and 2) the duration of the F1, F2, and F3 transition from the steady state to the /ai/ vowel (referred to as the transition manipulation). For the steady-state manipulation, two versions of the stimuli were constructed, the original and a shortened version. In the shortened version of RIGHT, the first 90 ms was removed from F1 and F2, and 95 ms was removed from F3. In the shortened version of LIGHT, the first 65 ms was removed from F1 and F2, and 70 ms was removed from F3. Note that although the shortened stimuli contained a shorter /r-l/ steady-state duration than the parameters specified by Klatt [1980], it seemed to be more "normal" sounding to CE listeners than the original stimuli based on Klatt's parameters. For the transition manipulation, three versions were constructed: the original, a moderately lengthened, and an extremely lengthened version. In the moderately lengthened version of RIGHT and LIGHT, F1, F2, and F3 transitions were lengthened by 30 ms. In the extremely lengthened version of RIGHT and LIGHT, F1, F2, and F3 transitions were lengthened by 60 ms. Altogether, 12 unique stimuli were produced using this procedure (2 words [RIGHT & LIGHT] X 2 steady-state durations[original and shortened] X 3 formant transition duration [unaltered, moderate, and extreme])

CE, Cantonese, and Japanese listeners were recruited from the Carleton University community. Six native speakers from each language group participated. CE listeners were monolingual English speakers whereas the Japanese and Cantonese listeners were bilingual (English plus their native language). All listeners reported no history of a speech of hearing disorder.

The stimuli were presented to listeners in a two-alternative forced choice (2AFC) identification task. Stimuli were presented over Sony MDR-P1 headphones at approximately 75 dB SPL. Listeners were seated in front of a computer monitor that displayed the printed forms of RIGHT and LIGHT. 250 ms later the auditory stimulus was then presented. The listeners were then required to move a cursor on the computer monitor by using a mouse to indicate whether they heard RIGHT or LIGHT. Each of the 12 stimuli was presented 15 times, making a total of 180 trials in the experiment. Stimuli were presented in a random order that varied from listener to listener. In addition to the identification task, each CE listener rated the quality the token on each trial using a 7-point scale, where 1 was "very clear", 4 "clear", and 7 "distorted" after each trial.

3. RESULTS

The CE listeners rated the stimuli as being clear (mean rating = 2.1). Moreover, no reliable differences among the stimuli were observed in the CE rating data. Thus, the stimuli used in the present experiment were consistently clear to CE listeners, regardless of durational manipulation. Analysis of the identification data indicated significant differences among the percentage of words correctly identified by the three groups of listeners, $F(2,180) = 58.02$, $p < .001$. The CE and Cantonese listeners identification performance (99.7, and 97.0%, respectively) exceeded that of the Japanese listeners (81.2%). In addition, there was a significant interaction between stimulus word (RIGHT vs. LIGHT) and steady-state duration (original vs. shortened), $F(1,180) = 9.45$, $p < .002$. This two-way interaction was subsumed, however, by a three-way interaction among group, stimulus word, and steady-state duration, $F(2,180) = 8.73$, $p < .001$, that is shown in Figure 1. The Japanese listeners identified the original steady-state version of /r/ more accurately than the shortened version whereas they identified the shortened version of /l/ more accurately than the original version of /l/. In contrast, the effect of duration and stimulus word was not important for CE and Cantonese listeners. No other statistically reliable effects were obtained.

4. DISCUSSION

The results of the present experiment provide partial support for the duration hypothesis. Although no effect of increased formant transition duration was found, increased steady state duration did seem to enhance performance for Japanese listeners, at least for /r/. Thus, /r-l/ steady-state duration seems to be an important acoustic cue for Japanese listeners. However, the difference in the effect of steady-state duration for /r/ and /l/ is somewhat puzzling as most of the literature on the perception of /r/ and /l/ by Japanese listeners treat the two phonemes as equivalent.

One factor that may account for some of the differences between /r/ and /l/ identification performance by the Japanese listeners is stimulus construction. Recall that to produce the shortened version of RIGHT approximately 90 ms was removed from the steady portion of the /r/ segment whereas for LIGHT, only 65 ms was removed from the steady-state portion of /l/. This difference in the length removed was necessary because of the duration of the steady state portion in the original stimuli; if a 90 ms section was removed from LIGHT, it would have interfered with the formant transition in the /l/ segment. However, this difference in stimulus construction does not account for why the shortened version of /l/ was identified more accurately than the original version. Additional research is needed to clarify this result. One option is to simply remove an equivalent 65 ms section from both the /r/ and /l/ segments

Further work is underway to investigate the role of duration in perception of word-final /r-l/. It will provide complementary information about the acoustic cues used by Japanese and Cantonese listeners in word-initial position. Additional work is also necessary to integrate findings obtained from duration manipulation experiments with the results of experiments in which formant frequencies are manipulated (e.g., Yamada & Tohkura, 1992).

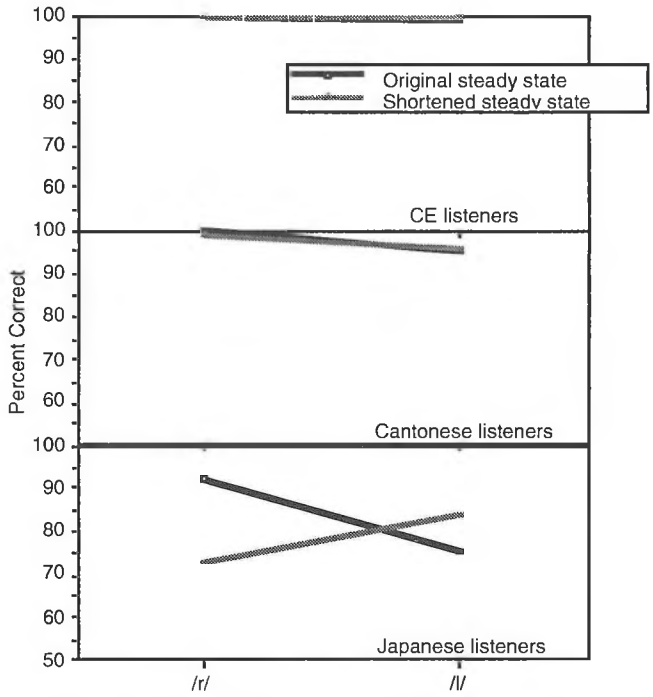

Figure 1. Identification performance (percent correct) for CE, Cantonese, and Japanese listeners presented synthesized RIGHT (/r/) and LIGHT (/l/) stimuli that varied in steady state duration.

5. REFERENCES

Dissosway-Huff, P., Port, R.F., & Pisoni, D.B. (1982). *Research on speech perception: Progress Report No. 8*. Bloomington, IN: Indiana University.

Goto, H. (1971). *Neuropsychologia*, **9**, 317-323

Henly, E., & Sheldon, A. (1986). *Language Learning*, **36**, 505-521.

Jamieson, D.G., Ramji, K.V., Neary, T.M. & Baxter, T.A. (1990). *Canadian Speech Research Environment (3.0)–User's manual.*

Klatt, D.H. (1980). *JASA*, **67**, 971-995.

Lively, S.E., Logan, J.S., & Pisoni, D.B. (1993). *JASA* , **94**, 1242 - 1255.

Logan, J.S., & BharrathSingh, K. (1994). *Canadian Acoustics*, **22**.

Logan, J.S., Lively, S.E., & Pisoni, D.B. (1991). *JASA*, **89**, 874-886.

MacKain, K., Best, C.T., & Strange, W. (1981). *Applied Psycholinguistics*, **2**, 369-390.

Mochizuki, M. (1981). *Journal of Phonetics*, **9**, 283-303.

Sheldon, A. & Strange, W. (1982). *Applied Psycholinguistics*, **3**, 243-261.

Yamada, R.A., & Tohkura, Y. (1992). *Speech perception, production and linguistic structure*., Tokyo: Ohm, pp. 155-174.

6. ACKNOWLEDGMENTS

Work supported by NSERC. Thanks to Linda Polka for providing useful information for developing the stimulus parameters.

Evaluation of US Image Echodensities During Contraction of the Lingual Musculature

Jeri L. Miller and **Kenneth L. Watkin**, Department of Communication Sciences and Disorders, Biomedical Engineering, McGill University
Montréal, Quebec

I. INTRODUCTION

B–mode ultrasound imaging has been used clinically to visualize the temporal and spatial movements of the tongue surface during speech production. Although these parameters provide important diagnostic information, the quantification of the acoustic signal during B–mode imaging of the tongue musculature has not been investigated. Hicks, Shawker, Jones, Linzer and Gerber (1984) analyzed the echo intensities of the pixel distribution within B–mode scans of muscle regions of the limb. They suggested that observed differences in pixel distributions were related to the degree of muscle contraction representing a physiological alteration in the muscle to fat–fibrous tissue ratio per cross–sectional area [1]. Any physiological or pathological condition which altered the composition of tissue would therefore be observed in the distribution of pixel intensities of a specific region of interest [2].

Given that the structural arrangement of the lingual musculature functionally alters during differing movements and postures, similar changes during the contraction of the intrinsic and extrinsic lingual muscle groups should be demonstrated by an alteration in the echo amplitudes of the acoustic signal. In addition, because the muscular composition of the tongue is not uniform throughout its length, individual muscle groups should be identifiable as differing echo amplitudes based on the extent of regional muscular contractions. Further, off–line image–processing of tissue echo intensities should detect significant differences in the acoustic properties of the ultrasound signal independent of transducer type and frequency.

Thus, the purpose of this study was to examine the physical properties of lingual musculature using off–line image processing of tissue echo intensities. We present preliminary data of a noninvasive method to describe and quantify the relationship between in vivo sonographic recordings of echo intensities and lingual muscle contractile state.

II. METHODS

One normal English speaker (female; age 35 years) was used. All testing was conducted using an ALOKA 2000 Ultrasound Unit. Two transducers were used with a resonant frequency of 5.0 MHz (convex) and 7.5 MHz (linear). The use of the same ultrasound unit was done to control for variability in system controls (e.g., dynamic range, pre– processing). Settings were maintained for each trial. Transducer characteristics included axial resolution of .4 mm (7.5 MHz) and .6 mm (5.0 MHz), respectively. Lateral resolution for both transducers was less the 1 mm or better. All images were collected in real–time at 10 frames per second using the video–acquisition board on a SGI Indigo R3000. To obtain relatively approximate replications of lingual force during tasks, a portable force measurement system containing a Force Sensing Resistor (FSR) was used [3,4]. The sensor was placed along the mid–line of the tongue blade. The subject pressed against the FSR until a force level as indicated by a liquid crystal display was achieved. Two force levels were approximated: 1) light press (700 grams force), and 2) hard press (2000 grams force).

III. PROCEDURES

The transducer was hand–held by the experimenter and placed submentally with the beam directed perpendicular to the tongue in mid– sagittal plane. The angle of the transducer was manipulated to achieve complete views of the lingual musculature from the anterior shadow of the mandible to the posterior shadow of the hyoid bone. Three trials per each hard press or light press task were made. A 30 second rest between trials was introduced to avoid fatigue effect. For each task, the subject isometrically contracted the tongue against the FSR/palate at the target level for 5 seconds.

All images were converted to an array of digitized picture elements (pixels) with an 8–bit resolution range. The converted images were then analyzed off–line on an IBM RISC workstation using image processing software. Ten consecutive frames were selected from one randomly designated trial for each task. Each frame was then analyzed to obtain moment statistics of gray level histograms of the complete image.

A grid overlay was generated for each image. Three x–axis coordinates were determined for all images to represent 'A–lines' of the anterior, mid, and posterior regions of the tongue. Within the designated A–line regions, the superior and inferior boundaries of the intrinsic, genioglossus, geniohyoid, and mylohyoid musculature were identified and corresponding xy coordinates of these muscle regions determined for each frame using a mouse–controlled cross–hair cursor displayed on the screen (Figure 1.0). For some tasks, the genioglossus did not extend to the posterior A–line region. Further, if the connective tissue fascia separating the geniohyoid and mylohyoid muscles at the tongue base were indistinguishable, the A–line measurement was completed for the geniohyoid only.

The pixel intensity distribution for each A–line region was then determined for each frame. The A–line intensity profiles represented an interpolated intensity scale from 0 to 1 (zero: white; 1: black). Mean and standard deviation values were automatically calculated and recorded for each region of interest.

The means of each A–line region for all ten images were pooled. Descriptive statistics were determined and included an analysis of kurtosis to determine pixel distribution in terms of peakedness of a curve, and skewness representing the symmetry of the pixel distribution. Significant differences between means were determined through ANOVA and nonparametric statistical analyses. Multiple pairwise comparisons were conducted for significant effects.

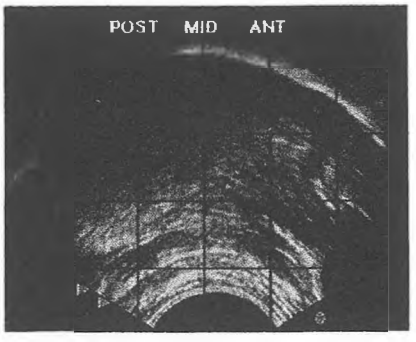

Figure 1.0. Example of gridded B–mode image containing A–line grid overlay.

IV. RESULTS

Results indicated the magnitude of echo intensities significantly differed as a function of contraction state. Significant differences in backscattered amplitudes were found between hard and light press tasks ($p < 0.0001$) for both transducer types, although the echo intensities were lower for the 5.0 MHz transducer (Tables 1.0–2.0). The data indicate the lowest echo intensities were found in the hard press task where the greatest levels of contraction were required. Higher echo intensities were found for light press tasks suggesting less contraction and a reconfiguration of the lingual musculature.

Within A–line regions significant differences ($p < 0.0001$) were found for all group means except the mid A–line region during the hard press task (5.0 MHz transducer). When the A–line regions from this image were reviewed, it was noted that the posture of the tongue was markedly different from that obtained with the 7.5 MHz transducer. Thus, postural differences may be one reason for this result. The data suggest that the extent of muscular contraction across regions of the tongue differ as measured by echo intensities.

Individual muscle groups within each A–line region were significant ($p < 0.05$) across tasks for the 7.5 MHz transducer. Results in individual muscles groups varied with the 5.0 MHz transducer. Overall, the results suggest that the contractile functions of individual muscle groups within A–line regions can be identified and may act functionally as semi–independent regions during different postural configurations.

In order to substantiate the findings of this subject, B–mode images were collected and analyzed for an additional subject. Results (Table 3.0) indicated that the same pattern of lower echo intensities for hard contraction vs. light contraction was maintained in this subject. The lowest echo intensities was found more posteriorly along the A–line regions. The lowest values representing the greatest contraction were found within the posterior geniohyoid and mylohyoid for both tasks. As in Subject 1, the mean pixel intensity values were greater than those obtained with the 5.0 MHz transducer.

IV. DISCUSSION

The data from this preliminary study support the hypothesis that echo intensities of the pixel distribution within B–mode scans of muscle regions differ as a function of degree of muscle contraction. The data from this investigation suggest that quantitative measures of echo intensities may provide useful information related to models of lingual muscle structure and function during speech and non–speech tasks. Tongue movements are recognized to result from the combination of extrinsic and intrinsic muscles in synergistic, antagonist, or protagonistic roles. In particular, the mylohyoid acts as the primary elevator of the floor of the mouth whereas the genioglossus serves to elevate the tongue [5]. The data from this study suggest that during maximum hard press isometric tasks, the base tongue musculature acts as the primary elevator of the tongue body with contractions within the genioglossus contributing to elevation more anteriorly. Higher variability occurs in light press postures where greater structural flexibility in achieving the task can occur.

Although distinct tongue muscle coordination is required for speech production, the role of the specific tongue muscles has not been completely investigated [5]. The observed differences in A–line echo intensity values suggest a means to visibly identify and quantify the unique muscular architecture of the tongue during a range of functional tasks. The data further suggest A–line analysis of regional echo intensities may provide a quantitative method to detect and measure changes to lingual tissue as a result of pathological conditions common in motor speech disorders or oral cancers, as well as the extent of muscular recovery as a result of myofunctional rehabilitation methods.

Table 1.0
Subject 1: Mean Pixel Echo Intensity of A–Line Muscle Regions: 7.5 MHz Transducer

SEGMENT	MEAN	INT	GG	G H	MH
HARD PRESS	.2295				
ANT	.3703	.4704	.3790	.2826	.1992
MID	.3889	.5224	.3501	.3012	.2125
POST	.4455	.4895	——	.4495	.3018
LIGHT PRESS	.2479				
ANT	.3673	.4385	.3275	.2920	.3834
MID	.4120	.5008	.3837	.2587	.2976
POST	.4515	.4740	.3336	.2670	——

Note. INT: intrinsic; GG: genioglossus; GH: geniohyoid; MH: mylohyoid. Dashed lines '—' indicate muscle region not within A–line region.

Table 2.0
Subject 1: Mean Pixel Echo Intensity of A–Line Muscle Regions: 5.0 MHz Transducer

SEGMENT	MEAN	INT	GG	GH	MH
HARD PRESS	.1673				
ANT	.2435	.2838	.1873	.1903	.4426
MID	.2809	.2863	.2670	.2815	.2838
POST	.2838	.3308	.2580	.2675	.2206
LIGHT PRESS		.1737			
ANT	.3134	.2994	.3179	.3558	.3118
MID	.3098	.3093	.3433	.3146	.2761
POST	.2765	.2892	——	.2450	.2308

Table 3.0
Subject 2: Mean Pixel Echo Intensity of A–Line Muscle Regions: 7.5 MHz Transducer

SEGMENT	MEAN	INT	GG	GH	MH
HARD PRESS	.3552				
ANT	.4666	.4805	.4440	.4814	.5968
MID	.4384	.4489	.4130	.4720	.4585
POST	.3723	.3906	——	.3570	.3243
LIGHT PRESS		.3710			
ANT	.4904	.4418	.4965	.5342	.5425
MID	.4711	.4837	.4794	.4965	.4691
P OST	.3921	.4003	——	.3615	.3648

REFERENCES

1. Hicks, JE., Shawker, TH., Jones, BL, Linzer, M., and Gerber, LH, (1984). Diagnostic ultrasound: Its use in the evaluation of muscle. *Archives of Physical Medicine and Rehabilitation*, Vol. 65, March, 129–131.

2. Wickline, SA, Pérez, JE, and Miller, JG,(1993). In KK Shung and GA. Thieme (Eds.), *Ultrasonic Scattering in Biological Tissues*, pp. 313–346. CRC Press: Boca Raton.

3. *Interlink Electronics*, Carpenteria, California.

4. Miller, J.L, and Watkin. KL, (1995). The effects of bolus volume and viscosity on anterior lingual force during swallowing. *Dysphagia , in-press .*

5. Miller, AJ., (1982). Deglutition. *Physiological Review*, 62(1), 129–184.

ACTIVE CONTROL OF SOUND WITH FOAM-PVDF COMPOSITE MATERIAL

C. Guigou, C. A. Gentry, J. Pan* and C. R. Fuller

Vibration and Acoustics Laboratories,
Department of Mechanical Engineering
Virginia Polytechnic Institute and State University,
Blacksburg VA 24061-0238, USA.

*Department of Mechanical and Materials Engineering
University of Western Australia
Nedland, WA 6907, Australia

1. Introduction

In this paper, the development and testing of foam-PVDF composite material designed for active noise reduction are discussed. A schematic of the composite material is shown in Figure 1 and consists of sinusoidally curved sections of the piezoelectric polymer film PVDF embedded in partially reticulated polyurethane acoustic foam. The transducer is designed to reduce sound by the action of the passive absorption of the foam (which is effective at higher frequencies) and the active input of the PVDF element driven by an oscillating electrical input (which is effective at lower frequencies).

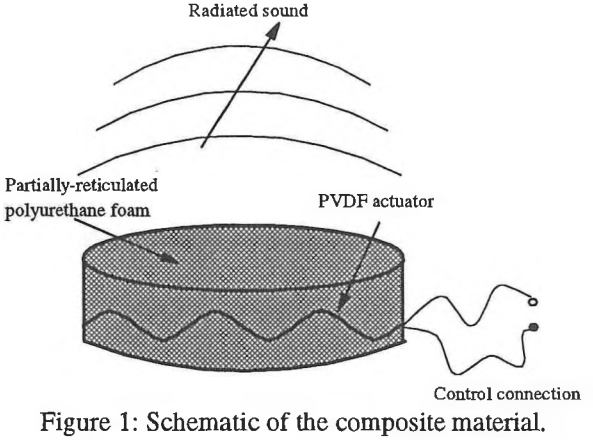

Figure 1: Schematic of the composite material.

2. Actuator Configuration

Much work has been performed to configure the active PVDF layers to behave in a linear sense as well as produce significant sound levels at low frequencies when driven by an oscillating voltage [1]. Figure 2 shows two configurations of the PVDF film presently under study. The main characteristic is that the PVDF is intentionally curved to couple the predominantly in-plane strain due to the piezoelectric effect and the vertical motion which is needed to accelerate fluid particles and hence radiate sound away from the surface of the material. The arrangement first suggested by Tibbetts [2] is shown in Figure 2. In the series-parallel configuration, the continuous PVDF film is broken up into cells in which the bottom surface electrodes are wired 180 out-of-phase into a single lead (or control channel). A slightly different configuration is the parallel arrangement in which the top and bottom electrodes are connected to their neighboring cell with a phase reversal, again into a single lead (or control channel). For these two arrangements, each cell moves in the same vertical direction under voltage activation and the sound radiation is increased. In addition, the non-linearities are canceled by the cell interaction.

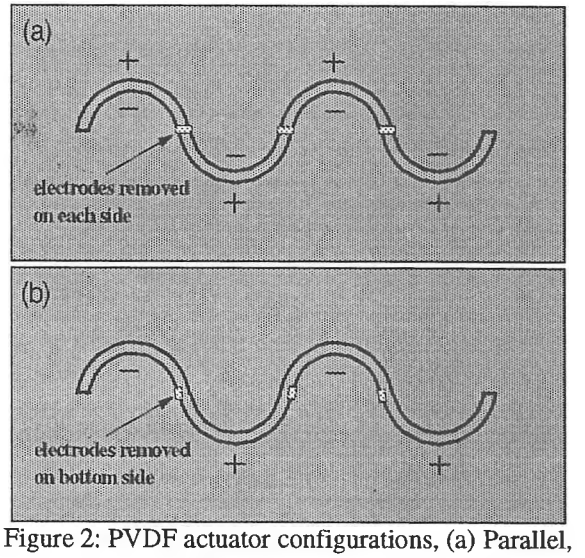

Figure 2: PVDF actuator configurations, (a) Parallel, (b) Series-parallel.

3. Radiation Control

The foam-PVDF composite active material was first mounted near the surface of an oscillating rigid piston mounted in a baffle and positioned in the VAL anechoic chamber at VPI&SU. The piston was of 15 cm diameter while the foam was 5 cm thick with a single layer of 28 μm Ag metalized PVDF. The piston was driven with band limited random noise (0-1600 Hz) and the radiated sound was measured with a polar microphone traverse of radius 2 m from the piston. An active controller based upon the Filtered-x version of the feedforward LMS algorithm [3] was used to minimize radiated sound at an error microphone located normal to the piston at 2 m (far-field error sensor) and 0.15 m (near-field error sensor) distance. Figure 3 shows the sound pressure level (SPL) attenuation averaged over the radiation angles. The attenuation is relative to the radiation from the bare piston. The "passive" case

corresponds to the attenuation due to the foam-PVDF composite material installed and control not turned on, and the "passive/active" case to the attenuation due to the foam-PVDF composite material installed and the control activated. Control performance of the series-parallel and parallel configurations for the actuator was found similar. The difference between the two configurations was the voltage required for the actuator: the series-parallel requires about twice the voltage of the parallel actuator to control the same acoustic levels, but is associated with less non-linearity effects. The results obtained with the series-parallel actuator are shown in this section. In Figure 3, it is apparent that the passive foam works well above 500 Hz as attenuation of about 14 dB is obtained in average. The results also reveal that the active component provides significant additional attenuation in the 100-1100 Hz frequency range as a further sound reduction of 10 dB is observed. It can also be seen that the near-field error microphone performs as well as the far-field error microphone. Note that the active material is associated with global sound attenuation (reduction in all radiation angles). Note that above 1.1 kHz the control effect is not demonstrated mainly due to the number of coefficients in the FIR filter used to model the impulse response function of the system.

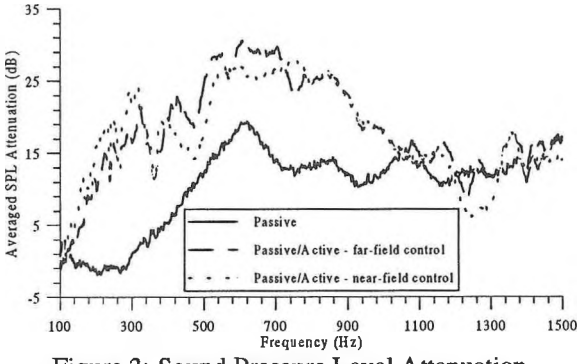

Figure 3: Sound Pressure Level Attenuation averaged over radiation angles (-90° to 90°).

4. Transmission Control

In this case, a rigid sandwich plate was added in front of the foam-PVDF composite active material. This corresponds to a simple local model for a fuselage structure with the active material mounted between the outer (excited by propellers and/or turbulent boundary layer) and inner skin (radiating inside the airplane). The piston (outer skin) was driven with band limited random noise 0-800 Hz. The sound radiation was minimized using either a microphone at 2 m distance or an accelerometer located at the center of the rigid plate.

The results corresponding to parallel configuration for the PVDF actuator are presented. Figure 4 shows the attenuation obtained due to the passive elements (composite material and sandwich plate) and due to the active control with the different error sensors investigated. It can be seen that the accelerometer performs as well as the far-field microphone, as in the low frequency region, the sandwich plate can be associated to a monopole radiator. Active control then results in an additional 10 dB global reduction in average in the frequency band 150-650 Hz.

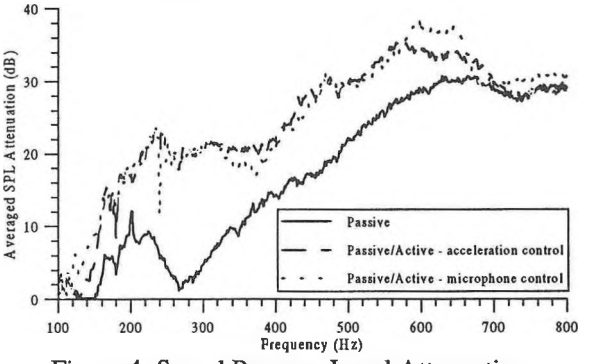

Figure 4: Sound Pressure Level Attenuation averaged over radiation angles (-90° to 90°).

5. Conclusions

The results presented demonstrate the potential of the active material composed of a foam-PVDF composite for reducing sound radiation as well as sound transmission. The device thus has the potential of simultaneously controlling low and high frequency sound in a very thin compact arrangement.

References

[1] C. Gentry, C. Guigou and C.R. Fuller, "Smart foam design and application in active structural acoustic control", presented at the 129th Meeting of the Acoustical Society of America, Washington, DC, June 1995.

[2] G.C. Tibbets, "Transducer having piezoelectric film arranged with alternating curvatures," United States Patent 4056742, Nov. 1977.

[3] P.A. Nelson and S.J. Elliott, "Active Control of Sound," Academic Press Limited, London, 1992.

Acknowledgments

The authors are grateful to NASA LaRC and the ONR for supporting this work as well as Dr. Marcus Bronzel of VAL-VPI&SU for developing and providing the controller.

MULTIMODAL SOUND PRESSURE FIELD IN A CYLINDRICAL DUCT

Fabienne Houïel, André L'Espérance
Groupe d'acoustique de l'Université de Sherbrooke
Université de Sherbrooke, Faculté des sciences appliquées, Département de génie mécanique
Sherbrooke(Québec), J1K 2R1, Canada

Introduction

Active control systems are used to reduce transmitted energy at the end of ducts. When high order modes propagate, the sound field becomes very complex and effective attenuation is more difficult to obtain. The first step in developing an active control system model is to accurately define the interior pressure field of the duct.
This paper presents a model able to predict the interior pressure field of a finite length circular duct when high order modes can no longer be neglected. The studied duct is close at one end and open at the other. As a first step, theoretical and experimental maps of the sound field in the circular duct are presented for zero modal impedance coefficients.

I. The model

A- Hypothesis. The sound pressure is calculated for a circular duct with a finite length (L), and an infinite flange at the open extremity. A velocity point source of strength Q_0 is located at (r_0,θ_0,z_0).
The pressure outside the duct ($z \geq 0$) is given by the Helmoltz integral :

$$P(r,\theta,z) = j\omega\rho \cdot \int_{r=0}^{a} \int_{\vartheta=0}^{2\pi} G(r,\theta,z;r',\theta',z) \cdot V^{+}(r',\theta',z) \cdot r' dr' d\theta \quad (1)$$

$V^{+}(r',\theta',z)$ is the axial velocity at the open end of the duct and G is the Green function of the semi-infinite space :

$$G(r,\theta,z;r',\theta',z) = \frac{e^{jkh}}{2\pi h}, \text{ with } h = r'^{2} + r^{2} - 2rr'\cos(\theta-\theta') + z^{2}$$

The pressure inside the duct ($z \leq 0$) is given by the following modal decomposition before and after the point source (r_0,θ_0,z_0) :

$$P^{-}(r,\theta,z) = \sum_{m=-\infty}^{+\infty} e^{jm\theta} \cdot \sum_{n=0}^{\infty} [A_{mn}^{-} e^{jk_z z} + B_{mn}^{-} e^{-jk_z z}] \cdot \Psi_{mn}(k_{mn} r) \quad (2)$$

$$P^{+}(r,\theta,z) = \sum_{m=-\infty}^{+\infty} e^{jm\theta} \cdot \sum_{n=0}^{\infty} [A_{mn}^{+} e^{jk_z z} + B_{mn}^{+} e^{-jk_z z}] \cdot \Psi_{mn}(k_{mn} r) \quad (3)$$

P^{+} and P^{-} are the generalized solutions of the Helmoltz equation (4) respecting the boundary condition (5) on the duct walls :

$$(\Delta + k^2)P = 0 \quad (4)$$

$$\frac{\partial P}{\partial r} = 0 \quad (5)$$

Equation (5) gives : $\Psi_{mn}(k_{mn}) = \dfrac{J_m(k_{mn} r)}{N_{mn}}$ (6)

where k_{mn} are determined using the boundary condition (5). The radial modes are orthogonal so it is convenient to choose a normalizing factor N_{mn} such that :

$$k^2 \int_0^a r \cdot \Psi_{mn}(k_{mn} r) \cdot dr = 1 \quad (7)$$

and $$N_{mn} = ka \cdot \left\{ \frac{1}{2} \cdot \left(1 - \frac{m^2}{k_{mn}^2 a^2} \right) J_m^2(k_{mn} a) \right\}^{1/2} \quad (8)$$

The dispersion relation gives : $k_z^2 = k^2 - k_{mn}^2$ (9)
The continuity of the pressure and the velocity inside the duct are:

$$P^{+}(r,\theta,z_0) = P^{-}(r,\theta,z_0) \quad (10)$$

$$V^{+}(r,\theta,z_0) - V^{-}(r,\theta,z_0) = Q_0 \cdot \delta(r - r_0) \cdot \delta(\theta - \theta_0) \quad (11)$$

B- Impedances-Pressure field. The acoustic pressure and the velocity at the open end of the duct can be expressed as :

$$P^{+}(r,\theta,0) = \sum_{m=-\infty}^{+\infty} e^{jm\theta} \cdot \sum_{n=0}^{\infty} P_{mn}^{+} \cdot \Psi_{mn}(k_{mn} r) \quad (12)$$

$$V^{+}(r,\theta,0) = \sum_{m=-\infty}^{+\infty} e^{jm\theta} \cdot \sum_{n=0}^{\infty} V_{mn}^{+} \cdot \left(\frac{k_z}{\rho\omega} \right) \cdot \Psi_{mn}(k_{mn} r) \quad (13)$$

A new expression of the pressure is found by subsituting equation (13) in equation (1) and by eliminating the function G as it is described in [1].
Equations (12) and (13) introduce a relation between the modal pressure amplitudes , the modal velocity amplitudes and the modal impedance coefficients :

$$P_{mn}^{+} = Z_{mn} V_{mn}^{+} \cdot \left(\frac{k_z}{\rho\omega} \right) \quad (14)$$

The coupling impedances are neglected.
Then, the generalized modal impedance becomes :

$$Z_{mn} = \int_0^{\pi/2} \sin\phi \cdot D_{mn}^2(\sin\phi) \cdot d\phi - j \int_0^{\infty} \cosh\xi \cdot D_{mn}^2(\cosh\xi) \cdot d\xi \quad (15)$$

$$\text{where } D_{mn}(\tau) = k^2 a \left\{ \frac{\tau k \cdot J_{m+1}(\tau k a) J_m(k_{mn} a) - k_{mn} J_m(\tau k a) J_{m+1}(k_{mn} a)}{N_{mn} \cdot (\tau^2 k - k_{mn}^2)} \right\} \quad (16)$$

Now, the interior problem has to be solved to find the modal amplitudes. The equations (10) and (11) have to be used to find the pressure before and after the source.
Finally, the pressure inside the duct is given by :

$$P^{-}(r,\theta,z) = \frac{k^2 r_0 Q_0 \rho\omega}{2k_z} \sum_{m=-\infty}^{+\infty} e^{jm(\theta-\theta_0)} \sum_{n=0}^{\infty} \frac{\left(e^{jk_z z_0} + R_{mn} e^{-jk_z z_0} \right)}{R_{mn} e^{2jk_z L} + 1} \times \left[e^{jk_z z} + e^{-jk_z (z+2L)} \right] \cdot \Psi_{mn}(k_{mn} r_0) \cdot \Psi_{mn}(k_{mn} r) \quad (17)$$

$$P^{+}(r,\theta,z) = \frac{k^2 r_0 Q_0 \rho\omega}{2k_z} \sum_{m=-\infty}^{+\infty} e^{jm(\theta-\theta_0)} \sum_{n=0}^{\infty} \frac{\left(e^{jk_z (z_0+2L)} + e^{-jk_z z_0} \right)}{R_{mn} e^{2jk_z L} + 1} \times \left[e^{jk_z z} + R_{mn} e^{-jk_z z} \right] \cdot \Psi_{mn}(k_{mn} r_0) \cdot \Psi_{mn}(k_{mn} r) \quad (18)$$

with the modal reflection coefficient :

$$R_{mn} = \frac{Z_{mn}\left(\frac{k_z}{\rho\omega} \right) + 1}{Z_{mn}\left(\frac{k_z}{\rho\omega} \right) - 1} \quad (19)$$

C- Theoretical results. This paragraph presents the preliminary results obtained by using zero modal impedance coefficients. It means that the exterior pressure was taken to be zero. The figure 1 shows the theoretical sound field map in a section of the duct.
The duct used for predictions is 3,30 meters long and has a radius of 0,147 m. The theoretical cut-on frequencies of this duct are given by the boundary condition (5) (table 1). For all tests, the source is located at 120 degrees, at 0.147 m on the radius and at 0.42 m of the closed extremity

Modes	Cut-on frequencies
00	0
10	671
20	1112
01	1396
30	1541

Table 1 : Cut-on frequencies of the duct used for measurements.

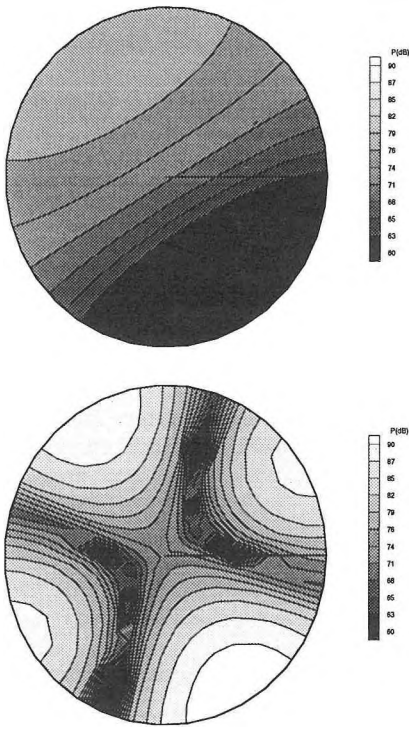

Fig 1 : Theoretical maps of the sound field at 1000 Hz and 1200 Hz at 2,95 m of the noise source in the duct.

The modes propagate according to the table 1. Hence, the first graphic is a superposition of modes (0,0) and (1,0) while for the second one the (2,0) mode is also present.

II. Pressure field measurements

A- Experimental setup. This second paragraph describes the measurements of the sound field in the same circular duct as used previously. The duct is placed in a semi-anechoïc room. To measure the sound pressure, five microphones are placed on a radius. This set of microphones can rotate around the axis of the duct by 10 degre steps. On a given section, this represents 210 measurement points.
The duct used for measurements is the identical to the duct used for the predictions. The source is also similarly located.

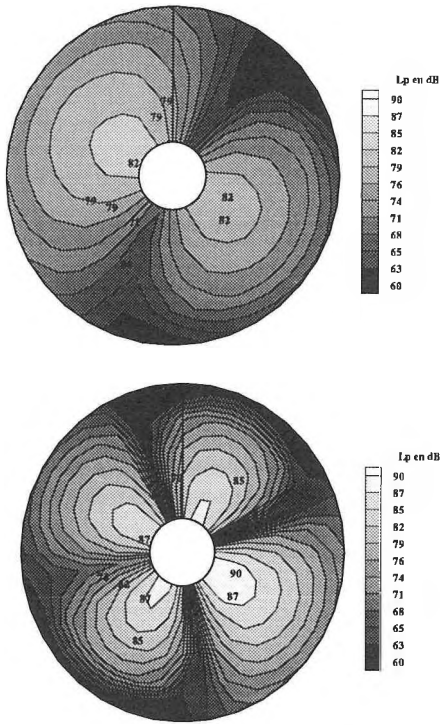

Fig 2 : Experimental maps of the sound field for 1000 Hz and 1100 Hz at 2,95 m of the noise source.

B- Experimental results. The fig 2 shows experimental maps of sound field for 1000 Hz and 1200 Hz. The modes propagate according to the table 1. In practice, the cut-on frequencies of modes do not really exist. We can say that the mode influence increase as the frequency is approaching its cut-on frequency.

III. Comparaison between theoretical and experimental results

It is important to note that when high modes propagate the sound field is the result of modes superposition as the equations (2) and (3) suppose it. Thus it is difficult to identify each mode independantly.
If we compare theoretical map (fig 1) and experimental map (fig 2), we can see two important differences :

i) the nodal lines are not exactly at the same place,
ii) the maximum and the minimum levels do not have the same repartition.

The zero modal impedance coefficients may be the cause of these differences. Further studies using non zero impedance coefficients with theory shown here will soon be conducted.

Conclusion

A model of the interior pressure field of finite length circular duct when high order modes propagate has been presented. The studied duct is closed at one end and baffled at its other open end. Theoritical and experimental results have shown important differencies for a zero modal impedance coefficient hypothesis. Theoretical cases with non zero modal impedance coefficients, calculated with the theory presented will now be computed.

[1] Zorumski W. E., *Generalized radiation of impedances coefficients of circular and annular ducts*, (1973) J. acoust. Soc. Am., vol 54 (6), p1667-1673.

A robust, low-computational, near optimal convergence speed, multi-channel Filtered-X LMS algorithm

Martin Bouchard, Mechanical Engineering
Bruno Paillard, Electrical Engineering
University of Sherbrooke
2500 Boul. Université, Sherbrooke
J1K 2R1

1.0 Introduction

A widely used algorithm for real-time implementations of multi-channel active control systems is the multi-channel Filtered-X LMS, and a normalisation of the algorithm has been published [1] : the NLMS. The drawback of these algorithms is their slow broadband convergence speed for strongly correlated reference signals. In this paper, a normalised fast convergence algorithm that has nearly the same low computational load than the Filtered-X LMS will be presented.

2.0 A new fast convergence algorithm

To describe the algorithms, here are some definitions for the different elements of a feedforward FIR adaptive control system :

Nx : number of reference sensors
Ny : number of output actuators
Ne : number of error sensors
W(i,j,iter):adaptive filter between i^{th} input sensor and j^{th} output actuator, after « iter » optimisation iterations
ΔW(i,j,iter):modification to the adaptive filter between i^{th} input sensor and j^{th} output actuator, after « iter » optimisation iterations
H(j,m) : filter modeling the path between the j^{th} output actuator and the m^{th} error sensor
Lw : length of the adaptive filters W(i,j,iter)
Lh : length of the filters H(j,m)
X(i,k) : vector of the Lh last samples at time k from the i^{th} input sensor
e(m,k) : residual error associated to the m^{th} error sensor, at time k
d(m,k) : sample from the m^{th} error sensor, at time k
V(i,j,m,k):vector of the Lw last samples of the filtered reference signal, calculated by filtering X(i,k) with H(j,m)

$X(i,k)^T$ = [x(i,k-Lh+1) ... x(i,k)]
$H(j,m)^T$ = [h(j,m,Lh) ... h(j,m,1)]
$W(i,j,iter)^T$ = [w(i,j,iter,Lw) ... w(i,j,iter,1)]
$\Delta W(i,j,iter)^T$ = [Δw(i,j,iter,Lw) ... Δw(i,j,iter,1)]
$V(i,j,m,k)^T$ = [v(i,j,m,k-Lw+1) ... v(i,j,m,k)].

In practice, a Filtered-X LMS algorithm is often divided into two parts : the control part (real-time part) and the optimisation part. As shown in Figure 1, instead of optimizing directly the adaptive filters W(i,j,iter) with the signals from the error sensors, variation filters ΔW(i,j,iter) are optimized with the residual errors, i.e. the signals that have not been cancelled by both the W(i,j,iter) and ΔW(i,j,iter) filters. The real-time control task of the W(i,j,iter) filters is executed at every sample, but the optimisation of the ΔW(i,j,iter) filters is calculated during idle processor time (whenever the processor is not executing a real-time control task). After some number of optimisation iterations, the values of ΔW(i,j,iter) are added to W(i,j,iter) and then cleared to start a new optimisation cycle.

The basic equations of a Filtered-X LMS are then («*» denotes a scalar product):

$$v(i,j,m,k) = X(i,k)^T * H(j,m) \qquad \text{(eq. 1)}$$

$$e(m,k) = \sum_i \sum_j V(i,j,m,k)^T * \Delta W(i,j,iter) + d(m,k) \qquad \text{(eq. 2)}$$

$$\Delta W(i,j,iter+1) = \Delta W(i,j,iter) - u \sum_m V(i,j,m,k) e(m,k) \qquad \text{(eq. 3).}$$

Now to describe the NLMS, an interlaced notation that will make the global correlation matrix of the filtered reference signals appear « block Toeplitz » will be introduced. We shall make use of that block Toeplitz property later.

If the following matrices are defined :

$$V(k) = \begin{bmatrix} \begin{bmatrix} v(1,1,1,k-Lw+1) \\ v(Nx,Ny,1,k-Lw+1) \end{bmatrix} & \cdots & \begin{bmatrix} v(1,1,Ne,k-Lw+1) \\ v(Nx,Ny,Ne,k-Lw+1) \end{bmatrix} \\ \begin{bmatrix} v(1,1,1,k) \\ v(Nx,Ny,1,k) \end{bmatrix} & & \begin{bmatrix} v(1,1,Ne,k) \\ v(Nx,Ny,Ne,k) \end{bmatrix} \end{bmatrix}$$

$$\Delta W(iter) = \begin{bmatrix} \begin{bmatrix} w(1,1,iter,Lw-1) \\ w(Nx,Ny,iter,Lw-1) \end{bmatrix} \\ \begin{bmatrix} w(1,1,iter,1) \\ w(Nx,Ny,iter,1) \end{bmatrix} \end{bmatrix}$$

$$E(k) = \begin{bmatrix} e(1,k) \\ e(Ne,k) \end{bmatrix} \qquad D(k) = \begin{bmatrix} d(1,k) \\ d(Ne,k) \end{bmatrix}$$

then equations 2 and 3 for the Filtered-X LMS algorithm can now be re-written in a compact way:

$$E(k) = V(k)^T \Delta W(iter) + D(k) \qquad \text{(eq. 4)}$$

$$\Delta W(iter+1) = \Delta W(iter) - uV(k)E(k) \qquad \text{(eq. 5).}$$

The NLMS algorithm recurrence equation can easily be written with that same notation (equations 1 and 4 are still valid for the NLMS):

$$\Delta W(iter+1) = \Delta W(iter) - uV(k)(V(k)^T V(k))^{-1} E(k) \qquad \text{(eq. 6).}$$

Introducing the inverse of the Ne×Ne matrix $V(k)^T V(k)$ in the recurrence equation 6 sets the range of u for which the algorithm is to converge (that range is independent of the filtered reference signals statistics) : $0 < u < 2$. At the opposite, the valid range of step sizes for equations 3 or 5 for the Filtered-X LMS depends on the filtered reference signals statistics and is the following (for $u \ll 1/$(any eigenvalue of $E[V(k)V(k)^T]$) [4]) :

$$0 < u < 2/\text{Trace}(E[V(k)V(k)^T])$$

$E[V(k)V(k)^T]$ is the NxNyLw × NxNyLw global correlation matrix of all the filtered reference signals (not to be confused with the instantaneous $V(k)^T V(k)$ of dimension Ne × Ne in equation 6). For now on, the former will be called Rvv.This correlation matrix is block Toeplitz because of the interlaced notation chosen for V(k) and ΔW(iter).

The main drawback of the Filtered-X LMS is its low broadband convergence speed when the filtered reference signals are strongly correlated. To achieve optimal convergence speed, the Filtered-X Newton-LMS algorithm can be used [2]. The Filtered-X Newton-LMS algorithm recurrence equation is (again equations 1 and 4 are valid for the Filtered-X Newton-LMS) :

$$\Delta W(iter+1) = \Delta W(iter) - u\, Rvv^{-1} V(k)\, E(k) \qquad \text{(eq. 7)}.$$

The matrix product with Rvv^{-1} ,requiring a lot of computational power, makes this algorithm unpractical for real-time systems with a large number of coefficients (Lw). Still, this algorithm achieves the optimal convergence speed and is the fastest of all stochastic gradient algorithms. The valid range of u for which the algorithm converges is (for $u << 1$): $0 < u < 2/NxNyLw$.

It is a well known fact in digital signal processing that the discrete cosine transform (DCT) can almost orthogonalize a strongly correlated signal. In [3], a fast convergence mono-channel Filtered-X LMS algorithm based on a transform domain optimisation (DCT transform) was presented. Orthogonalizing many filtered reference signals between each other is the same as diagonalizing the global correlation matrix Rvv. Let the new filtered reference matrix C(k) be defined as:

$$C(i,j,m,k)^T = [c(i,j,m,Lw) \ldots c(i,j,m,1)]$$
$$= \text{discrete cosine transform } (v(i,j,m,k-Lw+1) \ldots v(i,j,m,k))$$
$$= \text{discrete cosine transform } (V(i,j,m,k)^T) \qquad \text{(eq.8)}$$

$$\text{and } C(k) = \begin{bmatrix} \begin{bmatrix} \begin{bmatrix} c(1,1,1,Lw) \\ c(Nx,Ny,1,Lw) \end{bmatrix} \\ \vdots \\ \begin{bmatrix} c(1,1,1,1) \\ c(Nx,Ny,1,1) \end{bmatrix} \end{bmatrix} \cdots \begin{bmatrix} \begin{bmatrix} c(1,1,Ne,Lw) \\ c(Nx,Ny,Ne,Lw) \end{bmatrix} \\ \vdots \\ \begin{bmatrix} c(1,1,Ne,1) \\ c(Nx,Ny,Ne,1) \end{bmatrix} \end{bmatrix} \end{bmatrix}$$

The discrete cosine transform on the different filtered reference signals can make Rcc ($=E[C(k)C(k)^T]$) approximately block diagonal, which means that the autocorrelation of the different filtered reference signals has been almost eliminated by the discrete cosine transform, and that the intercorrelation between the different filtered reference signals has also been almost eliminated except between components at the same frequency.

The matrix that has nul elements outside of the main block diagonal and that has the elements of Rcc in the main block diagonal is called RDcc ($RDcc \approx Rcc$). The filtered reference matrix Cn(k) is then introduced:

$$Cn(k) = RDcc^{-1/2\,T}\, C(k) \qquad \text{(eq.9)}$$

and the new global correlation matrix will be:

$$\begin{aligned} Rcncn &= E[Cn(k)\, Cn(k)^T] \\ &= E[RDcc^{-1/2\,T}\, Rcc\, RDcc^{-1/2}] \\ &\approx E[RDcc^{-1/2\,T}\, RDcc\, RDcc^{-1/2}] \\ &= I \end{aligned} \qquad \text{(eq.10)}.$$

So the filtered reference signals are now almost uncorrelated and the convergence behavior is almost optimal. Note that $RDcc^{-1/2\,T}$ in eq.9 requires only the product of the main block diagonal unlike Rvv^{-1} in eq.7 for the Newton-LMS (much less computations for a large Lw). The equations for the COS-NLMS algorithm are (equation 1 remains valid, $\Delta\Omega(iter)$ is the transform domain equivalent of the time domain $\Delta W(iter)$) :

$$E(k) = Cn(k)^T\, \Delta\Omega(iter) + D(k) \qquad \text{(eq.11)}$$

$$\Delta\Omega\,(iter+1) = \Delta\Omega(iter) - u Cn(k)\, (Cn(k)^T\, Cn(k))^{-1}\, E(k) \qquad \text{(eq.12)}$$

After an optimisation sequence is complete, an inverse discrete cosine transform is performed on each adaptive filter of $\Delta\Omega(iter)$ to calculate all the adaptive filters of $\Delta W(iter)$ (so that the real-time control computations can still be performed in the time domain):

$$\Delta W(i,j,iter)^T = [\Delta w(i,j,iter,lw) \ldots \Delta w(i,j,iter,1)]$$
$$= \text{inverse discrete cosine transform}(\Delta\omega(i,j,iter,lw) \ldots \Delta\omega(i,j,iter,1))$$
$$= \text{inverse discrete cosine transform } (\Delta\Omega(i,j,iter)^T) \qquad \text{(eq.13)}.$$

Figure 2 shows an implementation of the COS-NLMS algorithm. Just like the NLMS, the range of u for which the algorithm converges is : $0 < u < 2$.

Some active control experiments in a duct have been performed to compare the NLMS and the COS-NLMS algorithms. Figure 3 shows some typical convergence curves for the two algorithms. As it is shown in that figure, the COS-NLMS has a faster convergence behavior than the NLMS.

3.0 Conclusion

A robust low computational approximation of the Newton-LMS algorithm was developped : the COS-NLMS algorithm. Real experiments of active control of noise in a duct have shown the effective gain of convergence speed provided by the COS-NLMS over the NLMS (or over the standard Filtered-X LMS).

Acknowledgments

Financial support for this work was provided by the « Institut de Recherche en Santé et Sécurité au Travail » (IRSST).

References

[1] DOUGLAS, S., OLKIN, J. (avril 1993) *Multiple-Input, Multiple Output, Multiple-Error Adaptive Feedforward Control Using the Filtered-X Normalised LMS Algorithm*, Proceedings of the second conference on recent advances in active control of sound and vibration, Blacksburgh(VA), 743-754.

[2] WIDROW, B., STEARNS, S.D. (1985) *Adaptive Signal Processing*, Englewood Cliffs, Prentice Hall, 99-116, 142-147.

[3] PAILLARD, B., BERRY, A., LE DINH, C.T., NICOLAS, J. (1995) *Accelerating The Convergence Of The Filtered-X LMS Algorithm Through Transform-Domain Optimization*, To be published in Mechanical Systems and Signal Processing.

[4] HAYKIN, S. (1991) *Adaptive Filter Theory*, Englewood Cliffs, Second edition, Prentice Hall

Figures

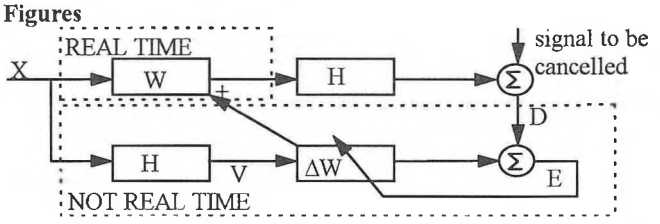

Figure 1: an implementation of the Filtered-X LMS algorithm.

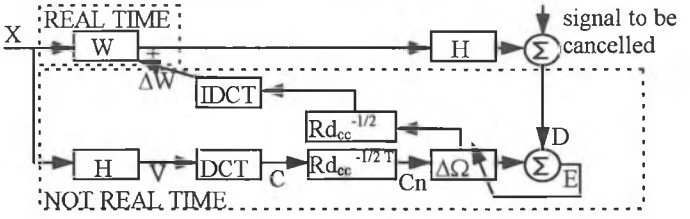

Figure 2: an implementation of the COS-NLMS algorithm.

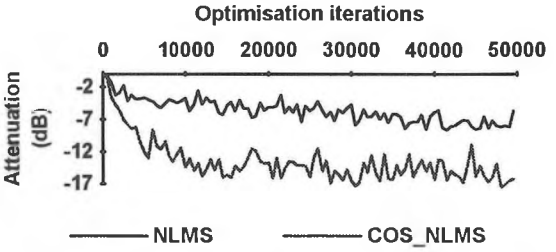

Figure 3 : results of active noise control in a duct

ACTIVE NOISE CONTROL SYSTEM TO REDUCE THE NOISE EMITTED BY A LARGE INDUSTRIAL STACK

André L'Espérance, Martin Bouchard, Fabienne Houiel, Mechanical Engineering Department, University of Sherbrooke
Sherbrooke, Québec, Canada

Jean-Claude Dubé *Aluminerie Lauralco Inc.*, 1 Boul. des Sources, Deschambault, (Qué), Canada, G0A 1S0

Introduction

A precise analysis of the noise emitted by an aluminum plant has shown that one of the main noise source was a 320 Hz emitted by an exhaust stack of 40 m high and 1,8 m of diameter. This pure tone noise was generated by the two blowers of the chimney. Because the classical cost effective solutions were not practical for this chimney (silencers, stack stuffers), the active noise control (ANC) solution was investigated. Commonly used single channel ANC systems [1] were however not applicable to the chimney, since high order acoustical modes propagate in the chimney. In fact, at the operation temperature (120 °C), 5 modes propagate in the chimney: modes (0,0), (1,0), (2,0), (0,1) & (3,0).

A higher modes ANC system was thus developed to control higher modes in a circular duct. To represent the propagation case of the real chimney, a scale model has been tested in a laboratory. The efficiency of the system was analyzed for different numbers and locations of control sources and error sensors. Conclusions obtained with this scale model were used for the installation of an ANC system in the real chimney stack.

1.0 Experimental set-up with the scale model

The scale model was a PVC duct of 3.30 m long having a diameter of 0.30 m. Figure 1 shows the basic arrangement upon which the tests have been conducted. The primary source was located at 0,40 m of the extremity closed by a reflecting cap. The secondary sources were placed at about 1 m away from this extremity, and the microphones are all disposed on the same section at 0.10 m of the open extremity of the duct. In this scale model, similar propagation conditions is obtained at 1700 Hz (same λ/diameter than in the real chimney)..

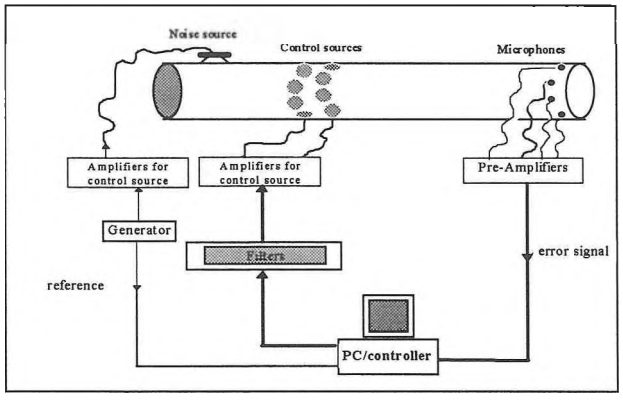

Figure 1 : Schematic of the general set-up

Amplifiers for the control sources and pre-amplifiers for the microphones are linked to a personal computer having a digital signal processing board which acts as the controller. Our controller used a common Multi-Input Multi-Output (MIMO) Filtered-X LMS algorithm[2].

Various preliminary measurements with different numbers and positions for the error microphones were conducted with the basic test arrangement described in figure 1. These measurements have shown that the location of the error microphones should be in an error sensors plane perpendicular to the cross section of the duct (patent pending). In this plane, the number and the location of the error sensors are determined such that the maximum distance between each error sensor and the boundary of the area under the influence of this error sensor is less or equal to approximately one-third of the wavelength of the maximum frequency to be attenuated. The number and location of the error sensors in the error sensors plane can be determined using the k mean algorithm[3].

2.0 Global attenuation as a function of the number of microphones

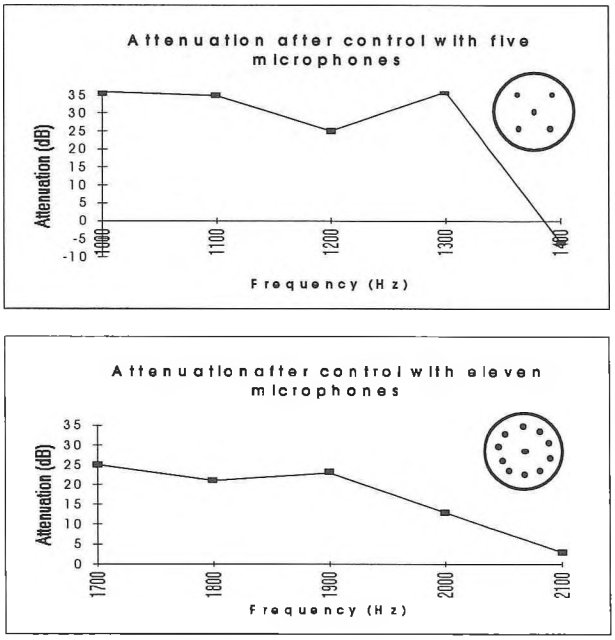

Figures 2a and 2b: Attenuation measurement results for the first source arrangement: a) 5 microphones, b)11 microphones.

Figures 2a and 2b give the global attenuation obtained as a function of the frequency for 5 and 11 error sensors in the error sensors plane respectively. With five error sensors, the ANC system is efficient up to 1300 Hz, but with 11 sensors, it is efficient up to about 2000 Hz (note that the cut off frequency for a single channal is about 900 Hz).

The positions of the error sensors plane and the control sources were also modified to evaluate their influence on the global attenuation obtained. Results have shown that the location of the speakers or of the microphones plane may change only slightly the general effectiveness and the cut-off frequency of the system. (mainly due to the effectiveness of the controller at the different controlling points).

3.0 Installation in the real chimney stack

According to the experimental results obtained in the scale model, a 10 channel MIMO controller was required to reduce the 320 Hz pure in the real stack. In this case, 9 of these sensors were located on a ring at 0.79 m of the wall, equally spaced at 40 ° intervals, and the last one was located in the middle. For convenience this error sensors plane and the 10 control sources have been installed in an existing turret located in the middle of the chimney. Figure 3 shows the installation of the control sources in the turret.

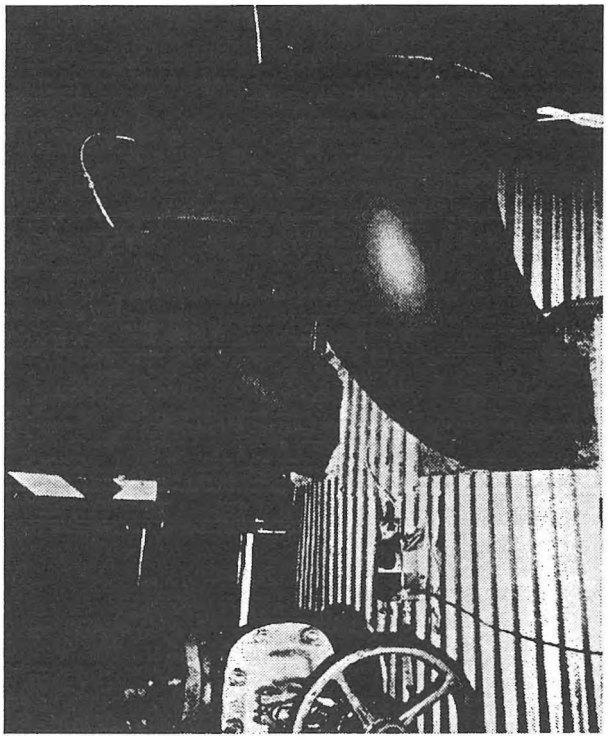

Figure 3 Installation of the speakers in the stack.

Using this 10 channels ANC system, the sound pressure level before and after the control have been measured at about 500 m of the stack. These measurements have shown that the noise reduction of the 320 Hz was about 7 dB(A) (figure 4).

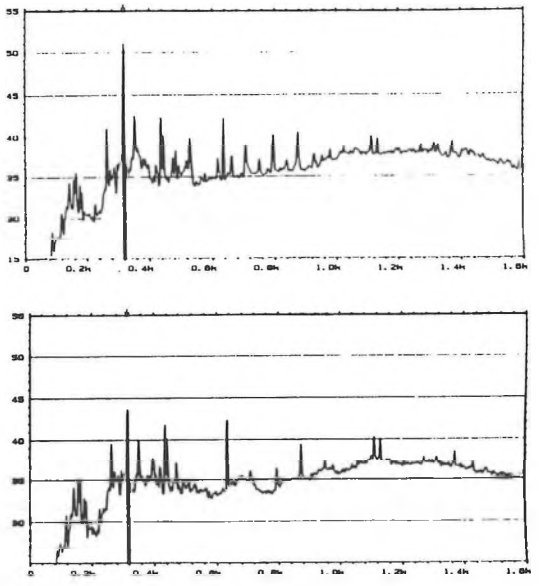

Figure 4 Noise spectral before and after the control at about 500 m from the chimney..

Some additional investigations have shown that the factor that have limited the noise reduction to 7 dB was the rapid variations of the 320 Hz level at the error sensors due to the asynchronicity of the two blowers. Simulations from records taken in the chimney have however shown that with some fine tuning of the controller, the global attenuation in the error sensor plane could be now increased to 12-13 dB.

It is now planed to install a permanent ANC system with this fine tuned controller to solve the noise problem related to this stack.

4.0 Conclusion

As long as a MIMO controller can reduce the noise level at the error points then, using the error sensors plane concept (patent pending), global attenuation can be obtained with ANC system at high frequencies for any type of duct shapes. The locations of the speakers or of the microphones plane changes only slightly the global efficiency of the system.

A 10 channel MIMO ANC system has been installed on an industrial stack and a 7-8 dB(A) noise reduction of 320 Hz has been obtained. It is however expected that 12 -13 dB(A) noise reduction can now be obtained with some fine tuning of the controller.

References

1. S. S. Wise et al., " Case Histories of active noise control on industrial fans and air handlers used for heating, ventilating and air conditioning". Proc. of Inter-Noise 92, Toronto Canada, p.307-312 (1992).
2. S. Douglas, J. Olkin, " Multiple input, multiple output, multiple error adaptive feedforward control using the filtered-X normalized LMS algorithm" , Proc. Recent Advances on Active Control, 1993
3. J. Markhoul " Vector quantization in speech coding ", Proc. IEEE, **73**, No 11, p. 1551-1588, 1985.

ACTIVE CONTROL OF PLATE VOLUME DISPLACEMENT: SIMULATION AND EXPERIMENTAL RESULTS

F. Charette, A. Berry and **C. Guigou**
Groupe d'Acoustique de l'Université de Sherbrooke
Department of Mechanical Engineering
Sherbrooke University, Sherbrooke, Qc. J1K 2R1

Vibration and Acoustics Laboratories
Department of Mechanical Engineering
V.P.I & S.U., Blacksburg, Virginia, U.S.

1. INTRODUCTION

The two main strategies for actively controlling sound fields are the Active Noise Control (ANC) and the Active Structural Acoustic Control (ASAC), first proposed by [Fuller 1990]. The ANC approach is based on controlling the acoustic field itself by using loudspeakers as secondary sources, while the ASAC approach directly modifies the response of the radiating structure by using structural transducers as secondary sources. In general, the ASAC approach has been proved to require a smaller number of secondary sources for a global control of the acoustic field. Recently, piezoceramic actuators embedded in or bonded to the structure have been successfully used as structural secondary sources for active noise applications, see [Fuller *et al.* 1989], [Clark *et al.* 1992] and [Crawley *et al.* 1987]. These distributed actuators overcome many of the disadvantages of shakers.

In ASAC, the other component of prime importance is the error sensor, which defines the type of information to be minimized by the controller. Polyvinylidene fluoride (PVDF) materials have been suggested as error sensors in the active control of structural vibration [Lee *et al.* 1990], [Gu *et al.* 1992], and more recently in the active control of sound radiation [Clark *et al.* 1992a,1993], [Guigou *et al.* 1994] and [Snyder *et al.* 1993], as an alternative to discrete microphones located in the acoustic field. [Guigou *et al.* 1994] developped a volume displacement sensor for beam using a single shaped PVDF strip. With this sensor, they have successfully implemented an active control of volume displacement for flexural beams and observed significant attenuation of the radiated sound field when active control was implemented. A similar approach was used by [Charette *et al.* 1995] to developed volume displacement sensor for 2D structure, i.e. rectangular plates. This plate volume displacement sensor is made of several shaped strips of PVDF film. This paper presents experimental results of an active control of volume displacement for a clamped plate using this PVDF volume displacement sensor as the error sensor.

2. ACTIVE CONTROL SIMULATION OF A PLATE VOLUME DISPLACEMENT

Active control simulation, for the clamped plate and actuators described in Tables 1 and 2, is performed to verify the efficiency of the proposed strategy (i.e. the minimization of the volume displacement) in reducing the sound radiation. To this end, the far-field radiated power and radiation efficiency are shown before and after control in Figure 1.

TABLE 1: Clamped plate characteristics

Length	50.0 cm
Width	39.8 cm
Thickness	3.15 mm
Young mod. (E)	6.5×10^{10} Pa
Density (ρ)	2800 Kg/m^3

It can be observed that below 220Hz, the radiation efficiency before control follows that of a monopole (about 6dB/oct.). Under control, in that frequency region, the radiation efficiency is changed to that of a dipole (about 12dB/oct.). The control of the plate volume displacement gives the largest sound power reduction in the frequency range where the radiation efficiency is reduced, since it decreases the plate capacity to induce sound in the acoustic medium.

TABLE 2: Ceramic piezo characteristics

	Primary	Secondary
Length	3.81 cm	3.81 cm
Width	3.18 cm	3.18 cm
Thickness	0.19 mm	0.19 mm
Pos. along the x axis	16.0 cm	19.0 cm
Pos. along y axis	30.0 cm	15.0 cm
Young mod. (E)	6.3×10^{10} Pa	6.3×10^{10} Pa
Density (ρ)	7750 Kg/m^3	7750 Kg/m^3

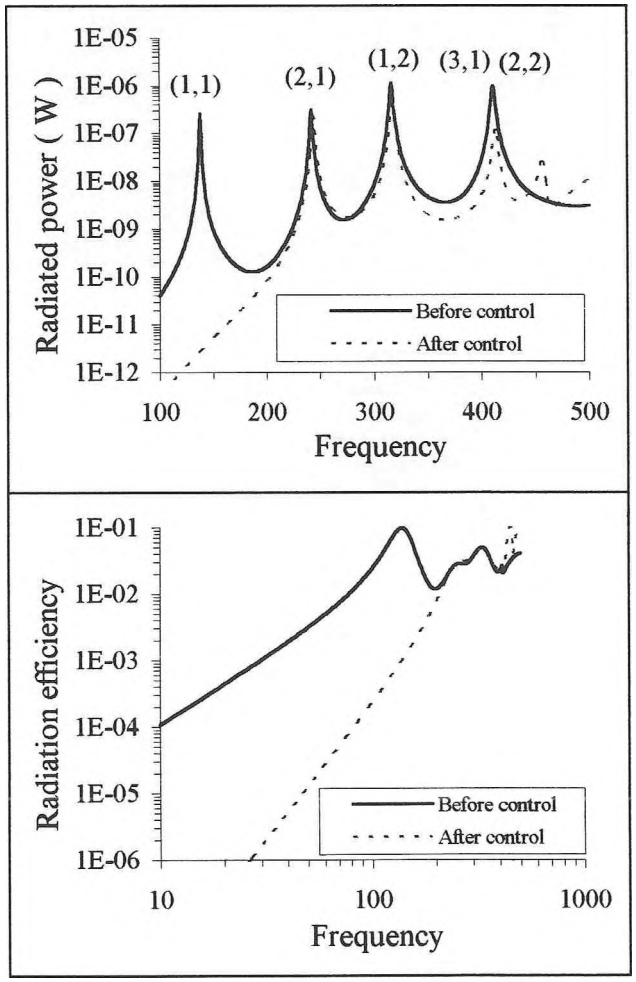

Figure 1: Theoretical simulation of the active control of volume displacement.

Over 220Hz, the radiation efficiency is approximately the same before and after control. In this frequency range, the control mechanism becomes mostly an attenuation of the plate vibration. The control efficiency near a mode depends mainly on the volume displacement of that mode. The (3,3) mode (413Hz) is thus controlled, while the (2,1) (243Hz), the (1,2) (319Hz) and the (2,2) (415Hz) which have low volume displacement are practically not controlled.

It can be noted, that a peak appears at 460Hz after control. This is caused by the control actuator which as a low authority near this frequency. Due to his dimensions and position, near 460Hz the control actuator as difficulty to generate volume displacement. This implies a high voltage is needed to control and associated with this high voltage is a global increase in the vibration level which in turn yields the regeneration of radiated power. An optimization of the control actuator characteristics should allow to prevent such regeneration of the radiated power.

3. EXPERIMENTAL RESULTS

An experimental implementation using the plate of the previous section was done. Eigth different frequencies were actively controlled using a LMS feedforward algorithm. Due to lack of space, only the results for the mode (1,1) at 140Hz are presented.

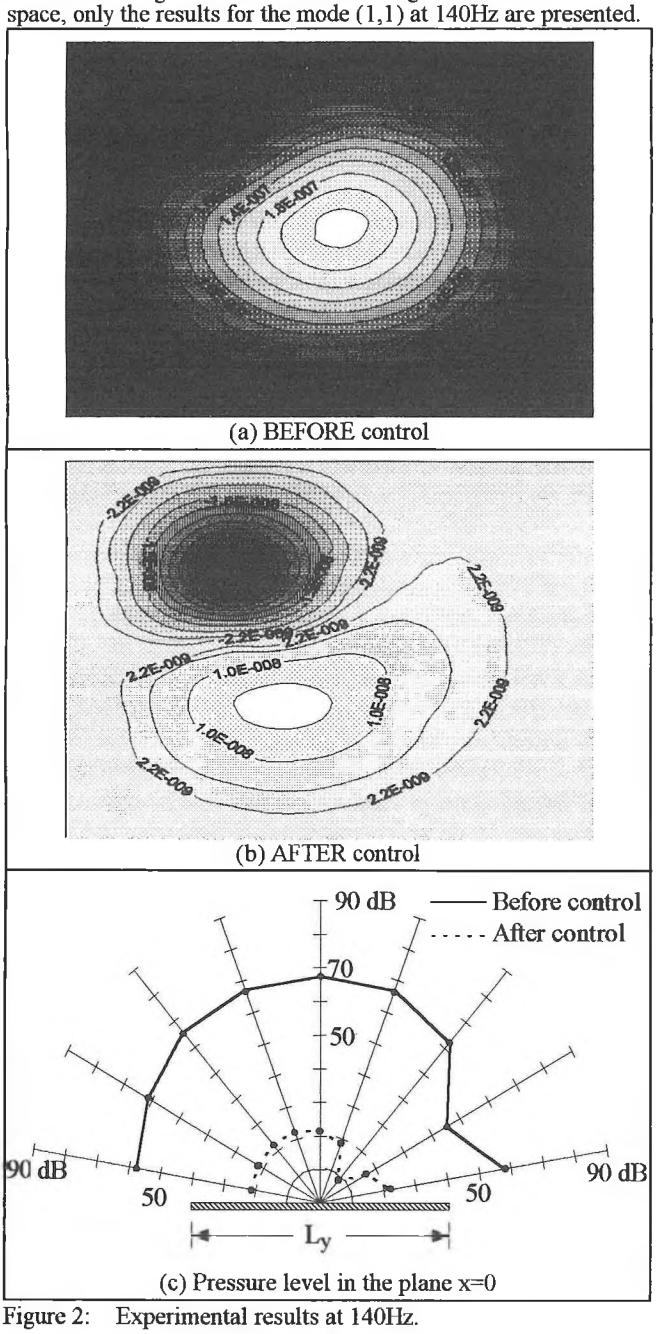

Figure 2: Experimental results at 140Hz.

Figure 2(a) and 2(b) shows the plate transversal displacement before and after control respectively. Those two plot demonstrate that the plate displacement go from a monopole type radiator to a dipole one. This confirm that the PVDF volume displacement sensor works properly. Figure 2(c) presents pressure level measurements made in the plane x=0. This plot shows a significant attenuation (between 40 and 50dB) in the pressure level at this frequenecy. Such attenuation is possible because at this frequency the control of the volume displacement minimizes the radiation efficiency and the vibration level simultaneously.

CONCLUSIONS

At low frequencies, passive control methods are generally inefficient for reducing the sound power radiated by a structure. However, the results presented in this paper clearly shows that the active control of volume displacement provides significant attenuation of sound radiation at those frequencies.

For the clamped plate considered here, the results indicates that below 220Hz the active control of volume displacement reduces the plate radiation efficiency and vibration level simultaneously. While over 220Hz, the control of volume displacement corresponds mainly to a reduction of the vibration level.

Using extended transducers, such as PVDF film, allows to have a single error channel to reduce the sound power radiated. This greatly simplifies the implementation of an active control system in the real world.

ACKNOWLEDGEMENT

This work was funded in part by the F.C.A.R. (Fonds pour la formation de chercheurs et l'aide à la recherche) and the I.R.S.S.T. (Institut de recherche en santé et sécurité au travail).

REFERENCES

Charette F. , Guigou C. and Berry A. "Development of volume velocity sensors for plates using PVDF film", *Proceedings of ACTIVE95 The 1995 International Symposium on Active Control of Sound and Vibration*, pages 241-252 (1995).

Clark R.L. and Fuller C.R. "Experiments on active control of structurally radiated sound using multiple piezoelectric actuators", *J. Acoust. Soc. Am.* **91**(6), pages 3313-3320 (1992).

Clark R.L. and Fuller C.R. "Modal sensing of efficient acoustic radiators with PVDF distributed sensors in active structural acoustic approaches", *J. Acoust. Soc. Am.* **91**(6), pages 3321-3329 (1992a).

Clark R.L., Burdisso R.A. and Fuller C.R. "Design approaches for shaping polyvinylidene fluoride sensors in active structural acoustic control (ASAC)", *Journal of Intelligent Material Systems and Structures*, **4**, pages 354-365 (1993).

Crawley E.F. and de Luis J. "Use of piezoelectric actuators as elements of intelligent structures", *AIAA Journal*, **25**(10), pages 1373-1385 (1987).

Fuller C.R., Hansen C.H. and Snyder S.D. "Active control of structurally radiated noise using piezoceramic actuator", *Proceedings of Inter-Noise 89*, pages 509-511 (1989).

Fuller C.R. "Active control of sound transmission/radiation from elastic plates by vibrational inputs: I. Analysis", *Journal of Sound and Vibration*, **136**(1), pages 1-15 (1990).

Gu Yi, Clark R.L., Fuller C.R. and Zander A.C. "Experiments on active control of plate vibration using piezoelectric actuators and polyvinylidene (PVDF) modal sensors", submitted to the *Journal of Sound and Vibration*, (1992).

Guigou C., Charette F. and Berry A. "Active control of sound by minimization of volume velocity on finite beam", *Proceedings of the Third International Congress on Air- and Structure-borne Sound and vibration*, pages 1507-1514 (1994).

Lee C.K., Moon F.C., "Modal sensors / actuators", *Transactions of the ASME*, **57**, pages 434-441 (1990).

Snyder S.D., Hansen C.H. and Tanaka N. "Shaped vibration sensors for feedforward control of structural radiation", *Proceedings of the Second Conference on the Recent Advances in Active Control of Sound and vibration*, pages 177-188 (1993).

ACTIVE ENHANCEMENT OF THE TRANSMISSION LOSS OF A PANEL VIA MINIMIZATION OF THE VOLUME VELOVITY: THEORETICAL AND EXPERIMENTAL RESULTS.

Marta Ruiz, Alain Berry, Francois Charette
G.A.U.S., Dép. de Génie Mécanique
Université de Sherbrooke, Sherbrooke (Québec) Canada J1K 2R1
Catherine Guigou
VAL, Dep. of Mechanical Engineering
VPI&SU, Blacksburg, VA 24061-0238, USA

I- INTRODUCTION

Among the different methods of active control of sound, the ASAC (Active Structural Acoustical Control) as employed in this study, presents the advantage of avoiding the cumbersome ,heavy and expensive microphones and speakers which are used in the ANC (Active Noise Control). The control of the acoustic radiated field is performed in modifying the response of the vibrating structure , with some piezoceramic actuators bonded on the plate. The error sensor is also bonded on the structure and provides the controller with a unique information: the volume displacement . Such a sensor, is said extended and has been adjusted in the GAUS[1],[2]. This strategy consisting in minimizing the volume displacement appears to be appropriate for the control of the transmission loss since this quantity has a good correlation with the radiation.
The present parametrical and experimental study has consisted in verifying the efficiency and the limits of this strategy on the control of the different vibrational and acoustics indicators, particularly the transmission loss of a plate.

II- STATEMENT OF THE PROBLEM:

A typical problem of transmission consists in studying how a partition-wall transmits the perturbation generated by an acoustic wave from a room to the other. In order to simplify the study of the control a thin rectangular plate, baffled in a wall has been excited by an acoustic wave and controlled by a pair of piezoceramic actuators bonded on the structure. These materials have the charateristic of contract or expand themselves when submitted to a current, flexural and distributed moments are generated along the edges , which permits to excitate the plate. Although some forces used as actuators conduct to better results than piezoceramic ones particularly in the low frequency range, their use is still not easy and expensive which is not the case for the piezoceramics . In order to achieve the parametrical study, the minimization of the volume displacement has been added in a program existing in the GAUS and determining all the acoustical indicators by a variational method, for a plate with general boundary conditions. [3][4].

III - THEORY

The total volume displacement (sum of the displacement over the panel surface) can be expressed as the sum of the primary volume displacement generated by the excitation (D_p) and the secondary volume displacement (D_s) generated by a control actuator which applied voltage should be the unity:

$$D_{tot} = \int_S W(x,y)dS = D_p + V \cdot D_s \qquad (1)$$

where V is the voltage corresponding to the actuator.
The displacement may be expanded with the polynomial functions chosen to form the basis.
As the displacement is:

$$W(x,y) = \sum_n \sum_m a_{nm}^{tot} (\tfrac{2}{a}x)^n (\tfrac{2}{b}y)^m dxdy \qquad (2)$$

where a and b are the dimensions of the plate and a_{nm}^{tot} the modal contribution, which permits, after some simplifications, to write the total volume displacement :

$$D_{tot} = \sum_{n,m\ odd} a_{nm}^{excit} \tfrac{ab}{nm} + \sum_{n,m\ odd} a_{nm}^{cont} \tfrac{ab}{nm} \qquad (3)$$

One can verify here that only the (odd,odd) modes participate to the volume displacement.

Minimizing this volume displacement is like finding V_c, the control voltage which has a quite simple expression:

$$V_c = -D_p / D_s \qquad (4)$$

The transmission loss of the panel is:

$$TL(dB) = 10\log_{10}(\tfrac{W^i}{W^t}) \qquad (5)$$

where W^i is the incident power and W^t the transmited power calculated in the far-field:
The more large this indicator will be, the more efficient the panel will be in term of transmission.
In this model, the sensor is assumed to be perfect in the whole frequency range, which is not the case for real sensors .

IV- RESULTS AND DISCUSSION

The results presented here, are for an aluminium plate which dimensions are 0.38×0.30×0.0016 m, the assumed damping factor being 5%, it is clamped and excited by a normal wave so that only

the modes whose volume displacement is not zero, are excited. Some thin piezos (0.038×0.032m) are located on the center of the plate, one on each side. The figure 1 shows that the efficiency of the control is good in a frequency domain where the symmetric (non-zero volume displacement) modes radiate significantly more than the other (zero volume displacement) modes, and consequently where the strategy of minimizing the volume displacement is relevant. The first mode is the one which is the most attenuated for it is also the one with the larger volume displacement. The antiresonances of the transmission loss correspond to the resonances of the quadratic velocity and represent the modes of the plate, however, after application of the control, the plate is excited on new frequencies (450 Hz) , this can be explained by the presence of such a weak secondary volume displacement that the voltage Vc (formula 4) applied on the piezos becomes very high, without achieving an efficient control. The figure 2 shows, nevertheless, that in the low frequency domain, the efficiency on the reduction of the transmited power is not questioned. Finally, the figure 3 shows the increase of the vibrations generated by the control. One can see that, for the first and most radiating mode, the vibration level has decreased. But it has to be known that the center of the plate is the best place for the piezo to be located, in the experiments the piezos can not be there because the sensor is also on the center.

V- CONCLUSION

The strategy of control by minimization of the volume displacement could be of great interest for the research in the "smart" structures area. It conducts to an interesting enhancement of the transmission loss of a thin plate in the frequency range where the volume displacement is sufficiently high, that is to say, at low frequencies.
The experimental results will be presented during the conference.

VI-ACKNOWLEDGEMENT

This work has been funded by the FCAR (Fonds pour la formation de chercheurs et l'aide à la recherche)

VII- REFERENCES

[1]: C. Guigou, F. Charette and A. Berry, "Active control of sound by minimization of volume velocity on finite beam", Proceedings of the Third International Congress on Air- and Structure-borne Sound and Vibration, pages 1507-1514 (1994).
[2]: F. Charette, C. Guigou, and A. Berry, "Development of volume velocity sensors for plates using PVDF film ", Proceedings of ACTIVE95 The 1995 International Symposium on Active Control of Sound and Vibration, pages 241-252 (1995).
[3]: R. Woodcock , "Modélisation de la transparence acoustique de structures simples et multicouches de type composite avec condictions limites quelconques ", PhD thesis. Université de Sherbrooke, Québec (1993).
[4]: A. Berry, J.-L. Guyader, J. Nicolas, "A general formulation for sound radiation from rectangular, baffled plates with arbitrary conditions", J.Acoust.Soc.Am,vol 88,n°6,p.2792-2802.

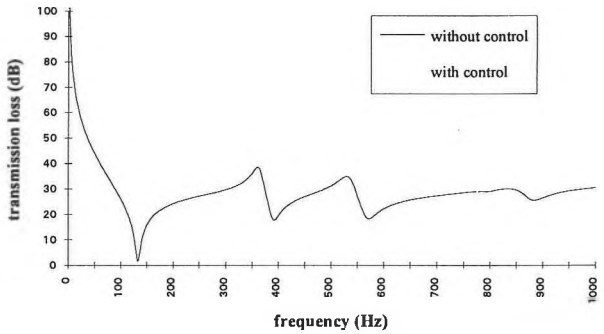

Figure 1: predicted **transmission loss** for a clamped plate excited by a normal incident wave

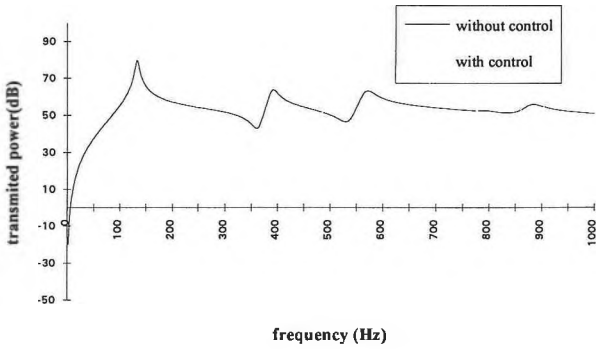

Figure 2: predicted **transmited power** for a clamped plate excited by a normal incident wave

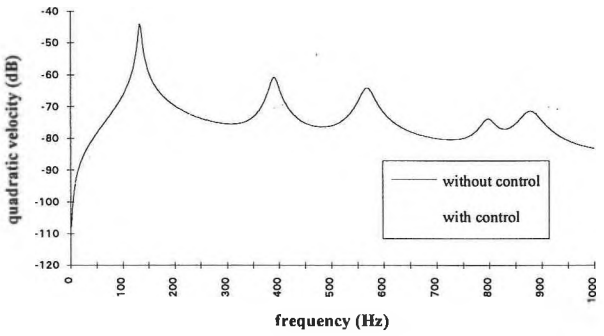

Figure 3: predicted **quadratic velocity** for a clamped plate excited by a normal incident wave

Active control of acoustic radiation using strain sensors

Patrice Masson, Alain Berry and Jean Nicolas
GAUS, Université de Sherbrooke,
Sherbrooke, Qué, J1K 2R1

INTRODUCTION

Sensing approaches used in active structural acoustic control (ASAC) are mainly concerned with monitoring acceleration, velocity or displacement of the structure, typically by means of accelerometers [1] or PVDF [2], thereby eliminating the need for far-field acoustic sensor(s). The radiation of the structure is estimated from this information, either directly [3] or from a model [4] of the radiating structure. The direct approach has the advantage of not being dependent on the accuracy of any model.

A new strategy is herein presented, where the estimation of acoustic radiation involves monitoring the *strain field* of the structure at discrete points. Such an information is *directly* given by fiber optics strain sensors, for example, so that significant gain is expected at this level. Two approaches are presented using the second derivative of the displacement, or strain, information. The ASAC is performed in the wavenumber domain and the cost function is defined as the radiated acoustic power.

COST FUNCTION IN THE WAVENUMBER DOMAIN

The acoustic radiation from a simply supported rectangular plate excited by a point disturbance will be considered (see Figure 1). A piezoelectric patch (PZT) is used for the control.

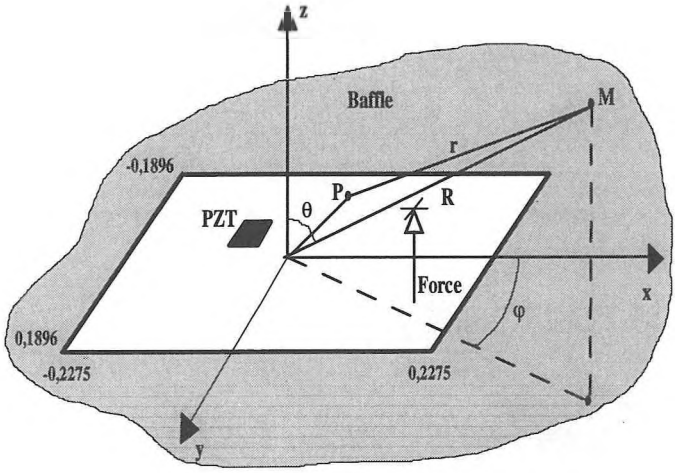

Figure 1 : Situation considered (dimensions in meters)

Assuming harmonic displacement, a far-field approximation to pressure is given by:

$$p(R,\theta,\varphi) = -\frac{\omega^2 \rho_o}{2\pi}\frac{e^{-ikR}}{R}\tilde{w}(\lambda,\mu) \qquad (1)$$

where λ and μ are the x and y components of the structural wavenumber, ω is the angular frequency , k is the acoustic wavenumber, ρ_o is the density of the fluid and $\tilde{w}(\lambda,\mu)$ is the Fourier transform of the normal displacement field $w(x,y)$.

The resulting pressure at a point M is the sum of a primary pressure field p_p associated with the disturbance and a secondary pressure field p_s associated with the control:

$$p(R,\theta,\varphi) = p_p(R,\theta,\varphi) + V_s\, p_s(R,\theta,\varphi) \qquad (2)$$

where V_s is the control voltage (complex) applied to the PZT.

The cost function is taken to be the radiated acoustic power Π which is given in the wavenumber domain by:

$$\Pi = \frac{1}{2\rho_o\omega}\left[\alpha_{pp^*} + V_s^*\alpha_{ps^*} + V_s\,\alpha_{p^*s} + |V_s|^2\,\alpha_{ss^*}\right] \qquad (3)$$

where the α's are obtained by integration in the supersonic region (A and B are associated with p and s):

$$\alpha_{AB^*} = \int_{-k}^{k}\int_{-\sqrt{k^2-\lambda^2}}^{\sqrt{k^2-\lambda^2}} \frac{\left(p_A\, p_B^*\right)}{\sqrt{k^2-\lambda^2-\mu^2}}\, d\mu\; d\lambda \qquad (4)$$

PRESSURE FROM DISCRETE STRAIN INFORMATION

Two formulations are proposed in order to express the pressure in Eq. (4) in terms of the discrete strain information. The first formulation is obtained by integrating Eq. (1) twice by parts while the second utilizes a finite difference scheme to estimate the displacement field to be Fourier transformed in Eq. (1).

1. Integration by parts of Fourier transform

Integrating twice by parts the Fourier transform in Eq.(1) gives:

$$\tilde{w}(\lambda,\mu) = \sum_{i=1}^{2} I_i - \frac{1}{\lambda^2}\,FT\left[\frac{\partial^2 w(x,y)}{\partial x^2}\right] \qquad (5)$$

where I_i is a boundary term associated with an edge i parallel to the y axis and FT denotes the discrete Fourier transform. The displacement and the rotation at the corners, as well as the second derivatives of the displacement may appear in the boundary terms. However, depending on the edge conditions, some of these terms can be simplified or expressed in terms of strain measurements along the edges.

2. Finite differences approach

Using a central finite difference scheme, the displacement at discrete $p \times q$ points (separated in the x direction by a distance h) on the plate can be *reconstructed* from the strain measurements by:

$$\frac{1}{h^2}\begin{bmatrix} -2h & -2 & 2 & & \\ & 1 & -2 & 1 & \\ & & \ddots & & \\ & & 2 & -2 & 2h \end{bmatrix}\begin{bmatrix} w'_{1,1} & \cdots & w'_{1,q} \\ w_{1,1} & \cdots & w_{1,q} \\ \vdots & & \vdots \\ w_{p,1} & \cdots & w_{p,q} \\ w'_{p,1} & \cdots & w'_{p,q} \end{bmatrix} = \begin{bmatrix} w''_{1,1} & \cdots & w''_{1,q} \\ \vdots & & \vdots \\ w''_{p,1} & \cdots & w''_{p,q} \end{bmatrix} \tag{6}$$

This linear system can be solved if two conditions on w or w' are given as boundary conditions. The corresponding system is then obtained:

$$[A_{p,p}][w_{p,q}] = [w''_{p,q}] - [A_{p,2}][w_{2,q}] \tag{7}$$

SIMULATION RESULTS

A first series of simulations was performed to validate the radiated sound power calculation with respect to the approach used. Figure 2 presents the radiated acoustic power as obtained with the two approaches, using a 16 × 16 array of sensors, and how it compares with a reference analytic curve (EOLE). The finite differences approach seems better on the whole range, up to 1300 Hz. Other results with 6 × 6 sensors showed good agreement up to 500 Hz with the finite differences approach.

Optimal control simulations were also conducted to assess the performance of our control scheme. Figure 3 presents the effect of active control on the radiated power using the finite differences approach and one 0,06 m × 0,04 m PZT located at x = -0,08 m, y = 0,07 m. As a result of the control, the reduction of the amplitudes in the supersonic region of the wavenumber spectrum is presented in Figure 4.

CONCLUSION

Strain sensors showed to be both simple and effective to evaluate the radiated sound power. For a simply supported plate, with 16 × 16 strain sensors, the finite differences approach allows good agreement with the analytic reference up to 1300 Hz. Both approaches were validated within optimal control situation and good performance was obtained. Future work includes the validation for other boundary conditions and the use of more than one actuator. The use of cubic splines as an alternative to finite differences will be investigated.

ACKNOWLEDGMENT

This research was supported by the *Fonds pour la formation de Chercheurs et Aide à la Recherche* (FCAR), Quebec, Canada.

REFERENCES

1. J.P. Maillard and C.R. Fuller, "Advanced time domain sensing for structural acoustic systems", Submitted for publication in the *J. Acoust. Soc. Am.*, 1994.
2. R.L. Clark and C.R. Fuller, "Modal sensing of efficient acoustic radiators with polyvinylidene fluoride distributed sensors in active structural acoustic control approaches", *J. Acoust. Soc. Am.*, **91**, 1992, pp.3321-3329.
3. S.D. Sommerfeldt and B.L. Scott, "Estimating acoustic radiation using wavenumber sensors", *Proc. Noise-Con 94*, Ft. Lauderdale, 1994, pp.279-284.
4. R.L. Clark and C.R. Fuller, "A model reference approach for implementing active structural acoustic control", *J. Acoust. Soc. Am.*, **92**, 1992, pp.1534-1544.

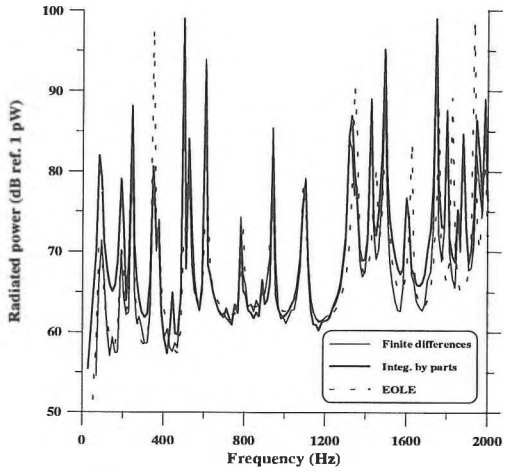

Figure 2 : Comparison of the two approaches

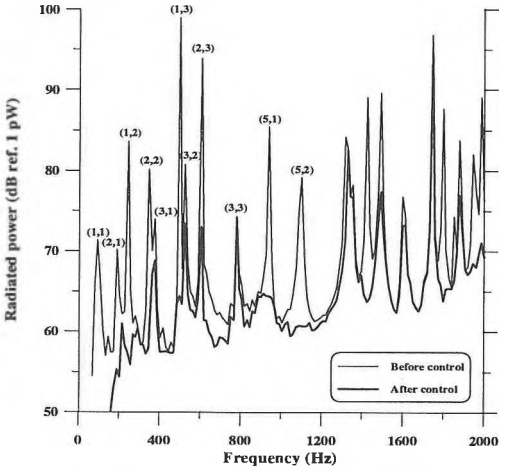

Figure 3 : Effect of active control, 16 × 16 strain sensors

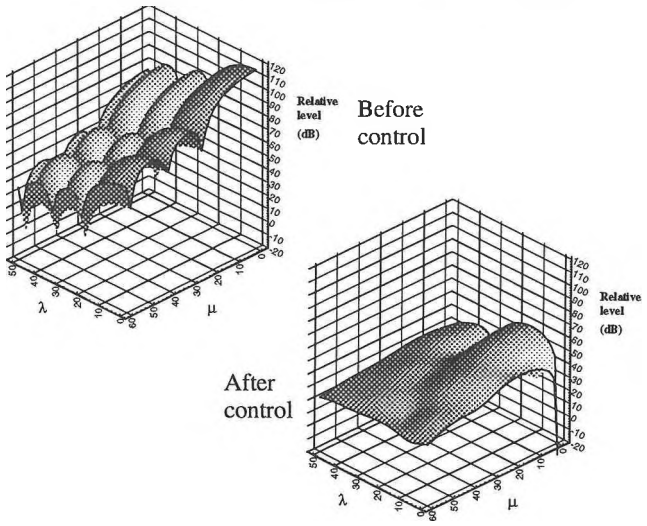

Figure 4 : Effect of control on the wavenumber spectrum, mode (1,1)

ÉTUDE VIBROACOUSTIQUE D'UNE COQUE CYLINDRIQUE SOUMISE À UNE EXCITATION SOLIDIENNE

Sylvain Boily, étudiant M. Sc. A.
François Charron, Professeur
G.A.U.S., Dép. de Génie Mécanique
Université de Sherbrooke, Sherbrooke (Québec) Canada J1K 2R1

I- INTRODUCTION

L'industrie aéronautique s'intéresse de plus en plus aux problèmes de bruit dans les avions et aux moyens pour les réduire. Une coque cylindrique est une représentation simplifiée d'une carlingue d'avion. Un tel modèle peut permettre d'évaluer l'effet de matériaux susceptibles de réduire le bruit et/ou les vibrations.

Cette étude porte sur la modélisation par éléments finis d'une coque cylindrique et de la cavité intérieure associée. On présente trois configurations: le système coque-cavité, le système coque-cavité avec un matériau absorbant et finalement une coque cylindrique sur laquelle est ajoutée une mince bande de matériau visco-contraint (sans cavité acoustique).

II- LES ÉQUATIONS DU PROBLÈME

Système coque-cavité

La discrétisation par éléments finis du problème structure-cavité acoustique avec une excitation solidienne donne le système couplé d'équations suivant (formulation u-p) [1],

$$-\omega^2\begin{bmatrix}[M_s] & [0]\\ [A]^T & [M_f]\end{bmatrix}\begin{Bmatrix}u_s\\ P_f\end{Bmatrix}+\begin{bmatrix}[\bar{K}_s] & -[A]\\ [0] & [\bar{K}_f]\end{bmatrix}\begin{Bmatrix}u_s\\ P_f\end{Bmatrix}=\begin{Bmatrix}F_s\\ 0\end{Bmatrix}$$

où $[M_s]$ et $[K_s]$ sont les matrices de masse et de rigidité de la structure. $[M_f]$ et $[K_f]$ sont les matrices pour le fluide. $[A]$ est la matrice de couplage des noeuds à l'interface fluide-structure. Afin de réduire la taille de ce système, on projette les déplacements u_s sur la base des modes propres de la structure $[\varphi_s]$ et la pression p_f sur la base des modes propres de cavité $[\varphi_f]$. Après manipulation, on obtient le système suivant, en coordonnées modales,

$$-\omega^2\begin{bmatrix}[m_s] & [0]\\ [a] & [m_f]\end{bmatrix}\begin{Bmatrix}q_s\\ q_f\end{Bmatrix}+\begin{bmatrix}[\bar{k}_s] & -[a]^T\\ [0] & [\bar{k}_f]\end{bmatrix}\begin{Bmatrix}q_s\\ q_f\end{Bmatrix}=\begin{Bmatrix}[\varphi_s]^T\{F_s\}\\ 0\end{Bmatrix}$$

où les inconnues sont maintenant les déplacements modaux q_s et les pressions modales q_f. Le nombre de d.d.l. est la somme des modes de structure et de cavité retenus.

Matériau absorbant

Le matériau absorbant est caractérisé par son impédance acoustique spécifique. En utilisant l'analogie mécanique représentée à la figure 1, on écrit l'impédance équivalente avec la relation suivante,

$$z = C + j\left(\omega M - \frac{K}{\omega}\right)$$

où C est la résistance acoustique et $\omega M - \frac{K}{\omega}$ est la réactance acoustique.

Matériau viscoélastique

On utilise l'approche proposée par Johnson et Kienholz [2]. Le matériau viscoélastique est modélisé par un module de cisaillement complexe, $G^*=(1+j\eta)G$, où G est le module de cisaillement et η le facteur de perte. On note que G et η sont considérés constants sur la bande de fréquences étudiée (80-480 Hz). Le viscoélastique est modélisé par des éléments de volume (3D) afin de bien représenter les déformations en cisaillement transversal.

III- DESCRIPTION DES MODÈLES NUMÉRIQUES

La figure 2 présente le maillage du modèle pour le système coque-cavité acoustique. Le système consiste en une coque cylindrique fermée à ses extrémités par des fonds rigides, avec à l'intérieur la cavité acoustique. Des éléments de plaques linéaires (5 d.d.l. par noeuds) sont utilisés pour la coque et les fonds rigides alors que des éléments de volume (1 d.d.l. par noeuds) forment la cavité. Le critère heuristique de 5 à 6 éléments par longueur d'onde fut utilisé pour le maillage.

L'ajout de l'absorbant est effectué en ajoutant une couche d'éléments absorbant à l'interface fluide-structure, ce qui a pour effet de réduire les dimensions de la cavité.

La figure 3 montre le maillage de la coque avec la bande de matériau visco-contraint au milieu ainsi qu'une vue de coupe. Des éléments de volume (3 d.d.l. par noeud) modélise le matériau viscoélastique alors que la couche supérieure utilise des éléments de plaque.

IV- RÉSULTATS ET ANALYSES

Les résultats sont systématiquement comparés à des résultats expérimentaux. L'excitation mécanique (ponctuelle, harmonique, normale à la coque, située à 0,4 m sur la coque) est la même dans les trois configurations.

Système coque-cavité

Pour ce cas, les conditions aux limites sont de type libre-libre. La figure 4 montre la pression quadratique moyenne $\langle P^2\rangle$ pour trois bases modales de cavité: 0-600 Hz, 0-2000 Hz et 0-2850 Hz. On constate que pour obtenir une réponse acoustique à chacun des modes de structure, on doit garder tous les modes acoustiques jusqu'à 2850 Hz, afin que chaque mode de structure se trouve couplé à au moins un mode de cavité. La figure 5 compare $\langle P^2\rangle$ numérique avec des résultats expérimentaux. On obtient une bonne comparaison.

Système coque-cavité avec matériau absorbant

La figure 6 compare $\langle P^2\rangle$ numérique avec des résultats expérimentaux. Il faut noter que les effets de masse et d'amortissement ajoutés du matériau absorbant sont inclus dans le modèle. La

réduction de $<P^2>$ est due aux propriétés amortissantes du matériau et non reliée à l'absorption. Ce phénomène s'explique par la faible épaisseur de l'absorbant pour la bande de fréquences étudiée.

Coque avec matériau visco-contraint

Les conditions aux limites pour ce cas sont de type appui simple. La figure 7 compare $<V^2>$ numérique avec des résultats expérimentaux. On obtient une très bonne corrélation.

V- CONCLUSION

La modélisation par éléments finis d'une coque cylindrique et de la cavité acoustique associée a été présentée. Trois configurations furent étudiées, soit le système coque-cavité, le système coque-cavité avec matériau absorbant et la coque avec matériau visco-contraint. Les corrélations obtenues avec les montages expérimentaux sont bonnes.

VI-REMERCIEMENTS

Les auteurs remercient le C.R.S.N.G et Canadair Inc. pour le support financier de cette étude ainsi que Jean-Marie Guérin pour les résultats expérimentaux.

VII- RÉFÉRENCES

[1]: H. J.-P. Morand et R. Ohayon, "Interactions fluides-structures", Paris, Éd. Masson, 224p. (1992).

[2]: C. D. Johnson and D. A. Kienholz, "Finite Element Prediction of Damping in Structures with Constrained Viscoelastic Layers", *AIAA Journal,* **20**(9), 1284-1290 (1982).

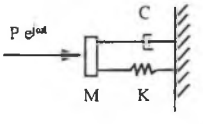

Figure 1. Modèle mécanique équivalent pour l'impédance acoustique spécifique d'un matériau absorbant

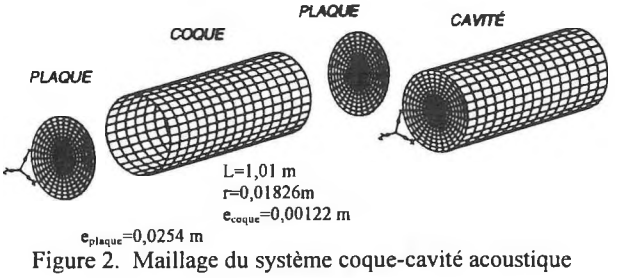

Figure 2. Maillage du système coque-cavité acoustique

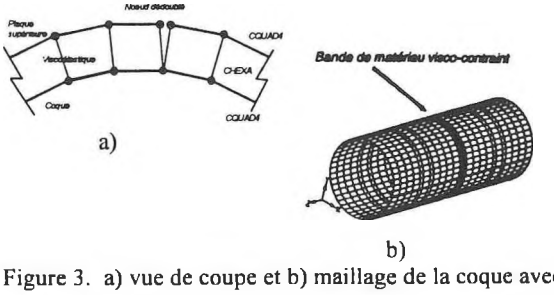

Figure 3. a) vue de coupe et b) maillage de la coque avec visco-contraint

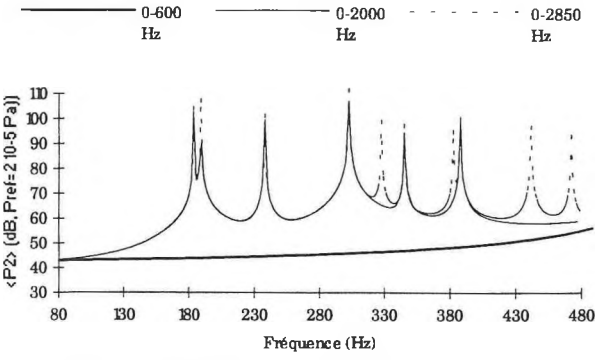

Figure 4. Comparaison de $<P^2>$ pour trois cas de base modale

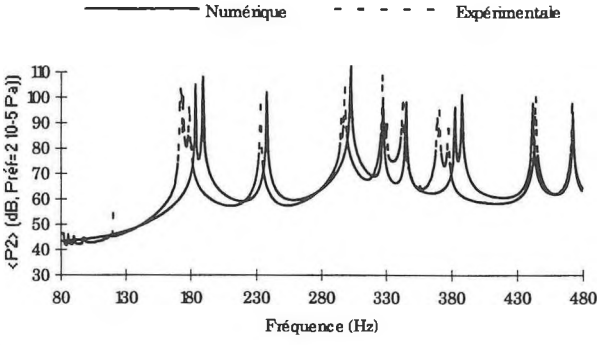

Figure 5. Comparaison de $<P^2>$, système coque-cavité

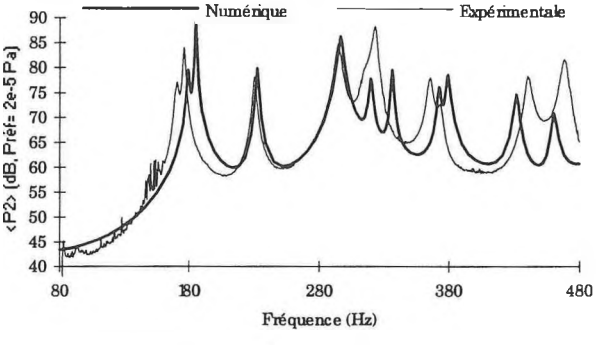

Figure 6. Comparaison de $<P^2>$, coque-cavité avec absorbant

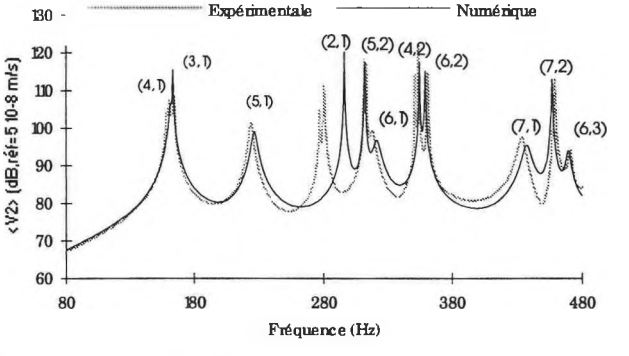

Figure 7. Comparaison de $<V^2>$, coque avec visco-contraint

On the computation of acoustic modes of cavities with irregular shapes

J. Missaoui and L. Cheng
Department of Mechanical Engineering
Laval University Quebec, Canada, G1K 7P4

1. Introduction

Reducing noise level needs a better understanding of the mechanism of noise transmission into cavities. For this purpose and due to the large number of degree of freedom needed for the Finite Element Method, more physical methods are needed to calculate the acoustic properties with less time computation, it is especially the case when the sound and structure are coupled. Among them one finds the following ones: Green function method based development [1] and the acoustoelastic theory [2]–[3]. The first one, similar to that used in ref. [4], considers a perturbation in the boundary shape. The second one is based on a subdivision of the interior space to a series of rectangular sub-cavities connected by vibrating membranes. Due to the reasonable deviation of the irregular cavity considered as a limitation in the Green function method and the increased number of sub-cavities used in the acoustoelastic theory, an alternative approach which is a combination of the two cited methods is presented. A major advantage of the proposed method is that analytical expressions for regular sub-cavities can be used while others can be characterized by a linear combination of the known eigenfunction of their bounded cavities.

2. Modelling of the acoustic properties

Based on Green theorem, the acoustic pressure inside a cavity can be expressed as an integral equation including the boundary and the membrane effects .

$$p_c = \int_{S_b} (G\frac{\partial p}{\partial \mathbf{n}} - p\frac{\partial G}{\partial \mathbf{n}})ds + \int_{S_m} (G\frac{\partial \bar{p}}{\partial \mathbf{n}} - \bar{p}\frac{\partial G}{\partial \mathbf{n}})ds \quad (1)$$

where: G is Green's function for a Neumann boundary, $\mathbf{n}$ is the outward normal vector of the boundary surface S_b, $\bar{p}$ is the pressure drop across the membrane S_m, c is the sound speed inside the cavity.

In the combined approach (see Figure 1), the acoustic pressure inside irregular sub-cavity is expressed as a linear combination of a know orthogonal functions: $\psi(r) = \sum_n A_n \phi_n(r)$ ($\phi_n(r)$ represents the spatial shape of the regular sub-cavity enclosing the irregular one). By a physical observation, if the approximated cavity presents a large deviation with respect to the bounding one, a minimal subdivision of the irregular cavity is necessary. A membrane without rigidity and mass is imagined to exist separating the two sub-cavities. Using equation (1), and allowing a continuous pressure across the membrane, the final coupled modal equations are derived as a function of the modal coordinate q_m of the vibrating membrane *in vacuo*.

$$A_n^i(\Lambda_n^{i2} - \omega^2)V_i M_n^i = -\rho c^2 \sum_m \ddot{q}_m L_{nm}^{ii} \quad (2)$$

$$A_n^j(\Lambda_n^{j2} - \omega^2)V_j M_n^j + c^2 \sum_{n'} A_{n'} B_{nn'} = \rho c^2 \sum_m \ddot{q}_m L_{nm}^{ij}$$

$$\bar{p} = 0 : \sum_n b_n^i L_{nm}^{ii} = \sum_n b_n^j L_{nm}^{ij}$$

where L_{nm}^{ij} is the modal acoustoelastic coupling coefficient between membrane (i) and hard walled mode of sub-cavity (j), the term $B_{nn'} = \int_s \phi_{n'} \frac{\partial \phi_n}{\partial \mathbf{n}} ds$ can be done analytically or numerically depending on the irregularity of the sub-cavity shape.
It should be noted that the proposed approach is in fact an extension of the Green function method by taking advantage that certain sub-cavities of regular shape may exist in the whole system.

3. Illustrative example

Figure 2 shows a cross-section of an irregular cylindrical cavity used to predict the acoustic characteristics inside a simplified aircraft cabin. Only natural acoustic frequencies are presented and compared to published results calculated by Finite difference method [5]. In Table 1, the Green function method using the cylindrical bounding cavity modes is used for a floor angle

($\theta_f = 49°$). Better results can be obtained for a reasonable deviation of the irregular cavity from the cylindrical one. In Table 2, results obtained by the combined approach are presented and compared to the Finite difference method.

4. Conclusion

It was shown that it is possible to use a combined analytical approach for the determination of the acoustic characteristics. This approach permits a minimal discretization of the irregular cavity, a saving in computational time compared to the acoustoelastic approach. However, the Green function method seems to be more accurate when the irregular cavity does not present a large deviation in boundary shape when compared to its bounding regular cavity.

References

[1] G. P. Succi 1987 *JASA*. 81(6),1688–1694. The interior acoustic field of an automobile cabin.

[2] E.H. Dowell, G.F. Gorman, and D.A. Smith 1977 *JSV* 52(4),519–542. Acoustoelasticity: General theory, acoustic natural modes and forced response to sinusoidal excitation, including comparison with experiment.

[3] Chao, Chen-Fu B. 1981 *Modal Analysis of interior noise fields* Ph.D. thesis Princeton University

[4] P.M. Morse and H. Feshbach 1953 *Methods of Theoretical Physics*

[5] L.D. Pope, E.G. Wilby and J.F. Wilby 1984 *Analytical predictor of the interior noise for cylindrical models of Aircraft fuselage for prescribed exterior noise fields*

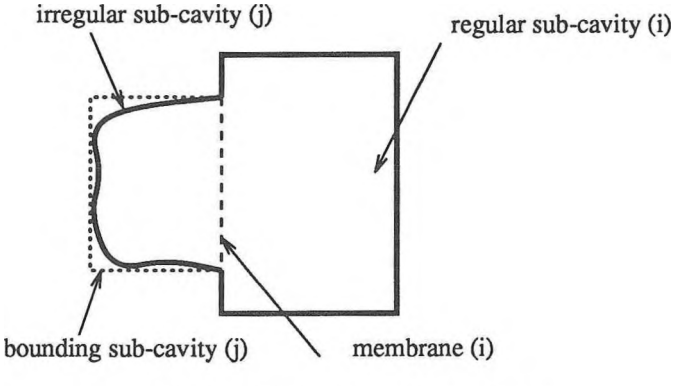

Figure 1: Combined approach

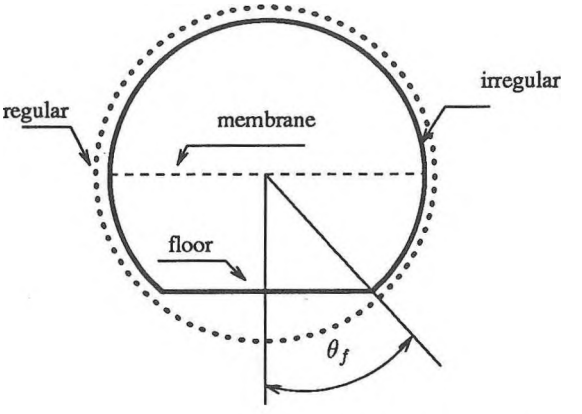

Figure 2: Irregular cylindrical cavity

Table 1: Finite difference and Green function method

Mode	Ref. [5]	Green function method	
	f_n (Hz)	f_n (Hz)	Error (%)
1	96.416	96.210	-0.21
2	113.002	114.847	1.63
3	166.997	169.457	1.45
4	178.748	179.937	0.66
5	212.718	217.642	2.26
6	238.019	243.739	2.31
7	243.915	246.772	1.17
8	280.915	284.653	1.33
9	283.663	286.643	1.05
10	305.542	295.714	-3.21

Table 2: Finite difference and Combined approach

Mode	Ref. [5]	Present work	
	f_n (Hz)	f_n (Hz)	Error (%)
1	96.416	96.5	0.080
2	113.002	116.0	2.65
3	166.997	166.25	-0.44
4	178.748	180.5	0.98
5	212.718	213.25	0.25
6	238.019	230.0	-3.37
7	243.915	246.0	0.85
8	280.915	278.0	-1.03
9	283.663	290.0	2.23
10	305.542	294.75	-3.53

NEWS/INFORMATIONS

CONFERENCES

130th Meeting of the Acoustical Society of America: 27 November - 1 December 1995, St. Louis, Missouri, USA. Contact: Elaine Moran, Acoustical Society of America, 500 Sunnyside Blvd., Woodbury, NY II797, USA. Tel: (516) 576-2360; Fax: (516) 349-7669.

Forum Acusticum 1996: 1-4 April 1996, Antwerp, Belgium. Contact: Convention Secretariat, Technological Institute K VIV, Desguinlei 214, B-2018 Antwerpen, Belgium. Tel: +32 (0)3 216-0996; Fax: +32 (0)3 216-0689.

4th Acoustical Engineering Student's Congress: 20-22 October 1995, Valdivia, Chile. Contact: M. G. Vinuales, Escuela de Inginieria Acustica, Faculdad de Ciencias de la Ingenieria, Universidad Austral de Chile, PO Box 567 Valdivia, Chile. Tel: +56 63 217368/221338; Fax: +56 63 213-986; E-mail: ingeacus@valdivia.uca.uach.cl.

Inter-Noise '96: 30 July - 2 August 1996, Liverpool, UK. Theme: Noise, the next 25 years - scientists, engineers and legislators in partnership. Contact: Cathy Mackenzie, Institute of Acoustics, Agriculture House, 5 Holywell Hill, St. Albans, Herts, ALI IEU, UK. Tel: +44 1727 848195; Fax: +44 1727 850553.

COURSES

Noise Control for Buildings, Manufacturing Plants, Equipment and Products: 13-17 November 1995, Sheraton World Hotel, Orlando, Florida. Contact: Hoover & Keith Inc., 11381 Meadowglen, Suite 1, Houston, Texas 77082, USA. Tel: (713) 496-9876; Fax: (713) 496-0016.

CONFÉRENCES

130e Rencontre de l'Acoustical Society of America: 27 novembre - 1 décembre 1995, St. Louis, Missouri, États-Unis. Contact: Elaine Moran, Acoustical Society of America, 500 Sunnyside Blvd., Woodbury, NY II797, États-Unis. Tél: (516) 576-2360, télécopieur: (516) 349-7669.

Forum Acusticum 1996: 1-4 avril 1996, Antwerp, Belgique. Contact: Secrétariat de conférence, Technological Institute K VIV, Desguinlei 214, B-2018 Antwerpen, Belgique. Tel: +32 (0)3 216-0996; télécopieur: +32 (0)3 216-0689.

4e congrès des étudiants en ingénierie acoustique: 20-22 octobre 1995, Valdivia, Chile. Contact: M. G. Vinuales, Escuela de Inginieria Acustica, Faculdad de Ciencias de la Ingenieria, Universidad Austral de Chile, PO Box 567 Valdivia, Chile. Tel: +56 63 217368/221338; télécopieur: +56 63 213986; courrier électronique: ingeacus@valdivia.uca.uach.cl.

Inter-Noise '96: 30 juillet - 2 août 1996, Liverpool, UK. Thème: Le bruit - les prochains 25 ans - chercheurs, ingénieurs et législateurs en partenariat. Contact: Cathy Mackenzie, Institute of Acoustics, Agriculture House, 5 Holywell Hill, St. Albans, Herts, ALI IEU, UK. Tel: +44 1727 848195; télécopieur: +44 1727 850553.

COURS

Contrôle du bruit pour les édifices, les industries maufacturières, les équipments et les produits: 13-17 novembre 1995, l'hotel Sheraton World, Orlando, Floride. Contact: Hoover & Keith Inc., 11381 Meadowglen, Suite 1, Houston, Texas 77082, États-Unis. Tel: (713) 496-9876; télécopieur: (713) 496-0016.

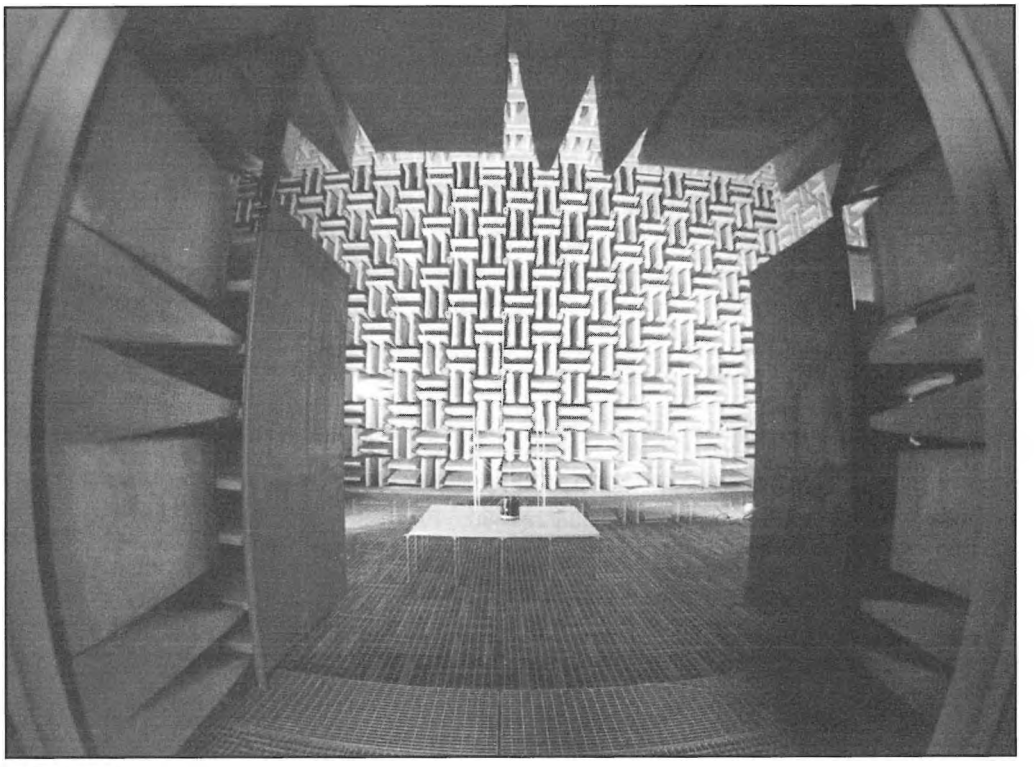

LARGE ACOUSTICAL ANECHOIC CHAMBER

AT HEALTH CANADA'S RADIATION PROTECTION BUREAU AVAILABLE ON A FEE-FOR-SERVICE BASIS

This facility features a unique combination of a quiet, echo-free environment, large size and versatility for generating and characterizing sound fields. Although not meant to replace commercially available anechoic chambers, there is a wide range of appropriate engineering, research and development applications which could be of interest to the private sector, universities, as well as government departments and agencies.

Availability of the facility will be based on the demands of the Bureau's noise protection program.

Let us know your needs by contacting:

Stephen Bly, Health Canada
Room 228A, 775 Brookfield Road
Ottawa, Ontario K1A 1C1
Phone: (613) 954-0308
Fax: (613) 941-1734
E-mail: sbly@hpb.hwc.ca

We will be pleased to provide more information, including cost estimates, scheduling and availability of equipment.

Characteristics:

- 12.7 x 8.7 x 7.8 m (l x w x h) wedge tip to wedge tip
- anechoic from 50 to 20 000 Hz
- inaudible background noise

Options:

- microphone positioning robot
- hemi-anechoic environment for distributed loads up to 1200 kg/m^2

Some applications:

- active noise control systems
- engineering noise controls
- audio entertainment systems
- psychoacoustics

Health Canada Santé Canada

Canada

The Canadian Acoustical Association
l'Association Canadienne d'Acoustique

ANNONCE DE PRIX

Plusieurs prix, dont les objectifs généraux sont décrits ci-dessous, sont décernés par l'Association Canadienne d'Acoustique. Pour les quatre premiers prix, les candidats doivent soumettre un formulaire de demande ainsi que la documentation associée au coordonnateur de prix avant le dernier jour de février de l'année durant laquelle le prix sera décerné. Toutes les demandes seront analysées par des sous-comités nommés par le président et la chambre des directeurs de l'Association. Les décisions seront finales et sans appel. L'Association se réserve le droit de ne pas décerner les prix une année donnée. Les candidats doivent être membres de l'Association. La préférence sera donnée aux citoyens et aux résidents permanents du Canada. Les candidats potentiels peuvent se procurer de plus amples détails sur les prix, leurs conditions d'éligibilité, ainsi que des formulaires de demande auprès du coordonnateur de prix.

Prix Post-Doctoral Edgar et Millicent Shaw en Acoustique

Ce prix est attribué à un(e) candidat(e) hautement qualifié(e) et détenteur(rice) d'un doctorat ou l'équivalent, qui a complèté(e) ses études et sa formation de chercheur, et qui désire acquérir jusqu'à deux années de formation supervisée de recherche dans un établissement reconnu. Le thème de recherche proposée doit être relié à un domaine de l'acoustique, de la psycho-acoustique, de la communication verbale ou du bruit. La recherche doit être menée dans un autre milieu que celui où le candidat a obtenu son doctorat. Le prix est de $3000 pour une recherche plein temps de 12 mois avec possibilité de renouvellement pour une deuxième année. Coordonnatrice: Sharon Abel, Mount Sinai Hospital, 600 University Avenue, Toronto, ON M5G 1X6. Les récipiendaires antérieur(e)s sont:

1990	*Li Cheng*	*Université de Sherbrooke*
1993	*Roland Woodcock*	*University of British Columbia*
1994	*John Osler*	*Defense Research Establishment Atlantic*

Prix Étudiant Alexander Graham Bell en Communication Verbale et Acoustique Comportementale

Ce prix sera décerné à un(e) étudiant(e) inscrit(e) dans une institution académique canadienne et menant un projet de recherche en communication verbale ou acoustique comportementale. Il consiste en un montant en argent de $800 qui sera décerné annuellement. Coordonnateur: Don Jamieson, Department of Communicative Disorders, University of Western Ontario, London, ON N6G 1H1. Les récipiendaires antérieur(e)s sont:

1990	*Bradley Frankland*	*Dalhousie University*
1991	*Steven D. Turnbull*	*University of New Brunswick*
	Fangxin Chen	*University of Alberta*
	Leonard E. Cornelisse	*University of Western Ontario*
1993	*Aloknath De*	*McGill University*
1994	*Michael Lantz*	*Queen's University*

Prix Étudiant Fessenden en Acoustique Sous-marine

Ce prix sera décerné à un(e) étudiant(e) inscrit(e) dans une institution académique canadienne et menant un projet de recherche en acoustique sous-marine ou dans une discipline scientifique reliée à l'acoustique sous-marine. Il consiste en un montant en argent de $500 qui sera décerné annuellement. Coordonnateur: David Chapman, DREA, PO Box 1012, Dartmouth, NS B2Y 3Z7.

1992	*Daniela Dilorio*	*University of Victoria*
1993	*Douglas J. Wilson*	*Memorial University*
1994	*Craig L. McNeil*	*University of Victoria*

Prix Étudiant Eckel en Controle du Bruit

Ce prix sera décerné à un(e) étudiant(e) inscrit(e) dans une institution académique canadienne dans n'importe quelle discipline de l'acoustique et menant un projet de recherche relié à l'avancement de la pratique en contrôle du bruit. Il consiste en un montant en argent de $500 qui sera décerné annuellement. Ce prix a été inauguré en 1991. Coordonnateur: Murray Hodgson, Occupational Hygiene Programme, University of British Columbia, 2206 East Mall, Vancouver, BC V6T 1Z3.

1994	*Todd Busch*	*University of British Columbia*

Prix des Directeurs

Trois prix sont décernés, à tous les ans, aux auteurs des trois meilleurs articles publiés dans l'*Acoustique Canadienne*. Tout manuscrit rapportant des résultats originaux ou faisant le point sur l'état des connaissances dans un domaine particulier sont éligibles; les notes techniques ne le sont pas. Le premier prix, de $500, est décerné à un(e) étudiant(e) gradué(e). Le deuxième et le troisième prix, de $250 chacun, sont décernés à des auteurs professionnels âgés de moins de 30 ans et de 30 ans et plus, respectivement. Coordonnateur: Blaise Gosselin, Hydro Québec, 16^{e} étage, 75 boul. René Lévesque ouest, Montréal, QC H2Z 1A4.

Prix de Presentation Étudiant

Trois prix, de $500 chacun, sont décernés annuellement aux étudiant(e)s sous-gradué(e)s ou gradué(e)s présentant les meilleures communications lors de la Semaine de l'Acoustique Canadienne. La demande doit se faire lors de la soumission du résumé. Coordonnateur: Alberto Behar, 45 Meadowcliffe Drive, Scarborough, ON M1M 2X8.

The Canadian Acoustical Association
l'Association Canadienne d'Acoustique

PRIZE ANNOUNCEMENT

A number of prizes, whose general objectives are described below, are offered by the Canadian Acoustical Association. As to the first four prizes, applicants must submit an application form and supporting documentation to the prize coordinator before the end of February of the year the award is to be made. Applications are reviewed by subcommittees named by the President and Board of Directors of the Association. Decisions are final and cannot be appealed. The Association reserves the right not to make the awards in any given year. Applicants must be members of the Canadian Acoustical Association. Preference will be given to citizens and permanent residents of Canada. Potential applicants can obtain full details, eligibility conditions and application forms from the appropriate prize coordinator.

Edgar and Millicent Shaw Postdoctoral Prize in Acoustics

This prize is made to a highly qualified candidate holding a Ph.D. degree or the equivalent, who has completed all formal academic and research training and who wishes to acquire up to two years supervised research training in an established setting. The proposed research must be related to some area of acoustics, psychoacoustics, speech communication or noise. The research must be carried out in a setting other than the one in which the Ph.D. degree was earned. The prize is for $3000 for full-time research for twelve months, and may be renewed for a second year. Coordinator: Sharon Abel, Mount Sinai Hospital, 600 University Avenue, Toronto, ON M5G 1X6. Past recipients are:

1990	*Li Cheng*	*Université de Sherbrooke*
1993	*Roland Woodcock*	*University of British Columbia*
1994	*John Osler*	*Defense Research Establishment Atlantic*

Alexander Graham Bell Graduate Student Prize In Speech Communication and Behavioural Acoustics

The prize is made to a graduate student enrolled at a Canadian academic institution and conducting research in the field of speech communication or behavioural acoustics. It consists of an $800 cash prize to be awarded annually. Coordinator: Don Jamieson, Department of Communicative Disorders, University of Western Ontario, London, ON N6G 1H1. Past recipients are:

1990	*Bradley Frankland*	*Dalhousie University*
1991	*Steven D. Turnbull*	*University of New Brunswick*
	Fangxin Chen	*University of Alberta*
	Leonard E. Cornelisse	*University of Western Ontario*
1993	*Aloknath De*	*McGill University*
1994	*Michael Lantz*	*Queen's University*

Fessenden Student Prize in Underwater Acoustics

The prize is made to a graduate student enrolled at a Canadian university and conducting research in underwater acoustics or in a branch of science closely connected to underwater acoustics. It consists of $500 cash prize to be awarded annually. Coordinator: David Chapman, DREA, PO Box 1012, Dartmouth, NS B2Y 3Z7.

1992	*Daniela Dilorio*	*University of Victoria*
1993	*Douglas J. Wilson*	*Memorial University*
1994	*Craig L. McNeil*	*University of Victoria*

Eckel Student Prize in Noise Control

The prize is made to a graduate student enrolled at a Canadian academic institution pursuing studies in any discipline of acoustics and conducting research related to the advancement of the practice of noise control. It consists of a $500 cash prize to be awarded annually. The prize was inaugurated in 1991. Coordinator: Murray Hodgson, Occupational Hygiene Programme, University of British Columbia, 2206 East Mall, Vancouver, BC V6T 1Z3.

1994	*Todd Busch*	*University of British Columbia*

Directors' Awards

Three awards are made annually to the authors of the best papers published in *Canadian Acoustics*. All papers reporting new results as well as review and tutorial papers are eligible; technical notes are not. The first award, for $500, is made to a graduate student author. The second and third awards, each for $250, are made to professional authors under 30 years of age and 30 years of age or older, respectively. Coordinator: Blaise Gosselin, Hydro Québec, 16^{e} étage, 75 boul. René Lévesque ouest, Montréal, QC H2Z 1A4.

Student Presentation Awards

Three awards of $500 each are made annually to the undergraduate or graduate students making the best presentations during the technical sessions of Acoustics Week in Canada. Application must be made at the time of submission of the abstract. Coordinator: Alberto Behar, 45 Meadowcliffe Drive, Scarborough, ON M1M 2X8.

INSTRUCTIONS TO AUTHORS
PREPARATION OF MANUSCRIPT

Submissions: The original manuscript and two copies should be sent to the Editor-in-Chief.

General Presentation: Papers should be submitted in camera-ready format. Paper size 8.5" x 11". If you have access to a word processor, copy as closely as possible the format of the articles in Canadian Acoustics 18(4) 1990. All text in Times-Roman 10 pt font, with single (12 pt) spacing. Main body of text in two columns separated by 0.25". One line space between paragraphs.

Margins: Top - title page: 1.25"; other pages, 0.75"; bottom, 1" minimum; sides, 0.75".

Title: Bold, 14 pt with 14 pt spacing, upper case, centered.

Authors/addresses: Names and full mailing addresses, 10 pt with single (12 pt) spacing, upper and lower case, centered. Names in bold text.

Abstracts: English and French versions. Headings, 12 pt bold, upper case, centered. Indent text 0.5" on both sides.

Headings: Headings to be in 12 pt bold, Times-Roman font. Number at the left margin and indent text 0.5". Main headings, numbered as 1, 2, 3, ... to be in upper case. Sub-headings numbered as 1.1, 1.2, 1.3, ... in upper and lower case. Sub-sub-headings not numbered, in upper and lower case, underlined.

Equations: Minimize. Place in text if short. Numbered.

Figures/Tables: Keep small. Insert in text at top or bottom of page. Name as "Figure 1, 2, ..." Caption in 9 pt with single (12 pt) spacing. Leave 0.5" between text.

Photographs: Submit original glossy, black and white photograph.

References: Cite in text and list at end in any consistent format, 9 pt with single (12 pt) spacing.

Page numbers: In light pencil at the bottom of each page.

Reprints: Can be ordered at time of acceptance of paper.

DIRECTIVES A L'INTENTION DES AUTEURS
PREPARATION DES MANUSCRITS

Soumissions: Le manuscrit original ainsi que deux copies doivent être soumis au rédacteur-en-chef.

Présentation générale: Le manuscript doit comprendre le collage. Dimensions des pages, 8.5" x 11". Si vous avez accès à un système de traitement de texte, dans la mesure du possible, suivre le format des articles dans l'Acoustique Canadienne 18(4) 1990. Tout le texte doit être en caractères Times-Roman, 10 pt et à simple (12 pt) interligne. Le texte principal doit être en deux colonnes séparées d'un espace de 0.25". Les paragraphes sont séparés d'un espace d'une ligne.

Marges: Dans le haut - page titre, 1.25"; autres pages, 0.75"; dans le bas, 1" minimum; latérales, 0.75".

Titre du manuscrit: 14 pt à 14 pt interligne, lettres majuscules, caractères gras. Centré.

Auteurs/adresses: Noms et adresses postales. Lettres majuscules et minuscules, 10 pt à simple (12 pt) interligne. Centré. Les noms doivent être en caractères gras.

Sommaire: En versions anglaise et française. Titre en 12 pt, lettres majuscules, caractères gras, centré. Paragraphe 0.5" en alinéa de la marge, des 2 cotés.

Titres des sections: Tous en caractères gras, 12 pt, Times-Roman. Premiers titres: numéroter 1, 2, 3, ..., en lettres majuscules; sous-titres: numéroter 1.1, 1.2, 1.3, ..., en lettres majuscules et minuscules; sous-sous-titres: ne pas numéroter, en lettres majuscules et minuscules et soulignés.

Equations: Les minimiser. Les insérer dans le texte si elles sont courtes. Les numéroter.

Figures/Tableaux: De petites tailles. Les insérer dans le texte dans le haut ou dans le bas de la page. Les nommer "Figure 1, 2, 3,..." Légende en 9 pt à simple (12 pt) interligne. Laisser un espace de 0.5" entre le texte.

Photographies: Soumettre la photographie originale sur papier glacé, noir et blanc.

Références: Les citer dans le texte et en faire la liste à la fin du document, en format uniforme, 9 pt à simple (12 pt) interligne.

Pagination: Au crayon pâle, au bas de chaque page.

Tirés-à-part: Ils peuvent être commandés au moment de l'acceptation du manuscrit.

WHAT'S NEW ??

Promotions
Deaths
New jobs
Moves
Retirements
Degrees awarded
Distinctions
Other news

Do you have any news that you would like to share with *Canadian Acoustics* readers? If so, fill in and send this form to:

QUOI DE NEUF ??

Promotions
Décès
Offre d'emploi
Déménagements
Retraites
Obtention de diplômes
Distinctions
Autres nouvelles

Avez-vous des nouvelles que vous aimeriez partager avec les lecteurs de l'*Acoustique Canadienne*? Si oui, écrivez-les et envoyer le formulaire à:

Jim Desormeaux, Ontario Hydro, 1549 Victoria Street East, Whitby, Ontario L1N 9E3

The Canadian Acoustical Association

l'Association Canadienne d'Acoustique

SUBSCRIPTION INVOICE

Subscription for the current calendar year is due January 31. New subscriptions received before July 1 will be applied to the current year and include that year's back issues of *Canadian Acoustics*, if available. Subscriptions received from July 1 will be applied to the next year.

Check ONE Item Only:

CAA Membership	$35
CAA Student membership	$10
Corporate Subscription	$35
Sustaining Subscription	$150

Total Remitted $_____

INFORMATION FOR MEMBERSHIP DIRECTORY

Check areas of interest (max 3):

1. Architectural Acoustics _____
2. Engineering Acoustics / Noise Control _____
3. Physical Acoustics / Ultrasound _____
4. Musical Acoustics / Electroacoustics _____
5. Psychological / Physiological Acoustics _____
6. Shock and Vibration _____
7. Hearing Sciences _____
8. Speech Sciences _____
9. Underwater Acoustics _____
10. Signal Processing / Numerical Methods _____
11. Other _____

PLEASE TYPE NAME AND ADDRESS BELOW:

VEUILLEZ ECRIRE VOTRE NOM ET VOTRE ADRESSE CI-DESSOUS:

FACTURE D'ABONNEMENT

L'abonnement pour la présente année est dû le 31 janvier. Les nouveaux abonnements reçus avant le 1 juillet s'appliquent à l'année courante et incluent les anciens numéros (non-épuisés) de *l'Acoustique Canadienne* de cette année. Les abonnements reçus après le 1 juillet s'appliquent à l'année suivante.

Cocher la case appropriée :

Membre individuel	
Membre étudiant(e)	
Membre de société	
Abonnement de soutien	

Versement total

RENSEIGNEMENT POUR L'ANNUAIRE DES MEMBRES

Cocher vos champs d'intérêt (max. 3):

1. Acoustique architecturale _____
2. Génie acoustique / Contrôle du bruit _____
3. Acoustique physique / Ultrasons _____
4. Acoustique musicale / Electroacoustique _____
5. Physio/psycho-acoustique _____
6. Chocs et vibrations _____
7. Audition _____
8. Parole _____
9. Acoustique sous-marine _____
10. Traitement des signaux / Méthodes numériques _____
11. Autre _____

Business telephone number (_____) _____ Numéro de téléphone au bureau
Business facsimile number (_____) _____ Numéro de télécopieur au bureau
Business E-Mail number _____ Numéro de courier électronique au bureau

Faites parvenir ce formulaire à l'adresse suivante en prenant soin d'y joindre un chèque fait au nom de L'ASSOCIATION CANADIENNE D'ACOUSTIQUE:

Make cheques payable to THE CANADIAN ACOUSTICAL ASSOCIATION. Mail this form with payment to:

Trevor R. T. Nightingale
Secretary, Canadian Acoustical Association
P. O. Box 74068
Ottawa, Ontario K1M 2H9

The Canadian Acoustical Association
l'Association Canadienne d'Acoustique

SUSTAINING SUBSCRIBERS / ABONNES DE SOUTIEN

The Canadian Acoustical Association gratefully acknowledges the financial assistance of the Sustaining Subscribers listed below. Annual donations (of $150.00 or more) enable the journal to be distributed to all at a reasonable cost. Sustaining Subscribers receive the journal free of charge. Please address donation (made payable to the Canadian Acoustical Association) to the Secretary of the Association.

L'Association Canadienne d'Acoustique tient à témoigner sa reconnaissance à l'égard de ses Abonnés de Soutien en publiant ci-dessous leur nom et leur adresse. En amortissant les coûts de publication et de distribution, les dons annuels (de $150.00 et plus) rendent le journal accessible à tous nos membres. Les Abonnés de Soutien reçoivent le journal gratuitement. Pour devenir un Abonné de Soutien, faites parvenir vos dons (chèque ou mandat-poste fait au nom de l'Association Canadienne d'Acoustique) au secrétaire de l'Association.

Acoustec Inc.
935 rue Newton, suite 103
Québec, Québec G1P 4M2
Tél: (418) 877-6351

Atlantic Acoustical Associates
P. O. Box 96, Station M
Halifax, NS B3J 2L4

H.L. Blachford Ltd.
Noise Control Products
Engineering / Manufacturing
Mississauga: Tel.: (905) 823-3200
Montreal: Tel: (514) 938-9775
Vancouver: Tel: (604) 263-1561

Bolstad Engineering Associates Ltd.
5110 - 97A Street
Edmonton, Alberta T6B 2R9
Tel: (403) 434-9386

Canadian Home Acoustics Inc.
PO Box 388
9 Doble Street
Sunderland, Ontario L0C 1H0
Tel: (905) 357-3303

J.E. Coulter Associates Engineering
Suite 507, 1200 Sheppard Avenue East
Willowdale, Ontario M2K 2S5
Tel: (416) 502-8598

Dalimar Instruments Inc.
193, Joseph Carrier
Vaudreuil-Dorion, Québec J7V 5V5
Tél: (514) 453-0033

Eckel Industries of Canada Ltd.
Noise Control Products, Audiometric
Rooms - Anechoic Chambers
P.O. Box 776
Morrisburg, Ontario K0C 1X0
Tel: (613) 543-2967

Environmental Acoustics Inc.
Unit 22, 5359 Timberlea Blvd.
Mississauga, Ontario L4W 4N5
Tel: (905) 238-1077

Hatch Associates Ltd.
Attn.: Tim Kelsall
2800 Speakman Drive
Mississauga, Ontario L5K 2R7
Tel: (905) 855-7600

Industrial Metal Fabricators (Chatham) Ltd.
Environmental Noise Control
288 Inshes Avenue
Chatham, Ontario N7M 5L1
Tel: (519) 354-4270

Integral DX Engineering Inc.
907 Admiral Avenue
Ottawa, Ontario K1Z 6L6
Tel: (613) 761-1565

Lalonde, Girouard, Letendre & Assoc.
2271 boul. Fernand-Lafontaine
Longueuil, Québec J4G 2R7
Tél: (514) 651-6710

Mechanical Engineering Acoustics and Noise Unit
University of Alberta
6720 - 30th St.
Edmonton, Alberta T6P 1J6
Tel: (403) 466-6465

MJM Conseillers en Acoustique Inc.
M.J.M. Acoustical Consultants Inc.
Bureau 440, 6555 Côte des Neiges
Montréal, Québec H3S 2A6
Tél: (514) 737-9811

Nelson Industries Inc.
Corporate Research Department
P.O. Box 600
Stoughton, Wisconsin, USA 53589-0600
Tel: (608) 873-4373

OZA Inspections Ltd.
PO Box 271
Grimsby, Ontario L3M 4G5
Tel: (905) 945-5471

Peutz & Associés
103 Bd. Magenta
F-75010 Paris, France
Tél: (33) 42-85-84-85

Scantek Inc.
Sound and Vibration Instrumentation
916 Gist Avenue
Silver Spring, Maryland, USA 20910
Tel: (301) 495-7738

SNC/Lavalin Environment Inc.
2 Felix Martin Place
Montreal, QC H2Z 1Z3
Tel: (514) 393-1000

Spaarg Engineering Limited
Noise and Vibration Analysis
822 Lounsborough Street
Windsor, Ontario N9G 1G3
Tel: (519) 972-0677

Tacet Engineering Limited
Consultants in Vibration & Acoustical Design
111 Ava Road
Toronto, Ontario M6C 1W2
Tel: (416) 782-0298

Valcoustics Canada Ltd.
30 Wertheim Court, Unit 25
Richmond Hill, Ontario L4B 1B9
Tel: (905) 764-5223

Wilrep Ltd.
Unit C10 - 1515 Matheson Blvd. E.
Mississauga, Ontario L4W 2P5
Tel: (905) 625-8944